

Characterization of Emissions and Air Quality Modeling for Predicting the Impacts of Prescribed Burns at DoD Lands

SI-1647

Lead Principal Investigator:

Dr. Mehmet Talat Odman
Georgia Institute of Technology
School of Civil and Environmental Engineering
311 Ferst Drive
Atlanta, GA 30332-0512
Email: odman@gatech.edu
Phone: (404) 894-2783
Fax: (404) 894-8266

Co-Principal Investigators:

Dr. Gary L. Achtemeier
USDA Forest Service
Center for Forest Disturbance Science
Athens, GA 30602

Dr. Armistead G. Russell
Georgia Institute of Technology
School of Civil and Environmental Engineering
Atlanta, GA 30332-0512

December 31, 2010

Table of Contents

| | |
|---|-----|
| Executive Summary | 1 |
| Objective | 7 |
| Background | 7 |
| State of Emissions Estimates | 8 |
| State of Models | 8 |
| Materials and Methods | 10 |
| Estimating Fuel Loads | 11 |
| Adaptive Grids | 11 |
| Adaptation Step | 12 |
| Solution Step | 14 |
| Daysmoke | 15 |
| Fort Benning Field Study | 15 |
| Model Evaluation | 17 |
| Results and Accomplishments | 17 |
| 1. Emissions Estimation | 17 |
| Subtask 1.1: Fuel Loading and Fuel Consumption Estimation | 17 |
| Subtask 1.2: Initial Emissions Estimation | 17 |
| Subtask 1.3: Collection of Fort Benning Samples for Measurements at Fire Sciences Lab | 17 |
| Subtask 1.4: Final Emissions Estimation | 19 |
| 2. Model Development | 20 |
| Subtask 2.1: Incorporation of the Adaptive Grid Method in CMAQ | 20 |
| Subtask 2.2: Initial Coupling of Daysmoke with CMAQ | 24 |
| Subtask 2.3: Modification of Daysmoke and Adaptive Grid CMAQ models | 24 |
| Subtask 2.4: Final Coupling of the Models | 24 |
| 3. Field Measurements | 32 |
| Subtask 3.1: Exploration of Fort Benning Site and Preliminary Data Collection | 32 |
| Subtask 3.2: Intensive Data Collection and Analysis | 32 |
| Subtask 3.3: Final Data Collection | 32 |
| 4. Model Evaluation | 32 |
| Subtask 4.1: Initial Evaluation of the Models | 32 |
| Subtask 4.2: Re-Evaluation with Newly Collected Data | 32 |
| Subtask 4.3: Final Evaluation with Other Data | 32 |
| 5. Simulations of Alternative Burning Strategies | 36 |
| Subtask 5.1: Identifying Burning Options | 36 |
| Concluding Summary | 37 |
| Lessons Learned from the Analysis of Field Studies | 41 |
| References | 42 |
| Appendix A: List of Technical Publications | A-1 |
| Articles or Papers Published in Peer-reviewed Journals | A-1 |
| Published Technical Abstracts | A-1 |
| Appendix B: Variable time-step algorithm | B-1 |
| Appendix C: Adaptive grid CMAQ | C-1 |
| Appendix D: Study plan for Eglin AFB | D-1 |

Appendix E: Evaluation of Daysmoke with collected dataE-1

List of Acronyms

| | |
|-------------------|--|
| AP-42 | Compilation of Air Pollutant emission factors |
| AFB | Air Force Base |
| AGM | Adaptive Grid Model |
| AG-CMAQ | Adaptive Grid CMAQ |
| AGD-CMAQ | Adaptive Grid CMAQ coupled with Daysmoke |
| AQM | Air Quality Model |
| ASHFALL | A plume model to simulate deposition of ash from sugar cane fires |
| CALPUFF | California Air Resources Board's Gaussian puff dispersion model. |
| CMAQ | Community Multiscale Air Quality model |
| CMAS | Community Modeling & Analysis System |
| CO | Carbon monoxide |
| CONSUME | A fuel consumption model |
| DDM | Decoupled Direct Method |
| DoD | Department of Defense |
| DSAGA | Dynamic Solution Adaptive Grid Algorithm |
| EPA | Environmental Protection Agency |
| FCCS | Fuel Characteristic Classification System |
| FS | Forest Service |
| GIT | Georgia Institute of Technology |
| MAQSIP | Multiscale Air Quality Simulation Platform |
| MM5 | Fifth-Generation NCAR / Penn State Mesoscale Model |
| MODIS | Moderate resolution Imaging Spectroradiometer |
| NASA | National Aeronautical and Space Administration |
| NCAR | National Center for Atmospheric Research |
| NCSU | North Carolina State University |
| NFDRS | National Fire Danger Rating System |
| NO | Nitric oxide |
| NO ₂ | Nitrogen dioxide |
| NO _x | Oxides of nitrogen |
| NO _y | Sum of NO _x and its oxidation products |
| O ₃ | Ozone |
| OAQPS | Office of Air Quality Planning and Standards |
| PBL | Planetary Boundary Layer |
| PI | Principal Investigator |
| PM | Particulate Matter |
| PM _{2.5} | PM with aerodynamic diameter smaller than 2.5 microns |
| PM ₁₀ | PM with aerodynamic diameter smaller than 10 microns |
| RCW | Red-Cockaded Woodpecker |
| Rx-CADRE | Prescribed Fire Combustion and Atmospheric Research Experiment |
| SCICHEM | Second-order Closure Integrated puff model with Chemistry |
| SERDP | Strategic Environmental Research and Development Program |
| SHRMC-4S | Southern High-Resolution Modeling Consortium Southern Smoke Simulation System |
| SO ₂ | Sulfur dioxide |

| | |
|----------|---|
| SOA | Secondary Organic Aerosol |
| SON | Statement of Need |
| SRS | Savannah River Site |
| TAC | Technical Advisory Committee |
| TSI | Thermo-Systems, Inc. |
| UGA | University of Georgia |
| UMASS | University of Massachusetts |
| USDA | United States Department of Agriculture |
| USFS | United States Forest Service |
| UXO | Unexploded Ordnance |
| VARTSTEP | Variable Time-Step Algorithm |
| VOC | Volatile Organic Compounds |
| WRAP | Western Regional Air Partnership |
| WRF | Weather Research and Forecasting model |

List of Figures

| | |
|---|----|
| Figure 1. Technical approach. | 10 |
| Figure 2. Intersection of an adapting grid cell with the area-source emissions grid..... | 13 |
| Figure 3. Transport with VARTSTEP algorithm. | 15 |
| Figure 4. Fort Benning sampling grid..... | 16 |
| Figure 5. Comparison of emission factors for burn units at Ft. Benning. | 18 |
| Figure 6. The wind fields obtained by standard MM5 (left) and adaptive MM5 but no grid adaptation (right) in applications to the 9 April 2008 burn at Ft. Benning. The domain is 91 x 94 cells of 1.33 km resolution covering Ft. Benning and surrounding areas in Georgia and Alabama..... | 21 |
| Figure 7. The wind field obtained by WRF in an application to the 15 April 2008 burn at Ft. Benning. The grid resolution is 1.33 km. | 22 |
| Figure 8. Comparison of zonal wind profiles in applications to the Holloman Air Force Base (Xiao et al., 2007). The Adaptive Grid MM5 (both with and without grid adaptation) agreed better with the Radiosonde observations than the standard MM5, even in the PBL although the focus of this application was the stratosphere..... | 23 |
| Figure 9. Determination of Daysmoke-adaptive grid CMAQ interface: a) Top view of a Daysmoke output divided by fine 100X100 grid, b) Top view of a Daysmoke output divided by adaptive grid, c) Top view of a Daysmoke output with “wall” in purple | 25 |
| Figure 10. Plots of concentration error versus downwind distance at a) 16:30Z, b) 17:30Z and c) 18:30Z. | 28 |
| Figure 11. Distance of the wall over time during the Feb. 28,2007 Atlanta burn case: blue for the Oconee burn and pink for the Piedmont burn. | 29 |
| Figure 12. Measured (red) and modeled PM _{2.5} concentrations using standard CMAQ (dark blue), AG-CMAQ (light blue), and AGD-CMAQ (green) at the Mc Donough, South DeKalb, Confederate Avenue, Fort McPherson, Jefferson Street and Fire Station 8 air quality monitoring sites in the Atlanta metropolitan area. | 30 |
| Figure 13. Mean normalized error for modeled PM _{2.5} concentrations using standard CMAQ (blue), AG-CMAQ (red), AGD-CMAQ (green) at the Mc Donough, South DeKalb, Confederate Avenue, Fort McPherson, Jefferson Street and Fire Station 8 sites in Atlanta metropolitan area. | 31 |
| Figure 14. Daysmoke performance for each burn event and at each monitor: difference of modeled PM _{2.5} from observed (top), classification of the burn event by the trend of concentration with distance downwind (middle), and ratio of modeled to observed PM _{2.5} (bottom)..... | 34 |
| Figure 15. PM _{2.5} concentrations predicted by CMAQ and AG-CMAQ along with measurements at South DeKalb on 28 February 2007 (top). The bottom panels, where the location of the South DeKalb site is marked by the pink dot, show simulated PM _{2.5} at three different instances indicated by the arrow tails. | 36 |

List of Tables

| | |
|---|-----------|
| Table 1. Comparison of flaming emissions factors (g/kg) | 18 |
| Table 2. Comparison of smoldering emissions factors (g/kg) | 19 |

Acknowledgements

This research is sponsored by the Strategic Environmental Research and Development Program (SERDP). The United States Department of Agriculture (USDA) Forest Service is sharing the cost.

Executive Summary

Prescribed burning (PB) is an effective and economical land management tool for improving and maintaining an ecosystem, reducing wildfire risk, and improving training realism at Department of Defense (DoD) facilities. However, pollutants emitted from prescribed fires may be transported downwind, mix with emissions from other sources, form other pollutants, and contribute to poor air quality of urban areas in the region. Compliance of those urban areas with ambient air quality standards may require tougher restrictions on DoD's air emissions in the future. Since the alternatives of PB are costly, it is important for DoD to be able to control the emissions from its PB operations and to minimize their air quality impacts. Therefore it is necessary to better characterize PB emissions and to more accurately predict their air quality impacts.

The objectives of this project are (1) to improve the characterization of PB emissions; (2) develop a simulation model that can accurately predict the impacts of prescribed burns on regional air quality; (3) collect field data most relevant to the modeling of PB plumes; (4) validate the model through evaluations with field data; and (5) assess alternative burning strategies for southeastern DoD facilities. Fort Benning is selected as the host DoD installation for this project because of the large size of its PB operation and its proximity to a major metropolitan area: Columbus-Phenix City, which is beleaguered with air quality issues.

Current estimates of PB emissions are based on studies mostly conducted in the West during 1970s and 1980s. They may not be able to characterize the diverse ecosystem and environmental conditions of the Southeast. For example, some prior studies by the Forest Service (FS) suggest that fine particulate matter (PM_{2.5}) emissions from southeastern burns may be much smaller than the current estimates. This is a problem for the fidelity of all air quality simulations. On the other hand, there is no definite answer to how to place these emissions in regional-scale air quality models. Local plume models and regional AQMs have advanced our knowledge of smoke transport and dispersion to a certain level. To increase our understanding, there is now a need for a proper model for prescribed fire plumes in regional scale simulations.

In this project a new classification system developed by the U.S. Forest Service is being applied to the characterization of fuel beds on DoD lands. PB emission factors are derived from prior field measurements of particulate matter (PM), carbon monoxide (CO), and volatile organic compounds (VOC) in the Southeast, and they are being compared to those in AP-42 tables recommended by the U.S. Environmental Protection Agency. "Daysmoke," a dynamical-stochastic plume model designed specifically for prescribed burns, and the Community Multiscale Air Quality (CMAQ) model are being coupled using the improved grid resolution provided by the Dynamic Solution Adaptive Grid Algorithm (DSAGA). This will enable accurate representation of plume dynamics and chemistry at local scales as well as accurate prediction of impacts over regional scales.

The models are being evaluated using existing data first. Additional data needs are fulfilled by a real-time ground-based downwind monitoring component that focuses on the PB operation at Fort Benning, Georgia. The models are being validated by reconciling the differences between model predictions and measurements. The data to be collected by other investigators at Southwestern U.S. and at Camp Lejeune, NC will also be used to evaluate the models for fuel types and loadings different from Fort Benning's. Finally, using the validated, coupled models, various scenarios will be simulated to quantify the air quality impacts of forest management options, such as changing the burning times, frequencies, and methods. The direct sensitivity

analysis method recently incorporated into CMAQ will be instrumental both in simulating the impacts and in understanding the uncertainties in model predictions.

The fuels survey at Fort Benning was completed and a model based on photo series was prepared for estimating fuel loads on any Fort Benning burn unit. Fuel loadings increase rapidly after a burn as shrubs become a significant part of the fuel bed. The increase slows down in time and a plateau is reached after approximately 5 years. This model provides a crosswalk to FCCS fuel classification system. Emissions were estimated for each burn monitored at Fort Benning: there were 3 burns in April 2008, 6 burns in January 2009, and 2 burns in April 2009. The fuel loads were input to CONSUME, which yields total fuel consumption, and then to FEPS for time varying consumption. The emissions are calculated by applying emission factors to the fuel consumptions. Emission factors used here were derived from extensive field studies of prescribed burns conducted by the Forest Service in the Southeastern U.S. in 1990's. To provide input to a parallel project, fuel samples were collected at Fort Benning and shipped to the Fire Science Laboratory in Missoula, MT for emission measurements. The emission factors measured in the laboratory were in general agreement with the USFS southeastern fuels emission factors used in our modeling. A sensitivity analysis was conducted to determine the important parameters of the models used in estimating emissions. Fuel moisture, involvement in flaming phase, duration of ignition, and emission factors are, by far, the most sensitive parameters. The likely ranges of these parameters were tested to determine the level of uncertainty in emission predictions. The uncertainties that were identified in this manner will later be used in estimating the uncertainties in downwind concentration predictions by the dispersion models. The sensitivity analysis extends to the air quality model now where the impact of vertical distribution of emissions on concentrations downwind is being studied.

Emission inputs are critical to dispersion model performance. While we have a certain level of confidence in emission factors, the fuel loads and fuel consumptions are more uncertain. As part of the Prescribed Fire Combustion and Atmospheric Research Experiment (Rx-CADRE) at Eglin Air Force Base (AFB) in February 2011, fuel load and fuel consumption data will be collected. By conducting our field study at Eglin AFB, during Rx-CADRE, we are hoping to benefit from these data, especially fuel consumption data, for more accurate emissions inputs to the Daysmoke plume dispersion model.

An adaptive grid version of MM5 that can provide meteorological inputs at the scales targeted for chemistry/transport modeling in this project (~100 m) was tested. This model was originally developed to resolve optical turbulence in the upper troposphere. Here, the model was applied to the simulation of boundary layer meteorology during the 9 April 2008 PB case. In this application, to better resolve the meteorology around the PB plume, the model was dynamically adapting to the externally supplied PM_{2.5} concentrations (which are high in the PB plume) from an earlier chemistry/transport simulation. Compared to a standard fixed grid MM5 simulation, as well as a WRF simulation, adaptive MM5 produced much more variability in the wind fields and the influence of the terrain was more apparent. Standard MM5 and WRF were under too much synoptic influence and the wind fields they produced were excessively damped and smooth.

Encouraged with this result, which indicated that the adaptive MM5 provides a significant improvement over the original model, we submitted a proposal to SERDP for high-resolution meteorological modeling with adaptive MM5. The goal of the proposed work was to continue the development and validation of adaptive MM5 to achieve full meteorology model functionality, which would result in unprecedented resolution of wind fields. The proposal was

rejected; therefore, meteorological inputs will continue to be interpolated from 1-km resolution MM5 or WRF simulations.

The incorporation of the adaptive grid algorithm into the CMAQ model was completed. The Adaptive Grid version of CMAQ (AG-CMAQ) is built in CMAQ Version 4.5 by keeping all the functionality and features of the host. AG-CMAQ also includes the variable time step algorithm (VARTSTEP) to improve computational efficiency (Odman and Hu, 2010; Appendix B). The code was verified by simulating the April 9, 2008 burn and comparing the results to those of an earlier simulation by CMAQ with fixed, uniform grid. AG-CMAQ increased the grid resolution in the regions of highest PM_{2.5} as it should. In a more rigorous verification aiming to match the results of standard CMAQ with a “non-adapting” run of the AG-CMAQ, all the differences in results were reconciled with the exception of very small (less than 0.1 μg m⁻³) differences in aerosol nitrates and secondary organic aerosols of biogenic origin. During this meticulous verification effort, three deeply hidden bugs were discovered in the official CMAQ code and reported to the modeling community. The highlights of AG-CMAQ development and verification were published in a journal article (Garcia-Menendez et al. 2010; Appendix C).

A thorough review of the Daysmoke model theory and computer code was completed. Several improvements to the model were implemented and tested. For example, the provision for adiabatic expansion allows for application to a wider range of smoke plume. The new transition from plume to free atmosphere at the plume top gives improved modeling for plume depth. The multi-core updraft feature is much more flexible now that it allows for cores of unequal sizes by assigning a stochastic flux component to each updraft core. A bug was discovered that increased plume vertical velocity by 0.5 - 1.0 m/s within the mixing layer. The parameterization of the entrainment coefficient was made a function of plume bent-overness. The detrainment coefficient was removed from being an additional degree of freedom. The free atmosphere horizontal velocity turbulence parameter, which was a constant, is made a function of the depth of the boundary layer. Finally, the model time steps, currently at 20 s, are being reduced (to be completed early next year) to capture the steep gradient in vertical velocity in the plume. Upon completion of the review of Daysmoke, a copy of the model code was transferred to GIT along with a draft write-up of the model theory.

Significant progress was made in the development of a coupling technique that can inject Daysmoke particles into the CMAQ grid cells without significant loss of accuracy. The technique is based on Fourier analysis. First, the smoke particle concentrations predicted by Daysmoke are represented as spectra of waves with different frequencies. Then, the waves whose frequencies cannot be supported by the adaptive CMAQ grid are identified. If the amplitudes of those waves are negligible, then the plume is handed over to CMAQ; otherwise the plume is continued to be followed by Daysmoke. A standalone analysis system was built by borrowing Fast Fourier Transform (FFT) algorithms from MATLAB. Analysis of several Daysmoke plumes showed that there exists an optimal downwind distance for hand over. This distance is a weak function of grid resolution; therefore the “wall” type coupling used so far is somewhat justified with the exception of the arbitrariness of the distance from the burn site to the wall. It was determined that the downwind distance of the wall should be calculated as a function of time.

Based on the findings of the Fourier analysis, we developed a coupling algorithm that sets the downwind distance for handover of Daysmoke plume to CMAQ as a function of time. Two conditions must be satisfied for handover: 1) the Daysmoke plume must reach its full height and 2) the difference between Daysmoke plume concentrations before handover and CMAQ grid cell

concentrations after handover (i.e., the concentration error incurred during handover) must be minimal. The coding of this algorithm was finished and the review and verification of the code has gone through its first cycle. The coupled system of the Adaptive Grid CMAQ (AG-CMAQ) with Daysmoke as the sub-grid scale plume model is named Adaptive Grid Daysmoke CMAQ (AGD-CMAQ). AGD-CMAQ is being evaluated by comparing its performance to the fixed grid CMAQ and adaptive grid CMAQ (AG-CMAQ).

After the preliminary data collection, which resulted in three monitored burns in April 2008, intensive field measurements in 2009 captured eight more burns: six in January and two in April. The burns were monitored by using three trucks equipped with real-time $PM_{2.5}$ and CO monitors covering a 60-degree arc emanating from the burn area and stretching along the predicted wind direction. In response to shifts in wind direction the trucks moved to different locations within their zones, respectively 1-3 km, 3-5 km, and 5-7 km downwind, according to dispatches from the fire tower. The exact locations of the sampler trucks have been tracked by GPS. The trucks remained at any given monitoring location for a minimum of 30 minutes. Each subsequent position was chosen based on a combination of wind shifts, real-time equipment levels, and road availability. All the real-time air samples collected were processed, controlled for quality, and quality assured. The measurements and related information have been posted to a web site for public access.

A thorough evaluation of the Daysmoke model was conducted using the collected field data (see Appendix E). $PM_{2.5}$ concentrations simulated by Daysmoke were compared to measurements at locations of the trucks that collected the air samples and for the times of collection. Analysis has shown that there is a relationship between the performance of the Daysmoke model and the gradient of the observed smoke by downwind distance. Daysmoke performance was the best on days when smoke concentration increased with distance downwind from the burn. On days when smoke concentrations decreased with distance, Daysmoke performance was not as good but still acceptable. On days characterized by extremely high smoke gradients, from very high smoke concentrations at 1-3 km downwind to almost no smoke at 5-7 km downwind, Daysmoke performance in predicting $PM_{2.5}$ concentrations was poor.

In general, the plume tops estimated by Daysmoke compare well with lidar measurements. The plume top and the number of updraft cores, which was confirmed by photographic data, are the two most important parameters in the determination of smoke levels by Daysmoke. Comparison of the $PM_{2.5}$ concentrations predicted by Daysmoke with real-time measurements from DustTrak instruments showed general agreement but there were several instances of divergence. Uncertainties remain related to the calibration of the DustTrack readings, estimated wind directions, ignition patterns, and the timing of emissions. Investigation of possible contamination by non-smoke PM sources led to the removal of only a small fraction of the data. WRF-simulated winds did not always line up the Daysmoke plume with truck locations. Most of the disparities in wind direction were within typical model prediction error. Occasionally, potential stability problems in WRF at 1.3-km resolution introduced unexpected oscillations to wind direction. This compromised efforts to match Daysmoke $PM_{2.5}$ with observed $PM_{2.5}$. The disparity was particularly notable for April 15, 2008 when truck positions were located SSE from the fire but WRF winds blew the Daysmoke plume to the SSW. Therefore, it is suggested that the WRF winds be validated with winds measured by a Doppler sodar during the next field experiment. A Doppler sodar was arranged for next year's field study to deal with the uncertainty in the wind directions.

The 2010 field study will be performed at Eglin AFB where fuels will be sampled before and after the burns for more accurate fuel loading and consumption data. PM_{2.5} data will be collected on mobile platforms and calibrated with more accurate PM_{2.5} measurements at a stationary site. In addition to plume measurements with ceilometer, vertical wind profiles will be measured with a Doppler sodar. A US EPA team will also join us with their tethered balloon, which will allow unique vertical profile measurements of the smoke plume. All these measurements during the 2011 field study are expected to substantially improve our ability to model emissions from prescribed burns and provide more accurate inputs to the Daysmoke plume dispersion model.

No burn monitored in 2009 carried smoke in the direction of regional monitors. So far, only the April 9, 2008 burn, under southeasterly winds, may have reached the monitor at Columbus, GA. A slight increase in PM_{2.5} was detected by the monitor few hours after the burn and this is believed to be a consequence of the PB plume hit. This leaves the historic Atlanta smoke incident (February 28, 2007) as the only other PB case for the evaluation of the coupled Daysmoke-CMAQ system. That case is ideal for regional model evaluation as the smoke was fully captured by the dense network of monitors in the metro-Atlanta area. The comparison of the CMAQ and AG-CMAQ results with observations showed improved replication of the plume and decrease in artificial dilution with AQ-CMAQ due to adaptive grid refinements. These results were published in a journal article (Garcia-Menendez et al. 2010; Appendix C).

Adaptive grid refinements increase the resolution only in the horizontal plane. A second set of simulations was conducted by increasing the vertical resolution. In these simulations the agreement between modeled and observed PM_{2.5} concentrations improved significantly. However, the models still underestimate PM_{2.5} levels. We believe this is in part due to the underestimation of secondary organic aerosol formation in CMAQ (as well as AG-CMAQ). Another possibility is the cooling effect of the dense smoke, which lowers the mixing height and leads to higher concentrations below the plume. This effect can only be modeled by feeding back PM levels from CMAQ to the meteorological driver.

Based on factors that can influence plume updraft dynamics, we reduced the number of cores used in Daysmoke for the burns at Oconee National Forest and the Piedmont Wildlife Refuge that led to the 28 February 2007 Atlanta smoke incident. We have also revised the fuel type used in FEPS upon further review of the information obtained from the Georgia Forestry Commission. As a result, the amount of PM_{2.5} emissions were reduced but the rise of the smoke plume in the atmosphere was enhanced. A sensitivity analysis is being conducted to determine the ideal profile for vertical distribution of the emissions so that a better agreement is obtained between predicted and observed pollutant concentrations.

The 28 February, 2007 Atlanta smoke incident is being used for the evaluation of the coupled Daysmoke and Adaptive Grid CMAQ (AGD-CMAQ) model as well. The initial results of the simulation with the coupled Daysmoke and Adaptive Grid CMAQ models (AGD-CMAQ) are superior to the results from the initial Daysmoke-CMAQ coupling as well as the Adaptive Grid CMAQ model. Not only the predicted PM_{2.5} concentrations were in better agreement with observations at downwind regional monitors, some long-range transport characteristics of the plumes were better simulated as well.

Finally, a survey was conducted among southeastern land managers to identify the most relevant burning scenarios to be simulated with our smoke impact prediction system. Varying the size of burn, ignition method, fuel moisture, season of burn, fuel loads, weather conditions, and time of burn were the most suggested burning options. Considering the priorities assigned to

each one of these options, various prescribed burning scenarios will be simulated to determine their potential impacts.

When finished, this project will integrate improved emissions data, important burn front information, and advanced plume modeling techniques in regional air quality models. It will enable more accurate prediction of the air quality impacts of prescribed burns. Using the developed simulation framework, DoD land managers will be able to plan their operations to minimize the impacts to regional air quality. The scientific community also will benefit from access to improved PB emissions and accurate models for the dispersion, transport, and chemistry of these emissions.

Objective

This project aims at improving the characterization of prescribed burn (PB) emissions, collecting field data most relevant to the modeling of PB plumes, and developing a simulation framework that can accurately predict the impacts of prescribed burns on regional air quality. Specific objectives are to:

1. Better characterize the fuel types and loads for the sites to be studied,
2. Accurately estimate emissions from the burns to be simulated,
3. Develop a sub-grid treatment for PB plumes in regional-scale air quality models
4. Increase the grid resolution for adequate coupling of the sub-grid scale plume models with regional-scale air quality models
5. Evaluate the coupled models with existing prescribed fire data
6. Identify and collect the data needed for model validation
7. Consider the effects of inherent uncertainties in model inputs on model results
8. Simulate the regional air quality impacts of DoD PB operations in the Southeast, and
9. Assess alternative burning strategies.

Background

The reasons for conducting PB operations at military installations include improving and maintaining endangered species habitat, reducing the risk of wildfires, preparing sites for seeding and planting, managing understory hardwoods, controlling disease, improving forage for grazing, enhancing appearance, and improving access. For example, at Fort Benning a major objective is to convert the landscape as close to its pre-settlement condition (longleaf pine forest) to protect the endangered red-cockaded woodpecker (RCW) habitat and prescribed burning is the most economical means. Approximately 30,000 acres must be prescribed burned each year during the growing season to reduce unwanted vegetation that would compete with longleaf seedlings. Prescribed burning is an efficient and effective means to reduce fire fuel build-up. Heavy roughs can build up posing a serious threat from wildfire to lives, property, and all natural resources. A burning rotation of approximately 3 years is usually adequate to fire proof pine stands and reduce this threat. Prescribed burning also controls brown spot disease, which is a fungal infection that weakens and eventually kills longleaf seedlings. Wildlife species such as deer, turkey, quail, and doves also benefit from prescribed burning. Prescribed burning on a regular basis also serves a military need by providing a safer training environment with improved access and visibility. Lastly, growing season burns have significantly reduced the tick population on the installation.

Smoke complaints and the threat of litigation from smoke-related incidents / accidents are major concerns of the PB operations. Fort Benning follows voluntary smoke management guidelines in an effort to minimize the adverse impacts from smoke. Particulate matter (PM) emissions and the effect of PB on ozone levels in Columbus-Phenix City metropolitan areas are also of concern. Forest fires produce nitrogen oxides (NO_x) and volatile organic compounds (VOC) emissions and form ozone (Cheng et al., 1998). PB emissions may be transported downwind, mix with emissions from other sources and contribute to poor air quality in urban areas. Recognizing the Columbus ozone problem, the majority of the burns (70-75%) were shifted to the January-April period. However the threat of PM pollution continues during this season. What is needed is an accurate forecasting system so that the PB operation can be conducted to minimize undesirable air quality impacts. Estimates of missions and models of dispersion, chemistry and long-range transport are the key components of such a system.

State of Emissions Estimates

Emission factors are estimates of the quantity of emissions of a pollutant species per amount of material burned. Wildland fire emission factors have been developed under either field or laboratory conditions. The U.S. EPA (1995) formed a table of default values (AP-42 Table) for fire emission factors of major species. Improvements were made through the EPA Office of Air Quality Planning and Standards (OAQPS) to obtain separate emission factors for flaming and smoldering and for different forest species. They are presented in Tables 38 and 39 in a report to EPA (Battye and Battye 2002). The Forest Service (FS) conducted extensive field experiments of prescribed fires in the Southeast in 1996 (Hao et al. 2002). Emission factors were estimated for various ecosystems at a number of National Forest, Wildlife Refuge, and Air Force Base. Georgia Institute of Technology (GIT) recently conducted measurements of prescribed burn at Fort Benning (Baumann, 2005) and provided an estimate of emission factors specific to that ecosystem.

Each set of emission factors is applied to the specific geographic, ecological and environmental circumstances of forest fuel and burn. The AP-42 Table has been widely used in developing regional and nation-wide emission inventory (WRAP 2002, Liu 2004), but it was developed based on studies conducted in the west during 1970s and 1980s. The FS measurements are specific for the Southeast. This region is characterized by a diverse ecosystem and environmental conditions, which leads to large variations in emission factors from one site to another. The GIT study (Baumann, 2005) is specific to Fort Benning. There are some noticeable differences in the magnitudes of emission factors from different sources. For example, in comparison with the $PM_{2.5}$ emission factor in the AP-42 Table for the Southeast, the median value of $PM_{2.5}$ emission factor from the FS measurements is about one third smaller, and the value from GIT measurements is much smaller. Thus, specific circumstance of fuel and burning needs to be taken into account when specifying a magnitude of emission factors for fire emission calculation.

State of Models

Reactive plume models, with a history dating back to early 1980s (Steward and Liu, 1981) are probably the most reliable tools to predict plume behavior. These models are developed to track plume dispersion and chemical transport using our best understanding of atmospheric turbulence and chemistry. Most of them are designed for plumes from industrial emission sources such as large power plants. CALPUFF is one of the most popular models (Earth Tech, 2000). It accounts for vertical wind shear by splitting the plume when necessary and offers a number of dispersion options under various atmospheric stability conditions. These features increase the fidelity of dispersion and downwind transport. However, its treatment of chemistry is highly simplified. SCICHEM (Karamchandani et al., 2000) has a more comprehensive treatment of plume chemistry, including some account of turbulent concentration fluctuations on chemical kinetics. But even SCICHEM is only reliable for large power plant plumes being transported steadily over rural regions with homogeneous land cover and relatively constant ambient conditions and, with no interference from other point source or urban plumes. When there is interaction between plumes, reactive plume models cannot accurately estimate the formation of secondary pollutants, such as ozone or SOA (Karamchandani et al., 2000). Hence, in geographic regions where emission sources are diverse and numerous, reactive plume models are not applicable in the long-range. The best use for these models is the study of local or short-range impacts of individual plumes.

A regional scale air quality model (AQM) can provide more realistic ambient concentrations to the reactive plume models. It can also account for the injection of emissions from other sources that cannot all be modeled individually due to computational limitations. There have been several attempts to couple reactive plume models with regional AQMs (e.g., Kumar and Russell, 1996; Gillani and Godowitch, 1999). Recently, SCICHEM has been coupled with CMAQ and, in an application to Central California, remarkably good agreement was obtained with NO_y and O_3 measurements up to 5-km distances downwind of the sources (Vijayaraghavan, et al., 2006). Hence more accurate ambient concentrations help the plume models in the short range. The other expectation from coupling the models is to be able to transfer accurate plume information from the sub-grid (i.e., reactive plume) model to the grid (i.e., regional air quality) model. This other side of the coin is known as the plume “hand-over” problem. Kumar and Russell (1996) proposed handing over the plume after 1-hr of tracking it with the sub-grid model. Another approach is to hand over when physical plume dimensions reach the grid scales (Karamchandani et al, 2002). Gillani and Pleim (1996) suggested that the chemical maturity of the plume should be used as a hand-over criterion. A power plant plume is considered “mature” when its NO_x -rich and O_3 -poor core levels off. This is the recommended criteria for SCICHEM coupled with CMAQ (Karamchandani et al., 2002). Satisfying this criterion often requires tracking the plume with the sub-grid model for long distances (~70 km). Prolonged tracking with the sub-grid model delays the interaction of the plume with all the other plumes in its surroundings.

To our knowledge, no improvement in agreement between predictions and observations at ground monitors beyond ~10 km downwind has been reported with coupled models. This led to the general impression in modeling circles that plume-in-grid (i.e., coupled) models are unnecessary. As a result, the computationally expensive plume-in-grid capability is often turned off in regional applications (Morris et al., 2005). One of our hypotheses in this research is that, in order for model coupling to be beneficial in the mid-to-long range, the plume should be handed over as quickly as possible but only when the grid resolution can support the structure of the plume. This of course requires very fine grid resolution (~250 m). The adaptive grid technique (Khan et al., 2004) is capable of providing this resolution at reasonable computational cost.

Without the plume-in-grid treatment, the only means left to include fire plumes in regional-scale AQMs such as CMAQ (Byun and Ching 1999) and WRF-chem (Grell et al, 2005) is to treat them as point sources (such as industrial stacks) and/or area sources (such as vehicle emissions in cities). Point source emissions go through plume rise calculations and they are distributed through the vertical layers of the models at the vertical column coinciding with the source location. Area sources are directly mixed into the surface layer. These oversimplifications of plume mixing with the environment are not adequate to simulate patterns of pollution dispersion and concentration over large multiple state areas. Prescribed burns are transient (occurring only once every few years in any particular area) and ground-level (not from elevated stacks) and thus do not qualify as point sources. Prescribed burns release considerable amounts of heat which leads to buoyant plumes capable of distributing smoke well above the ground and thus do not qualify as area sources either. Furthermore, fire intensity, hence heat production and emission rates, varies throughout the life of the burn with corresponding changes in plume dynamics.

Another problem is that none of these models includes the “human element” – how the burns are engineered by land managers. By the choice of firing method – head fire, back fire, mass ignition (where, when, and how much fire is dropped) – land managers can determine the timing

of heat production and how much heat is produced over the course of the burn. Thus the human element can be a major contributor to how high smoke goes and how much gets there during a period of evolving mixing layer height within a time-dependent wind field. One exception is the Daysmoke model (Achtemeier 1998) which was designed considering unique characteristics of prescribed fire plumes including the human element.

In summary, there is no simple method for determining where in regional-scale AQMs wildland fire plumes should be placed; nor how much smoke should be placed there and thus the contribution of emissions from wildland fire, especially to the particulate matter (PM) loads, is problematic. Given that the prescribed burn programs, for example the one in the Southeast, release large amounts of PM_{2.5}, carbon monoxide and NO_x, this is also a problem for the fidelity of all regional air quality simulations. Local plume models and regional AQMs have advanced our knowledge of smoke transport and dispersion to a certain level. To increase our understanding, there is now a need for a proper subgrid model for prescribed fire plumes in regional scale models and an appropriate coupling methodology.

Materials and Methods

The overall technical approach is summarized in Figure 1. The emissions estimation task is followed by model development and simulations. Then the model predictions are evaluated with field data. There will be several cycles of these tasks including new field measurements. Finally, alternative burning strategies will be simulated using the evaluated modeling system.

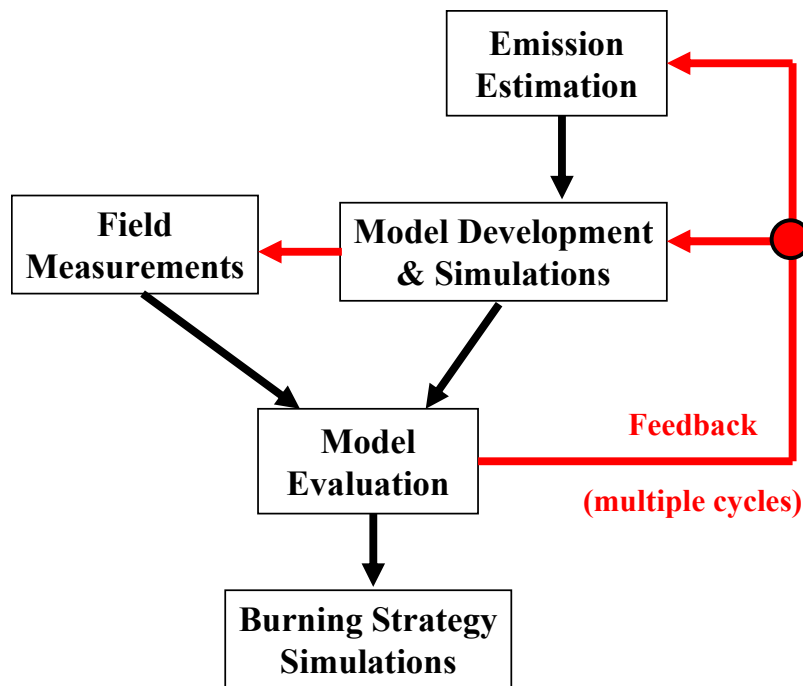


Figure 1. Technical approach.

As part of the emission estimation task a new classification system developed by the Forest Service (FS) is applied to the characterization of fuel beds on DoD lands. PB emission factors are derived from prior field measurements of particulate matter, carbon monoxide, and volatile organic compounds in the Southeast. The models used in the project are “Daysmoke,” a

dynamical-stochastic plume model designed specifically for prescribed burns, and the Community Multiscale Air Quality (CMAQ) model. These two models will be coupled using the improved grid resolution provided by the Adaptive Grid Model (AGM) technology. The goal is to enable accurate representation of plume dynamics and chemistry at local scales for accurate prediction of the air quality impacts over regional scales. The models are evaluated using available data. Additional data needs will be identified and fulfilled by a real-time downwind monitoring component that focuses on the PB operation at Fort Benning, Georgia. The models will be validated by reconciling the differences between model predictions and measurements.

Estimating Fuel Loads

An estimate of the fuel load in a burn unit is the starting point for any attempt to calculate the emissions from a wildland fire. Detailed measurements of fuel loads are time consuming to obtain and are therefore not done as part of a land manager's normal burn planning. Wildland fuel photo series (Ottmar et al., 2000, 2003; Scholl and Waldrop, 1999) represent a practical tool developed for land managers. It allows fuel loads to be estimated by comparing site conditions against a collection of photographs with known fuel loadings. A limitation of photo series is that they are not produced for every locality/ecosystem type, as is the case for Fort Benning in the Piedmont of Georgia.

This study utilizes a combination of photo series developed for nearby ecosystems (*Scholl and Waldrop, 1999; Ottmar et al., 2000, 2003*). For a subset of burn units available on Fort Benning representing the two major soil types (clay vs. sand) and fire return intervals from 1 to 5 years, three technicians visually surveyed each site and described the site in terms of photo series fuel types. This description was often highly qualitative (e.g., site looks like fuel type *n*, but could also be *m*). The descriptions were then translated into fuel loadings by weighted averages of the fuel bed components. If only one fuel model was specified, its weight was set to 1.0. For cases with multiple fuel models, weights were based on any qualifiers used in the description. No qualifiers provided equal weighting, while a qualifier of “more like” received a larger weight (in the case of two fuel models, if models *n* and *m* both were applicable, but the site looked more like *n*, it received a weight of 0.67 while *m* received a weight of 0.33). Every observer's fuel load estimates for a site were subsequently averaged to provide a final fuel load estimate for a burn unit.

Adaptive Grids

An adaptive grid algorithm can better resolve the dynamics and chemistry needed for accurate simulation of a PB plume. Such an algorithm has been developed at North Carolina State University and recently included into the MM5 numerical weather prediction model for the purpose of predicting atmospheric optical turbulence (Xiao et al., 2006). The same algorithm was incorporated in MAQSIP, an air quality model which served as the prototype to CMAQ (Odman et al., 2001; 2002). It was shown to lead to greater precision in the simulation of transport and dispersion of pollutants released during a fire event (Unal and Odman, 2003).

An adaptive grid AQM simulation has two fundamental steps: a grid adaptation step, that is responsible for repositioning of grid nodes according to the grid resolution requirements, and a solution step, that simulates the physical and chemical processes that occur in the atmosphere. The solution (i.e., concentration fields) remains unchanged during the adaptation step, and the weight function clusters the grid nodes in regions where finer resolution grids are required. In preparation for the solution step, the fields of meteorological inputs and emissions must be

mapped onto the new grid locations. This task is also considered part of the adaptation step and is undertaken by efficient search and intersection algorithms. During the solution step, the grid nodes remain fixed while the solution is advanced in time. Ideally, the adaptation step should be repeated after each solution step owing to the change in resolution requirements. However, since the mapping of meteorological and emissions data is computationally expensive, we have chosen to apply the adaptation step less frequently. Whereas, the solution is advanced in time by 1 hour in several time steps, the adaptation step is performed once every hour. In order to ensure numerical stability, we require that the Courant number be smaller than unity while determining the time step of the solution. The rest of this section consists of a more detailed description of the adaptation and solution steps.

Adaptation Step

The key to adaptation is a weight function that determines where grid nodes need to be clustered for a more accurate solution. Such a weight function, w , can be built from a linear combination of the errors in the concentrations of various chemical species:

$$w \propto \sum_n \alpha_n \nabla^2 c_n \quad (1)$$

where ∇^2 , the Laplacian, represents the error in c_n , the computed value of the concentration of species n . The chemical mechanisms used in AQMs usually have a large number of species. Due to non-homogeneous distribution of emissions and disparate residence times, each species may have very different resolution requirements. Determining α_n such that pollutant concentrations (e.g., ozone) can be estimated most accurately is a current research topic. Here, all α_n are set to zero, except the one for nitric oxide (NO). Further, the grid adaptation is restricted to the horizontal plane, and the same grid structure, which is determined by the surface layer NO concentrations, is used for all vertical layers. This, combined with the requirement that the Courant number should be less than unity, may result in very small solution time steps because of high wind speeds aloft. Adaptation in the vertical direction is possible but more complicated.

The grid nodes are repositioned by using the weight function. The new position of the grid node i , \bar{P}_i^{new} , is calculated as:

$$\bar{P}_i^{new} = \frac{\sum_{k=1}^4 w_k \bar{P}_k}{\sum_{k=1}^4 w_k} \quad (2)$$

where \bar{P}_k , $k = 1, \dots, 4$, are the original positions of the centroids of the four cells that share the grid node i , and w_k is the weight function value associated with each centroid.

Once the grid nodes are repositioned, cell-averaged species concentrations must be recomputed for the adapted grid cells. Holding the concentration field fixed and moving the grid is numerically equivalent to simulating the advection process on a fixed grid. Therefore, we use a high-order accurate and monotonic advection scheme known as the piecewise parabolic method (Collela and Woodward, 1984) to interpolate concentrations from the old to the new grid locations.

The calculation of the weight function, the movement of the grid nodes, and the interpolation of species concentration from the old to the new grid locations are three distinct tasks of an iterative process. The process continues until the maximum grid node movement is less than a preset tolerance. A very small tolerance may lead to a large number of iterations. On the other hand, a large tolerance may not ensure adequate resolution of the solution field. Currently, we

stop iterating when, for any grid node, the movement is less than 5% of the minimum distance between the node in question and the four nodes to which it is connected.

After the grid nodes are repositioned, emissions and meteorological data must be processed to generate the necessary inputs for the solution step. Note that, unlike the practice with fixed grid AQMs, this processing could not be performed prior to the simulation because there is no *a priori* knowledge of where the nodes would be located at any given time. In case of meteorological data, an ideal solution would be to run a meteorological model (MM), which can operate on the same adaptive grid, in parallel with the AQM. This would ensure dynamic consistency of meteorological inputs, but such a MM is currently nonexistent. Therefore, hourly meteorological data are obtained from a high-resolution, fixed-grid MM simulation and interpolated onto the adaptive grid. For mass conservation, as a minimum requirement, the vertical wind components are readjusted later during the solution step as described in Odman and Russell (2000).

The processing of emission data is computationally expensive, requiring identification of various emission sources in the adapted grid cells. Here, we treat all emission sources in two categories: point and area sources. For simplicity, the mobile sources have been included in the area-source category, but treating them as line sources would yield better resolution. For the point sources, the grid cell containing the location of each stack must be identified. The search may be quite expensive if there are thousands of stacks in the modeling domain. However, assuming that the cell containing the stack before adaptation would still be in close proximity of the stack after adaptation, the search can be localized. The localization of the search provides significant savings over more general, global searches. As for the area sources, they are first mapped onto a uniform high-resolution *emissions grid* using geographic information systems. This is done in order to avoid higher computational costs associated with processing of emissions from highly irregular geometric shapes presented by highways and counties. Around each adaptive grid cell there is a box of emissions grid cells $E_i, i = 1, \dots, n$, as illustrated in Figure 2. Once each E_i is identified, then their polygonal intersections with the adaptive grid cell are determined. Finally, the areas of these polygons, S_i , are multiplied by the emission fluxes of E_i and summed over n to yield the total mass emitted into the adaptive grid cell. This process is performed for all adaptive grid cells.

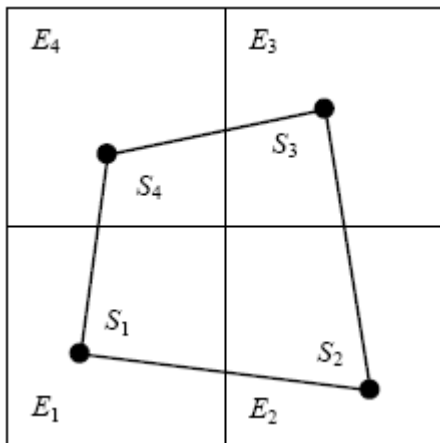


Figure 2. Intersection of an adapting grid cell with the area-source emissions grid.

The final step in preparation for the solution step is reestablishing a uniform grid for easy computation of the solution. This requires computation of a transformation from the (x, y) space where the grid is non-uniform to the (ξ, η) space where the grid would be uniform. The calculation of the Jacobian of the transformation and other necessary metrics (i.e., $\partial\xi/\partial x, \partial\xi/\partial y, \partial\eta/\partial x, \partial\eta/\partial y$) concludes the adaptation step.

Solution Step

The atmospheric diffusion equation in the (ξ, η, σ) space can be written as

$$\begin{aligned} \frac{\partial(Jc_n)}{\partial t} + \frac{\partial(Jv^\xi c_n)}{\partial \xi} + \frac{\partial(Jv^\eta c_n)}{\partial \eta} + \frac{\partial(Jv^\sigma c_n)}{\partial \sigma} + \frac{\partial}{\partial \xi} \left(JK^{\xi\xi} \frac{\partial c_n}{\partial \xi} \right) \\ + \frac{\partial}{\partial \eta} \left(JK^{\eta\eta} \frac{\partial c_n}{\partial \eta} \right) + \frac{\partial}{\partial \sigma} \left(JK^{\sigma\sigma} \frac{\partial c_n}{\partial \sigma} \right) = JR_n + JS_n \end{aligned} \quad (3)$$

where c_n , R_n , and S_n are the concentration, chemical reaction, and emission terms of species n , respectively, and σ is a terrain-following vertical coordinate. J is the Jacobian of the coordinate transformation:

$$J = \frac{1}{m^2} \frac{\partial z}{\partial \sigma} \left(\frac{\partial x}{\partial \xi} \frac{\partial y}{\partial \eta} - \frac{\partial y}{\partial \xi} \frac{\partial x}{\partial \eta} \right) \quad (4)$$

where m is the scale factor of a conformal map projection in the horizontal. The components of the wind vector in ξ and η directions are v^ξ and v^η :

$$\begin{aligned} v^\xi &= m \frac{\partial \xi}{\partial x} U + m \frac{\partial \xi}{\partial y} V \\ v^\eta &= m \frac{\partial \eta}{\partial x} U + m \frac{\partial \eta}{\partial y} V \end{aligned} \quad (5)$$

where U and V are real horizontal wind velocities rotated in the map's coordinate directions. The turbulent diffusivity tensor is assumed to be diagonal, and its elements are $K^{\xi\xi}$, $K^{\eta\eta}$, and $K^{\sigma\sigma}$.

$K^{\sigma\sigma}$ can be expressed in terms of the vertical diffusivity K^z as:

$$K^{\sigma\sigma} = \left(\frac{\partial \sigma}{\partial z} \right)^2 K^z. \quad (6)$$

The expressions for v^σ (the wind component in the σ direction), $K^{\xi\xi}$, and $K^{\eta\eta}$ are omitted here due to space limitations. Since the grid is uniform in the (ξ, η) space, solution algorithms can be taken directly from existing AQMs.

One drawback of adaptive grids in air quality modeling has been the demand for large computational resources. It has been noted however that the demand can be significantly reduced if the time-step restriction, which advances all grid cells with the same short time step required by the smallest grid cell, can be lifted. Odman and Hu (2007) developed a variable time step algorithm for this purpose. In this algorithm:

- Every cell is assigned its own local time step, Δt_i , which is an integer multiple of the global time step Δt and an integer divisor of 60 minutes. For example., if the global time step is 5 minutes, the local time step can be 5, 10, 15, 20, 30, or 60 minutes.
- The model clock time, t , is advanced by the global time step.

- When $t=N\times\Delta t_i$ chemistry, aerosol and cloud processes are applied for the duration of Δt_i
- Transport processes require a reservoir to store the fluxes as shown in Figure 3.

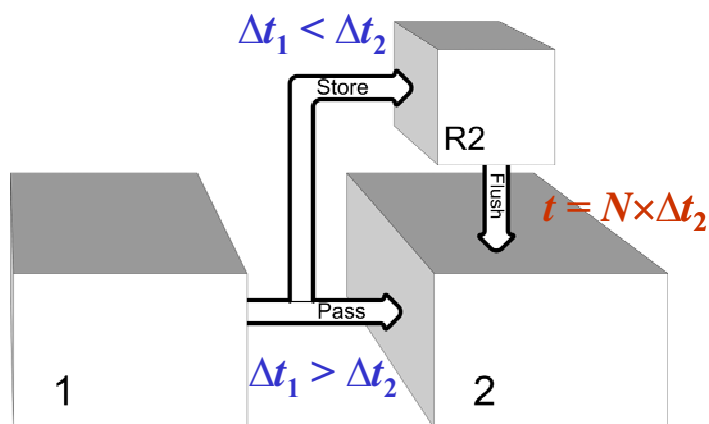


Figure 3. Transport with VARTSTEP algorithm.

A complete description of the VARTSTEP algorithm can be found in Odman and Hu (2010), which is included here as Appendix B. The adaptive grid algorithm described above, including VARTSTEP, has been incorporated into CMAQ. Verification of the adaptive grid CMAQ code and an evaluation of the model can be found in Garcia-Menendez et al. (2010), which is also included in this report as Appendix C.

Daysmoke

Daysmoke is an extension of ASHFALL, a plume model developed to simulate deposition of ash from sugar cane fires (Achtemeier 1998). As adapted for prescribed fire, Daysmoke consists of four models one of which is an Entraining Turret Model (ETM). From photogrammetric analysis of video footage of smoke plumes from burning sugar cane, Achtemeier and Adkins (1997) determined that a rising smoke plume could be described by a train of rising turrets of heated air that sweep out a three-dimensional volume on expanding through entrainment of surrounding air through the sides and bottoms as they ascend.

The governing equations made no allowance for adiabatic expansion in the rising plume. For prescribed fires for which smoke plumes seldom rise above 2 km, omission of adiabatic expansion amounted to an error of approximately 3%, a negligible error given the sizes of errors in other estimations for plume rise calculations such as fuel loading. However, should Daysmoke be used for estimating plume rise from wildfires from which plumes may rise to 10 km, errors of omission of adiabatic expansion may increase to 30%. Thus adiabatic expansion has been built into the governing equations for Daysmoke.

Fort Benning Field Study

Prescribed burns were monitored at Fort Benning using a ground-based real-time measurement technique. Each day, using the burn plan provided by the Fort Benning crew, the UGA team laid out a grid on a site map (Figure 4). The grid consisted of a 60 degree arc emanating from the burn compartment and stretching along the predicted wind direction. This arc was divided into three sampling zones: Zone 1: 1-3 km; Zone 2: 3-5 km; Zone 3: 5-7 km. A truck was assigned to each zone. Each truck was equipped with two DustTrak $PM_{2.5}$ monitors

and two Langan CO monitors at a sampling height of 8 feet. Each truck monitored multiple locations in its zone with a minimum of 30 minutes at each location. Sampling was started at ignition and continued until approximately one hour after completion. Initial sampling locations were on the most direct downwind position from a burn location. Each subsequent position was chosen based on a combination of wind shifts, real-time measurement levels, and road availability. The truck positions were recorded using Trimble Juno ST GPS units. During the monitoring, the FS team operating from a fire tower collected plume rise information and photographic data and coordinated the data collection by the UGA trucks confirming wind shifts. At the same time, Lidar measurements of the smoke plume were taken by the University of Massachusetts (UMASS).

PM_{2.5} was sampled at 30-second intervals with TSI DustTrak Model 8520 aerosol monitors (DustTrak: range 0.01 mg/m³ to 100 mg/m³; resolution 0.01 mg/m³) with dataloggers (TSI, Minneapolis, MN). CO was sampled at 30-second intervals by two monitors: Langan CO Monitor Model T15v CO monitor (resolution 0.1 ppm) with datalogger (Langan Products, Inc., San Francisco, CA); and PAC III Monitor (resolution 1 ppm) with datalogger (SKC, Inc.). These instruments were calibrated before the study in the Air Quality Lab at the University of Georgia (UGA) and the DustTrak monitors were zero calibrated in the field each day. In addition, all DustTrak monitors were also factor calibrated and serviced at the start of the project.

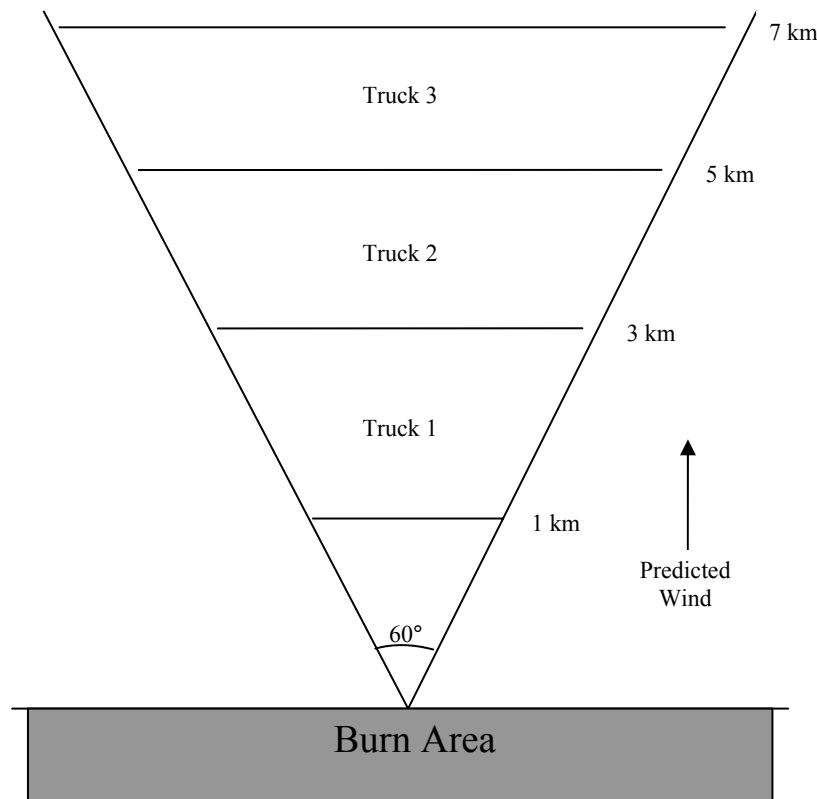


Figure 4. Fort Benning sampling grid.

Model Evaluation

Many prescribed burning events, including some historic cases, are being simulated. Model predictions are compared to available data as well as to the “base model” predictions in terms of various plume dispersion and air quality parameters. Improved agreement of predictions with data indicates success. The data being used includes observations from networks such as the Clean Air Status Trends Network (CASTNet), the Speciated Trends Network (STN), and the Interagency Monitoring of Protected Visual Environments (IMPROVE). These networks are relatively sparse around the study sites and the closest monitors are typically located at 25 km or larger distances. On the other hand, most measurements are within a 2-km radius of the burn plots. The data collection component of this study is targeting the mid-range (approximately 10 km downwind from the burn plots). After initial evaluations, the gaps in data are being identified and filled with ground-based mobile measurements at Fort Benning. The model is re-evaluated with the new data. Two cycles of this data-collection and model evaluation process already took place during model development: after each cycle the model has been revised and/or refined as necessary.

At Fort Benning, the particle composition data collected by Baumann et al (2005) during the spring of 2004 offers a unique opportunity to evaluate the PM_{2.5} speciation skill of the models. In addition to these on-site measurements, there are 4 PM_{2.5} monitors within 15-25 km of the base and several other air quality monitors in the Columbus-Phenix City area. Also, remote sensing images of the smoke plumes are being used for model evaluation. Furthermore, photographic data is being used to determine the number of updraft cores (a critical measurement for Daysmoke) and to estimate the height of smoke plumes.

Results and Accomplishments

1. Emissions Estimation

Subtask 1.1: Fuel Loading and Fuel Consumption Estimation

This subtask was completed in 2008; its results and accomplishments were included in the first interim report.

Subtask 1.2: Initial Emissions Estimation

This subtask was completed in 2009; its results and accomplishments were included in the second interim report.

Subtask 1.3: Collection of Fort Benning Samples for Measurements at Fire Sciences Lab

Recall that we collected 1-square-meter samples from a Fort Benning plot (Burn Unit I3) that was burned on January 23, 2009. This plot was previously burned on 9 March 2006; therefore, it had a 3-year old rough. The samples were collected at 5 different locations of this 455-acre plot: (1) Planted slash mixed longleaf pine, 44 years old; (2) Shortleaf pine, 70 years old; (3) Planted loblolly pine, 20 years old; (4) Loblolly pine, 68 years old; and (5) Planted longleaf, 4 years old. The collected samples were shipped to the Fire Science Laboratory in Missoula, MT for analysis.

This year, the results of the laboratory work on Ft. Benning fuel samples were released. The emission factors measured in the Fire Sciences Laboratory (marked SMRFS) were compared to existing sets, namely the USFS southeastern fuels set (marked Urbanski), the Georgia Tech Ft. Benning set (Marked Baumann), and the EPA AP-42 set (see Figure 5 **Error! Reference source**

not found.) The values of the emission factors are listed in Table 1 and Table 2. The USFS southeastern emission factors are generally in closest agreement with the laboratory measurements. This increases the confidence in the emission factors used in our modeling.

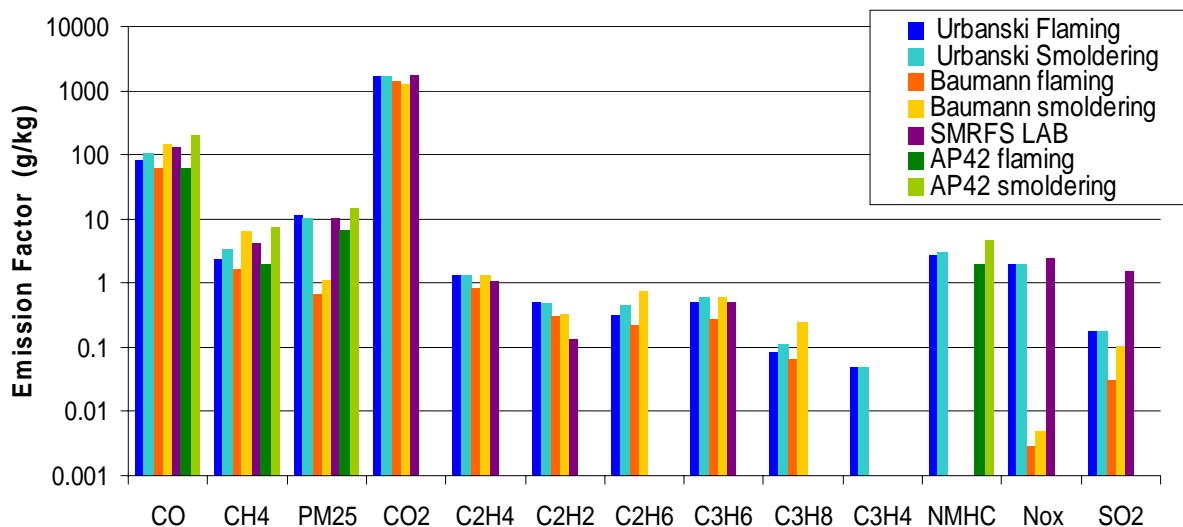


Figure 5. Comparison of emission factors for burn units at Ft. Benning.

Table 1. Comparison of flaming emissions factors (g/kg)

| | AP42 | Baumann | Urbanski | SMRFS |
|------|------|---------|----------|-------|
| CO | 63.0 | 63.7 | 82.0 | 128.6 |
| CH4 | 2.00 | 1.63 | 2.32 | 4.25 |
| PM25 | 6.70 | 0.66 | 11.50 | 10.30 |
| CO2 | | 1437 | 1664 | 1710 |
| C2H4 | | 0.8400 | 1.300 | 1.048 |
| C2H2 | | 0.2986 | 0.500 | 0.138 |
| C2H6 | | 0.2179 | 0.320 | |
| C3H6 | | 0.2664 | 0.510 | 0.500 |
| C3H8 | | 0.0635 | 0.086 | |
| C3H4 | | | 0.050 | |
| NMHC | 2.00 | | 2.770 | |
| NOx | | 0.0029 | 2.000 | 2.468 |
| SO2 | | 0.0312 | 0.175 | 1.547 |

Table 2. Comparison of smoldering emissions factors (g/kg)

| | AP42 | Baumann | Urbanski |
|------|-------------|----------------|-----------------|
| CO | 205 | 149.28 | 106 |
| CH4 | 7.4 | 6.49 | 3.42 |
| PM25 | 14.7 | 1.1453 | 10.5 |
| CO2 | | 1247.68 | 1649 |
| C2H4 | | 1.357 | 1.3 |
| C2H2 | | 0.3277 | 0.48 |
| C2H6 | | 0.7387 | 0.46 |
| C3H6 | | 0.584 | 0.59 |
| C3H8 | | 0.2476 | 0.11 |
| C3H4 | | | 0.05 |
| NMHC | 4.6 | | 3 |
| NOx | | 0.005 | 2 |
| SO2 | | 0.1035 | 0.175 |

Subtask 1.4: Final Emissions Estimation

Emission inputs are critical to the performance of a dispersion model like Daysmoke; therefore, one of our objectives is to provide more accurate emissions inputs to Daysmoke. Having addressed the uncertainty in emission factors in Subtask 1.3, we now would like to increase our confidence in fuel loads and fuel consumptions. Recall that our emission estimates so far relied on photo series for fuel loads and a model (CONSUME) for fuel consumption. In February 2011, as part of the Prescribed Fire Combustion and Atmospheric Research Experiment (Rx-CADRE), Dr. Roger Ottmar of USFS will conduct a field study at Eglin Air Force Base (AFB) to collect fuel loading and fuel consumption field data. During this study, each fuelbed type in a burn unit will be sampled before and after the burn for fuels, which include trees, shrubs, grasses, small woody fuels, and litter. We are planning to take advantage of this study by conducting our plume measurements at Eglin AFB, during Rx-CADRE. By doing so, we will have the opportunity to use fuel loading and consumption field data to estimate the emissions. We will also compare this technique to the previously used photo-series method as well as to the consumption model Consume (Version 3.0). These comparisons will give us an idea about the uncertainty of the fuel loading estimates used in all the other burns and help us assess the accuracy of the model CONSUME. A detailed study plan was prepared for our field campaign at Eglin AFB and it is included in this report as Appendix D.

Recall that a sensitivity analysis was conducted to determine the important parameters of the emission models last year. This year the sensitivity analysis took a different direction by focusing on the sensitivities of downwind pollutant concentrations to emissions. For this, we are using the decoupled direct method (DDM) incorporated into the CMAQ model (Napelenok et al, 2008). Our objective is to determine the changes to prescribed burning emissions that are needed in order to get a better agreement between predicted and observed pollutant concentrations. Implicit in this approach is the assumption that the wind speed/direction inputs to the CMAQ model are accurate. In the past, DDM has been used to estimate the uncertainties in emissions of various sources. What is new in our study is the use of DDM not just to look at the sensitivity to the amount of fire emissions but also to the vertical distribution of those emissions. We are calculating the sensitivities of downwind pollutant concentrations to the amount of emissions injected into each vertical layer of the CMAQ model. This way, we will be able to determine the ideal profile for distributing the fire emissions in the vertical. By comparing this ideal profile to the profile generated by the Daysmoke model (recall that Daysmoke is being used as an injector of fire emissions into CMAQ) it is possible to get a better idea on how to set certain parameters of Daysmoke, for example the number of updraft cores which has a significant impact on the vertical structure of the fire plume.

2. Model Development

Subtask 2.1: Incorporation of the Adaptive Grid Method in CMAQ

This subtask was completed in 2009; its results and accomplishments were included in the second interim report. However, we continued our efforts for incorporating Adaptive Grid MM5 in our modeling system as summarized below. We also published the highlights of our work on the development of Adaptive Grid CMAQ in a journal article (Garcia-Menendez et al. 2010; also included here as Appendix C)

Adaptive Grid MM5

Adaptive MM5 was used in an application to the 9 April 2008 burn at Ft. Benning. The comparison to standard MM5 in terms of the wind fields obtained showed that Adaptive MM5 was promising in the PBL (Figure 6). The wind field obtained by WRF is very similar to the standard MM5 wind field. Too much synoptic influence, excessive damping, and smoothing of the terrain in MM5 and WRF lead to very little variability in the wind fields. The wind fields by adaptive grid MM5 have much more variability, even without grid adaptation. This is due to less damping in the model. Also, the influence of the terrain on the wind fields is more apparent.

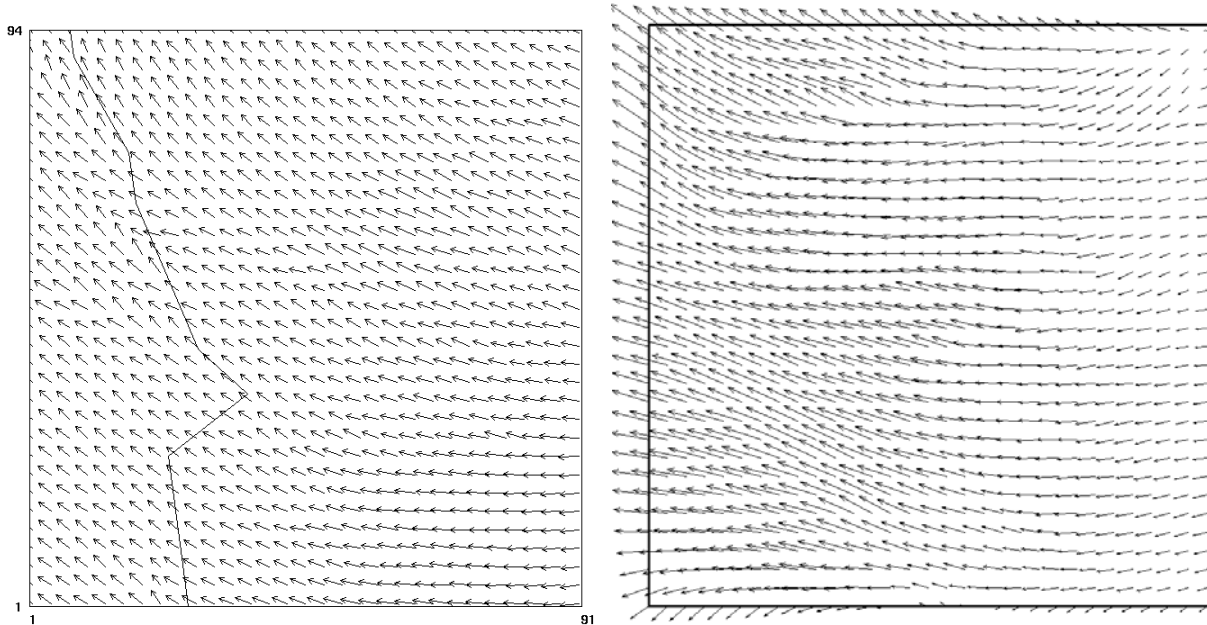


Figure 6. The wind fields obtained by standard MM5 (left) and adaptive MM5 but no grid adaptation (right) in applications to the 9 April 2008 burn at Ft. Benning. The domain is 91 x 94 cells of 1.33 km resolution covering Ft. Benning and surrounding areas in Georgia and Alabama.

With the WRF wind fields, in addition to the lack of variability due to excessive damping and lack of resolution of the terrain, we discovered some stability issues. During the simulation of the 15 April 15, 2008 burn we have noticed significant disagreement between the predicted wind direction and the direction suggested by the position of our ground units that were chasing the plume to measure its concentration. When we took a close look at the wind fields we have noticed a pattern of alternating NNW and NNE winds during the burn (Figure 7). Since October 2009, when we first announced this problem to the community, we followed several suggestions but found no solution to this problem. The suggestions included 1) reducing the time step, and 2) increasing the damping coefficient. We tried using several different values of both parameters but did not see significant improvement in the wind fields: the oscillatory wind direction pattern persisted in all cases.

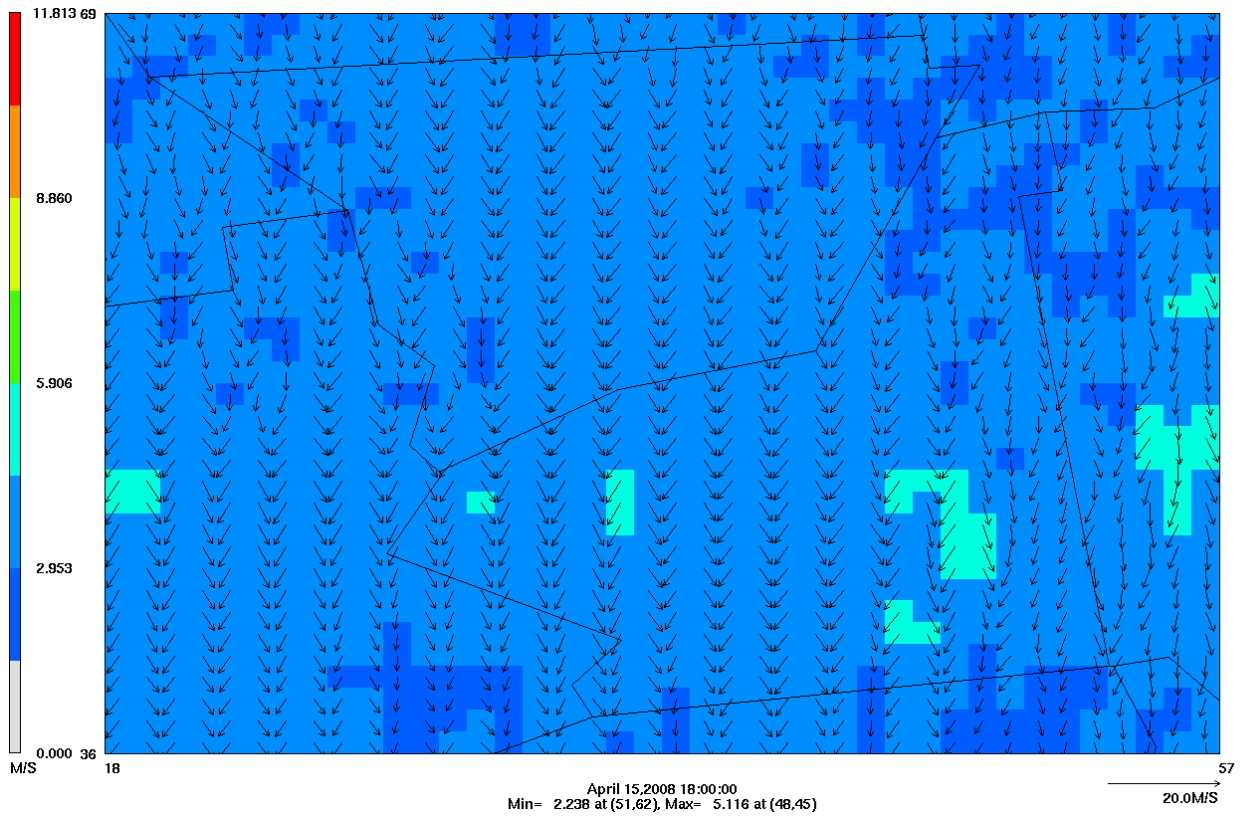


Figure 7. The wind field obtained by WRF in an application to the 15 April 2008 burn at Ft. Benning. The grid resolution is 1.33 km.

The lack of wind field variation in the Ft. Benning application of standard MM5 mirrors the lack of wind variation found in the stratosphere application (Xiao, 2006), as compared to detailed ~1.5 m radiosonde observations by AFRL (Figure 3). WRF was also reported to show much reduced variation. It should be noted that all model comparisons used the same input conditions and initial grids. The resulting poor prediction of optical turbulence levels using the output of the standard MM5 and WRF led to the research effort to develop the adaptive MM5, including a sophisticated LES/RANS turbulence model for direct output of the optical structure function.

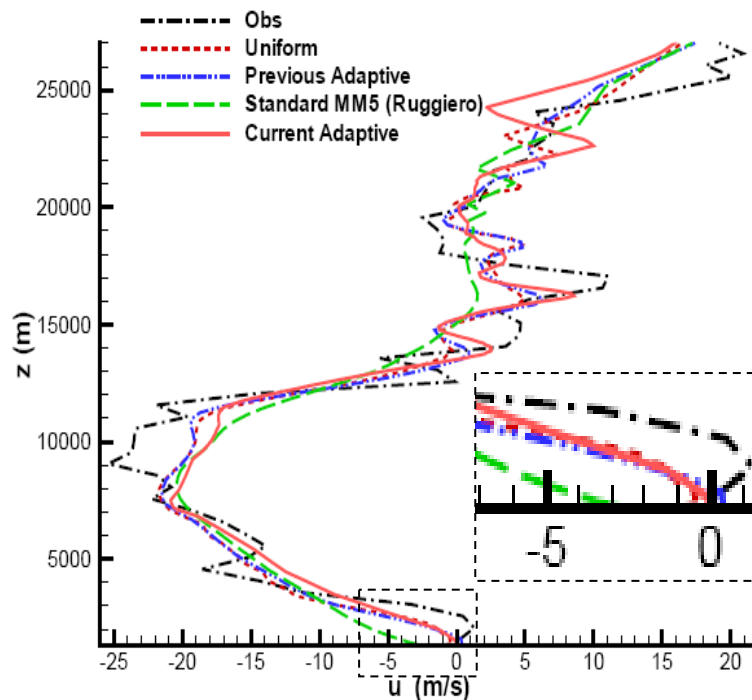


Figure 8. Comparison of zonal wind profiles in applications to the Holloman Air Force Base (Xiao et al., 2007). The Adaptive Grid MM5 (both with and without grid adaptation) agreed better with the Radiosonde observations than the standard MM5, even in the PBL although the focus of this application was the stratosphere.

The adaptive MM5 wind field results in the stratosphere showed increased variability as compared with radiosonde observations when no adaptation was used, thereby indicating the benefit of the NCSU LES/RANS turbulence model (Figure 8). When mesh adaptation was used, the wind field variability approached that of the binned radiosonde observations. The improved agreement with observed winds in the PBL (Figure 8 inset) show the potential of adaptive MM5 for benefiting the proposed prescribed burning applications. The dramatic improvements over the standard MM5 results also demonstrate the need for duplicating the adaptive capability in WRF in the future.

Encouraged by these findings, which indicate that the adaptive MM5 provides a significant improvement over the original model, we submitted a proposal to SERDP for high-resolution meteorological modeling with adaptive MM5. The goal of the proposed work was to continue the development and validation of adaptive MM5 to achieve full meteorology model functionality, thereby resulting in a heretofore unobtainable capability to resolve local detail in wind fields required for accurate fire plume propagation.

Since our proposal was rejected, the application of the adaptive grid MM5 model will not be pursued any further in this project. The meteorological inputs for the adaptive grid CMAQ model will be derived through interpolation from coarser resolution uniform grid simulations.

Adaptive Grid CMAQ

We published the highlights of our work on the development of Adaptive Grid CMAQ in a journal article (Garcia-Menendez et al. 2010; also included here as Appendix C)

Subtask 2.2: Initial Coupling of Daysmoke with CMAQ

This subtask was completed in 2008; its results and accomplishments were included in the first interim report.

Subtask 2.3: Modification of Daysmoke and Adaptive Grid CMAQ models

This subtask was completed in 2009; its results and accomplishments were included in the second interim report. Important modifications made to the Adaptive Grid CMAQ model were reported in Garcia-Menendez et al. (2010) which is also included here as Appendix C.

The analyses under Subtask 4.3 below have revealed two additional glitches with Daysmoke. First, an equation to add 1° C to the surface temperature was added to ensure there will be no zero-depth mixing layers. Second, a subroutine that shifts plume data to account for ignitions that are not at the beginning of an hour had to be revised. These modifications were included both in the stand-alone version of Daysmoke and the version being coupled with CMAQ.

Subtask 2.4: Final Coupling of the Models

Coupling Daysmoke with CMAQ

Recall that we started to use Fourier analysis to determine the optimal downwind distance for handing the Daysmoke plume to CMAQ last year. This year, we continued the analysis to better understand the relationship between this distance, the plume structure and the resolution of the grid. We analyzed several plumes and various grids generated through adaptation to PM_{2.5} concentrations (background plus fire emissions). We also started calculating the optimal handover distance (i.e., where the error incurred due to handover is the smallest) as a function of time. Based on the findings of the Fourier analysis, we developed a coupling algorithm that sets the downwind distance for handover of Daysmoke plume to CMAQ as a function of time. Two conditions must be satisfied for handover: 1) the Daysmoke plume must reach its full height and 2) the difference between Daysmoke plume concentrations before handover and CMAQ grid cell concentrations after handover (i.e., the concentration error incurred during handover) must be minimal. Analysis of several burn plumes has shown that the downwind distance where these two conditions are satisfied changes in time. The coding of this algorithm was finished and the review and verification of the code has gone through its first cycle. Initial testing produced satisfactory results and the evaluation of the coupled models will be discussed below.

Description of Coupling Algorithm

Our new modeling system consists of the Adaptive Grid CMAQ (AG-CMAQ) coupled with Daysmoke as the sub-grid scale plume model. The coupled system is called Adaptive Grid Daysmoke CMAQ (AGD-CMAQ), and the purpose of this model is to be able to obtain more accurate characterization of plume concentrations in a grid model. The resultant model is tested by simulating a real air pollution episode and its performance is compared to that of fixed grid CMAQ and original AG-CMAQ.

Daysmoke (Liu et al., 2010) is responsible for tracking the trajectories of emitted smoke parcels during each CMAQ time step. At the end of the time step, there is a process called

“handover” which will check for certain conditions and determine the interface where Daysmoke shares its information with CMAQ. Handover consists of 5 major parts. First, it will convert smoke emissions that Daysmoke keeps track in units of mass to concentration by dividing the smoke plume boundaries into a 100 by 100 grid for each adaptive grid layer (Figure 9a). Secondly, the smoke emissions are also converted into concentrations using the adaptive grid from AG-CMAQ which has already been adapted according to a fire tracer (Figure 9b).

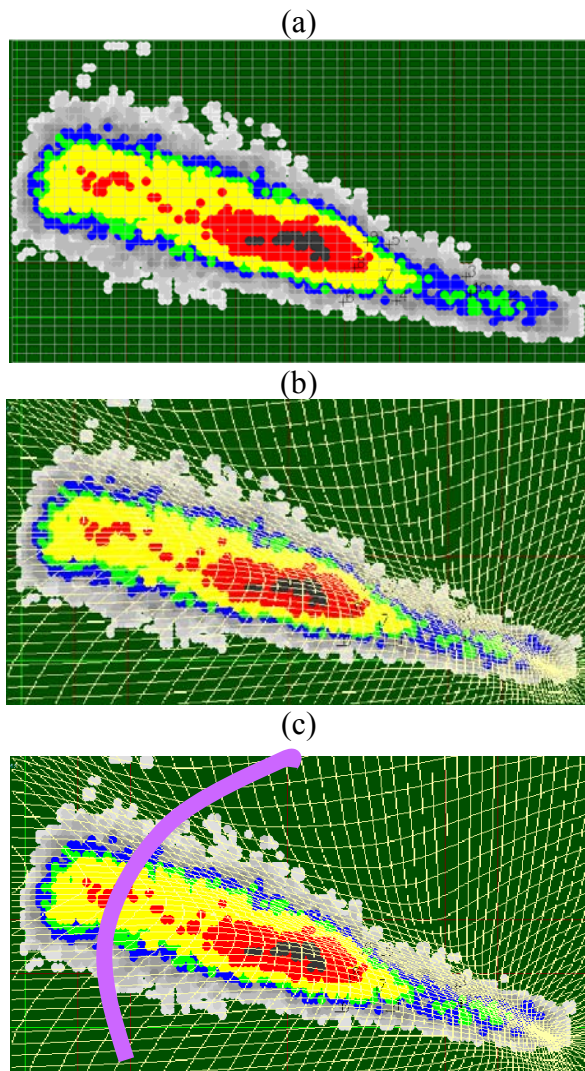


Figure 9. Determination of Daysmoke-adaptive grid CMAQ interface: a) Top view of a Daysmoke output divided by fine 100X100 grid, b) Top view of a Daysmoke output divided by adaptive grid, c) Top view of a Daysmoke output with “wall” in purple

The concentrations calculated in these two different grids are then compared by adding up the differences of the concentrations for every one hundredth of the total downwind distance of the plume, about 10 to 15 meters. The equation used to calculate the normalized concentration difference is as follows.

$$Normalized\ Difference_{downwind,j} = \frac{1}{nlays \times 100} \sum_k^{nlays} \left[\sum_i^{100} \frac{2 \times |C_{adaptive} - C_{fine}|_i}{(C_{adaptive} + C_{fine})_i} \right]_k \quad (7)$$

Here $C_{adaptive, i}$ is the concentration in the adaptive grid at row i , $C_{fine, i}$ is the concentration in fine (100×100) grid, and k is the height layer counter.

The interface where Daysmoke emissions are transferred into AG-CMAQ is named “the wall”, and the wall must satisfy two boundary conditions. First, the wall must be set after the plume is fully developed, and it can not be farther than 16 km from the fire. Second, the wall must be set at a certain distance from the fire where the concentration difference is minimum. This way the outputs from the sub grid model are carried over to the air quality model with least possible compromise in vertical and spatial resolution.

Any emission parcel beyond the wall is inserted into the appropriate grid cell of AG-CMAQ at appropriate times. All other particles remain in Daysmoke and their trajectories are recalculated until those parcels travel beyond the wall. This process will continue until all of the parcels emitted from the fire have been inserted into grid cells and converted into grid concentrations in AG-CMAQ.

Case Study

In the southeastern U.S., prescribed burns are used as a wildfire prevention and habitat restoration strategy. In the morning of Feb. 28 2007, there were two planned forest fires 80 km upwind from Atlanta. It was not till late afternoon the same day that the air quality in the Atlanta metropolitan area was impacted by the heavy smoke from the two prescribed burns. Fine particulate matter levels at monitoring sites throughout the area increased to nearly 150 $\mu\text{g}/\text{m}^3$ (Hu *et al.*, 2008).

The two prescribed fires that affected air quality in Atlanta were at Oconee National Forrest and Piedmont National Wildlife Refuge. With both sites combined, about 3,000 acres were burned for as long as 5 hours. The smoke from the burns was completely gone when it started raining at noon the next day. The emissions from the two burns are estimated using FEPS. The same meteorology used in CMAQ is also applied to Daysmoke. Feb. 28 Atlanta smoke episode has already been simulated with a 4 km fixed grid photochemical model and is discussed in Hu *et al.*, 2008. The first approach of combining Daysmoke with AG-CMAQ, where the output emissions from Daysmoke were injected into an AG-CMAQ column, is discussed in Garcia–Menendez *et al.* 2010. In this study, the event was simulated with AGD-CMAQ, which consists of CMAQ version 4.5 combined with Daysmoke using the “handover” described above.

Analysis of Handover Error

During the simulation of the Feb. 28 2007 Atlanta smoke case the handover process for the two fires was kept track. The plots of the normalized concentration error analysis are shown in Figure 10. In these plots, the blue line represents the normalized error at a certain downwind distance for the Oconee burn, and the pink line represents the same error for the Piedmont burn. The walls are drawn at the minimum error closest to the fire, and the light blue line represents the wall set for the Oconee burn and the orange line is where the wall is set for the Piedmont burn. The plots for 16:30Z and 18:30Z show cases where the concentration error tends to minimize as distance from the fire increases. Note that the wall is much closer to the fire at 18:30Z since it is towards the end of the fire, when both burns are in the smoldering phase. At

17:30Z, the Piedmont burn shows a pattern where the error decreases farther away from the fire. On the other hand, the Oconee burn displays a minimum error closer to the fire, which is why we set a condition that the wall be drawn at least 2 km away from the fire and where the plume is fully developed.

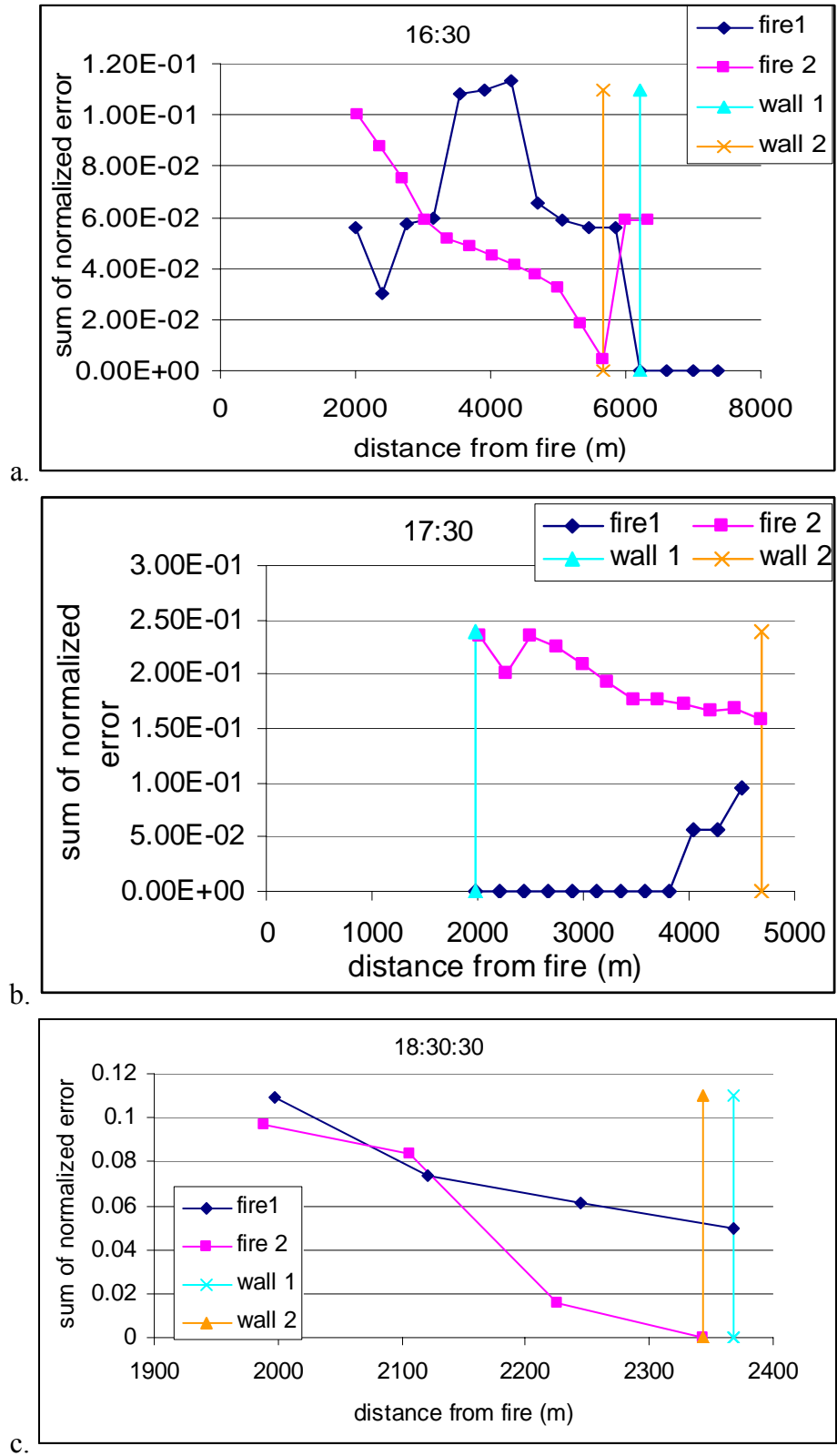


Figure 10. Plots of concentration error versus downwind distance at a) 16:30Z, b) 17:30Z and c) 18:30Z.

Figure 11 shows another result from handover where the dots represent the location of where the wall was set for Oconee and Piedmont burns. Only the period when both burns were active is shown. One can see that as the plume starts to develop, the downwind distance of the wall increases and reaches its maximum around 16:24Z. As both fires start to calm down, the distance of the wall tends to stay steady between 2 to 3 km. Towards 19:00Z the Piedmont fire has stopped flaming and went into the smoldering phase, which explains the sudden decrease in the distance of the wall.

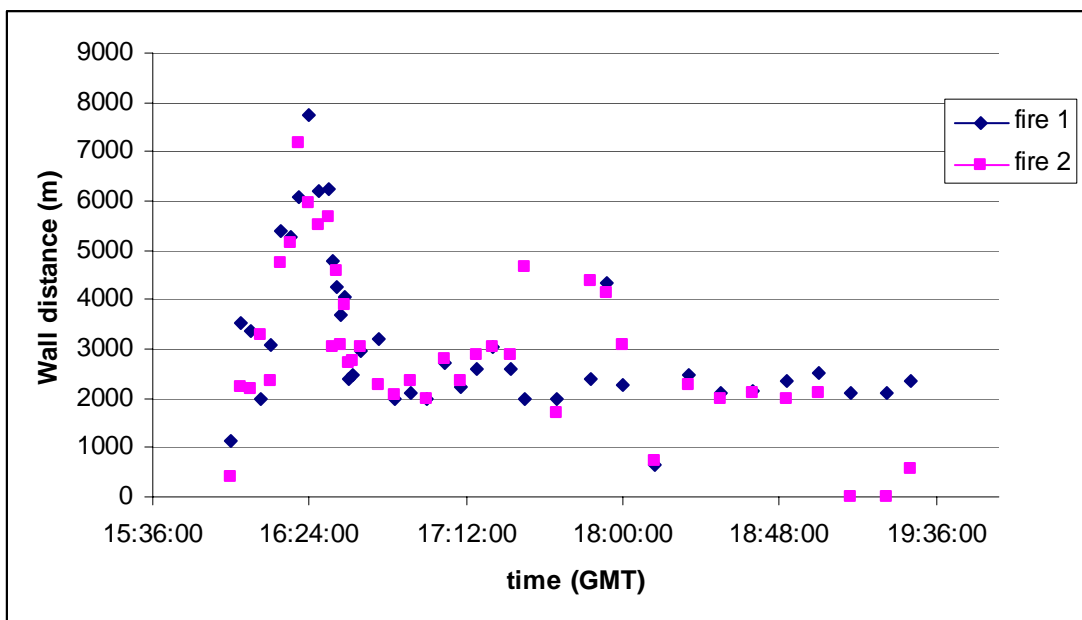


Figure 11. Distance of the wall over time during the Feb. 28,2007 Atlanta burn case: blue for the Oconee burn and pink for the Piedmont burn.

Evaluation of the Coupled Model

The Feb. 28, 2007 Atlanta smoke incident is simulated using three different CMAQ versions mentioned before (i.e., CMAQ, AG-CMAQ and AGD-CMAQ) and the results are compared here. Model inputs and setup are kept the same as those used for the fixed-grid simulation covering Northeastern Georgia as described in *Hu et al., 2008*. Grid refinement in AG-CMAQ and AGD-CMAQ is driven by fire related PM_{2.5} concentrations. The simulation starts at 21Z on Feb. 27 and finishes at 05Z on Mar. 1 using an output time step of 30min. The first burn started at 15Z on Feb. 28, which is also when grids start to adapt, consistent with the initial emissions release from the fires. The concentration peaks from the fires were observed at 6 monitoring sites in/around Atlanta and the sites are numbered from the station closest to the fire in the graphs below.

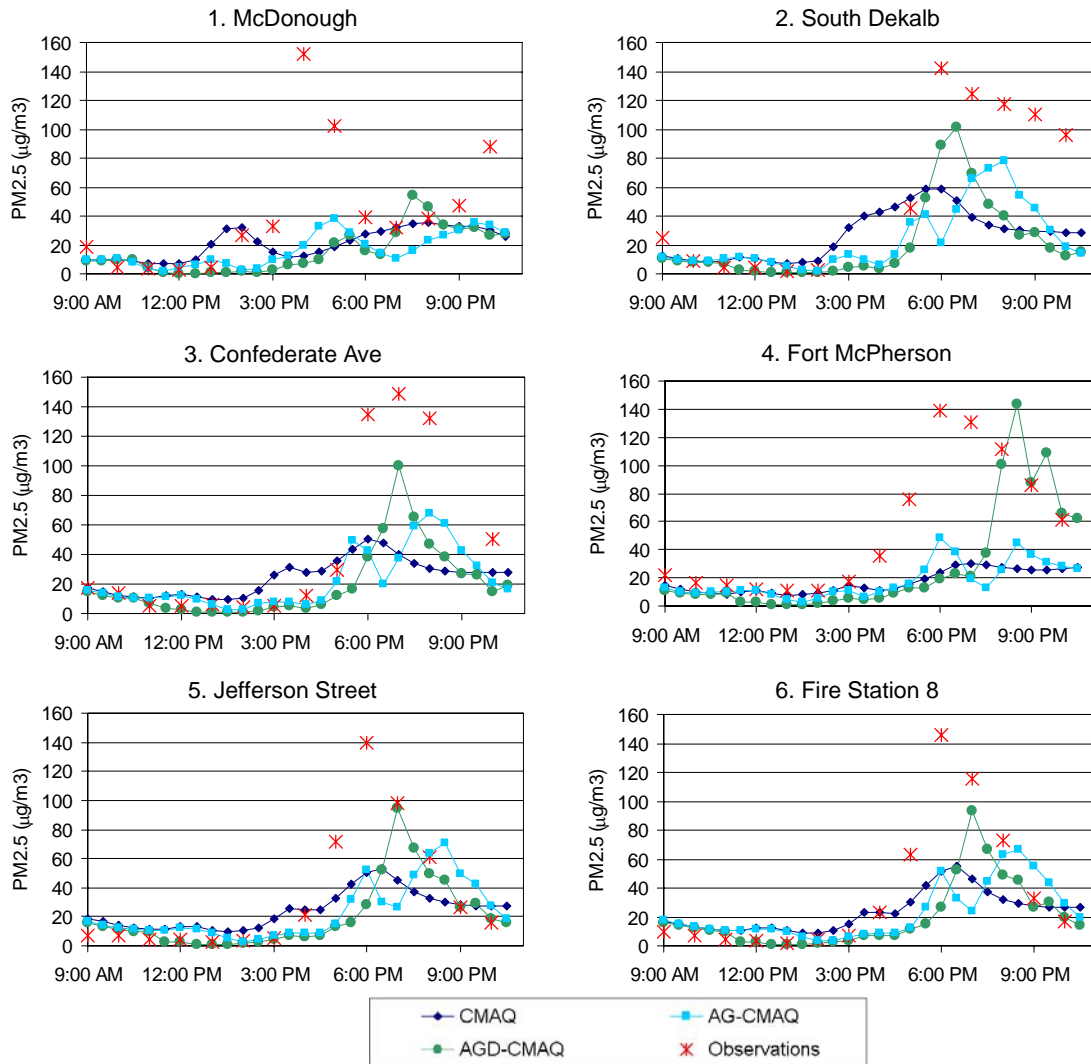


Figure 12. Measured (red) and modeled PM_{2.5} concentrations using standard CMAQ (dark blue), AG-CMAQ (light blue), and AGD-CMAQ (green) at the Mc Donough, South DeKalb, Confederate Avenue, Fort McPherson, Jefferson Street and Fire Station 8 air quality monitoring sites in the Atlanta metropolitan area.

Figure 1 compares the performances of standard CMAQ, AG-CMAQ and AGD-CMAQ to the hourly measured concentrations at sites near Atlanta that experienced a significant increase in PM_{2.5} concentration from 9am to 10:30pm EST. Significant differences can be observed in all three simulations. The artificial dilution effect in uniform grid is thought to be the reason why the standard CMAQ concentrations consistently under-predict peak PM_{2.5} concentrations and concentrations generally start to increase sooner than the other two models with adaptive grids. AG-CMAQ reduces the initial over prediction of PM_{2.5} concentrations and predicts higher concentration peaks compared to standard CMAQ results. The double concentration peak behavior is observed with a fixed grid as well but more significantly in AG-CMAQ. The two peaks appear in AG-CMAQ because the two smoke plumes from the two burn sites remain separated and reach out to Atlanta consecutively. On the other hand, the double concentration peaks are no longer apparent in AGD-CMAQ. AGD-CMAQ tends to predict higher concentration peaks, and seems to predict the closest to the observations for most of the

monitoring sites. To compare the performances quantitatively, the mean normalized errors were calculated and they are shown in Figure 2.

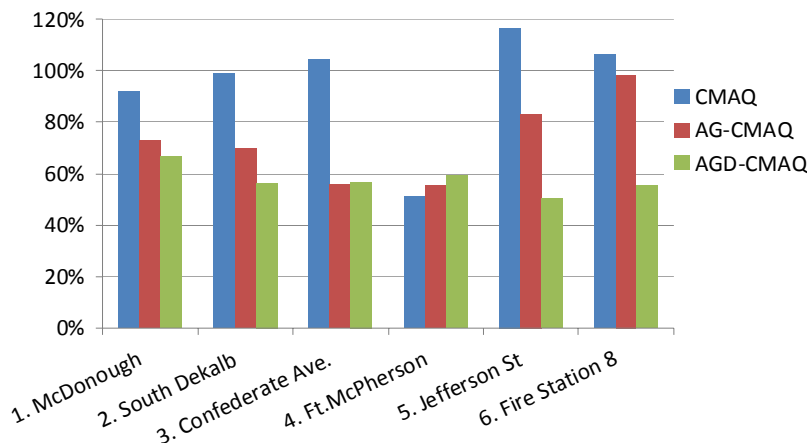


Figure 13. Mean normalized error for modeled PM_{2.5} concentrations using standard CMAQ (blue), AG-CMAQ (red), AGD-CMAQ (green) at the Mc Donough, South DeKalb, Confederate Avenue, Fort McPherson, Jefferson Street and Fire Station 8 sites in Atlanta metropolitan area.

The mean normalized error is calculated for the duration of the fires using the following equation, where for every hour i up to N , C_{observed} is the measured PM_{2.5} concentration and C_{model} is the predicted PM_{2.5} concentration.

$$\text{mean normalized error} = \frac{1}{N} \sum_i^N \left(\frac{|C_{\text{observed}} - C_{\text{model}}|}{C_{\text{observed}}} \right) \quad (8)$$

On average, AGD-CMAQ performs the best followed by AG-CMAQ then standard CMAQ. 5 out of 6 times AGD-CMAQ has much lower error than standard CMAQ has, except for Fort McPherson. Going back to the concentration plot for Fort McPherson in Figure 1, AGD-CMAQ was the only model that captured the PM_{2.5} concentration peak well, but it over predicted the concentrations at times. AG-CMAQ performs better than AGD-CMAQ does for Confederate Ave. site as well but only by 0.83%. Decrease in artificial dilution is achieved through adaptive grid refinement. On top of that, deciding when and where to carry the information from the sub grid model to the air quality model improves the plume impact predictions. We believe that the simulation with AGD-CMAQ better describes local dispersion of fire emissions and their regional air quality impacts.

Chemical Coupling of Daysmoke with CMAQ

A white-paper proposal for building a reactive version of Daysmoke to better model ozone and secondary organic aerosol formations in the prescribed burn plume was turned down by SERDP. We are hoping to build on our initial efforts in this project (see second interim report) with funding from other agencies in the future, and develop an air quality model with reactive sub-grid scale plume treatment capability.

3. Field Measurements

Subtask 3.1: Exploration of Fort Benning Site and Preliminary Data Collection

This subtask was completed in 2008; its results and accomplishments were included in the first interim report.

Subtask 3.2: Intensive Data Collection and Analysis

This subtask was completed in 2009; its results and accomplishments were included in the second interim report.

Subtask 3.3: Final Data Collection

The 2010 field study was postponed to 2011 in order to give the Technical Advisory Committee (TAC) a chance to review the model evaluation cycles we performed so far. at the In-Progress Review (IPR) meeting on May 7. In accordance with the TAC guidance, we revised our field study plan. Revisions include smoke sampling of 2-3 burns at Eglin AFB where fuels will be sampled before and after the burns for more accurate fuel loading and consumption data. The fuels study will be conducted by Dr. Roger Ottmar of the USFS.

Dr. Roby Greenwald of Emory University will collect PM_{2.5} data with mobile platforms and calibrate these data with more accurate PM_{2.5} measurements at a stationary site where he will also measure CO and CO₂ to determine the transition of the burn from flaming to smoldering phases. The US Forest Service team lead by Dr. Gary Achtemeier will continue the plume measurements with their ceilometer and add vertical wind profile measurements with a Doppler sodar. A US EPA team headed by Dr. Brian Gullett will also join us with their tethered balloon which will allow unique vertical profile measurements of the smoke plume. All these measurements during the 2011 field study are expected to substantially improve our ability to model emissions from prescribed burns and provide more accurate inputs to the Daysmoke plume dispersion model. The revised study plan is included here as Appendix D.

4. Model Evaluation

Subtask 4.1: Initial Evaluation of the Models

This subtask was completed in 2008; its results and accomplishments were included in the first interim report.

Subtask 4.2: Re-Evaluation with Newly Collected Data

This subtask was completed in 2009; its results and accomplishments were included in the second interim report. It was later realized (in December 2009) that the PM_{2.5} data reported by UGA and used in model evaluations were direct instrument readings that were not properly calibrated. The evaluation with the collected data had to be redone in 2010. However, since this task was marked as completed, we were reporting any further model evaluations under Subtask 4.3, Final Evaluation with Other Data. We will do the same in this interim report.

Subtask 4.3: Final Evaluation with Other Data

One of our goals is to use the data collected in other projects (SI-1648 and SI-1649) in our model evaluations. The burns we are focusing on are those conducted on November 5 and 11, 2009 at Vandenberg AFB and on February 11 and 12, 2010 at Camp Lejeune MCB. The data

collected during these burns are still being analyzed but are expected to be ready soon. We sent specific descriptions of the data we need for model evaluation to other project PIs. As the first step of modeling Vandenberg and Camp Lejeune burns, the meteorological modeling with WRF was completed.

Analysis of Burns Monitored at Ft. Benning

The analyses conducted under Subtask 4.3 last year revealed that the field data reported by UGA was not properly calibrated. UGA recommended dividing the values used so far by 3.64. Since this is a very large adjustment to the data used in Daysmoke evaluations, all analyses performed so far had to be repeated. These analyses are included in this report as Appendix E.

The advantage of Daysmoke over existing plume models is the ability to account for complex plume structures interpreted as updraft cores. The drawback is that Daysmoke makes no provision for determining the updraft core numbers. From a few studies unrelated to the Fort Benning project, it was assumed that 6 updraft cores were adequate for a typical prescribed burn. The analyses for the Fort Benning data show that the assumption cannot be sustained. Therefore, core numbers are now determined subjectively for each burn from a list of factors that can influence plume updraft dynamics. Some of these factors are:

- Size of burn area – a small burn area should be expected to produce only one updraft core; large burn areas can support many updraft cores.
- Shape of burn area – a burn area that is highly irregular in shape will require an irregular distribution of fire leading to many updraft cores. This problem can be amplified when wind direction maximizes irregularities.
- Heterogeneity of fuels – fuels that burn hot relative to surrounding fuels will develop stronger convective currents and will tend to form updraft cores.
- Fuel type, moisture, and loadings – all three factors relate to heat production. High heat production will develop convective columns and lead to fewer updraft cores; low heat production will lead to many updraft cores
- Distribution of fire on landscape - fire distributed along a long linear line will produce many updraft cores; fire spread evenly over length and depth (mass ignition, stripping) will organize convective columns into fewer updraft cores.
- Amount of fire on landscape – a small amount of fire will reduce emissions per second but decrease heat thus minimizing convective organization. The result is many updraft cores. A large amount of fire will produce the opposite. The result is fewer updraft cores.
- Distribution of canopy gaps – hot air trapped beneath a dense canopy will flow to the gaps thus creating convective columns that produce updraft cores there. Thin (or no) canopies will not be a factor in updraft core development.
- Transport wind speed – strong winds inhibit convective organization thus leading to many updraft cores. Weak winds allow convective organization resulting in few updraft cores.
- Mixing layer depth – a shallow mixing layer inhibits convective organization thus leading to many updraft cores. A deep mixing layer has less adverse impact on convective organization so fewer updraft cores should be expected.

The differences between PM_{2.5} concentrations calculated by Daysmoke and observed by each truck are shown in the top panel of Figure 14. The middle panel classifies each day according to downwind smoke gradients. On 3 days shown by orange, smoke concentrations increased with distance downwind from the burn, and Daysmoke performed well on these days. On 3 days

shown by magenta, smoke concentrations decreased with distance downwind from the burn, and Daysmoke performance was average on these days. On two days shown by brown, extremely high $PM_{2.5}$ concentrations at Truck 1 rapidly decreased to almost no smoke at Truck 3, and Daysmoke performed poorly on these days. On 2 days shown by light blue, smoke was not measured at the trucks. The event average factor of departure in the bottom panel of Figure 14 shows that on a per truck basis, Daysmoke was off by a factor greater than 2 on 7 out of 30 events.

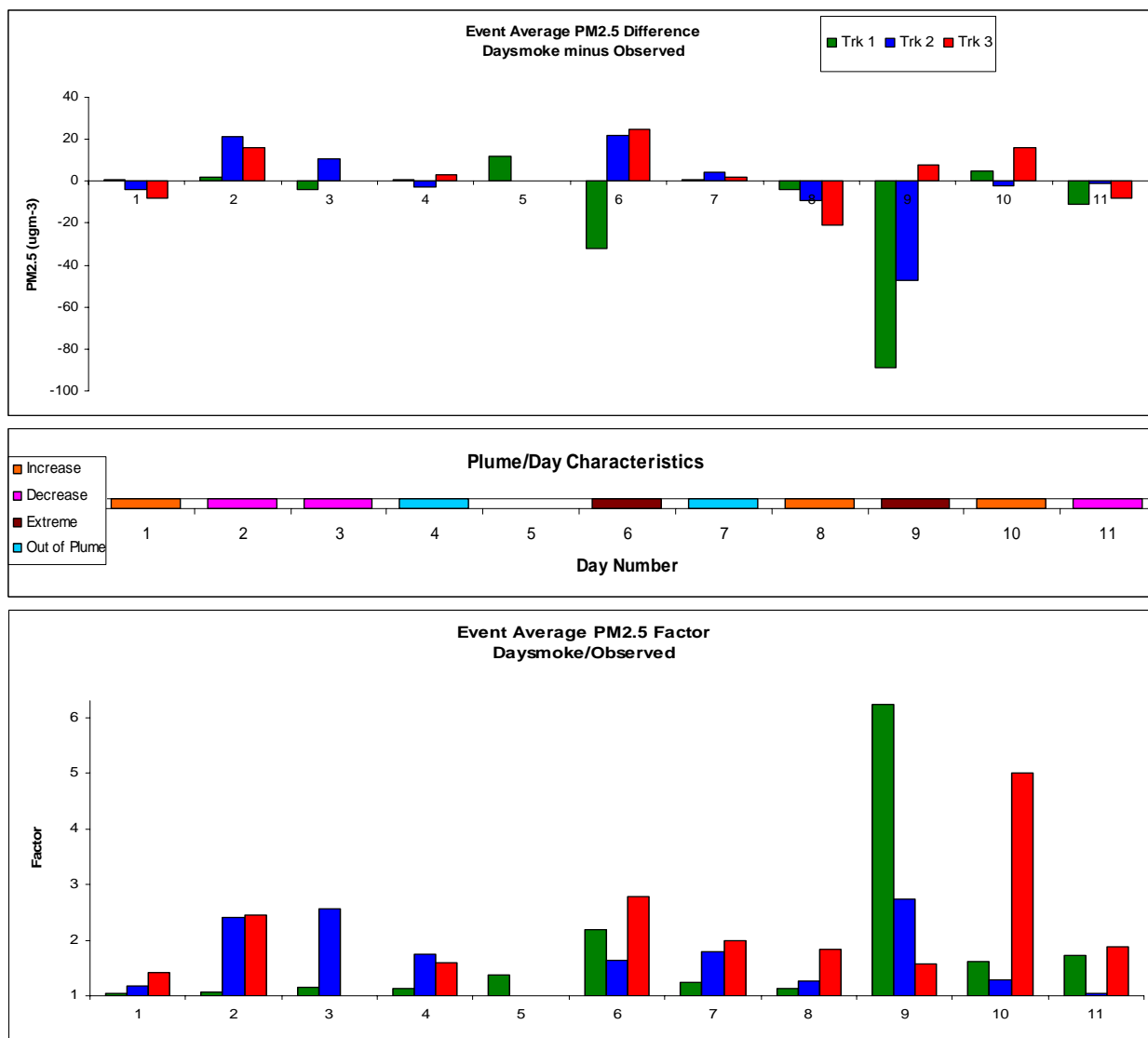


Figure 14. Daysmoke performance for each burn event and at each monitor: difference of modeled $PM_{2.5}$ from observed (top), classification of the burn event by the trend of concentration with distance downwind (middle), and ratio of modeled to observed $PM_{2.5}$ (bottom).

The analysis in Figure 14 has shown a relationship between the performance of the model and the gradient of the observed smoke by downwind distance. Daysmoke performance was the best on days when smoke concentration increased with distance downwind from the burn. On days when smoke concentrations decreased with distance, Daysmoke performance was not as

good but still acceptable. On days characterized by extremely high smoke gradients, from very high smoke concentrations at 1-3 km downwind to almost no smoke at 5-7 km downwind, Daysmoke performance in predicting PM_{2.5} concentrations was poor.

Atlanta February 28, 2007 Smoke Incident

Recall that we are using the February 28, 2007 Atlanta smoke incident as the primary evaluation case for our air quality models since the impacts of the burns were detected at several regional monitors around Atlanta. The results of the simulation of this incident by the adaptive grid CMAQ model were published in Atmospheric Pollution Research (Garcia-Menendez et al., 2010). The investigation of the reasons for the underestimation of PM_{2.5} concentrations continues. As discussed under Subtask 1.4 above, a sensitivity analysis is being conducted to determine the vertical plume profile which leads to the best agreement between modeled and observed concentrations.

Based on criteria listed above we revised (reduced) the number of cores used in Daysmoke for the burns at Oconee National Forest and the Piedmont Wildlife Refuge that led to the Atlanta smoke incident. We have also revised the fuel type used in FEPS upon further review of the information obtained from the Georgia Forestry Commission. As a result, the amount of PM_{2.5} emissions were reduced but the rise of the smoke plume in the atmosphere was enhanced. As a result, not only the predicted PM_{2.5} concentrations were in better agreement with observations at downwind regional monitors, some long-range transport characteristics of the plumes were better simulated as well (Figure 15).

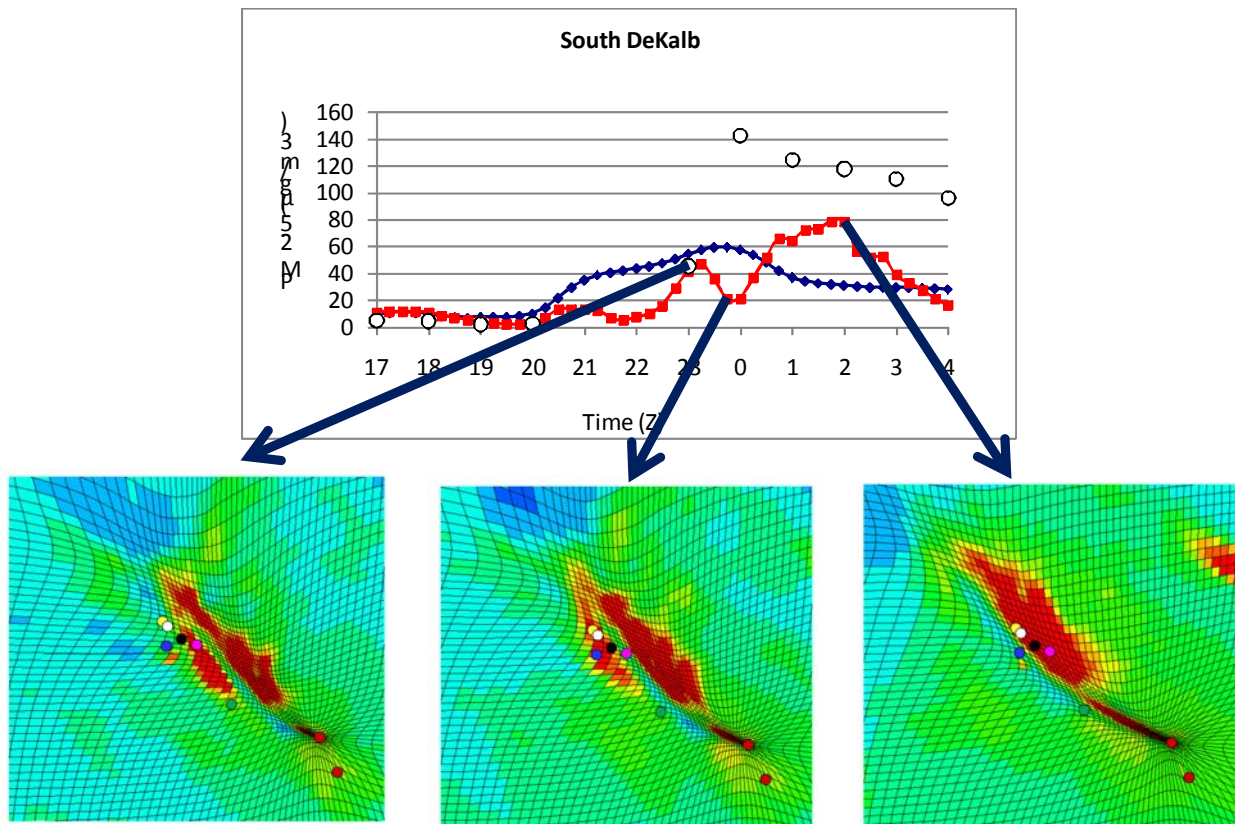


Figure 15. PM_{2.5} concentrations predicted by CMAQ and AG-CMAQ along with measurements at South DeKalb on 28 February 2007 (top). The bottom panels, where the location of the South DeKalb site is marked by the pink dot, show simulated PM_{2.5} at three different instances indicated by the arrow tails.

Figure 15 shows modeled PM_{2.5} concentrations using static grid CMAQ (blue) and adaptive grid CMAQ (red), along with site measurements at the South DeKalb station during Feb. 28/Mar. 1, 2007. Gridded concentration maps explain the peaks and trough in the AG-CMAQ modeled concentration, where the South DeKalb site is the pink circle. The initial peak corresponds to a plume from the smaller westernmost fire. The second peak corresponds to the larger Oconee fire plume. The transition between plumes leads to a trough in the station's pollutant levels.

As discussed under Subtask 2.4, we are using the February 28, 2007 Atlanta smoke incident for the evaluation of the coupled Daysmoke and Adaptive Grid CMAQ (AGD-CMAQ) model as well. We will continue to use this incident as our primary evaluation case for the revised/enhanced versions of the coupled modeling system in the future.

5. Simulations of Alternative Burning Strategies

Subtask 5.1: Identifying Burning Options

Prescribed burning experts consisting mostly of DoD and other land managers in the Southeast were surveyed. The goal of the survey was to identify the most relevant burning scenarios to be simulated with our smoke impact prediction system. Varying the size of burn, ignition method, fuel moisture, season of burn, fuel loads, weather conditions, and time of burn

were the most suggested burning options. Considering the priorities assigned to each one of these options, scenarios related to the following factors will be simulated.

1. Frequency of burn: We will vary the fire return interval (e.g., from 2 to 5 years) to study the impact of varying fuel loads and fuel types. Comparing fire suppression conditions with regularly burned healthy forests would illustrate the impacts of fuel accumulation vs. frequent low intensity burning, which is more cost effective. Is it beneficial to bring the fire suppressed parcels into the PB cycle?
2. Season of burn: How would the season (e.g., winter vs. summer) affect the PB impacts? The weather and background atmospheric composition would be different in each season. The fuel moisture, especially for woody fuels may also change from season to season. The contrast of traditional winter/spring burning with summer would illustrate the challenges of conducting PB during poor air quality periods.
3. Size of burn: We will vary the size of the burn (e.g., 300 vs. 600 acres) and the proximity of the burn plots (e.g., two 300 acre plots 5 miles away vs. next to each other). How far apart do parcels have to be from one another such that if subject to PB simultaneously, their impacts will not superimpose upon each other?
4. Ignition type: Hand stripping vs. aerial burning result in very different plumes. What impact to downwind concentrations of PM_{2.5} will occur if a 1000 acre burn is conducted at a constant rate of spread (representative of hand ignition), versus substantially increasing the number of acres burned for the first hour or two and then allow a constant rate of spread (for example 500 acres consumed in the first two hours; more representative of aerial ignition).
5. Time of burn: The burn can be conducted during different times of the day to make the impact of PB plume different due to varying meteorological conditions.

Concluding Summary

The fuels survey at Fort Benning was completed and a model based on photo series was prepared for estimating fuel loads on any Fort Benning burn unit. Fuel loadings increase rapidly after a burn as shrubs become a significant part of the fuel bed. The increase slows down in time and a plateau is reached after approximately 5 years. This model provides a crosswalk to FCCS fuel classification system. Emissions were estimated for each burn monitored at Fort Benning: there were 3 burns in April 2008, 6 burns in January 2009, and 2 burns in April 2009. The fuel loads were input to CONSUME, which yields total fuel consumption, and then to FEPS for time varying consumption. The emissions are calculated by applying emission factors to the fuel consumptions. Emission factors used here were derived from extensive field studies of prescribed burns conducted by the Forest Service in the Southeastern U.S. in 1990's. To provide input to a parallel project, fuel samples were collected at Fort Benning and shipped to the Fire Science Laboratory in Missoula, MT for emission measurements. The emission factors measured in the laboratory were in general agreement with the USFS southeastern fuels emission factors used in our modeling.

A sensitivity analysis was conducted to determine the important parameters of the models used in estimating emissions. Fuel moisture, involvement in flaming phase, duration of ignition, and emission factors are, by far, the most sensitive parameters. The likely ranges of these parameters were tested to determine the level of uncertainty in emission predictions. The uncertainties that were identified in this manner will later be used in estimating the uncertainties in downwind concentration predictions by the dispersion models. The sensitivity analysis was

extended to the air quality model where the impact of vertical distribution of emissions on concentrations downwind is being studied.

An adaptive grid version of MM5 that can provide meteorological inputs at the scales targeted for chemistry/transport modeling in this project (~100 m) was tested. This model was originally developed to resolve optical turbulence in the upper troposphere. Here, the model was applied to the simulation of boundary layer meteorology during the 9 April 2008 PB case. In this application, to better resolve the meteorology around the PB plume, the model was dynamically adapting to the externally supplied PM_{2.5} concentrations (which are high in the PB plume) from an earlier chemistry/transport simulation. Compared to a standard fixed grid MM5 simulation, there were some significant differences in model results, especially in wind speeds, that could not be explained in terms of grid adaptations. Compared to a standard fixed grid MM5 simulation, as well as a WRF simulation, adaptive MM5 produced much more variability in the wind fields and the influence of the terrain was more apparent. These results were encouraging in terms of providing wind field resolution never achieved before, which could translate in much more accurate transport simulation of prescribed burn plumes. However, since we do not have any resources to continue the development and validation of adaptive MM5, meteorological inputs will be interpolated from 1-km resolution MM5 or WRF simulations.

The incorporation of the adaptive grid algorithm into the CMAQ model was completed. The Adaptive Grid version of CMAQ (AG-CMAQ) is built in CMAQ Version 4.5 by keeping all the functionality and features of the host. AG-CMAQ also includes the variable time step algorithm (VARTSTEP) to improve computational efficiency. The code was verified by simulating the April 9, 2008 burn and comparing the results to those of an earlier simulation by CMAQ with fixed, uniform grid. AG-CMAQ increased the grid resolution in the regions of highest PM_{2.5} as it should. In a more rigorous verification aiming to match the results of standard CMAQ with a “non-adapting” run of the AG-CMAQ, all the differences in results were reconciled with the exception of very small (less than 0.1 $\mu\text{g m}^{-3}$) differences in aerosol nitrates and secondary organic aerosols of biogenic origin. During this meticulous verification effort, three deeply hidden bugs were discovered in the official CMAQ code and reported to the modeling community. The VARTSTEP algorithm and the newly developed AG-CMAQ model were documented in two journal articles published in *Atmospheric Pollution Research* (Odman and Hu, 2010 and Garcia-Menendez et al., 2010).

A thorough review of the Daysmoke model theory and computer code was completed. Several improvements to the model were implemented and tested. For example, the provision for adiabatic expansion allows for application to a wider range of smoke plume. The new transition from plume to free atmosphere at the plume top gives improved modeling for plume depth. The multi-core updraft feature is much more flexible now that it allows for cores of unequal sizes by assigning a stochastic flux component to each updraft core. A bug was discovered that increased plume vertical velocity by 0.5 - 1.0 m/s within the mixing layer. The parameterization of the entrainment coefficient was made a function of plume bent-overness. The detrainment coefficient was removed from being an additional degree of freedom. The free atmosphere horizontal velocity turbulence parameter, which was a constant, is made a function of the depth of the boundary layer. Finally, the model time steps, currently at 20 s, are being reduced (to be completed early next year) to capture the steep gradient in vertical velocity in the plume. Upon completion of the review of Daysmoke, a copy of the model code was transferred to GIT along with a draft write-up of the model theory.

Significant progress was made in the development of a coupling technique that can inject Daysmoke particles into the CMAQ grid cells without significant loss of accuracy. The technique is based on Fourier analysis. First, the smoke particle concentrations predicted by Daysmoke are represented as spectra of waves with different frequencies. Then, the waves whose frequencies cannot be supported by the adaptive CMAQ grid are identified. If the amplitudes of those waves are negligible, then the plume is handed over to CMAQ; otherwise the plume is continued to be followed by Daysmoke. A standalone analysis system was built by borrowing Fast Fourier Transform (FFT) algorithms from MATLAB. The incorporation of these algorithms into the FORTRAN code of CMAQ and Daysmoke has started. Analysis of several Daysmoke plumes showed that there exists an optimal downwind distance for hand over. This distance is a weak function of grid resolution; therefore the “wall” type coupling used so far is somewhat justified with the exception of the arbitrariness of the distance from the burn site to the wall. It was determined that the downwind distance of the wall should be calculated as a function of time.

The combination of finer grid resolution and sub-grid scale modeling can provide more detailed simulations of the prescribed burn plume evolution. An adaptive grid version of CMAQ has been coupled with Daysmoke, to create adaptive grid Daysmoke-CMAQ (AGD-CMAQ). In AGD-CMAQ, smoke emissions are first tracked by Daysmoke as parcels then inserted into the grid cells of AG-CMAQ at appropriate times and places using a procedure called “handover”. AGD-CMAQ’s benefits have been verified in an application to the Feb. 28, 2007 Atlanta smoke incident. In the future, the model evaluation will continue for other burn cases, especially for a series of prescribed burns at Fort Benning, GA. We are also in the process of having the grid system adapt to minimize the error during the handover process. A Fourier analysis technique will be used to determine the right moment to hand over the plume from the sub-grid scale plume model to the air quality model.

After the preliminary data collection, which resulted in three monitored burns in April 2008, this year’s intensive field measurements captured eight more burns: six in January and two in April. The burns were monitored by using three trucks equipped with real-time PM_{2.5} and CO monitors covering a 60-degree arc emanating from the burn area and stretching along the predicted wind direction. In response to shifts in wind direction the trucks moved to different locations within their zones, respectively 1-3 km, 3-5 km, and 5-7 km downwind, according to dispatches from the fire tower. The exact locations of the sampler trucks have been tracked by GPS. The trucks remained at any given monitoring location for a minimum of 30 minutes. Each subsequent position was chosen based on a combination of wind shifts, real-time equipment levels, and road availability. All the real-time air samples collected were processed, controlled for quality, and quality assured. The measurements and related information have been posted to a web site for public access.

A thorough evaluation of the Daysmoke model was conducted using the collected field data. The plume tops estimated by Daysmoke compares well with lidar measurements. The plume top and the number of updraft cores, which was confirmed by photographic data, are the two most important parameters in the determination of smoke levels by Daysmoke. Comparison of the PM_{2.5} concentrations predicted by Daysmoke with real-time measurements from DustTrak instruments showed general agreement but there were several instances of divergence. Uncertainties remain related to the calibration of the DustTrack readings, estimated wind directions, ignition patterns, and the timing of emissions. Investigation of possible contamination by non-smoke PM sources led to the removal of only a small fraction of the data. WRF-

simulated winds did not always line up the Daysmoke plume with truck locations. Most of the disparities in wind direction were within typical model prediction error. Occasionally, potential stability problems in WRF at 1.3-km resolution introduced unexpected oscillations to wind direction. This compromised efforts to match Daysmoke PM_{2.5} with observed PM_{2.5}. The disparity was particularly notable for April 15, 2008 when truck positions were located SSE from the fire but WRF winds blew the Daysmoke plume to the SSW. Therefore, it is suggested that the WRF winds be validated with winds measured by a Doppler sodar during the next field experiment. A Doppler sodar was arranged for next year's field study to deal with the uncertainty in the wind directions.

The comparison of PM_{2.5} concentrations simulated by Daysmoke to measurements had to be redone due to a calibration issue with the DustTrak instrument. Re-analysis (Appendix E) has shown a relationship between the performance of the model and the gradient of the observed smoke by downwind distance. Daysmoke performance was the best on days when smoke concentration increased with distance downwind from the burn. On days when smoke concentrations decreased with distance, Daysmoke performance was not as good but still acceptable. On days characterized by extremely high smoke gradients, from very high smoke concentrations at 1-3 km downwind to almost no smoke at 5-7 km downwind, Daysmoke performance in predicting PM_{2.5} concentrations was poor.

The 2010 field study will be performed at Eglin AFB where fuels will be sampled before and after the burns for more accurate fuel loading and consumption data. PM_{2.5} data will be collected on mobile platforms and calibrated with more accurate PM_{2.5} measurements at a stationary site. In addition to plume measurements with ceilometer, vertical wind profiles will be measured with a Doppler sodar. A US EPA team will also join us with their tethered balloon, which will allow unique vertical profile measurements of the smoke plume. All these measurements during the 2011 field study are expected to substantially improve our ability to model emissions from prescribed burns and provide more accurate inputs to the Daysmoke plume dispersion model.

No burn monitored in 2009 carried smoke in the direction of regional monitors. So far, only the April 9, 2008 burn, under southeasterly winds, may have reached the monitor at Columbus, GA. A slight increase in PM_{2.5} was detected by the monitor few hours after the burn and this is believed to be a consequence of the PB plume hit. This leaves the historic Atlanta smoke incident (February 28, 2009) as the only other PB case for the evaluation of the coupled Daysmoke-CMAQ system. That case is ideal for regional model evaluation as the smoke was fully captured by the dense network of monitors in the metro-Atlanta area. The comparison of the CMAQ and AG-CMAQ results with observations showed improved replication of the plume and decrease in artificial dilution due to adaptive grid refinements of AQ-CMAQ.

A second set of simulations was conducted with increased vertical resolution. In these simulations the agreement between modeled and observed PM_{2.5} concentrations improved significantly. However, the models still underestimate PM_{2.5} levels. We believe this is in part due to the underestimation of secondary organic aerosol formation in CMAQ (as well as AG-CMAQ). Another possibility is the cooling effect of the dense smoke, which lowers the mixing height and leads to higher concentrations below the plume. This effect can only be modeled by feeding back PM levels from CMAQ to the meteorological driver.

Based on factors that can influence plume updraft dynamics, we reduced the number of cores used in Daysmoke for the burns at Oconee National Forest and the Piedmont Wildlife Refuge that led to the 28 February 2007 Atlanta smoke incident. We have also revised the fuel type used in FEPS upon further review of the information obtained from the Georgia Forestry Commission.

As a result, the amount of PM_{2.5} emissions were reduced but the rise of the smoke plume in the atmosphere was enhanced. A sensitivity analysis is being conducted to determine the ideal profile for vertical distribution of the emissions so that a better agreement is obtained between predicted and observed pollutant concentrations.

The Atlanta smoke incident is being used for the evaluation of the coupled Daysmoke and Adaptive Grid CMAQ (AGD-CMAQ) model as well. The initial results of the simulation with the coupled Daysmoke and Adaptive Grid CMAQ models (AGD-CMAQ) are superior to the results from the initial Daysmoke-CMAQ coupling as well as the Adaptive Grid CMAQ model. Not only the predicted PM_{2.5} concentrations were in better agreement with observations at downwind regional monitors, some long-range transport characteristics of the plumes were better simulated as well.

A survey was conducted to identify the most relevant burning scenarios for which land managers would be interested in finding out potential impacts. Changing the frequency of the burn, season of the burn, size of the burn, ignition type, and time of the burn were among the scenarios of most interest. The smoke impact prediction system being developed in this project will be used to simulate several prescribed burning scenarios to determine their potential air quality impacts.

Lessons Learned from the Analysis of Field Studies

The analysis of the prescribed burns at Fort Benning generally confirmed the strategy used by UGA ground crews in moving trucks to new locations when winds shifted to blow the plume elsewhere. On the other hand, it revealed several modeling limitations and some deficiencies in the experimental design.

1. Daysmoke represents the burn area as a square equal in size to the actual burn area. When the actual burn area is highly irregular, some discrepancy should be expected when comparing Daysmoke simulated PM_{2.5} concentrations with observed concentrations, especially close in to the burn area. Correcting the problem would require specification of the geometric shape of the burn site,
2. Daysmoke discharges smoke uniformly over the square burn area throughout the course of the burn. With highly irregular burn areas, ignition may proceed from one side to the opposite side thus giving a progression of the fire and smoke emissions across the landscape. Correcting the problem knowledge of how land managers spread fire over the landscape, and knowledge of the distribution of fuel types and fuel loadings. A fire spread/relative emissions production model (Rabbit Rules) under development at USFS can map fire and emissions over a landscape with heterogeneous distribution of fuels.
3. PM_{2.5} concentrations generated by Daysmoke for the weak plumes match with smoke distributions produced by Gaussian smoke models. Maximum smoke concentrations are found immediately downwind from the burn site. However, for the moderately weak plumes, Daysmoke placed maximum concentrations 4 – 10 miles downwind from the burn site. If correct, Daysmoke presents a significant departure from existing concepts and models. The current experimental design places three trucks from 1 – 4 miles downwind from the burn. When conditions permit, the truck placements should be stretched as far downwind as logistical conditions permit.
4. Differences between observed wind directions (as determined by observed PM_{2.5} at truck locations) and modeled wind directions (as determined by Daysmoke simulated

PM_{2.5} at truck locations) have been found during the course of several burns. The discrepancies may be caused by differences between observed and WRF wind directions and/or failure of Daysmoke to spread the plume properly. A Doppler lidar will be deployed at Fort Benning to measure wind directions during experimental prescribed burns. These winds would provide validation for the WRF model winds. Knowing the accuracy of the WRF winds will enable us to determine the proper value for the plume spread coefficient.

5. The field protocol called for the mobile samplers to be turned on at time of ignition and turned off when firing was complete. This procedure did not allow sufficient time for smoke to travel from the burn site down wind past the truck locations. Thus several of the observed PM_{2.5} records end with high smoke concentrations still being measured. The data collection should be extended for at least an additional one half hour after firing is complete to allow for smoke to pass the most distant truck.

References

- Achtemeier GL (1998) Predicting dispersion and deposition of ash from burning cane. *Sugar Cane*, **1**, 17-22.
- Achtemeier GL, Adkins CW (1997) Ash and smoke plumes produced from burning sugar cane. *Sugar Cane* **2**, 16-21.
- Achtemeier GL (2005) On plume rise – matching Daysmoke with Briggs Equations for industrial stacks. J3.4, Sixth Symposium on Fire and Forest Meteorology, Canmore, CA, American Meteorological Society, Boston, MA.
- Battye, B. W. and R. Battye, 2002: Development of emissions inventory methods for wildland fire (final report). Prepared for U.S. Environmental Protection Agency, Research Triangle Park, NC, U.S.A. (<http://www.epa.gov/ttn/chief/ap42/ch13/related/firerept.pdf>)
- Baumann, K., 2005: Study of air quality impacts resulting from prescribed burning - Focus on sub-regional PM_{2.5} and source apportionment. Technical Report, Georgia Institute of Technology, 83pp.
- Byun, D.W. and J. Ching, 1999: Science algorithms of the EPA Model-3 community multiscale air quality (CMAQ) modeling system. Research Triangle Park (NC): EPA/600/R-99/030, National Exposure Research Laboratory.
- Cheng L., McDonald K.M., Angle R.P. and Sandhu H.S., 1998: Forest fire enhanced photochemical air pollution: A case study. *Atmos. Environ.*, **32**, 673-681.
- Earth Tech, Inc., 2000: A user's guide for the CALPUFF dispersion model version 5. Concord, MA.
- Garcia-Menendez, F., A. Yano, Y. Hu, and M. T. Odman, 2010: An adaptive grid version of CMAQ for improving the resolution of plumes. *Atmos. Pol. Res.*, **1**, 239-249 (doi: 10.5094/APR.2010.031).
- Gillani, N. V., and J. E. Pleim, 1996: Subgrid scale features of anthropogenic emissions of NO_x and VOC in the context of regional Eulerian models. *Atmos. Environ.*, **30**, 2043–2059.
- Gillani, N. V., and J. M. Godowitch, 1999: Plume-in-grid treatment of major point source

- Emissions. Chapter 9, Science algorithms of the EPA Model-3 community multiscale air quality (CMAQ) modeling system (Byun, D.W. and J. Ching, eds.), Research Triangle Park (NC): EPA/600/R-99/030, National Exposure Research Laboratory.
- Grell, G. A., S. E. Peckham, R. Schmitz, S. A. McKeen, G. Frost, W. C. Skamarock and B. Eder, 2005: Fully coupled online chemistry within the WRF model. *Atmos. Environ.*, 39, 6957-6975.
- Hao, W.M., D.E. Ward, R.A. Babbitt, R. E. Susott, S. P. Baker, R. Ottmar, R.E. Vihnanek, and D. Wade, 2002: Emissions of trace gases and aerosol particles from biomass fires in the southeastern and central United States, USDA Forest Service.
- Hu, Y., M. T. Odman, M. E. Chang, W. Jackson, S. Lee., E. S. Edgerton, K. Baumann, A. G. Russell, 2008: Simulation of air quality impacts from prescribed fires on an urban area. *Environ. Sci. Technol.*, 42(10), 3676-3682.
- Karamchandani, P., L. Santos, I. Sykes, Y. Zhang, C. Tonne, and C. Seigneur, 2000: Development and evaluation of a state-of-the-science reactive plume model. *Environmental Science & Technology*, 34, 870-880.
- Karamchandani, P., Seigneur, C., Vijayaraghavan, K., Wu, S.-Y., 2002 : Development and application of a state-of-the science plume-in-grid model. *J. Geophys. Res.*, 107, 4403–4415.
- Khan, M. N., M. T. Odman and H. Karimi, 2004: Evaluation of algorithms developed for adaptive grid air quality modeling. *Computers, Environment and Urban Systems*, 9, 718-734.
- Kumar, N.; Russell, A. G., 1996: Development of a computationally efficient, reactive subgrid-scale plume model and the impact in the northeastern United States using increasing levels of chemical detail. *J. Geophys. Res.*, 101, 16737-16744.
- Liu, Y. –Q., 2004: Variability of wildland fire emissions across the continuous United States. *Atmos. Environ.*, 38, 3489-3499.
- Liu, Y., G. L. Achtemeier, S. L. Goodrick, and W. A. Jackson, 2010: Important parameters for smoke plume rise simulation with Daysmoke, *Atmos. Pol. Res.*, 1, 250- 259.
- Morris R. E., McNally D.E., Tesche T.W., Tonnesen G., Boylan J. W., Brewer P., 2005: Preliminary evaluation of the community multiscale air, quality model for 2002 over the southeastern United States. *J. Air & Waste Manage. Assoc.*, 55 (11), 1694-1708.
- Napelenok, S. L., D. S. Cohan, M. T. Odman and S. Tonse, 2008: Extension and evaluation of sensitivity analysis capabilities in a photochemical model, *Environmental Modelling and Software*, 23 (8), 994-999.
- Odman, M. T., M. N. Khan, and D. S. McRae, 2001: Adaptive grids in air pollution modeling: Towards an operational model. *Air Pollution Modeling and Its Application XIV*, (S.-E. Gryning and F. A. Schiermeier, Eds.), New York: Kluwer Academic/Plenum Publishers, 541-549.
- Odman, M. T., M. N. Khan, R. K. Srivastava, and D. S. McRae, 2002: Initial application of the adaptive grid air pollution model. *Air Pollution Modeling and its Application XV* (C. Borrego and G. Schayes, Eds.), New York: Kluwer Academic/Plenum Publishers, 319-328.

- Odman, M.T., Hu, Y., 2007: A variable time-step algorithm for air quality models. *Air Pollution Modeling and its Application XVII* (C. Borrego and A.-L. Norman, Eds.), New York: Springer, 411-420.
- Odman, M. T. and Y. Hu, 2010: A variable time-step algorithm for air quality models. *Atmos. Pol. Res.*, **1**, 229-238 (doi: 10.5094/APR.2010.030).
- Ottmar, R.D., R.E. Vihnanek and J.W. Mathey, 2000. Stereo photo series for quantifying natural fuels. Volumes VI: Longleaf pine, pocosin and marshgrass types in the southeast United States. Publication of the National Wildfire Coordinating Group. PMS 835/NFES 2630.
- Ottmar, R.D., R.E. Vihnanek and J.W. Mathey, 2003. Stereo photo series for quantifying natural fuels. Volumes VIa: Sand hill, sand pine scrub and hardwoods with white pine types in the southeast United States. Publication of the National Wildfire Coordinating Group. PMS 835/NFES 2630 & PMS838/NFES 1119.
- Scholl, E.R. and T.A. Waldrop, 1999. Photos for estimating fuel loadings before and after prescribed burning in the upper coastal plain of the southeast. United States Dept. Agriculture, Forest Service Southern Research Station, General Technical Report GTR-SRS-26.
- Stewart, D. A., M. K. Liu, 1981: Development and Application of a Reactive Plume Model. *Atmos. Environ*, **15**, 2377-2393.
- U.S. EPA, 1995: Compilation of Air Pollutant Emission Factors, AP-42, fifth Edition, Vol. 1: Stationary Point and Area Sources. (<http://www.epa.gov/ttn/chief/ap42>)
- Unal, A. and M. T. Odman, 2003: Adaptive grid modeling for predicting the air quality impacts of biomass burning. 5th American Meteorological Society Symposium on Fire and Forest Meteorology, Orlando, Florida, November 16-20, 2003.
- Vijayaraghavan, K., Karamchandani, P., and Seigneur C., 2006: Plume-in-grid modeling of summer air pollution in Central California. *Atmos. Environ*, **40**, 5097–5109.
- WRAP (Western Regional Air Partnership), 2002: 1996 Fire Emission Inventory. Air Sciences, Inc. (<http://www.wrapair.org/forums/fejf/documents/emissions>)
- Xiao, X., D. S. McRae, H. A. Hassan, F. H. Ruggiero, G. Y. Jumper, 2006: Modeling Atmospheric Optical Turbulence, 44th AIAA Sciences Meeting and Exhibit, 09–12 January 2006, Reno, Nevada.

Appendix A: List of Technical Publications

Articles or Papers Published in Peer-reviewed Journals

- Liu, Y., S. Goodrick, G. Achtemeier, W. A. Jackson, J. J. Qu and W. Wang, 2009: Smoke Incursions into Urban Areas and Air Quality Effects: Simulation and Experiment of A Georgia Prescribed Burn. *International Journal of Wildland Fire*, **18**, 336-348.
- Odman, M. T. and Y. Hu, 2010: A variable time-step algorithm for air quality models. *Atmospheric Pollution Research*, **1**, 229-238 (doi: 10.5094/APR.2010.030).
- Garcia-Menendez, F., A. Yano, Y. Hu, and M. T. Odman, 2010: An adaptive grid version of CMAQ for improving the resolution of plumes. *Atmospheric Pollution Research*, **1**, 239-249 (doi: 10.5094/APR.2010.031).
- Liu, S., M. T. Odman, G. Achtemeier, S. Goodrick, S. L. Rathbun, and L. P. Naeher, Downwind Real-time PM_{2.5} and CO Monitoring during Prescribed Burns at Fort Benning, GA: Implications for Community Exposures, in preparation.

Published Technical Abstracts

- Odman, M. T., Y. Hu, D. S. McRae, G. L. Achtemeier, [A dynamic adaptive grid method for improved modeling of biomass burning plumes](#), 7th Annual CMAS Conference, Chapel Hill, NC, October 6, 2008.
- Odman, T., Y. Hu, S. Goodrick, Y. Liu, G. Achtemeier, L. Naeher, Preliminary Evaluation of a Modeling System for Predicting the Air Quality Impacts of Prescribed Burns, Partners in Environmental Technology Technical Symposium & Workshop, Washington, DC, December 2, 2008.
- Tsai, P.S., S. J. Frasier, S. Goodrick, G. L. Achtemeier, and M. T. Odman, [Combined Lidar and Radar Observations of Smoke Plumes from Prescribed Burns](#), Fourth Symposium on Lidar Atmospheric Applications, 89th American Meteorological Society Annual Meeting, Phoenix, AZ, 13 January 2009.
- Odman, M. T., Y. Hu, D. S. McRae, S. L. Goodrick, Y. Liu, G. L. Achtemeier, and L. P. Naeher, Predicting the Regional Air Quality Impacts of Prescribed Burns, 30th NATO/SPS International Technical Meeting on Air Pollution Modelling and its Application, San Francisco, CA, 18-22 May 2009.
- Achtemeier, G. L., Y. Liu, S. L. Goodrick, L. P. Naeher, and M. T. Odman, Results from Daysmoke for Weak Smoke Plumes, Eighth Symposium on Fire and Forest Meteorology, Kalispell, MT, 13-15 October 2009.
- Garcia-Menendez, F., Y. Hu, and M. T. Odman, [An adaptive grid version of CMAQ for improving the resolution of plumes](#), 8th Annual CMAS Conference, Chapel Hill, NC, October 20, 2009.
- Yano, A., Y. Hu, G. L. Achtemeier, and M. T. Odman, A sub-grid scale model for the treatment of biomass burning plumes in CMAQ, 8th Annual CMAS Conference, Chapel Hill, NC, October 19-21, 2009.

- Achtemeier, G. L., Y. Liu, S. L. Goodrick, L. P. Naeher, T. Odman, S. Frasier, and P. Tsai, Results from Daysmoke for Weak Smoke Plumes, 4th International Fire Ecology and Management Congress, Savannah, GA, 30 November - 4 December, 2009.
- Odman, T., Y. Hu, S. Goodrick, Y. Liu, G. Achtemeier, L. Naeher, Evaluation of a Modeling System for Predicting the Air Quality Impacts of Prescribed Burns, Partners in Environmental Technology Technical Symposium & Workshop, Washington, DC, December 2, 2009.
- Achtemeier, G. L., Y. Liu¹, S. L. Goodrick, L. P. Naeher, T. Odman, S. Frasier, and P. Tsai, [Results from Daysmoke for Weak Smoke Plumes](#), 16th Joint Conference on the Applications of Air Pollution Meteorology with the A&WMA, 17-21 January 2010 at Atlanta, GA.
- Odman, M. T., Y. Hu, A. Yano, F. Garcia-Menendez, G. L. Achtemeier, S. L. Goodrick, Y. Liu, D. S. Mcrae, L. Naeher, [Development of a modeling system for prescribed burn emissions and air quality impacts](#), 16th Joint Conference on the Applications of Air Pollution Meteorology with the A&WMA, 17-21 January 2010 at Atlanta, GA.
- Yano, A., F. Garcia-Menendez, Y. Hu, M. T. Odman, D. S. McRae, and G. L. Achtemeier, [Modeling biomass burnings by coupling a sub-grid scale plume model with Adaptive Grid CMAQ](#), 9th Annual CMAS Conference, Chapel Hill, NC, October 11-13, 2010.
- Garcia-Menendez, F., Y. Hu, and M. T. Odman, Evaluation of air quality models applied to wildland fire impact simulation, 9th Annual CMAS Conference, Chapel Hill, NC, October 11-13, 2010.
- Odman, M. T., F. Garcia-Menendez, A. Yano, Y. Hu, G. L. Achtemeier, and D. S. McRae, A High-Resolution Modeling System for Regional Carbonaceous Aerosols, 29th Annual Conference of the American Association for Aerosol Research, Portland, OR, October 25-29, 2010.
- Odman, T., F. Garcia-Menendez, A. Yano, Y. Hu, S. Goodrick, Y. Liu, G. Achtemeier, Predicting the Air Quality Impacts of Prescribed Burns, Partners in Environmental Technology Technical Symposium & Workshop, Washington, DC, December 1, 2010.

Appendix B: Variable time-step algorithm

Odman, M. T. and Y. Hu, 2010: A variable time-step algorithm for air quality models.
Atmospheric Pollution Research, **1**, 229-238 (doi: 10.5094/APR.2010.030).



A variable time-step algorithm for air quality models

M. Talat Odman, Yongtao Hu

School of Civil and Environmental Engineering, Georgia Institute of Technology 311 Ferst Drive, Atlanta, GA 30332-0512

ABSTRACT

In current air quality models, distinct process operators are applied sequentially to pollutant concentration fields. A common time step is used to synchronize all the processes. Usually, the characteristic time for advection, which is equal to the grid length divided by the wind speed, is selected as the common step. Since the same time step is used everywhere in the domain, the maximum wind speed and minimum grid length determine the step size. This leads to computational inefficiency in cells where process characteristic times are much longer than the time step.

A variable time-step algorithm was developed that allows each grid cell to have its own time step. Concentrations in cells with shorter time steps are updated using fluxes from cells with longer time steps. Fluxes from cells with shorter time steps to cells with longer time steps are kept in reservoirs. Concentrations in cells with longer time steps remain constant until the time levels are synchronized. At the time of synchronization the mass in each reservoir is added to the corresponding cell.

A two-dimensional implementation of the algorithm that uses the same time step in each vertical column is described. $PM_{2.5}$ estimates obtained by using variable time steps are, on average, within 3% of those obtained by using a single time step. Larger differences are observed for $PM_{2.5}$ components, especially for sulfate, which is 12% higher in winter. The differences in light extinction are also within 3% and those in ozone are within 1%. The computation time decreased by 50% in a winter episode largely due to the economy realized in aerosol equilibrium calculations. The time saved by this algorithm can be spent in increasing the process detail in air quality models or improving their computational accuracy.

Keywords:

Time-splitting
Process splitting
Particulate matter
Visibility
Ozone

Article History:

Received: 31 March 2010
Revised: 04 September 2010
Accepted: 07 September 2010

Corresponding Author:

M. Talat Odman
Tel: +1-404-894-2783
Fax: +1-404-894-8266
E-mail: talat.odman@ce.gatech.edu

© Author(s) 2010. This work is distributed under the Creative Commons Attribution 3.0 License.

doi: 10.5094/APR.2010.030

1. Introduction

Air quality models (AQMs) are based on the atmospheric transport and chemistry equation:

$$\frac{\partial c}{\partial t} + \nabla \cdot (uc) = \nabla \cdot (K\nabla c) + R(c) + S \quad (1)$$

where c is a vector of pollutant concentrations, u is the wind field, K represents parameterized atmospheric turbulence, R denotes chemical production (or loss) which is a nonlinear function of c and S includes various sources (e.g., emissions) and sinks (e.g., deposition). The dependence of the variables on the coordinates x and time t is not shown here for simplicity. Both u and K are given (usually provided by a prognostic meteorological model) so that the problem is linear with respect to the transport part. Characteristic times differ from one process to another. In particular, the range of characteristic times for chemical reactions in R spans several orders of magnitude.

After spatial discretization of Equation (1) a semi-discrete system of the following form is obtained:

$$\frac{\partial w}{\partial t} = F(w) \quad (2)$$

The variables of vector w consist of c and some other parameters and F is a vector function of w . The computational power required to solve this system is enormous due to the stiffness caused by the wide range of characteristic times. In addition, various numerical difficulties associated with special requirements of each transport and chemistry process must be dealt with. Therefore, in AQMs, Equation (2) is divided into smaller pieces. A common approach is process splitting (Blom and Verwer, 2000) where F is split into functions representing different processes:

$$\frac{\partial w}{\partial t} = F(w) \equiv F_A(w) + F_D(w) + F_R(w) \quad (3)$$

The function F_A is the advection dominated horizontal transport, F_D is the diffusion dominated vertical transport, and F_R contains chemical reaction terms. Terms for aerosol and cloud processes can also be added to the right hand side of Equation (3). Dry deposition is generally treated as a boundary condition of F_D . Emissions are usually made part of F_D or F_R . If they are made part of F_D then fresh emission plumes would be diffused before they had a chance to react with radicals in the environment. This is the choice made in the Community Multiscale Air Quality (CMAQ) model (Byun and Schere, 2006). On the other hand, if made part of F_R they would participate in chemical reactions before they had a chance to diffuse into the surrounding air. It is obvious that emissions should be made part of the process with shorter characteristic time but the relative magnitudes of the characteristic

times may differ from place to place and time to time. The Urban-to-Regional Multiscale (URM) model (Boylan et al., 2002) solves the problem by combining F_D and F_R into a single diffusion-chemistry function.

Splitting drastically reduces the computational resources required by Equation (2). It also allows using custom-built numerical solvers for each piece or process. It is much easier to deal with process-specific problems individually rather than trying to develop a general solver. For example, the advection operator is usually made nonlinear to achieve positivity either through filtering or flux-limiting. The only disadvantage of splitting is that it introduces an error into the solution (Lanser and Verwer, 1999).

Splitting methods are classified as first or second order based on the order of the splitting time step, Δt , in their error terms. Most splitting methods, including the one used in CMAQ, are first order (i.e., their splitting error term is second order in Δt). They advance the solution by Δt in time by applying process operators consecutively as follows:

$$w^{n+1} = \Phi_R(t^n; \Delta t) \Phi_D(t^n; \Delta t) \Phi_A(t^n; \Delta t) w^n \quad (4)$$

where Φ_A , Φ_D and Φ_R are the integrators for F_A , F_D and, F_R in Equation (3) respectively; for simplicity other processes are not shown. Strang splitting (Strang, 1968), which is believed to be second order, is also popular in AQMs. It advances the solution in time by the following sequence of operators:

$$w^{n+1} = \Phi_A(t^{n+\frac{1}{2}}; \frac{\Delta t}{2}) \Phi_D(t^{n+\frac{1}{2}}; \frac{\Delta t}{2}) \Phi_R(t^n; \Delta t) \Phi_D(t^n; \frac{\Delta t}{2}) \Phi_A(t^n; \frac{\Delta t}{2}) w^n \quad (5)$$

Note that the transport operators Φ_A and Φ_D are applied for one half of Δt , symmetrically around the chemistry operator Φ_R . Sportisse (2000) recently argued that, for R linear in c , Strang splitting is only first order unless the stiff operator Φ_R is applied last.

Processes with characteristic times shorter than the splitting time step can be advanced in several sub-time steps but this “sub-cycling” is internal to the process operators. It is the splitting time step that determines the frequency by which different processes with differing characteristic times are “synchronized” or “coupled.” Typically, the characteristic time for advection, which is equal to the grid size divided by the wind speed, is selected as the splitting time step (splitting will be dropped hereafter). Current AQMs use a single time step for the entire domain. In uniform grid AQMs the maximum wind speed in the domain limits the time step. In variable grid AQMs the characteristic time of a cell with relatively small grid size and high wind speed would be used as the global time step, Δt . Usually, a large fraction of the grid cells would have characteristic advection times larger than Δt due to either relatively low local wind speeds or larger grid sizes. Time stepping those cells with a Δt much smaller than their characteristic time step does not make the results more accurate; therefore, using a single time step for the entire domain is computationally inefficient.

A variable time-step algorithm is described in this paper. Its accuracy and computational efficiency were evaluated in comparison to using a single time step in a uniform grid AQM. Computing time saved by this algorithm can be used for increasing the details of processes modeled in AQMs, adding new processes, or improving computational accuracy. For example, AQMs can be coupled with the dynamics models and the feedbacks of aerosols on radiation and clouds can be modeled. Alternatively, the grid resolution can be increased for more accurate representation of emission plumes or cumulus convection. Some AQMs confronted the grid resolution issue by using variable grids that are either

static (Boylan et al., 2002; Park et al., 2004) or dynamic (Odman et al., 2002; Constantinescu et al., 2008). If the grid sizes in a variable grid differ by orders of magnitude, and, worse yet, smallest grid cells are collocated with strongest winds, the inefficiency of using a single global time step becomes unbearable even for the most powerful computers. This variable time-step algorithm has been the enabling technology for the adaptive grid version of CMAQ, which uses a dynamic variable grid (Garcia-Menendez et al., 2010).

2. Methodology

The variable time-step algorithm (VARTSTEP) is developed with the objective of enabling local time steps in AQMs. VARTSTEP allows each grid cell to advance by its own time step. The version of the algorithm described here is two-dimensional: it uses the same time step for an entire vertical column. Extension of the algorithm to third dimension should be straightforward. Here, VARTSTEP is implemented in the CMAQ model. CMAQ uses a global time step, Δt , determined as follows:

$$\Delta t = s \frac{\Delta x}{u^{max}} \quad (6)$$

In Equation (6), Δx is the uniform grid size, u^{max} is the maximum wind speed in the domain, and s is a factor of safety equal to 0.75. Starting with Version 4.3, the user can specify an altitude (as a vertical layer) above which wind speeds are not considered in determining the time step. Horizontal advection is applied multiple times (i.e., sub-cycled) above that altitude with a sub-time step that guarantees stability. This feature is preserved in the VARTSTEP version of CMAQ, which will be referred to as VARTSTEP-CMAQ hereafter.

The two-dimensional (2D) VARTSTEP assigns every vertical column i its own time step, Δt_i , called the local time step hereafter to differentiate from the global time step. The local time step must satisfy two conditions. The first condition is:

$$\frac{u_i^{max} \Delta t_i}{\Delta x_i} \leq 1 \quad (7)$$

where u_i^{max} is the maximum wind speed in vertical column i (up to the user-specified altitude) and Δx_i is the horizontal grid size for that vertical column (subscript i is used considering that grid size may be non-uniform). This is the well known Courant, Friedrichs and Lewy (CFL) stability condition for advection (Anderson et al., 1984). In process splitting, this condition also assures that fresh emissions are not transported by a horizontal distance longer than the grid length before other processes are applied at least once. The second condition requires that Δt_i be an integer multiple of the global time step, Δt , and an integer divisor of the output time step. The last part assures synchronization of processes among all the grid cells before the results are written out. Note that the global time step must be determined first, before the second condition can be used to determine the local time steps. The following example illustrates how the second condition is applied. Assuming an output time step of 60 min, if the global time step is 5 min, the local time steps can be 5, 10, 15, 20, 30, or 60 min. On the other hand, 25, 35, 40, 45, 50, or 55 min cannot be used as local time steps, although they are multiples of 5 min, because they do not divide 60 min evenly.

The model clock advances in increments equal to the global time step, Δt . When the clock strikes an integer multiple of the local time step, Δt_i , (i.e., $t = N \times \Delta t_i$) VARTSTEP applies process operators to the concentrations of vertical column i for the duration of Δt_i . In other words, instead of advancing the solution in m steps with the global time step Δt as:

$$\begin{aligned}
 w^{n+m} &= \Phi_R(t^{n+m-1}; \Delta t) \Phi_A(t^{n+m-1}; \Delta t) \Phi_D(t^{n+m-1}; \Delta t) \dots \\
 &\Phi_R(t^{n+k}; \Delta t) \Phi_A(t^{n+k}; \Delta t) \Phi_D(t^{n+k}; \Delta t) \dots \\
 &\Phi_R(t^n; \Delta t) \Phi_A(t^n; \Delta t) \Phi_D(t^n; \Delta t) w^n
 \end{aligned}
 \tag{8}$$

where $1 \leq k \leq m-2$, VARTSTEP advances it in one step with the local time step $\Delta t_i = m \times \Delta t$ as:

$$w^{n+m} = \Phi_R(t^n; m\Delta t) \Phi_A(t^n; m\Delta t) \Phi_D(t^n; m\Delta t) w^n
 \tag{9}$$

Since there is a single local time step for each vertical column, there are no difficulties involved in doing this with the vertical transport operator, Φ_D . The chemical reaction operator, Φ_R , does not pose any problems either since it is applied to one grid cell at a time. However, the horizontal transport operator, Φ_A , requires special attention since neighboring grid cells in the horizontal may have different time steps. Figure 1 illustrates how the transport between two cells might be handled. If $\Delta t_2 < \Delta t_1$, any horizontal flux (advective or diffusive) from Cell 1 must be passed to Cell 2 when it is time to update Cell 2 concentrations (i.e., when $t = N \times \Delta t_2$). This situation is illustrated by the arrow marked "Pass" in Figure 1. On the other hand, if $\Delta t_2 > \Delta t_1$ and $t \neq N \times \Delta t_2$ any flux from Cell 1 to Cell 2 is directed to a reservoir. This is shown in Figure 1 by the arrow marked "Store". When the time comes for updating Cell 2 concentrations (i.e., when $t = N \times \Delta t_2$) not only any possible flux from Cell 1 is passed to Cell 2, but the mass accumulated in the reservoir is also added to Cell 2. This is represented by the arrow marked "Flush" in Figure 1.

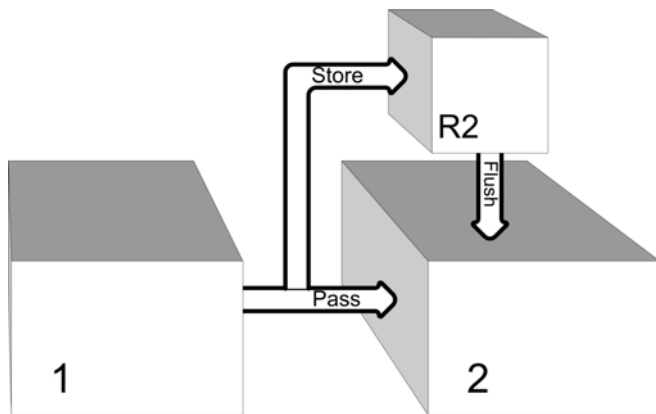


Figure 1. Concept of a reservoir used in VARTSTEP algorithm. The flux from Cell 1 is either passed directly to Cell 2 or stored in a reservoir which is flushed when it is time to update Cell 2 concentrations.

In practice, there is little computational gain in trying to calculate horizontal fluxes for the duration of each cell's local time step. There are also mass conservation concerns related to calculating the same flux at a grid cell interface twice, using one time step at the outflow side and another time step at the inflow side. It is much easier to calculate horizontal transport fluxes every global time step. In most transport schemes used in current AQMs, the calculation of a flux into or out of a cell does not only involve that cell's concentration but the concentrations of neighboring cells as well. Those concentrations may have been updated at a different time than the cell's own concentration. Horizontal transport fluxes are calculated using the latest updated concentration for each cell. The influxes are added to and outfluxes are subtracted from the cells' reservoirs. When the concentration of a cell is being updated, every local time step, the cell's reservoir is also flushed. This assures that all fluxes are eventually added to the appropriate cell and that mass is conserved. The process that advances a grid cell's concentration in time by the cell's local time step is illustrated in Figure 2.

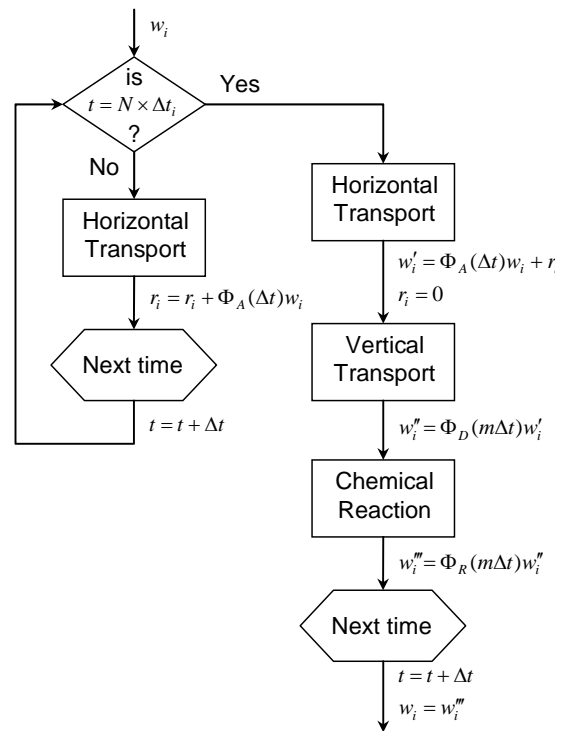


Figure 2. Flowchart of the VARTSTEP algorithm showing the sequence of the processes for advancing w_i , the solution for grid cell i , by one local time step $\Delta t_i = m\Delta t$.

3. Major Implementation Issues

In this section, the two-dimensional (2D) implementation of VARTSTEP in CMAQ is described. The discussion is limited to general issues and is intended to be useful for implementation in other air quality models. Remarks are made to aid a three-dimensional (3D) implementation in the future.

The first order splitting of Equation (4) is implemented in CMAQ as consecutive calls to various process modules inside a time step loop. Each module calculates the changes in pollutant concentrations resulting from a particular process (or processes) during the time step and applies them to the concentration array, CGRID. The specific order in which the process modules are called is as follows: vertical diffusion, which includes emissions and dry deposition; horizontal advection; vertical advection; horizontal diffusion; cloud processes; gas-phase chemistry; and aerosol processes. The CGRID array is four-dimensional consisting of 3D concentration fields for each and every pollutant species. The time step is set to the minimum characteristic time for advection among all grid cells.

In VARTSTEP-CMAQ, the time step loop advances the clock time by the global time step, TSTEP. In this 2D implementation of VARTSTEP, the local time steps assigned to each vertical column are stored in LOCSTEP, a 2D array with the dimensions of the horizontal grid. In a 3D implementation every grid cell would be assigned its own time step, hence, LOCSTEP would be a 3D array. LOCSTEP passes the local time step information to the process modules. Processes other than horizontal advection and diffusion are applied to vertical columns for the duration of the local time step. The decision to update pollutant concentrations is made based on whether the local time step evenly divides the clock time. The potential for computational time savings lies in processes that are applied less frequently and for periods longer than the global time step. In VARTSTEP-CMAQ, this is the case for vertical diffusion, cloud processes, gas-phase chemistry, and aerosol processes.

The local time steps of neighboring cells in a horizontal plane can be different; therefore, the implementation of VARTSTEP for horizontal transport is more complex compared to vertical transport where all the cells in a vertical column share the same local time step. In a 3D implementation, vertical transport, including transport due to convective clouds, would have to be treated in a way similar to the way horizontal transport is treated here. In VARTSTEP-CMAQ, the horizontal fluxes in and out of grid cells must be computed every global time step even though the cell concentrations are updated once per local time step. Calculation of fluxes that will not be used immediately may be unnecessary in other models. However, in CMAQ, flux parameters, namely wind velocity for advective flux and eddy diffusivity for diffusive flux, are evaluated at the middle of the time step through linear interpolation between two meteorological input records, typically one hour apart. Evaluating flux parameters at different times may lead to mass conservation problems. For example, suppose the wind velocity at the interface of two cells has one value when evaluated at the middle of the local time step of the first cell but another value when evaluated at the middle of the local time step of the second cell. This would yield a different flux leaving (or entering) the first cell than the flux entering (or leaving) the second cell. Having different fluxes on opposite sides of the cell interfaces would violate mass conservation. If the flux parameters were held constant during each output time step, horizontal transport could also be applied for the duration of the local time step.

VARTSTEP requires another array to store the fluxes into or out of cells whose local time steps are longer than the global time step and whose concentrations are not being updated immediately. This array, FGRID, fulfills the duty of the reservoirs described in Section 2. In CMAQ, horizontal transport processes (advection and diffusion) are applied to all horizontal planes, from the surface to the top, through a loop over vertical layers before CGRID is updated and handed over to another process. To be consistent with this structure, and, considering the possibility of a 3D implementation in the future, we chose to store the fluxes of each pollutant in a three-dimensional array. Further, since the fluxes of each pollutant must be kept in a different reservoir, we made the FGRID array four-dimensional, where the fourth dimension is indexed by pollutant species, just like the CGRID array. The FGRID array is the only significant burden of VARTSTEP on memory; therefore, if additional memory slightly larger than the size of the CGRID array is made available, full advantage can be taken from the algorithm's computational efficiency. Note that if the loops over vertical layers are taken out of horizontal process modules and these modules are called within a layers loop, then only the horizontal fluxes of one layer would have to be stored in a 2D array for each pollutant; therefore, FGRID can be a 3D array.

For mass conservation, horizontal transport schemes are usually in flux form; therefore, the calculation of horizontal fluxes is routine in most AQMs. In CMAQ, the preferred advection scheme is the Piecewise Parabolic Method of Collella and Woodward (1984). In this scheme, advective fluxes are calculated by fitting piecewise parabolas to the cell concentrations. Horizontal advection modules of CMAQ were modified not to update cell concentrations but to store already calculated lateral fluxes in the FGRID array. In CMAQ, advective outfluxes are limited such that they do not generate negative concentrations. No flux is allowed to remove more than the pollutant mass content of a cell. In VARTSTEP-CMAQ some of the cell content may already be committed to other outfluxes (e.g., advective flux in the orthogonal direction, advective flux in the same direction during a previous global time step, or diffusive flux) or influxes may have accumulated in the reservoir. Therefore, the outflux must be limited by the cell content plus the fluxes (positive or negative) stored in FGRID up to that point. The horizontal diffusion module was also modified to store the fluxes calculated by central differencing without updating the concentrations. In addition, flux

limiting was added to this module to take into account fluxes that are already committed.

When the local time step evenly divides the clock time, the cell concentrations in CGRID must be updated using the horizontal fluxes stored in FGRID. This can be done after the calls to horizontal transport modules. In VARTSTEP-CMAQ, instead of creating a separate module for this, the task was assigned to the vertical advection module, which already contains an update of CGRID based on LOCSTEP. This results in computational time savings by reducing the total number of conditional operations. However, the original process order had to be changed such that horizontal diffusion takes place before vertical advection. It should also be noted that VARTSTEP-CMAQ uses a vertical advection scheme that adjusts vertical velocities for strict mass conservation (Hu et al., 2006).

Vertical diffusion, which includes emissions and dry deposition, is the first process in CMAQ and it is followed by horizontal transport. The reason for this is most likely the desire to start each process cycle with fresh emissions and give diffusion priority because of its relatively short characteristic times. In VARTSTEP-CMAQ, if vertical diffusion were applied when the local time step evenly divides the clock time (i.e., $t = N \times \Delta t_i$), in cells with local time steps longer than the global time step, horizontal transport would start before emissions were injected and vertically diffused. On the other hand, there is no reason for applying vertical diffusion every global time step just to remain faithful to the original process order. Therefore, vertical diffusion was applied to each vertical column for the duration of the local time step at the beginning of the process cycle. Note that gas-phase chemistry, aerosol and cloud processes are applied when the local time step evenly divides the clock time, effectively taking place after horizontal transport. This would not be an issue in models where vertical diffusion and emissions are applied after horizontal transport.

The last important implementation issue is the time interpolation of meteorological parameters and emissions. In CMAQ, these parameters are evaluated at the middle of the global time step. The reading of input values and interpolation takes place for all the grid cells at once. Using this global interpolator may have some undesirable consequences. For example, assuming a 10 min global time step and hourly meteorological inputs, between 07:00 and 08:00, the interpolator would interpolate the parameters to 07:05, 07:15, 07:25, and so on. For a concentration update at 7:30, a cell with a local time step of 30 min should have its parameters at 07:15, which is the middle of the time step from 7:00 to 7:30, but the last available parameters from the global interpolator would be at 7:25. Having meteorological parameters and emission rates at a different time can violate mass conservation. For example, the total amount of emissions into cells with longer local time steps may be over/under-estimated. To avoid such consequences, a new interpolator was developed here for VARTSTEP-CMAQ that can evaluate time-dependent parameters for each grid cell at a different time. This way all the cell parameters can be evaluated at the middle of the local time step of that cell.

4. Results and Discussion

VARTSTEP was verified using a rotating-cone test. A right circular cone was introduced into a rotational wind field on a uniform grid (see the Supporting Material, SM, Figure S1a). The distance from the axis of rotation to the axis of the cone was equal to the diameter of the base circle; therefore, wind speeds increased by a factor of 3 across the base circle. Hence, the local time steps in the grid cells supporting the cone varied by a factor of 3 according to Equation (7). After one full rotation, the cone rotated by VARTSTEP was practically identical to the cone rotated by using a global time step (see the SM, Figures S1b and S1c). The small magnitude of the difference (see the SM, Figure S1d)

indicated that VARTSTEP is a viable alternative to the current time stepping algorithms in AQMs. Mass conservation was also tested and no mass conservation errors were found after one full rotation of the cone (see the SM, Figure S2).

To evaluate VARTSTEP–CMAQ, air quality simulations were performed in the Southeastern U.S. during a winter episode (1–20 January 2002) and a summer episode (12–27 July 2001). Version 4.3 of CMAQ was used for calculating the ambient fine particulate matter ($PM_{2.5}$) and ozone (O_3) concentrations. The horizontal grid resolution was 12 km over the domain shown in Figure 3. The global time steps were between the user–specified minimum of 5 min and the CFL condition imposed maximum of 7.5 min during the winter episode and 10 min during the summer episode. In addition to these simulations that served as a “benchmark”, a second set of simulations was conducted with VARTSTEP–CMAQ.

All computations were performed on a single processor 2.8 GHz Intel CPU with dedicated 4 gigabytes of memory. The total computation time for the simulation with VARTSTEP–CMAQ was 50% less than the benchmark CMAQ simulation for the winter episode, while the savings were only 13% for the summer episode (Table 1). This difference in savings is largely due to the load reduction of the aerosol module from 60% for the winter episode to 23% for the summer episode in CMAQ simulations. In Southeastern U.S., sulfate is the dominant PM species in summer, while nitrate is almost negligible. On the other hand, nitrate levels can exceed sulfate levels in winter. Nitrate equilibrium is much more complex than sulfate’s: it does not only depend on the availability of nitric acid but also on ammonia and sulfate, as well as temperature and relative humidity. The large CPU time spent in the aerosol module in winter is due to the computational intensity of nitrate equilibrium, as well as shorter time steps dictated by stronger winds. With VARTSTEP, the times spent in the vertical diffusion, clouds, and chemistry modules were all reduced, but almost all of the benefits are realized in the aerosol module. The gas–phase chemistry module of CMAQ uses an implicit chemical kinetics solver whose computation time does not respond to changes in the time step. A different solver with larger overhead could have benefited more from less frequent calls to the chemistry module.

Since horizontal transport modules are called every global time step, no benefit of VARTSTEP should be expected. The increase in the computation time of the horizontal advection module is due to the flux limiting that accounts for committed fluxes in FGRID. The increase in the computation time of the horizontal diffusion module is due to the computation and storage of diffusive fluxes needed by VARTSTEP; those fluxes were not

needed in the original module. The VARTSTEP burden in vertical advection is due to the update of concentrations.

Now that we have seen how VARTSTEP can reduce the computation time, the question is whether it can produce reliable air quality results. Daily average $PM_{2.5}$ concentrations for 17 January 2002 resulting from the two simulations are compared in Figure 3. Both simulations produced a similar $PM_{2.5}$ distribution over the Southeastern U.S. with a peak near Pensacola, Florida. The value of the peak is $65.8 \mu g m^{-3}$ according to the benchmark simulation and $62.9 \mu g m^{-3}$ according to the VARTSTEP–CMAQ simulation. $PM_{2.5}$ distributions were also similar for the summer episode, VARTSTEP producing slightly lower values over the Southeast (see the SM, Figure S3).

Daily average observations of $PM_{2.5}$ and its composition are available through the Interagency Monitoring of Protected Visual Environments (IMPROVE) network. The network covers areas designated as “Class-I” for visibility protection such as national parks and wilderness areas. There are 22 such observation sites in the region shown in Figure 3. Eight of these sites are clustered along the Southern Appalachian Mountains, six sites are distributed along the coastline, and the remaining eight sites are scattered throughout the domain. The objective here is not to evaluate modeled concentrations vis-à-vis observations, but to perform a detailed comparison of the VARTSTEP–CMAQ results with benchmark CMAQ results at these 22 sites where performance is of utmost concern. Figure 4 compares the two sets of model results for daily average $PM_{2.5}$ concentrations at these 22 sites during the 1–20 January 2002 and 12–27 July 2001 periods. Note that all comparisons provided here are for the model layer directly above the ground.

There is strong correlation $R^2 > 0.98$ between the benchmark and the results obtained with VARTSTEP–CMAQ with the exception of a few outliers. VARTSTEP–CMAQ results are higher than the benchmark, on average, by about 1 to 3%. Since visibility is the primary concern in this study and since different components of $PM_{2.5}$ affect visibility differently, it is important to accurately model not just the total $PM_{2.5}$ but its components as well. Sulfate and nitrate particles, in the presence of water vapor, and elemental carbon can be important visibility degradation agents; other particles are relatively less important (Malm et al., 2000). Daily average concentrations of sulfate, nitrate, ammonium, soil, elemental carbon, and organic carbon components of $PM_{2.5}$ were compared at the 22 Class-I areas. The scatter plots in Figure 5 (1–20 January 2002) and 6 (12–27 July 2001) have the concentrations calculated by VARTSTEP–CMAQ on the y -axis and those calculated by CMAQ Version 4.3 on the x -axis.

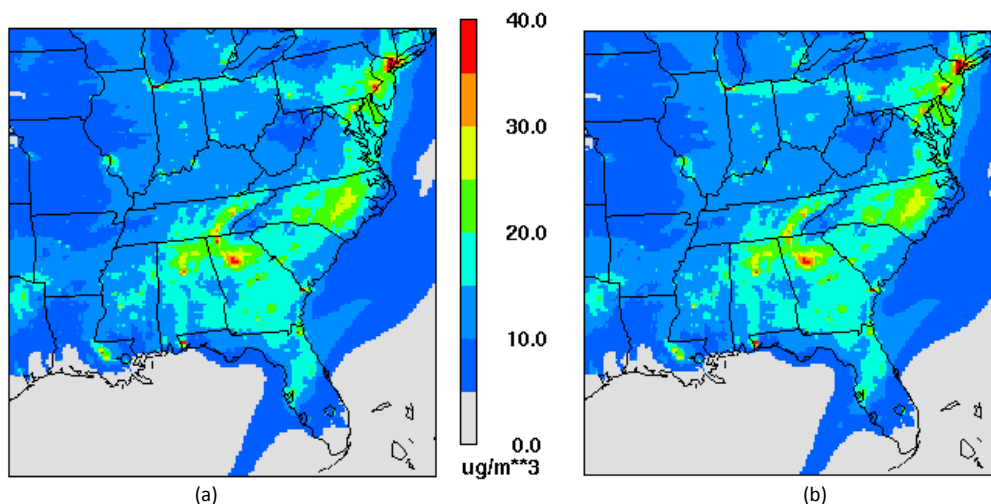


Figure 3. Daily average $PM_{2.5}$ concentrations ($\mu g m^{-3}$) over the Southeastern U.S. on 17 January 2002 as calculated by the benchmark CMAQ simulation (a) and the VARTSTEP–CMAQ simulation (b).

Table 1. CPU^a times per simulated day broken down by process for CMAQ (Version 4.3) and VARTSTEP–CMAQ, and the fraction of the total VARTSTEP savings attributed to each process

| Module | CMAQ (s) | | VARTSTEP–CMAQ (s) | | Fraction of Savings (or Burden) (%) | |
|----------------------|----------------|----------------|-------------------|----------------|-------------------------------------|----------------|
| | Winter episode | Summer episode | Winter episode | Summer episode | Winter episode | Summer episode |
| Vertical Diffusion | 4 148 | 3 226 | 1 850 | 1 398 | 7.51 | 52.5 |
| Horizontal Advection | 7 027 | 4 327 | 8 762 | 5 164 | (5.68) | (24.0) |
| Horizontal Diffusion | 481 | 391 | 1 517 | 1 159 | (3.39) | (22.1) |
| Vertical Advection | 1 027 | 733 | 2 126 | 1 426 | (3.59) | (19.9) |
| Clouds | 555 | 503 | 529 | 476 | 0.09 | 0.76 |
| Chemistry | 8 824 | 9 770 | 8 061 | 8 729 | 2.50 | 29.9 |
| Aerosols | 37 098 | 6 099 | 5 469 | 2 974 | 103 | 89.8 |
| Other | 2 470 | 1 663 | 2 726 | 1 906 | (0.8) | (6.95) |
| TOTAL | 61 630 | 26 712 | 31 040 | 23 232 | 100 | 100 |

^a Single processor 2.8 GHz Intel CPU with dedicated 4 GB memory

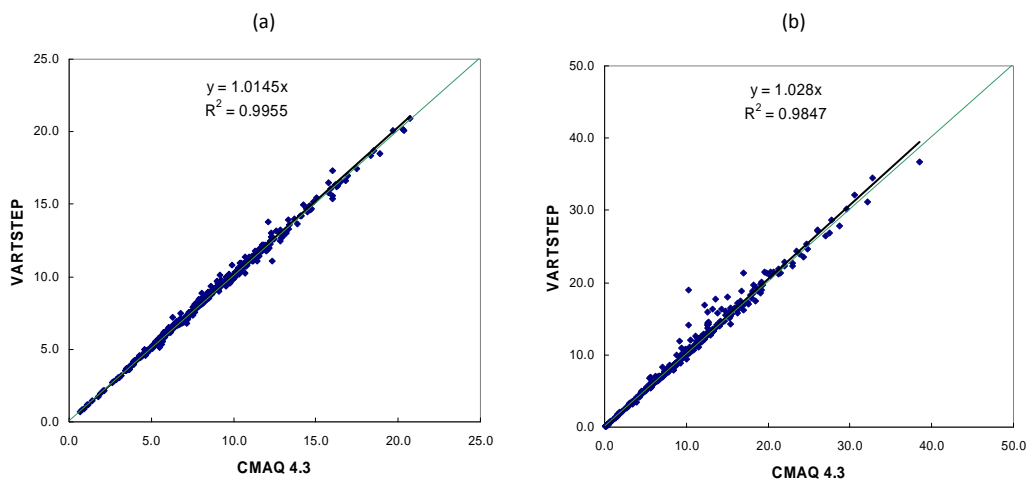


Figure 4. Comparison of daily average $PM_{2.5}$ concentrations ($\mu\text{g m}^{-3}$) calculated by VARTSTEP–CMAQ (y -axis) with the benchmark (x -axis) at 22 Class-I areas in the Southeastern U.S. during 1–20 January 2002 (a) and 12–27 July 2001 (b).

The two model results are highly correlated: R^2 is at least 0.94 (in the case of wintertime sulfate) and 0.98 or higher in the case of nitrate, ammonium soils, elemental carbon, and organic carbon for both episodes. For the winter episode, while sulfate concentrations calculated by VARTSTEP–CMAQ are, on average, 12% higher, the concentrations of nitrate are 5.0% lower than the benchmark (Figure 5). Sulfate is a smaller component of $PM_{2.5}$ than nitrate in winter when relative humidity is also low; therefore, compared to summertime, both sulfate and nitrate have a much smaller impact on visibility. Soil, the second largest component of $PM_{2.5}$, has no bias and ammonium is higher by 2.7%. Elemental carbon, an important contributor to light extinction, has no bias while organic carbon, which is the fourth largest component of $PM_{2.5}$, is 1.1% higher.

For the summer episode, the concentrations of all the $PM_{2.5}$ components calculated by VARTSTEP–CMAQ are highly correlated with the benchmark concentrations (Figure 6). Sulfate is the largest component of $PM_{2.5}$ during this period and, with high summertime relative humidity, it has the largest contribution to light extinction. Its concentrations are, on average, 3.6% higher. Organic carbon, which is the second largest component of $PM_{2.5}$, is higher by 4.6%. Ammonium and soil have almost no bias. Nitrate, the fifth largest summertime $PM_{2.5}$ component, is 5.5% lower. Elemental carbon, the smallest component, but an important visibility degradation agent, is lower by 3.5%.

To see the total impact of $PM_{2.5}$ components on visibility, light extinction, B_{ext} (Mm^{-1}), was calculated using the formula in Malm et al. (2000):

$$B_{\text{ext}} = 3f(RH)\left([SO_4^{2-}] + [NO_3^-] + [NH_4^+]\right) + 4[OC] + 10[EC] + [Soil] + 0.6[CM] + B_{\text{Rayleigh}} \quad (10)$$

where $[SO_4^{2-}]$, $[NO_3^-]$, $[NH_4^+]$, $[OC]$, $[EC]$, and $[Soil]$ are the concentrations ($\mu\text{g m}^{-3}$) of $PM_{2.5}$ associated with sulfate, nitrate, ammonium, organic carbon, elemental carbon, and soils, respectively; $[CM]$ is the concentration of coarse PM; $f(RH)$ is a dimensionless relative humidity adjustment factor, which is different for each Class-I area and varies by the time of the year; and B_{Rayleigh} is the Rayleigh scattering (10 Mm^{-1}). Daily average extinction coefficients derived from CMAQ and VARTSTEP–CMAQ concentrations were compared at the 22 Class-I areas (Figure 7). R^2 is 0.99 for both the 1–20 January 2002 and the 12–27 July 2001 episodes. On average, VARTSTEP–CMAQ light extinction is 1.6% higher than the benchmark during the winter episode and 2.5% higher during the summer episode.

Daily maximum 8-hr ozone concentrations were also compared at the 22 Class-I areas (Figure 8) to see the impact of oxidant concentrations on the $PM_{2.5}$ results above. The correlation between the benchmark and the results obtained with VARTSTEP–

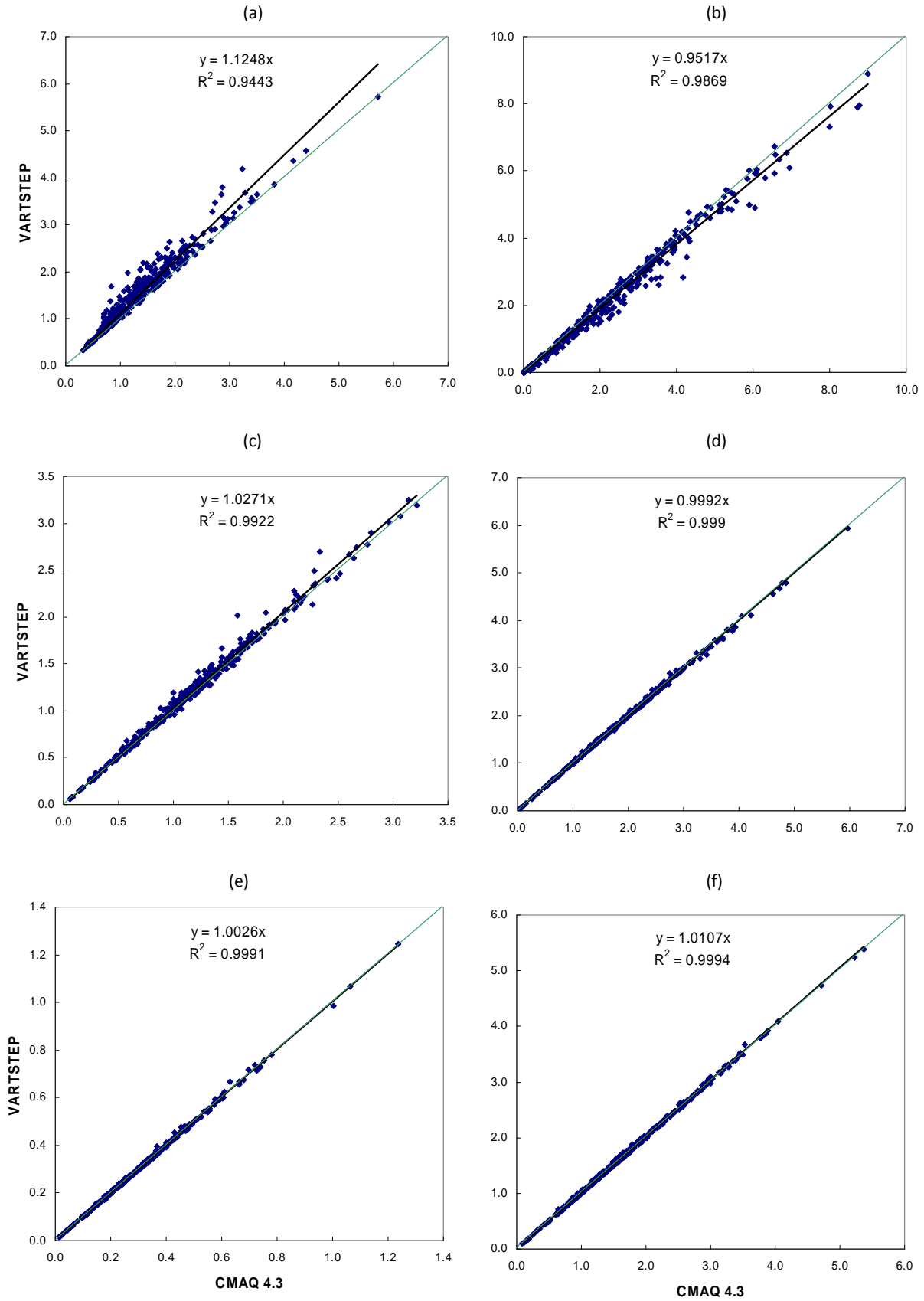


Figure 5. Comparison of daily average concentrations ($\mu\text{g m}^{-3}$) calculated by VARTSTEP–CMAQ (y-axis) with the benchmark (x-axis) for various components of $\text{PM}_{2.5}$ at 22 Class-I areas in the Southeastern U.S. during 1–20 January 2002: (a) Sulfate, (b) Nitrate, (c) Ammonium, (d) Soil, (e) Elemental Carbon, (f) Organic Carbon.

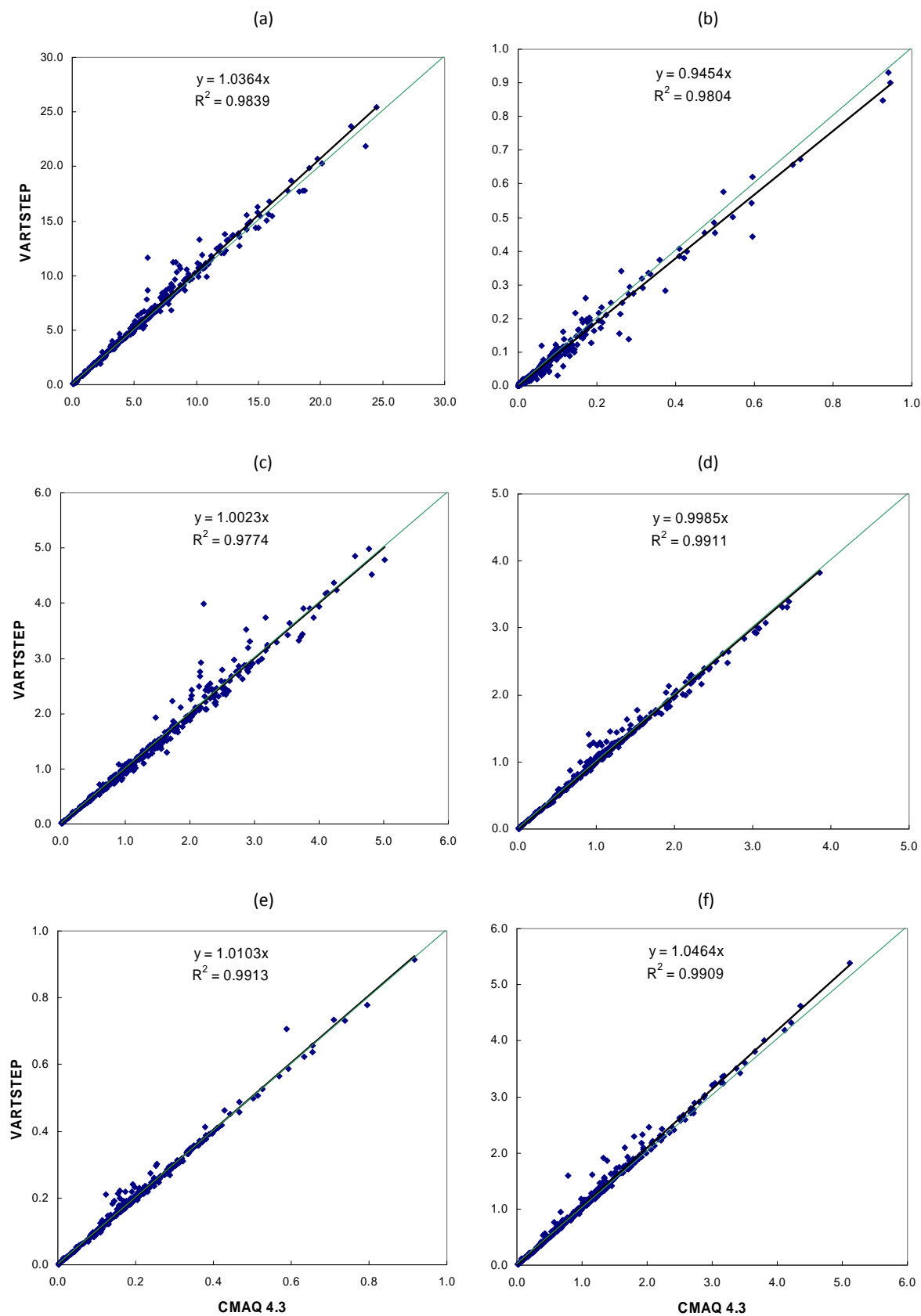


Figure 6. Comparison of daily average concentrations ($\mu\text{g m}^{-3}$) calculated by VARTSTEP-CMAQ (y-axis) with the benchmark (x-axis) for various components of $\text{PM}_{2.5}$ at 22 Class-I areas in the Southeastern U.S. during 12–27 July 2001: (a) Sulfate, (b) Nitrate, (c) Ammonium, (d) Soil, (e) Elemental Carbon, (f) Organic Carbon.

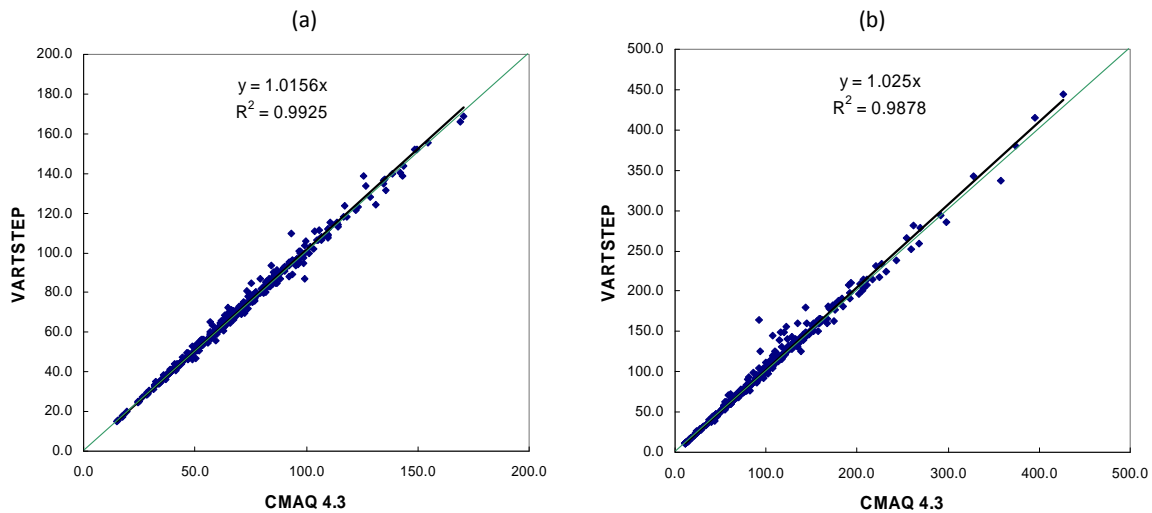


Figure 7. Comparison of daily average light extinction (Mm^{-1}) derived from VARTSTEP-CMAQ (y-axis) with the benchmark (x-axis) at 22 Class-I areas in the Southeastern U.S. during 1-20 January 2002 (a) and 12-27 July 2001 (b).

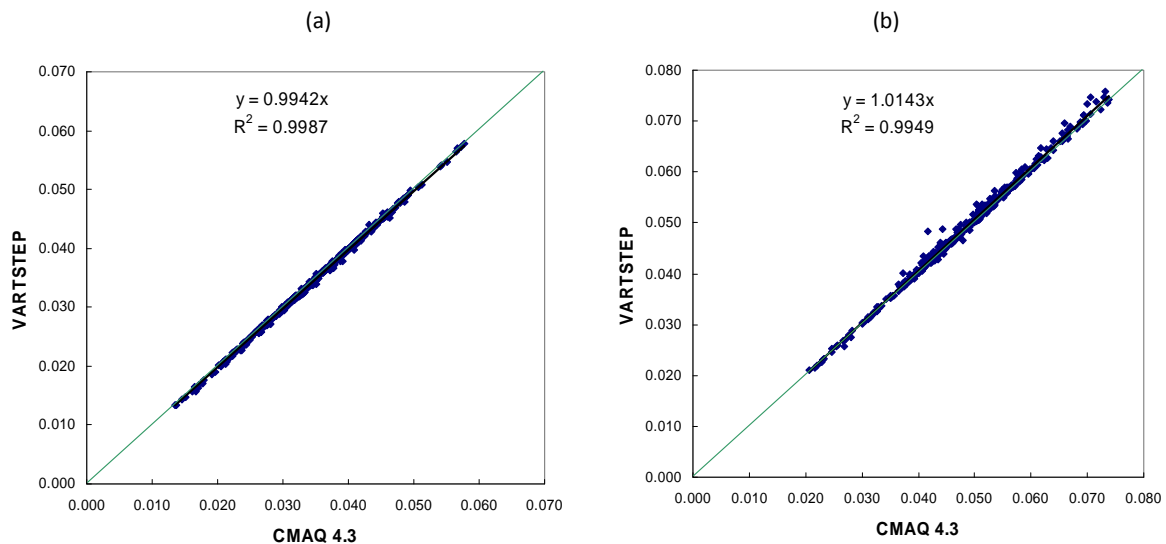


Figure 8. Comparison of daily maximum 8-hr O_3 concentrations (ppm) calculated by VARTSTEP-CMAQ (y-axis) with the benchmark (x-axis) at 22 Class-I areas in the Southeastern U.S. during 1-20 January 2002 (a) and 12-27 July 2001 (b).

CMAQ is strong for both the summer ($R^2 = 1.00$) and the winter episodes ($R^2 = 0.99$). On average, the VARTSTEP-CMAQ ozone concentrations are 1% lower in winter and 1% higher in summer compared to the benchmark.

The higher sulfate and lower nitrate concentrations calculated by VARTSTEP-CMAQ can be explained as follows. With VARTSTEP, the time steps are longer and different processes are coupled less frequently. Therefore, turbulent mixing and dry deposition, which are both performed in the vertical diffusion module, can operate longer on freshly emitted pollutants (emissions are also part of vertical diffusion) before those pollutants have a chance to take part in photochemical reactions in the chemistry module or change phase through condensation (or evaporation) in the aerosol module. The majority of SO_2 emissions are from elevated sources while almost all of the NH_3 emissions are from ground-level sources. In CMAQ (and VARTSTEP-CMAQ), aerosol equilibrium is such that free ammonia first neutralizes sulfate before any ammonium nitrate is formed. Enhanced mixing in VARTSTEP-CMAQ brings more SO_2 in contact with ammonia; therefore, more sulfate is formed whereas the amount of nitrate is diminished. This effect of enhanced mixing is more pronounced in the shallower wintertime boundary layer.

5. Conclusions

Current AQMs use a single, global time step to synchronize different processes in all of the grid cells. When the local characteristic time for various processes is longer than this global time step, computations are inefficient because a result with similar accuracy can be obtained by using a longer time step. The variable time-step algorithm, VARTSTEP, was developed to improve computational efficiency by using local time steps that are more in tune with characteristic process times of each grid cell. A two-dimensional version of the algorithm was implemented in CMAQ; it reduced the computation time by as much as 50% (13% for the less computationally intensive summertime episode). In CMAQ the characteristic time for advection is used to synchronize various processes. Since the CMAQ grid is uniform, all of the variability in local time steps comes from the wind speeds. In a non-uniform grid model such as the adaptive grid version of CMAQ (Garcia-Mendez et al., 2010) the variability would be amplified by varying grid lengths. With larger variability in local time steps, VARTSTEP would provide larger speedups compared to the single, global time step alternative.

The differences between concentration estimates of VARTSTEP–CMAQ and benchmark CMAQ are within 3% for PM_{2.5} but can be larger for certain PM_{2.5} components, especially sulfate and nitrate. Due to enhanced mixing of elevated sulfur emissions with ground-level ammonia emissions, and since free ammonia prefers to neutralize sulfate over nitrate in CMAQ, VARTSTEP results in higher sulfate and lower nitrate concentrations. This is more pronounced in the shallower wintertime boundary layer, when sulfate calculated by VARTSTEP–CMAQ is 12% higher. According to Morris et al. (2005), CMAQ underestimates sulfate by approximately the same amount during the same winter period. This does not necessarily mean that VARTSTEP–CMAQ is a better model than CMAQ. In fact, CMAQ should be more representative of the real atmosphere since it couples the processes, which happen simultaneously in reality, more frequently. However, a possible existing error in CMAQ, for example limited vertical mixing in the boundary layer, may be compensating for the less frequent coupling, leading to the right amount of mixing between the elevated SO₂ and ground-level ammonia emissions in VARTSTEP–CMAQ. More analysis is needed to investigate the exact reason for this favorable result with VARTSTEP–CMAQ.

In the Southeastern U.S., sulfate is a much smaller component of PM_{2.5} in winter (compared to summer); therefore, along with 5.0% lower nitrate, the PM_{2.5} calculated by VARTSTEP is only 1.5% higher than the benchmark. Since different PM_{2.5} components have very different contributions to light extinction, and since sulfate and nitrate are two important contributors, the results for visibility may be very different even though total PM_{2.5} is very similar. Light extinctions were calculated using the IMPROVE formula (Malm et al., 2000). The light extinction calculated from VARTSTEP–CMAQ is 1.6% higher than the benchmark in winter and 2.5% higher in summer. Finally, for ozone, the differences are within 1% in both winter and summer. Clearly, VARTSTEP–CMAQ can produce PM_{2.5}, visibility, and ozone result very similar to CMAQ with greater computational efficiency. The same assessment can be made for most PM_{2.5} components with a few exceptions, sulfates and nitrates in particular. In wintertime source apportionments, VARTSTEP–CMAQ is likely to attribute greater air quality impacts than CMAQ to SO₂ emitting sources, such as coal-fired power plants.

Acknowledgements

This research was supported in part by the Visibility Improvement State and Tribal Association of the Southeast (VISTAS) and by the U.S. Department of Defense, through the Strategic Environmental Research and Development Program (SERDP).

Supporting Material Available

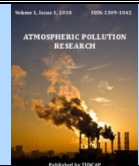
Rotating cone test: (a) Initial cone (b) after 1 rotation using global time step, (c) after 1 rotation with VARTSTEP, (d) difference created by VARTSTEP (Figure S1); Total mass in the grid cells after each time step of the rotating cone test (Figure S2); Daily average PM_{2.5} concentrations over the Southeastern U.S. on 16 July 2001 as calculated by the benchmark CMAQ simulation and the VARTSTEP–CMAQ simulation (Figure S3). This information is available free of charge via the Internet at <http://www.atmospolres.com>.

References

- Anderson, D.A., Tannehill, J.C., Pletcher, R.H., 1984. Computational Fluid Mechanics and Heat Transfer, Hemisphere Publishing Corp, New York, pp. 70-77.
- Blom, J.G., Verwer, J.G., 2000. A comparison of integration methods for atmospheric transport-chemistry problems. *Journal of Computational and Applied Mathematics* 126, 381-396.
- Boylan, J.W., Odman, M.T., Wilkinson, J.G., Russell, A.G., Doty, K.G., Norris, W.B., McNider, R.T., 2002. Development of a comprehensive, multiscale “one atmosphere” modeling system: application to the Southern Appalachian Mountains. *Atmospheric Environment* 36, 3721-3734.
- Byun, D., Schere, K.L., 2006. Review of the governing equations, computational algorithms, and other components of the Models-3 Community Multiscale Air Quality (CMAQ) modeling system. *Applied Mechanics Reviews* 59, 51-77.
- Collela, P., Woodward, P.R., 1984. The piecewise parabolic method (PPM) for gas-dynamical simulations. *Journal of Computational Physics* 54, 174-201.
- Constantinescu, E.M., Sandu, A., Carmichael, G.R., 2008. Modeling atmospheric chemistry and transport with dynamic adaptive resolution. *Computational Geosciences* 12, 133-151.
- Garcia-Menendez, F., Yano, A., Hu, Y., Odman, M.T., 2010. An adaptive grid version of CMAQ for improving the resolution of plumes. *Atmospheric Pollution Research* 1, 239-249.
- Hu, Y., Odman, M.T., Russell, A.G., 2006. Mass conservation in the Community Multiscale Air Quality model. *Atmospheric Environment* 40, 1199-1204.
- Lanser, D., Verwer, J.G., 1999. Analysis of operator splitting for advection-diffusion-reaction problems from air pollution modeling. *Journal of Computational and Applied Mathematics* 111, 201-216.
- Malm, W.C., Pitchford, M.L., Scruggs, M., Sisler, J.F., Ames, R., Copeland, S., Gebhart, G.A., Day, D.E., 2000. *Spatial and Seasonal Patterns and Temporal Variability of Haze and its Constituents in the United States, Report III*, ISSN: 0737-5352-47, Colorado State University: Fort Collins, CO, pp. 3.1-3.38.
- Morris, R.E., McNally, D.E., Tesche, T.W., Tonnesen, G., Boylan, J.W., Brewer, P., 2005. Preliminary evaluation of the Community Multiscale Air Quality Model for 2002 over the Southeastern United States. *Journal of the Air and Waste Management Association* 55, 1694-1708.
- Odman, M.T., Khan, M.N., Srivastava, R.K., McRae, D.S., 2002. Initial application of the adaptive grid air pollution model, in *Air Pollution Modeling and its Application XV*, edited by C. Borrego and G. Schayes, Academic/Plenum Publishers, New York, pp. 319-328.
- Park, R.J., Pickering, K.E., Allen, D.J., Stenchikov, G.L., Fox-Rabinovitz, M.S., 2004. Global simulation of tropospheric ozone using the University of Maryland Chemical Transport Model (UMD-CTM): 2. Regional transport and chemistry over the central United States using a stretched grid. *Journal of Geophysical Research D: Atmospheres* 109, art. no. D09303.
- Sportisse, B., 2000. An analysis of operator splitting techniques in the stiff case. *Journal of Computational Physics* 161, 140-168.
- Strang, G., 1968. On the construction and comparison of difference schemes. *SIAM Journal of Numerical Analysis* 5, 506-517.

Appendix C: Adaptive grid CMAQ

Garcia-Menendez, F., A. Yano, Y. Hu, and M. T. Odman, 2010: An adaptive grid version of CMAQ for improving the resolution of plumes. *Atmospheric Pollution Research*, 1, 239-249 (doi: 10.5094/APR.2010.031).



An adaptive grid version of CMAQ for improving the resolution of plumes

Fernando Garcia–Menendez, Aika Yano, Yongtao Hu, M. Talat Odman

School of Civil and Environmental Engineering, Georgia Institute of Technology, 311 Ferst Drive, Atlanta, GA 30332-0512, USA

ABSTRACT

Atmospheric pollutant plumes are not well resolved in current air quality models due to limitations in grid resolution. Examples of these include power plant and biomass burning plumes. Adequate resolution of these plumes necessitates multiscale air quality modeling at much finer scales than currently employed and we believe that adaptive grids could be the best approach to accurate fine-scale modeling of air pollution dynamics and chemistry. An adaptive grid version of the CMAQ model with all necessary functions for tracking gaseous pollutants and particulate matter has been developed. The model incorporates a dynamic, solution-adaptive grid algorithm and a variable time step algorithm into CMAQ, while retaining the original functionality, concept of modularity, and grid topology.

The adaptive model was evaluated by comparing its performance to that of the standard, static grid CMAQ in simulating particulate matter concentrations from a biomass burning air pollution incident affecting a large urban area. The adaptive grid model significantly reduced numerical diffusion, produced better defined plumes, and exhibited closer agreement with monitoring site measurements. The adaptive grid also allows impacts at specified locations to be attributed to a specific pollutant source and provides insight into air pollution dynamics unattainable with a static grid model. Potential applications of adaptive grid modeling need not be limited to air quality simulation, but could be useful in meteorological and climate models as well.

Keywords:

Adaptive mesh refinement
Modeling of plumes
Air quality
Biomass burning
Particulate matter

Article History:

Received: 11 April 2010
Revised: 20 August 2010
Accepted: 11 September 2010

Corresponding Author:

M. Talat Odman
Tel: +1-404-894-2783
Fax: +1-404-894-8266
E-mail: talat.odman@ce.gatech.edu

© Author(s) 2010. This work is distributed under the Creative Commons Attribution 3.0 License.

doi: 10.5094/APR.2010.031

1. Introduction

The dynamic and chemical processes of air pollution involve a wide range of scales. While the initial transformation of emissions and dispersion of plumes occur on relatively small scales, long-range transport engages much larger scales. Air quality models rely on their grids for explicit resolution of processes involved; the processes that occur on sub-grid scales are parameterized. Modeling large geographic regions with uniform resolution at the finest relevant scale is beyond the realm of current computers; therefore, regional models generally settle for coarser grid resolution. When emissions or plumes are injected into grid cells coarser in size than characteristic plume dimensions, they instantaneously mix with the contents of the grid cell. Such mixing is unrealistic; it dilutes the plumes and the details of the near-field chemistry are lost. Multiscale models have been proposed to surpass the limitations of single scale models. Conceptually, a multiscale model blends small scales with large scales and assigns the most appropriate scales to the phenomenon being modeled.

The approaches to multiscale air quality modeling generally fall into one of the following two categories. The first category features static grids that can be nested multiple levels deep for better resolution of finer scale processes. This is the approach taken in the Community Multiscale Air Quality Model (CMAQ) (Byun and Schere, 2006). The second approach involves grids whose resolutions continuously adapt to the needs of a particular phenomenon throughout the simulation. Note that we did not distinguish sub-grid modeling as a separate category in our classification. Embedding a sub-grid scale model into the grid

model (e.g., plume-in-grid modeling) is a multiscale modeling technique that can be used both with static grid nesting and dynamic grid adaptations.

In static grid nesting, finer grids (FGs) are nested inside coarser ones (CGs). Multilevel nests can be placed to resolve the plumes of interest; however, since wind direction can change during the simulation, there must be fine resolution all around the emission source (e.g., power plant or industrial facility). There are two types of grid nesting: one-way and two-way. In one-way nesting, the CG provides boundary conditions to the FG and no feedback is allowed from the FG to the CG; therefore, the CG and FG can be modeled sequentially. CMAQ uses one-way nesting. In two-way nesting, there is full interaction between the grids and all grids must be modeled simultaneously. The biggest limitation of static grid nesting is that resolution and the extent of each grid must be determined a priori and remain fixed throughout the simulation. One has to make sure that the right choices of scale and coverage are made at the beginning of the simulation.

In dynamic grid adaptations, the grid resolution changes continuously and automatically to improve the ability of the model, to capture detailed dynamics or follow the chemical evolution of plumes. For example, refining the grid where chemical reactivity is high can lead to better characterization of the interactions of pollutant plumes with ambient atmospheres. Similarly, the passage of a front, clouds, and other relevant dynamic features can all be better resolved if dynamic adaptations are used. Dynamic adaptive grids were suggested for use in

atmospheric modeling few decades ago, but did not gain wide-spread acceptance.

Several adaptive grid algorithms were developed specifically for air quality modeling during the last decade. Although these algorithms did not necessarily make their way into functional air quality models, they were quite useful in determining the limitations of alternative approaches. For example, Tomlin et al. (1997; 2000) developed an unstructured grid algorithm for the purpose of resolving pollutant plumes in the boundary layer (Tomlin et al., 1997; Ghorai et al., 2000; Tomlin et al., 2000). This algorithm could have been linked with an adaptive grid meteorology model that also employs unstructured grids (e.g., Bacon et al., 2000) and developed into a transport–chemistry coupled with dynamics modeling system. However, this did not happen. The reason may be the difficulties involved in transferring existing air pollution modeling technologies to unstructured grids. On the other hand, the adaptive grid algorithm developed by Srivastava et al. (2000; 2001a; 2001b) is based on structured grids and may be easier to implement in an air quality modeling system.

Although some adaptive grid air pollution models were developed (e.g., Odman et al., 2001; Odman et al., 2002; Constantinescu et al., 2008), they were limited to gas–phase chemistry. No effort has been reported towards the development of an adaptive grid transport–chemistry model for particulate matter (PM) or the incorporation of any adaptive grid capability into community models. However, dynamic grid adaptations in a community model such as CMAQ can significantly improve modeling, hence the assessment of the air quality impacts, of plumes from specific emission sources, such as power plants or biomass burns.

This paper continues with a description of how an adaptive grid version of the CMAQ model has been developed based on the adaptive grid algorithm by Srivastava et al. (2000) and the adaptive grid air pollution model by Odman et al. (2001). This is followed by a brief account of the model code verification. The adaptive grid version of CMAQ is then applied to the simulation of a biomass burning plume and compared to the standard, static grid version in terms of plume resolution and agreement with ground–level observations.

2. Model Development Methodology

The purpose of this work is to obtain more accurate solutions from the CMAQ model for better assessment of the air quality impacts of plumes. The accuracy of the solution of a numerical model can be increased by either using higher order approximations (a.k.a. p–refinement) or by refining the grid. There are two common grid refinement methods: (1) increasing the number of grid elements (h–refinement); and (2) maintaining the same number of grid elements but refining the grid by repositioning the nodes (r–refinement). In adaptive grid refinement, h– or r–, the objective is to generate an optimal grid with available computational resources for the most accurate solution.

The adaptive grid refinement method used here falls into the r–refinement category. It employs a constant number of grid nodes. An important characteristic of the algorithm is that it utilizes a structured grid that partitions a rectangular domain into N by M quadrilateral cells. The nodes move throughout the simulation but the topology of the grid remains the same. In other words, each node is still connected to the same neighboring nodes and each cell still has the same neighboring cells after the movement. However, the length of the links between nodes and the area of the grid cells change. One advantage of retaining the structure of the grid is that the non–uniform grid in the physical space can be mapped onto a uniform grid in the computational space through a coordinate transformation. The solution of partial differential equations that govern atmospheric diffusion is simpler

on a uniform grid. Another advantage that cannot be achieved by an unstructured grid is compatibility with CMAQ. Not only can the numerical solution schemes developed for CMAQ be used after the coordinate transformation, but the sub–grid parameterizations in CMAQ can be adopted as well (as long as they remain valid within the range of adaptive grid scales). Since these parameterizations assume a certain grid topology, they are generally incompatible with unstructured grids.

The time integration of the governing equations on a dynamic adaptive, i.e. moving, grid can be viewed as a two–step operation. In the first step, *the solution step*, the grid movement is frozen in time and the equations are solved on this stationary grid. In the second step, *the adaptation step*, the grid nodes are moved through the solution, i.e. concentration, fields obtained in the first step. As a result of the movement of the grid nodes to new locations, it will appear as if fluxes are crossing the faces of the grid cells. Ideally, the adaptation step should be repeated after each solution step owing to the change in resolution requirements. However, since frequent adaptations may be computationally restrictive, we have chosen to apply the adaptation step less frequently than the solution step. A logical choice was to perform grid adaptation once every output time step as, in CMAQ, the partial solutions for different processes are guaranteed to synchronize before the solution is outputted. However, considering that an hour, the typical output time step in CMAQ, may be too long without any adaptation, the output time step was reduced to 15 minutes.

Development of the adaptive grid CMAQ (AG–CMAQ) involved four major tasks: (1) reformulation of governing equations in general curvilinear coordinates; (2) implementation of spatially varying time steps; (3) incorporation of the adaptive grid algorithm; and, (4) consideration of meteorological data and emissions. The first two tasks are related to the solution step. The third and fourth tasks belong to the adaptation step. These four tasks will be described next. The section will end with a brief account of the code verification procedure.

2.1. Governing equations and coordinate transformation

CMAQ is based on the species continuity equation that relates the rate of change of the concentration of species n , c_n , to transport and chemistry as follows:

$$\frac{\partial(\gamma c_n)}{\partial t} + \frac{\partial(\gamma U c_n)}{\partial X} + \frac{\partial(\gamma V c_n)}{\partial Y} + \frac{\partial(\gamma \dot{\sigma} c_n)}{\partial \sigma} + \frac{\partial}{\partial X} \left(\gamma K^{xx} \frac{\partial c_n}{\partial X} \right) + \frac{\partial}{\partial Y} \left(\gamma K^{yy} \frac{\partial c_n}{\partial Y} \right) + \frac{\partial}{\partial \sigma} \left(\gamma K^{\sigma\sigma} \frac{\partial c_n}{\partial \sigma} \right) = \gamma R_n + \gamma S_n \quad (1)$$

where X and Y are the coordinates on a conformal map of Earth and σ is a terrain–following normalized vertical coordinate. Hence, the spherical shape of Earth and the irregularity of its surface already necessitated coordinate transformations, and γ is the Jacobian of these transformations:

$$\gamma = \frac{1}{m^2} \frac{\partial z}{\partial \sigma} \quad (2)$$

Here m is the scale factor of a conformal map projection, i.e., the ratio of the distance on map to distance on Earth. A popular normalized vertical coordinate is sigma–p (pressure) which is related to the altitude coordinate z as $\partial z / \partial \sigma = p^* / \rho g$, where p^* is the pressure difference between the surface and the top of the domain, ρ is the air density, and g is the gravitational acceleration. In Equation (1), U and V are the wind velocity components in the X and Y directions after scaling by m , and $\dot{\sigma}$ is a non–dimensional velocity component in the σ direction. K^{xx} ,

K^{yy} and $K^{\sigma\sigma}$ are the elements of the diagonal turbulent diffusivity tensor with $K^{\sigma\sigma}$ related to vertical diffusivity K^{zz} as:

$$K^{\sigma\sigma} = \left(\frac{\partial\sigma}{\partial z} \right)^2 K^{zz} \quad (3)$$

R_n and S_n are the chemical reaction and emission terms for species n . There are also terms related to aerosol and cloud processes in CMAQ, but they are not shown here for simplicity.

One more coordinate transformation was necessary to develop AG-CMAQ, and that is the transformation of the horizontal space from the (X, Y) coordinate system to a curvilinear coordinate system (ξ, η) :

$$\begin{aligned} \xi &= \xi(X, Y) \\ \eta &= \eta(X, Y) \end{aligned} \quad (4)$$

Through this transformation, the adaptive grid that is non-uniform in (X, Y) space becomes a uniform grid in (ξ, η) space. The governing equations in (ξ, η, σ) space can be derived from Equation (1) above through the use of the chain rule for derivatives:

$$\begin{aligned} \frac{\partial(Jc_n)}{\partial t} + \frac{\partial(Jv^\xi c_n)}{\partial \xi} + \frac{\partial(Jv^\eta c_n)}{\partial \eta} + \frac{\partial(J\sigma c_n)}{\partial \sigma} + \frac{\partial}{\partial \xi} \left(JK^{\xi\xi} \frac{\partial c_n}{\partial \xi} \right) \\ + \frac{\partial}{\partial \eta} \left(JK^{\eta\eta} \frac{\partial c_n}{\partial \eta} \right) + \frac{\partial}{\partial \sigma} \left(JK^{\sigma\sigma} \frac{\partial c_n}{\partial \sigma} \right) = JR_n + JS_n \end{aligned} \quad (5)$$

In this equation, the new Jacobian, J , is related to γ as:

$$J = \left(\frac{\partial X}{\partial \xi} \frac{\partial Y}{\partial \eta} - \frac{\partial Y}{\partial \xi} \frac{\partial X}{\partial \eta} \right) \gamma \quad (6)$$

and v^ξ and v^η are the non-dimensional components of the wind velocity vector in the ξ and η directions related to U and V as:

$$\begin{aligned} v^\xi &= \frac{\partial \xi}{\partial X} U + \frac{\partial \xi}{\partial Y} V \\ v^\eta &= \frac{\partial \eta}{\partial X} U + \frac{\partial \eta}{\partial Y} V \end{aligned} \quad (7)$$

The expressions for the elements of the turbulent diffusivity tensor $K^{\xi\xi}$, $K^{\eta\eta}$ are rather long and they will not be included here.

Now that the grid is uniform in (ξ, η) space, it is much easier to solve the Equation (5). In fact, since the finite difference stencils in the ξ and η directions are the same as the stencils used in the X and Y directions in CMAQ, the solution algorithms can be taken directly from CMAQ. In addition, the parameterizations that only involve the vertical direction (e.g., cumulus parameterization) are directly applicable since we did not transform the vertical coordinate. The metric derivatives in Equations (6) and (7) are calculated after each grid adaptation step using finite differences at the most appropriate locations (i.e., at the grid nodes or at the centers of the grid cells), stored as global variables, and then passed to various process modules that need them.

2.2. Variable time-step algorithm

In CMAQ, Equation (1) is solved using a method called process splitting where the rate of change of concentrations in one time step is broken into components associated with each process. These processes (i.e., advection, diffusion, and chemistry, as well as the aerosol and cloud processes) not shown in Equation (1), are

applied to the concentration fields sequentially. After all the processes are applied for one time step, the solution is complete. The time step used for advancing split processes in CMAQ is determined by the characteristic time for advection. The goal is to complete the process cycle before any material is advected by more than one grid cell distance. This is ensured by selecting a time step less than the grid size divided by the wind speed. This also satisfies the Courant stability condition for explicit advection schemes. Since the grid size is uniform in CMAQ, the maximum wind speed determines the time step for the entire domain. Note that using a time step much smaller than a cell's characteristic time step does not make the solution more accurate; therefore, having a single global time step is computationally inefficient. In AG-CMAQ, the grid size is not uniform and the minimum ratio of grid size to wind speed (i.e. a relatively small grid size and a relatively large wind speed) determines the time step. Since the smallest and largest grid sizes can differ by orders of magnitude, the inefficiency becomes a serious bottleneck. Odman and Hu (2007) developed an algorithm that overcomes the global time step limitation by allowing the use of local time steps.

In the variable time step algorithm, VARTSTEP (Odman and Hu, 2010), every cell is assigned its own local time step, which must be an integer multiple of the smallest time step in the domain and a whole divisor of the model's output time step. For example, if the smallest time step in the domain is 1 minute and the output time step is 15 minutes, the allowable local time steps are 1, 3, 5, and 15 minutes. Considering that the length scales may be as small as 10 m in AG-CMAQ, and with a 10 m s⁻¹ wind speed a time step of 1 s may be necessary, the lower bound for local time steps was decreased to 1 second. With this adjustment, there is now a much wider range of possible local time steps than in the above example. The model clock time, t , is advanced by the minimum time step in the domain. When the clock strikes a multiple of the local time step, the grid concentration is advanced by the local time step by applying the changes resulting from different processes.

Greatest computational savings can be expected in chemistry and aerosol processes that are independent from neighboring cell concentrations because the changes due to those processes can be computed at the frequency of the local time steps. On the other hand, transport processes involve neighboring cell concentrations; therefore, they must be computed more frequently than the local time step. The transport fluxes from neighboring cells must be kept in reservoirs until the concentrations are updated. This increases the memory requirements with respect to CMAQ by an array equal in size to the concentration array. Horizontal advection in all grid cells is computed at the frequency of the minimum time step in the domain. Chemistry and aerosol processes are computationally more intensive than horizontal advection in CMAQ (Odman and Hu, 2010). As a result, the local time stepping enabled by VARTSTEP makes AG-CMAQ much more computationally efficient than its predecessors (Odman et al., 2001; Odman et al., 2002).

2.3. Adaptive grid algorithm

As mentioned before, a simulation with AG-CMAQ has two fundamental steps: the solution step, as described above, and the grid adaptation step that will be described here. The purpose of grid adaptation is to locally increase or decrease grid resolution such that a more accurate solution can be obtained in the following solution step. The solution (i.e., concentration) fields remain unchanged during the adaptation step. The grid nodes are clustered in regions where finer resolution is needed for an accurate solution.

The grid adaptation methodology used here is based on the Dynamic Solution Adaptive Grid Algorithm (DSAGA) described in Srivastava et al. (2000). In this algorithm, the movement of the grid nodes is controlled by a weight function. The grid resolution is increased by clustering the grid nodes around regions where the

weight function bears large values. Since the number of nodes is constant, refinement of the grid in some regions of the domain is accompanied by coarsening in other regions where the weight function has smaller values. In this manner, a multiscale grid is obtained where the scales change gradually. Unlike nested grids, there are no fine-to-coarse grid interfaces, which may introduce numerical difficulties due to the abrupt change (i.e. discontinuity) of grid scales. In practice, the number of grid nodes is selected according to the computational resources available. By distributing the grid nodes automatically throughout the modeling domain, DSAGA makes optimal use of computational resources throughout the simulation.

The weight function must be able to determine where grid nodes are to be clustered for a more accurate solution. A linear combination of the errors in concentrations of various chemical species makes an ideal weight function because it will assume large values where the errors are large:

$$w = \sum_n \alpha_n \nabla^2 c_n \quad (8)$$

where w is the weight function; ∇^2 , the Laplacian, is a measure for the numerical error in C_n and α_n is a coefficient that adjusts the weight of the numerical error in species n with respect to the others. The different chemical mechanisms used in CMAQ all have a large number of species. Each one of these species may have very different resolution requirements. Therefore, no single set of α_n can guarantee accurate solutions for all applications. In what follows, the focus was on PM emissions from biomass burning; therefore, all α_n were set to zero, except for those of primary PM species. In applications involving secondary pollutants (e.g., ozone or secondary organic aerosols) the proper choice of α_n may not be as obvious and may require some experimentation. For example, a weight function combining nitrogen oxides (NO_x), volatile organic compounds (VOCs) and ozone is likely to produce the best grid for capturing ozone formation. Odman et al. (2002), Khan (2003), and Constantinescu et al. (2008) tried weight functions with different combinations of α_n for NO_x , VOC, and ozone, in applications to urban and power plant plumes.

The current grid adaptation in AG-CMAQ is in the horizontal plane only, i.e., the resulting grid is the same in all vertical layers. Therefore, surface or any other layer concentrations, or vertical column totals may be used in Equation (8). Using the weight function, the new position of the grid node i , \bar{P}_i^{new} , is calculated as follows:

$$\bar{P}_i^{new} = \frac{\sum_{k=1}^4 w_k \bar{P}_k}{\sum_{k=1}^4 w_k} \quad (9)$$

Here, \bar{P}_k , $k=1, \dots, 4$ are the original positions of the centroids of four grid cells that share the grid node i in the horizontal plane, and w_k is the value of the weight function at each centroid. Although only X and Y change and σ remains the same after adaptation, the grid node coordinates (X, Y, σ) were stored in a 3-D array, $XGRID$, to allow for vertical adaptation in the future. $XGRID$ is passed as an argument to all of the process modules.

The movement of grid nodes in a steady concentration field results in fluxes crossing the boundaries of the grid cells. In this respect, grid adaptation is similar to advection where the grid boundaries are fixed but the field is moving due to wind velocity. Another way of attacking the problem is to observe that after the grid adaptation each grid cell encloses a different portion of the domain, hence a different plot of the concentration field. Therefore, cell-average concentrations must be recomputed. This is more similar to interpolation. Since interpolation is numerically equivalent to advection (Smolarkiewicz and Grell, 1992), either

way of thinking is acceptable. We used a high-order accurate and monotonic advection scheme known as the piecewise parabolic method (Colella and Woodward, 1984) to determine the concentrations of grid cells after adaptation.

Grid adaptation is an iterative process that continues until the optimal grid is found. Note that the concentration field must be redistributed (i.e., interpolated as described above using the advection scheme) to the new grid locations and the weight function must be recalculated at every iteration. The grid is considered to have converged when the new positions in Equation (9) are the same, i.e., within a preset tolerance, as the old positions. A very small tolerance may lead to a large number of iterations. On the other hand, a large tolerance may not yield adequate grid resolution for minimizing the numerical error in concentrations. After rigorous testing with alternative values of the tolerance, we decided to stop iterating when, for any grid node, the movement is less than 5% of the minimum distance between the node in question and the four nodes to which it is connected in the horizontal plane.

2.4. Meteorological data and emissions

After the grid adaptation, meteorological data and emissions are needed on the new grid locations for the next solution step. For meteorological data, an ideal solution would be to have a meteorological model that can operate on the same adaptive grid and run in parallel with AG-CMAQ. The weight function that drives grid adaptations can include functions of meteorological variables such as vorticity. Such an adaptive grid meteorological model can also resolve local circulations that cannot be detected by static grid meteorological models, even at very fine (e.g., 1-km) grid resolutions. Recently, an adaptive grid version of the MM5 numerical weather prediction model was developed based on DSAGA for the purpose of predicting optical turbulence in the upper atmosphere (Xiao et al., 2006). However, at the time of the present study, that model was still under evaluation for applications within the boundary layer. In the absence of an adaptive grid meteorology model, the best available option was to obtain the data from a high-resolution, static-grid meteorological model, store it in a uniform grid input file at 15-minute frequency and, when needed in AG-CMAQ, interpolate onto the adaptive grid. The interpolation weights were calculated after each grid adaptation step and stored as global variables, in the same manner as the metric derivatives.

The processing of emissions is computationally expensive, requiring relocation of various emission sources in the adapted grid cells. Khan et al. (2005) developed efficient search and intersection algorithms for emissions processing. Here, we treated all emissions either as foreground or background emissions. For example, if AG-CMAQ is being used to resolve a biomass burning plume, the emissions from that burn are considered to be in the foreground, while all other emissions (e.g., power plant, industrial, traffic, and biogenic emissions) are in the background. If the foreground emissions are from a stack (e.g., a power plant), the position of the stack must be relocated on the grid as the cell containing the stack may have changed after grid adaptations. If the foreground emissions are from an area source (e.g. a forest fire) then the area of the source must be intersected with the adaptive grid. Since the focus is usually on a few foreground sources, these search and intersection operations are not very intensive. In order to avoid higher computational costs associated with processing of emissions, background emissions are all merged and mapped onto a uniform high-resolution *emissions grid*. Each adaptive grid cell intersects with a number of emissions grid cells. The polygonal intersections of emissions grid cells with adaptive grid cells are calculated and stored as global variables after the grid adaptation step. When emissions are needed during the solution step, the fluxes are read from the emissions input file and apportioned to

the adaptive grid cells using these polygonal intersections as described in Odman et al. (2002).

2.5. Code verification

The development of AG-CMAQ was a major undertaking. In addition to adding the adaptive grid related modules, important modifications had to be made to the base CMAQ code; however, special care was taken to remain faithful to the original modularity concept. Several rounds of code reviews were conducted by at least two authors critically examining the code together and making sure that it reflects the intent of the methodology. As a side benefit of these reviews, a few deeply hidden bugs were discovered in the base CMAQ code (see "Bug Alerts" under <http://people.ce.gatech.edu/~odman>). Finally, carefully designed tests were executed to complete the verification of the AG-CMAQ code.

Two of those code verification tests were most useful. In the first test, results from a standard, static-grid CMAQ simulation were compared to those obtained from AG-CMAQ without activating any grid adaptation. The measure of success in this test would be the similarity of results from the newly developed code to the benchmark. Emission data and model inputs corresponding to a controlled forest fire performed at Ft. Benning, Georgia on April 9, 2008 were used in the simulations. The results from the application of AG-CMAQ without adaptation were practically the same to those from the static grid CMAQ, except for very small and random differences, mostly in biogenic organic and nitrate aerosol concentrations ($< 0.1 \mu\text{g m}^{-3}$). A second verification test was carried out to observe the performance of AG-CMAQ with grid adaptation in the simulation of the same controlled forest fire. In this test, to refine the grid around the fire plume in AG-CMAQ, fine particulate matter ($\text{PM}_{2.5}$) concentration was used as the adaptation variable. Modeled surface-level $\text{PM}_{2.5}$ concentration fields are shown in Figure 1. The results from AG-CMAQ were as expected: grid resolution was increased in the regions of highest $\text{PM}_{2.5}$ concentration. In the area of highest resolution, grid cell size was reduced down to approximately $100 \text{ m} \times 100 \text{ m}$ from the initial grid dimensions of $1.3 \text{ km} \times 1.3 \text{ km}$. A reduction in the artificial dispersion of the plume, typical of photochemical models, was also evident from the simulation.

3. Model Evaluation Results and Discussion

In previous studies, the adaptive grid algorithm was evaluated using problems with increasing complexity and relevance to air quality modeling. Starting with pure advection tests (Srivastava et

al., 2000), idealized reactive flow (Srivastava et al., 2001a) and plume dispersion cases (Srivastava et al., 2001b) were simulated using DSAGA. The performance of the algorithm in tracking multiple urban and power plant plumes was also demonstrated (Khan et al., 2005). In all these applications, the adaptive grid solution was more accurate than the static, uniform grid solution with the same number of grid nodes. Here, the algorithm will be evaluated in AG-CMAQ by a regional-scale air quality simulation that involves a biomass burning event.

In the U.S., controlled forest fires, or prescribed burns, are successfully applied as a land management strategy. Prescribed burns are commonly carried out throughout the Southeastern U.S. and have proven to be effective towards accomplishing different objectives such as habitat restoration, wildfire prevention, endangered species protection, site preparation for seeding and planting, disease control, and appearance enhancement, among others. However, pollutants emitted from prescribed burns may be transported and react to form other pollutants, contributing to poor air quality in downwind urban areas. In the Southeastern U.S., prescribed burns are an important source of primary $\text{PM}_{2.5}$ and gaseous pollutants. One study found that in this region forest fires account for approximately 20% of $\text{PM}_{2.5}$ emissions, 8% of carbon monoxide emissions, and 6% of organic compound emissions (Lee et al., 2005).

Air pollution episodes caused by prescribed burning are excellent examples of highly concentrated events occurring at a finer, local scale with an impact that transitions into a larger, regional scale downwind. Prescribed burn plume development typically occurs at scales below those suitable for existing photochemical models due to limitations in grid resolution. In this initial evaluation of AG-CMAQ performance, we analyzed the simulation of a large prescribed burn incident affecting a large urban area. However, AG-CMAQ can be applied to any type of pollution plume and is not limited to those resulting from prescribed burns or forest fires. Our evaluation compares the performance of AG-CMAQ and a standard static grid version of CMAQ. Differences in the simulation results were determined from surface level pollutant concentrations and 3-dimensional visualizations of modeled plumes. Additionally, modeled concentrations are compared to measurements from 6 monitoring stations impacted by the analyzed smoke incident.

3.1. Application

On 28 February 2007, air quality in the Atlanta metropolitan area was impacted by heavy smoke caused by prescribed burns.

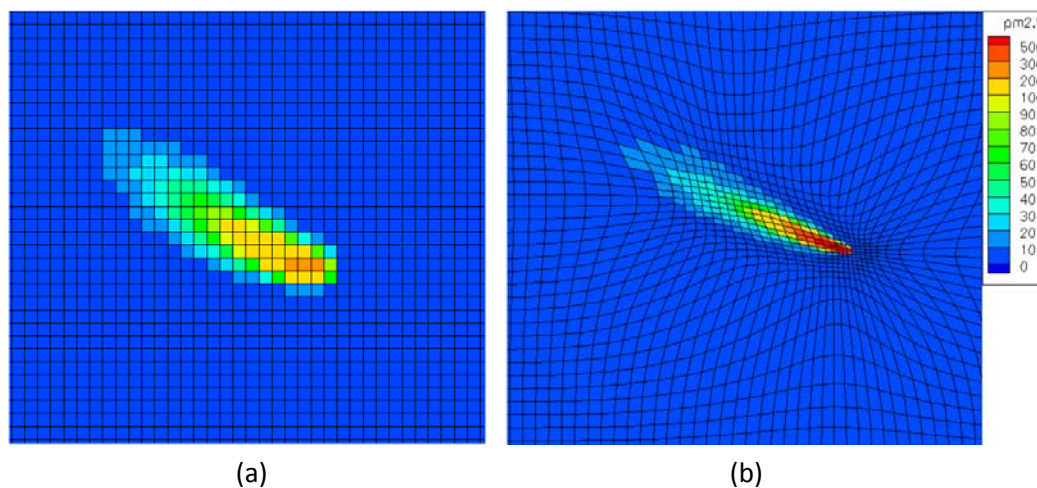


Figure 1. Comparison of $\text{PM}_{2.5}$ concentrations ($\mu\text{g m}^{-3}$) at Fort Benning, Georgia (U.S.A.) during a prescribed burn on 8 April 2008: **(a)** standard CMAQ with 1.33 km grid resolution, **(b)** adaptive CMAQ with dynamically adapting mesh. This figure was originally published in 'Air Pollution Modeling and its Application XX', D.G. Steyn, S.T. Rao, Springer Science + Business Media, 2010, p. 191.

Within hours, $PM_{2.5}$ levels at monitoring sites throughout the area increased to nearly $150 \mu\text{g m}^{-3}$ and ozone levels exhibited increments as large as 30 ppb (Hu et al., 2008). Although several prescribed burns were carried out throughout the day, the dramatic increase in pollution levels is mainly attributed to 2 prescribed burns 80 km southeast of Atlanta, one in the Oconee National Forest and another in Piedmont National Wildlife Refuge. In these burns, about 12 km^2 of land were subjected to treatment. Simulation of the 28 February Atlanta smoke episode with CMAQ at 4-km resolution has been previously carried out and is discussed in Hu et al. (2008). Though the predicted hourly maximum $PM_{2.5}$ in the Atlanta metropolitan area followed a trend similar to the observed hourly maximum $PM_{2.5}$ in the area, the simulation failed to place the plume in the right place at the right time. Since the smoke from prescribed burns was detected at multiple local monitoring sites, this event provides a unique opportunity to evaluate AG-CMAQ and compare its performance to standard CMAQ.

In this study, we used the Weather Research and Forecasting model (WRF, version 2.2) (Michalakes et al., 2005) for meteorology and the Sparse Matrix Operator Kernel Emissions model (SMOKE, version 2.1) (Coats, 1996) for emissions other than biomass burning. The WRF simulation started from a 12-km grid over the South-eastern U.S. and nested down to the 4-km grid over Georgia. Analysis products from the North American Mesoscale (NAM) model (nomads.ncdc.noaa.gov) were utilized to initialize WRF, constrain boundary conditions, and nudge simulated fields at 6-h intervals. The emission inventory used as input to SMOKE is projected from a 2002 “typical year” inventory developed for Southeastern U.S. (MACTEC, 2008). The biomass burning emissions were estimated by the Fire Emission Production Simulator (FEPS) (Sandberg et al., 2005) using the information collected and prepared after the burns (Hu et al., 2008). This information includes the actual area burned each hour, fuel moisture, fuel consumption estimated using the Consume 3.0 model (<http://www.fs.fed.us/pnw/fera/research/smoke/consume/index.shtml>), and hourly combustion phase (flaming or smoldering) information. We also used local meteorology and plume temperature data to estimate plume rise and vertical plume profile with Daysmoke, a plume-rise model specifically developed for prescribed burns (Liu et al., 2008). The number of updraft cores, which is an important parameter in Daysmoke, was set to 6 despite the large area of the burns, primarily because of the mass ignition techniques employed and hot burning temperatures; both of these factors should organize the plume in fewer updraft cores. Burn emissions were then injected into CMAQ grid cells, according to their horizontal position with respect to the burn area and, vertically, using the estimated hourly layer-fraction information. At the hour when burn emissions peaked, about 75% of the plume fell into layer 8 of CMAQ (out of 13 total), between 1 090 and 1 865 m above the ground.

3.2. Results

The simulation was initiated at 21:00 Z on 27 February and finalized at 05:00 Z on 1 March. Grid adaptation commenced at 15:00 Z on 28 February consistent with initial emissions from the Oconee National Forest and Piedmont National Wildlife Refuge fires. Grid refinement in AG-CMAQ was driven by $PM_{2.5}$ concentrations. Figure 2 shows $PM_{2.5}$ concentrations on the modeling domain at 04:45 Z on 1 March after full plume development from both the AG-CMAQ and standard CMAQ simulations. Visual inspection of the modeled $PM_{2.5}$ surface level concentration fields provides evidence of significant differences between the adaptive grid and static grid simulations. The artificial dilution effect commonly present in gridded photochemical models appears to decrease when applying an adaptive grid. The smoke plumes drawn with AG-CMAQ appear better defined and pollutant concentrations remain higher near plume cores. Most significantly

perhaps, plumes from the two different ongoing prescribed burns can be distinctly observed when applying an adaptive grid. By using a static grid, the plumes cannot be distinguished from each other and appear as a single thicker plume. We believe that in this case the results from AG-CMAQ allow for a better understanding of changes to local air quality and pollutant dispersion.

Analysis of simulated results was extended beyond surface layer concentrations to include pollutant concentrations and plume dynamics aloft. Figure 3 shows a three-dimensional (3D) plot of $PM_{2.5}$ concentrations which includes concentrations at the surface level and domain boundaries, as well as the 3D pollutant plume defined as a constant concentration surface for concentrations greater than $50 \mu\text{g m}^{-3}$. The tops of the plots face the North-western corner of the domain with plumes blowing in the direction of Atlanta. A comparison of the results produced by CMAQ and AG-CMAQ with the use of 3D visualizations provides insight into differences between the simulations not evident from simple surface-level concentration fields. Two differences between both model simulations are most striking. As was observed from the surface-level concentrations plots, the plumes from both targeted ongoing prescribed burns are undistinguishable and appear as a single merged plume using CMAQ results. However, the results from AG-CMAQ allow plumes from both prescribed burns to be distinctly observed. Unlike the static grid simulation, AG-CMAQ allows impacts from smoke plumes at specified locations to be attributed to a specific prescribed burn. It is also apparent that with the static grid simulation a significant portion of the smoke plume initially bifurcates from the main body of the plume directed towards Atlanta due to upper-level wind shear and heads north at a higher altitude (Figure 3a). This bifurcation is not perceived from surface-level concentration fields and more importantly is not present in the AG-CMAQ simulation. The detachment of a plume fragment could partially explain CMAQ's under-prediction of pollutant concentrations at monitoring sites.

Modeled concentrations from both static grid CMAQ and AG-CMAQ simulations were compared to concentration measurements at several air quality monitoring sites in the Atlanta metropolitan area that experienced a significant increase in $PM_{2.5}$ concentrations during the event. Results from both simulations are plotted along with hourly measurements at six monitoring sites in Figure 4. All sites are concentrated around the city of Atlanta with exception of the McDonough monitoring station located about 40 km away, halfway between the city of Atlanta and the location of the prescribed burns. The tendencies of modeled and observed concentrations at the sites considered are generally similar among each other with exception of the McDonough site. At all sites excluding McDonough, results from the static grid CMAQ simulation consistently under-predict maximum $PM_{2.5}$ concentrations by 58–70% of measured values. Additionally, the CMAQ results at these sites exhibit two distinct concentration peaks unlike the monitoring station observations. The simulation with AG-CMAQ results in higher concentration maximums at all locations, with exception of the McDonough site, by 27–40% relative to static grid CMAQ maximum concentrations.

The significance of the double peak behavior observed with the static grid results is lessened using AG-CMAQ as results show a more prominent concentration increase at a single major concentration spike. However, a delay of approximately 1 hour in concentration peaks is observed in the AG-CMAQ simulation with respect to static grid CMAQ results which exhibits timing more consistent with monitoring station measurements. Table 1 presents a statistical comparison of model error for CMAQ and AG-CMAQ relative to monitoring station measurements.

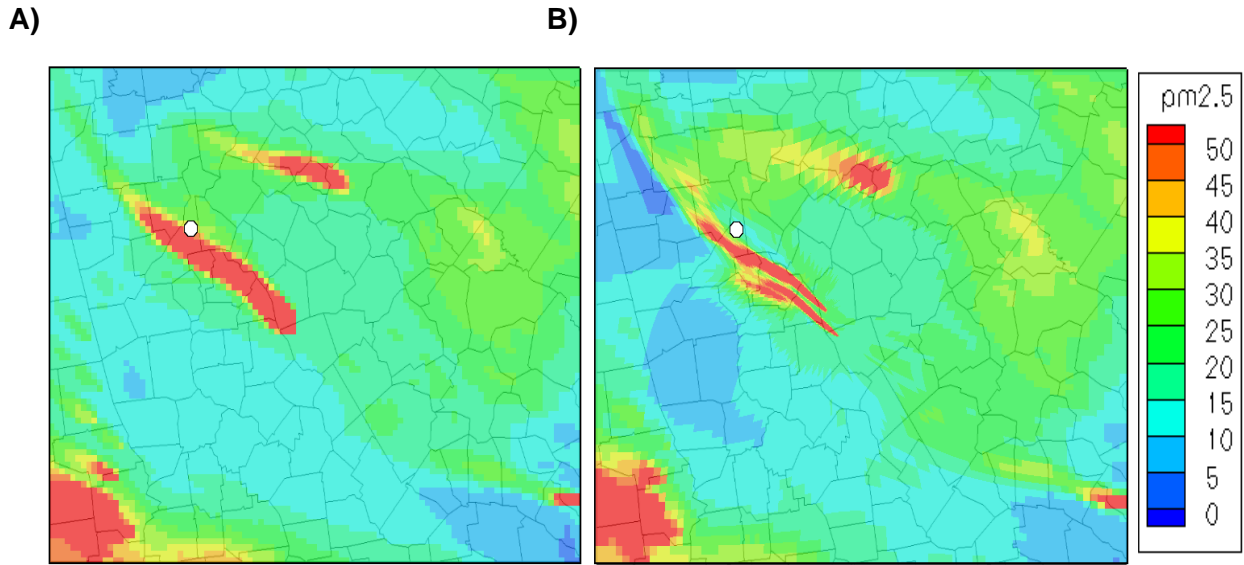


Figure 2. Simulated PM_{2.5} concentrations ($\mu\text{g m}^{-3}$) in the surface layer over Georgia, U.S.A. at 04:45 Z on 1 March 2007 using A) static grid CMAQ and B) AG-CMAQ. The location of Atlanta is denoted by a white circle.

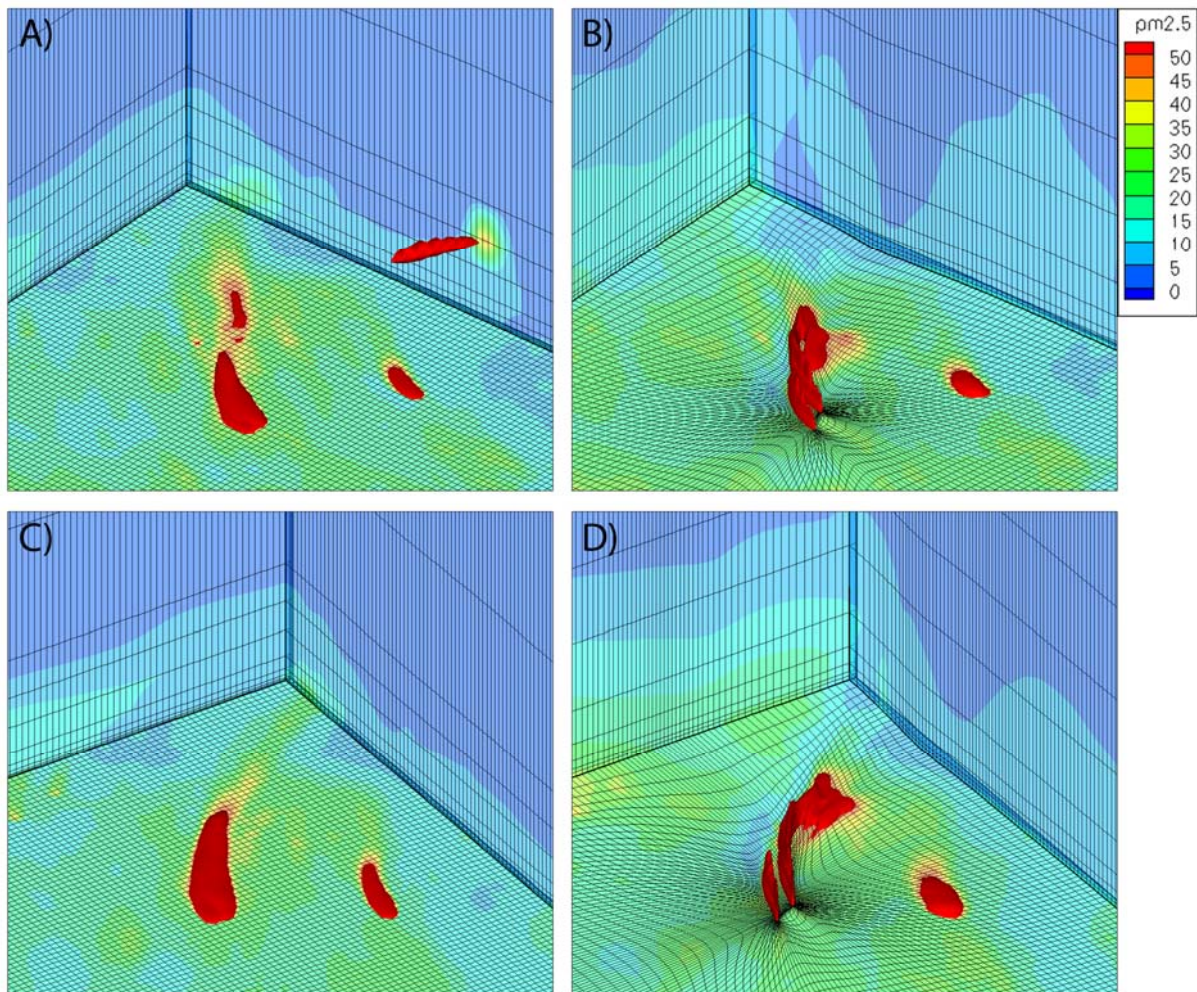


Figure 3. Three-dimensional visualization of smoke plumes and PM_{2.5} concentrations ($\mu\text{g m}^{-3}$) on 1 March 2007 at 0:30 Z using A) static grid CMAQ and B) AG-CMAQ, and at 2:15 Z using C) static grid CMAQ and D) AG-CMAQ.

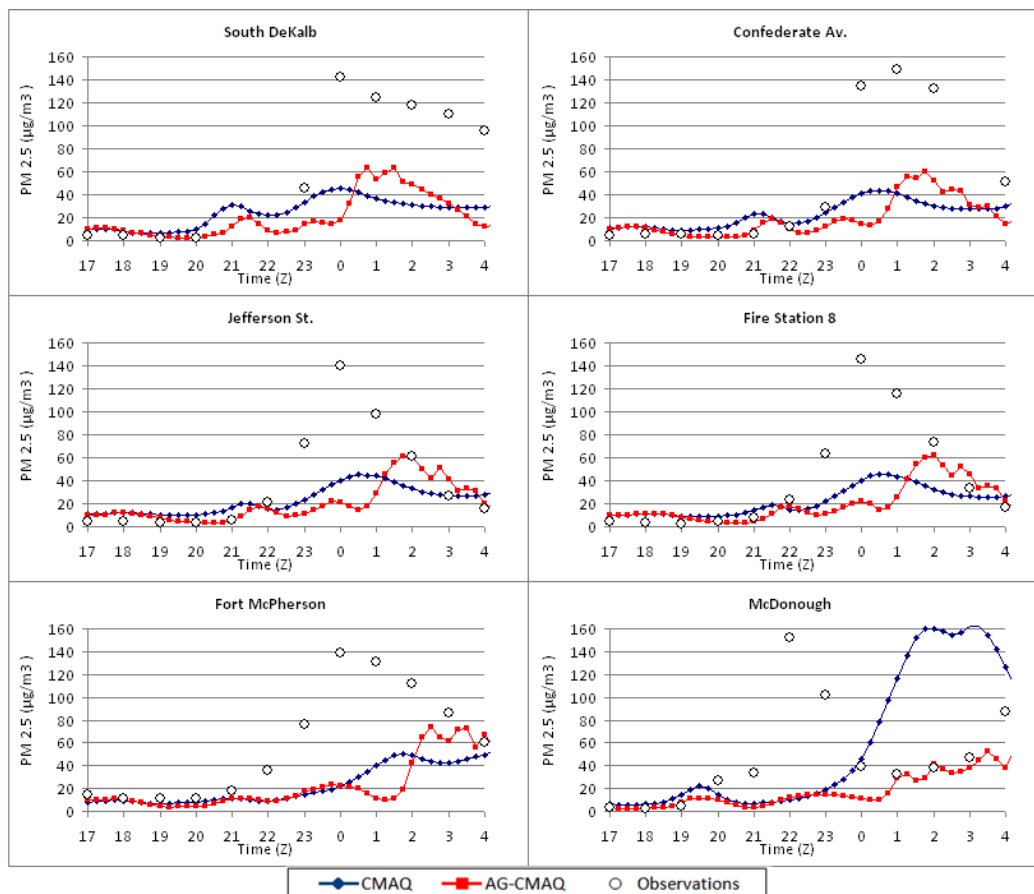


Figure 4. Modeled $PM_{2.5}$ concentrations ($\mu g m^{-3}$) using static grid CMAQ and AG–CMAQ along with concentration measurements at the South DeKalb, Confederate Avenue, Jefferson Street, Fire Station8, Fort McPherson, and McDonough air quality monitoring sites in the Atlanta metropolitan area.

Table 1. Model error metrics for CMAQ and AG–CMAQ relative to $PM_{2.5}$ observations at the Jefferson Street (JST), Confederate Avenue (CFA), McDonough (MCD), South DeKalb (SDK), Fort McPherson (FTM), and Fire Station 8 (FS8) monitoring sites and their averages (Avg.)

| | Mean Error ($\mu g/m^3$) ^a | | Mean Normalized Error (%) | | Normalized Mean Error (%) | | Mean Fractional Error (%) | |
|-------------|---|-------------|---------------------------|-------------|---------------------------|-------------|---------------------------|-------------|
| | CMAQ | AG-CMAQ | CMAQ | AG-CMAQ | CMAQ | AG-CMAQ | CMAQ | AG-CMAQ |
| JST | 21.9 | 21.7 | 114.1 | 71.4 | 65.4 | 65.0 | 78.0 | 58.3 |
| CFA | 28.9 | 29.4 | 82.8 | 57.0 | 66.4 | 67.5 | 66.5 | 58.3 |
| MCD | 47.2 | 27.6 | 131.3 | 58.6 | 111.8 | 65.3 | 92.5 | 64.3 |
| SDK | 39.0 | 40.5 | 94.9 | 70.1 | 68.5 | 71.0 | 85.7 | 78.6 |
| FTM | 32.2 | 33.3 | 48.6 | 52.3 | 60.6 | 62.7 | 69.7 | 74.4 |
| FS8 | 23.2 | 23.8 | 97.0 | 83.4 | 63.8 | 65.4 | 72.5 | 65.0 |
| Avg. | 32.1 | 29.4 | 94.8 | 65.5 | 72.7 | 66.2 | 77.5 | 66.5 |

^a Modeled concentration (m), observed concentration (o), Number of modeled/observed concentration pairs (N)

A closer look at the surface-level concentration fields along with the location of the six monitoring sites can explain some of the features observed on the time series plots. Four of the sites, South Dekalb, Confederate Av., Jefferson St., and Fire Station 8, are located in this order along a straight path downwind of the prescribed burns. Correspondingly, all increases in $PM_{2.5}$ concentrations recorded for these sites occur following the same timing pattern from the station closest to the prescribed burns to the furthest. Figure 5a shows surface-level concentrations and monitoring site locations from the static grid simulation at 22:30 Z on 28 February. The simulated plume appears fragmented into two segments. The initial segment is responsible for the first of two

concentration peaks observed in the CMAQ results. However, the initial plume segment has a tangential impact on all stations, leading to smaller concentration increases. The southwesternmost station (Fort McPherson) remains practically unaffected. The larger concentration peaks are caused by the more direct impact from the second plume segment. The plume segmentation observed in the CMAQ simulation is caused by the upper-level bifurcation previously described. Although an interruption in the modeled plume is apparent with CMAQ results, no distinction between smoke plumes from the different prescribed burns is appreciable.

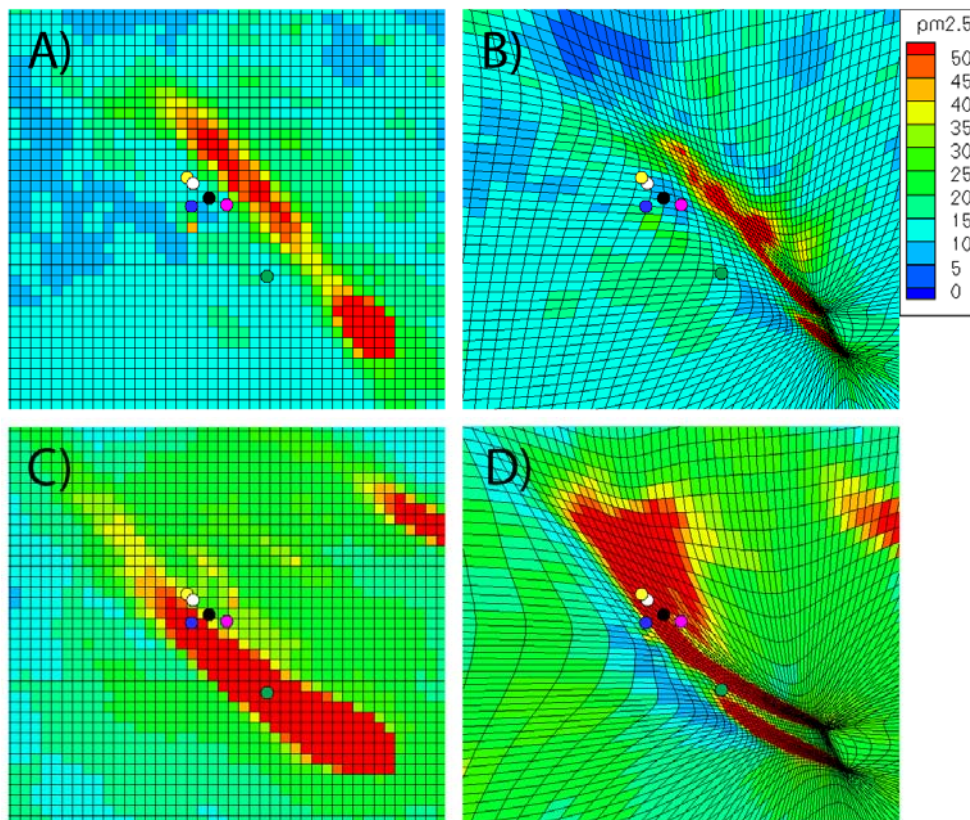


Figure 5. Simulated $PM_{2.5}$ concentrations ($\mu g m^{-3}$) on 28 February 2007 at 22:30 Z using **A)** static grid CMAQ and **B)** AG-CMAQ, and on 1 March at 02:00 Z using **C)** static grid CMAQ and **D)** AG-CMAQ. The locations of the McDonough (green), South DeKalb (pink), Confederate Avenue (black), Fort McPherson (blue), Jefferson Street (white), and Fire Station 8 (yellow) air quality monitoring sites are indicated by the colored circles.

Figure 5b shows surface-level concentrations and monitoring site locations from the AG-CMAQ simulation also at 22:30 Z. From these results no plume segmentation can be observed and plumes from both prescribed burns are clearly distinct. Once again, the earliest impact of the plume at monitoring sites is tangential, and avoids the Fort McPherson site.

Similar plots at 02:00 Z on 1 March for CMAQ and AG-CMAQ simulations are presented in Figures 5c and 5d respectively. The AG-CMAQ simulation indicates that the major modeled concentration peak is attributable to the more northern prescribed burn at Oconee National Forest. This conclusion cannot be derived from the static grid CMAQ results. The southernmost station at McDonough also merits special attention. While nested between plumes in Figure 5d, the site is affected by both plumes at different instances during the AG-CMAQ simulation. This may explain the site's unique double concentration peak recorded in the station measurements. If indeed these observations correspond to distinct hits from different plumes, such behavior can only be deduced with the increased resolution provided by the adaptive grid model, although the initial hit recorded in the measurements at the monitoring site is not perceived from modeled results since the smoke plume is oriented excessively to the east of the site.

3.3. Discussion

We believe that differences in simulated concentration fields produced by the static grid and adaptive grid models reflect the improved replication of plume dynamics and decrease in artificial dilution that was achieved through grid refinement. Nevertheless, the consistent under-prediction of maximum $PM_{2.5}$ concentrations observed from a static grid simulation, although ameliorated, persists throughout the adaptive grid simulation. It is likely that underestimations of fire induced volatile organic compound emissions and secondary organic aerosol formation are largely

responsible for the differences between modeled results and measurements, and that other inputs and processes unrelated to grid resolution contribute significantly to the error in pollutant concentrations. Uncertainties in plume rise, mixing layer height, and prescribed burn emission factors all contribute to model error and should be addressed in an attempt to achieve results more consistent with site measurements.

It is also undeniable that the surface-level concentrations are quite sensitive to wind direction and speed inputs from the meteorological model utilized. The sensitivity to winds becomes even greater when plumes are better defined as in the adaptive grid simulation. Small changes in wind direction can greatly change the impact plumes have on surface-level pollutant concentrations at specified locations. The performance of photochemical models will continue to be constrained by the limitations in fine-scale wind predictions inherent to meteorological models. To address this concern in the future, we plan to apply the grid refinement methodology in AG-CMAQ to meteorological models and develop weather models that can effectively adapt to air pollutant concentrations. Such adaptation will require continuous input of pollutant concentrations from the air quality model into the meteorological model. Therefore, coupled air quality and meteorological adaptive grid models will be created to operate simultaneously at finer scales and continuously exchange feedback.

Finally, the bifurcation observed in the 3D visualization of static grid results may indicate the importance of vertical resolution in achieving better results. Although AG-CMAQ currently provides increased resolution only along the horizontal plane, we plan to extend the grid refinement capability to include the model's vertical layering. This development would allow full grid adaptation of a 3-dimensional domain and may prove to be useful in simulating plume dynamics at even greater levels of detail. Extension of grid adaptation to the third dimension (i.e.,

vertical) would also be extremely useful in resolving cloud processes.

4. Conclusions

An adaptive grid air pollution model (AG-CMAQ) has been developed by integrating a dynamic, solution-adaptive grid algorithm into CMAQ. The model can efficiently refine the grid in response to any defined simulation variable or parameter. Although adaptive grid air pollution models have been previously explored, AG-CMAQ is unique in its capacity to model particulate matter and the first built onto an existing community model. We believe that adaptive grid modeling could potentially be the best approach to multiscale modeling of air pollution dynamics and chemistry.

The developed model was verified and its capabilities were demonstrated. The model proved to replicate results that were practically the same to those produced by the standard, static grid CMAQ when no grid adaptation was applied and effectively increased grid resolution in response to pollutant concentrations increases when adaptation was applied. AG-CMAQ performance was evaluated by simulating an air pollution incident affecting the Atlanta metropolitan area caused by two prescribed burns. The evaluation showed that AG-CMAQ successfully reduced the artificial diffusion inherent to photochemical models and produced better defined plumes compared to the standard CMAQ. Additionally, AG-CMAQ allowed both prescribed burn plumes to be distinctly observed and impacts at specific locations to be attributed to a particular prescribed burn. AG-CMAQ predicted PM_{2.5} concentrations with less error than CMAQ at most monitoring station locations affected during the incident. The mean fractional error was reduced by 15% on average, indicating significantly better agreement with site measurements.

The results of this study indicate that AG-CMAQ may provide understanding of air quality and atmospheric dynamics beyond that attainable through a static grid model. However, our evaluation indicates that despite the improvement, AG-CMAQ continues to under-predict PM_{2.5} concentrations. It is likely that the error can at least be partially attributed to processes unrelated to grid resolution within the air quality modeling system. Among these, the ability of meteorological models to simulate fine-scale and short-term variability in winds may be of greatest significance.

Adaptive grids are a tool that could prove useful for various applications beyond plume simulation. Grid refinement driven by reactivity may provide insight into atmospheric chemistry. The need for improved fine-scale wind modeling previously mentioned could be addressed by applying an adaptive grid within weather models. Indeed, adaptive mesh modeling is currently being discussed as a tool applicable to climate models to focus on small-scale processes that cannot be resolved in existing models. Some have even suggested that adaptive grid models may provide the only means of resolving these small-scale processes within a single model (Weller et al., 2010). The potential benefits that could be attained through adaptive grid modeling in the field of air pollution photochemical modeling are only briefly explored in this study. However, adaptive grids will likely lead to additional and greater advantages not necessarily restricted to air quality modeling, but encompassing different geophysical models as well.

Acknowledgements

This research was supported in part by the U.S. Department of Defense, through the Strategic Environmental Research and Development Program (SERDP) and by the U.S. Department of Agriculture Forest Service through the Joint Fire Science Program (JFSP).

References

- Bacon, D.P., Ahmad, N.N., Boybeyi, Z., Dunn, T.J., Hall, M.S., Lee, P.C.S., Sarma, R.A., Turner, M.D., Waight III, K.T., Young, S.H., Zack, J.W., 2000. A dynamically adapting weather and dispersion model: the operational multiscale environment model with grid adaptivity (OMEGA). *Monthly Weather Review* 128, 2044-2076.
- Byun, D., Schere, K.L., 2006. Review of the governing equations, computational algorithms, and other components of the models-3 Community Multiscale Air Quality (CMAQ) modeling system. *Applied Mechanics Reviews* 59, 51-77.
- Coats, C.J., Jr., 1996. High-performance algorithms in the Sparse Matrix Operator Kernel Emissions (SMOKE) modeling system. Preprints, *Ninth Joint Conference on Applications of Air Pollution Meteorology with A&WMA*, Atlanta, GA, American Meteorological Society, 584-588.
- Colella, P., Woodward, P.R., 1984. The piecewise parabolic method (PPM) for gas-dynamical simulations. *Journal of Computational Physics* 54, 174-201.
- Constantinescu, E.M., Sandu, A., Carmichael, G.R., 2008. Modeling atmospheric chemistry and transport with dynamic adaptive resolution. *Computational Geosciences* 12, 133-151.
- Ghorai, S., Tomlin, A.S., Berzins, M., 2000. Resolution of pollutant concentrations in the boundary layer using a fully 3D adaptive gridding technique. *Atmospheric Environment* 34, 2851-2863.
- Hu, Y.T., Odman, M.T., Chang, M.E., Jackson, W., Lee, S., Edgerton, E.S., Baumann, K., Russell, A.G. 2008. Simulation of air quality impacts from prescribed fires on an urban area. *Environmental Science and Technology* 42, 3676-3682.
- Khan, M.N., 2003. *Development and application of an adaptive grid air quality model*. Ph. D. Dissertation, School of Civil & Environmental Engineering, Georgia Institute of Technology, Atlanta, GA, 105-120.
- Khan, M.N., Odman, M.T., Karimi, H.A., 2005. Evaluation of algorithms developed for adaptive grid air quality modeling using surface elevation data. *Computers, Environment and Urban Systems* 29, 718-734.
- Lee, S., Baumann, K., Schauer, J.J., Sheesley, R.J., Naeher, L.P., Meinardi, S., Blake, D.R., Edgerton, E.S., Russell, A.G., Clements, M., 2005. Gaseous and particulate emissions from prescribed burning in Georgia. *Environmental Science and Technology* 39, 9049-9056.
- Liu, Y., Achtemeier, G., Goodrick, S., 2008. Sensitivity of air quality simulation to smoke plume rise. *Journal of Applied Remote Sensing* 2, art. no. 021503.
- MACTEC, 2008. *Documentation of the base G2 and best and final 2002 base year, 2009 and 2018 emission inventories for VISTAS*. Available online from: <http://www.vistas-sesarm.org/documents/VISTABF2003-20-2008.pdf>.
- Michalakes, J., Dudhia, J., Gill, D., Henderson, T., Klemp, J., Skamarock, W., Wang, W., 2005. The weather research and forecast model: software architecture and performance, in *Proceedings of the Eleventh ECMWF Workshop on the Use of High Performance Computing in Meteorology*. Eds. Walter Zwiefelhofer and George Mozdzynski, World Scientific, October 25-29, 2004, pp. 156 – 168.
- Odman, M.T., Hu, Y., 2010. A variable time-step algorithm for air quality models. *Atmospheric Pollution Research* 1, 229-238.
- Odman, M.T., Hu, Y., 2007. A variable time-step algorithm for air quality models. *Air Pollution Modeling and its Application XVII: Proceedings of the 27th NATO/CCMS International Technical Meeting on Air Pollution Modelling and Its Application*, held in Banff, Canada, October 24-29, 2004, pp. 411-420 (Eds. Borrego, C., Norman, A.L.), New York, Springer.
- Odman, M.T., Khan, M.N., Srivastava, R.K., McRae, D.S., 2002. Initial application of the adaptive grid air pollution model. *Air Pollution Modeling and its Application XV: Proceedings of the 25th NATO/CCMS International Technical Meeting on Air Pollution Modelling and Its Application*, held in Louvain-la-Neuve, Belgium, October 15-19, 2001, pp. 319-328 (Eds. Borrego, C., Schayes, G.), New York, Kluwer Academic/Plenum Publishers.

- Odman, M.T., Khan M.N., McRae, D.S., 2001. Adaptive grids in air pollution modeling: Towards an operational model, *Air Pollution Modeling and Its Application XIV, Proceedings of the 24th (Millennium) NATO/CCMS International Technical Meeting on Air Pollution Modeling and its Application*, held in Boulder, Colorado, May 15-19, 2000, pp. 541-549, (Eds. Gryning, S.E., Schiermeier, F.A.), New York: Kluwer Academic/Plenum Publishers.
- Sandberg, D.V., Anderson, G.K., Norheim, R.A., 2005. *Fire Emission Production Simulator Tutorial: Student Workbook*. USDA Forest Services, pp. 29-51.
- Smolarkiewicz, P.K., Grell, G.A., 1992. A class of monotone-interpolation schemes. *Journal of Computational Physics* 101, 431-440.
- Srivastava, R.K., McRae, D.S., Odman, M.T., 2001a. Simulation of a reacting pollutant puff using an adaptive grid algorithm. *Journal of Geophysical Research D:Atmospheres* 106, 24245-24257.
- Srivastava, R.K., McRae, D.S., Odman, M.T., 2001b. Simulation of dispersion of a power plant plume using an adaptive grid algorithm. *Atmospheric Environment* 35, 4801-4818.
- Srivastava, R.K., McRae, D.S., Odman, M.T., 2000. An adaptive grid algorithm for air-quality modeling. *Journal of Computational Physics* 165, 437-472.
- Tomlin, A.S., Ghorai, S., Hart, G., Berzins, M., 2000. 3-D Multi-scale air pollution modelling using adaptive unstructured meshes. *Environmental Modelling and Software* 15, 681-692.
- Tomlin, A., Berzins, M., Ware, J., Smith, J., Pilling, M.J., 1997. On the use of adaptive gridding methods for modelling chemical transport from multi-scale sources. *Atmospheric Environment* 31, 2945-2959.
- Weller, H., Ringler, T., Piggott, M., Wood, N., 2010. Challenges facing adaptive mesh modeling of the atmosphere and ocean. *Bulletin of the American Meteorological Society* 91, 105-108.
- Xiao, X., McRae, D.S., Hassan, H.A., Ruggiero, F.H., Jumper, G.Y., 2006. Modeling Atmospheric Optical Turbulence. *44th AIAA-Aerospace Sciences Meeting and Exhibit*, January 9-12, 2006, Reno, Nevada, AIAA-2006-0077.

Appendix D: Study plan for Eglin AFB

Study Plan (SI-1647):

Enhanced smoke and related measurements at Eglin Air Force Base

**Roby Greenwald¹, Brian Gullett², Roger Ottmar³, Warren E. Heilman⁴,
Scott Goodrick⁵, Yongqiang Liu⁵, Gary Achtemeier⁵ and Talat Odman⁶**

1. Emory University, Rollins School of Public Health
 2. U.S. Environmental Protection Agency, Office of Research and Development
 3. U.S. Forest Service, Pacific Northwest Research Station
 4. U.S. Forest Service, Northern Research Station
 5. U.S. Forest Service, Southern Research Station
 6. Georgia Institute of Technology, School of Civil and Environmental Engineering
-

1 Introduction

In 2008 and 2009 we monitored several prescribed burns (PB) at Ft. Benning, measured plume height and smoke (PM_{2.5} and CO) concentrations downwind of the plume, and used these data to assess the performance of Daysmoke, a smoke dispersion model. During our model evaluation cycles, we identified a few additional pieces of data we would like to have for more rigorous assessment of Daysmoke's performance. This study plan is prepared for the purpose of collecting these data that we believe are necessary for a more complete evaluation of the model. These data elements are wind speed/direction, fuel consumption, plume height, on-site calibration factors for real-time instruments, and ground-level and aerial smoke concentrations. Below, it will be explained how each one of these data elements would help better understand the skills and limitations of the Daysmoke model.

In our evaluations so far, Daysmoke was found to be very sensitive to the input wind speeds and directions. The errors in winds predicted by the meteorological models (MM5 and WRF), especially error in wind direction, are believed to significantly affect the plume transport by Daysmoke. Therefore, in our 2011 field study, we would like to measure the vertical profile of the winds, evaluate the uncertainty in the winds predicted by the meteorological models, and assess the impact of these uncertainties on Daysmoke predictions.

Emission inputs are critical to Daysmoke performance. While we have a certain level of confidence in emission factors, the fuel loads and fuel consumptions are more uncertain. As part of the Prescribed Fire Combustion and Atmospheric Research Experiment

(Rx-CADRE) at Eglin Air Force Base (AFB) in February 2011*, fuel load and fuel consumption data will be collected. By conducting our field study at Eglin AFB, during Rx-CADRE, we would like to benefit from these data, especially fuel consumption data, for more accurate emissions inputs to Daysmoke. Due to the coastal location of Eglin AFB, new challenges are likely, both from a sampling and modeling perspectives. Typically, burns are conducted under offshore winds at Eglin so that the smoke plume is blown to the Gulf of Mexico. For the ground-based mobile units, this might limit the sampling distances downwind from the burn plots. Also, the land/sea breeze effects might complicate the modeling. However, during the month of February, when the study is planned at Eglin, the effect of the land/sea breeze should be relatively small.

The number of updraft cores is an important parameter of Daysmoke that needs to be set by the user. The resulting plume height is very sensitive to the number of updraft cores. Therefore, plume height measurements are very useful in making an adequate selection for this important Daysmoke parameter. A ceilometer was purchased by the Forest Service for the purpose of measuring plume height. However, this ceilometer was not used in all prior burns; we would like to use it in all the burns we will monitor during our 2011 field campaign.

The calibration of real-time instruments used on mobile platforms has been a source of uncertainty in our prior measurements. The calibration factors employed were derived from other studies which may not accurately characterize the smoke conditions of monitored burns. Measurements with stationary but more precise instruments side-by-side with real-time instruments can be useful for deriving burn specific calibration factors. In our 2011 study, we would like to set up a stationary site to calibrate the instruments used on mobile platforms. If this site is set up in the short range (~1 km), downwind from the burn unit, it can also provide useful data for evaluation of Daysmoke.

The last data element we would like to have is smoke measurements on the ground and aloft. So far we evaluated the Daysmoke model only with ground-based measurements. By adding a balloon-lofted and tether-maneuvered instrument package, we can collect smoke concentration data that would allow the evaluation of Daysmoke aloft. This would be a major contribution to model evaluation considering that the only above ground evaluation possible so far was qualitative evaluation using lidar and ceilometer measurements. The smoke concentration data aloft will enable quantitative evaluation of the model above ground for the first time.

In the rest of this document we will discuss how we intend to collect these data elements which we would like to have for more rigorous evaluation of the Daysmoke PB plume dispersion model. Two of the data elements, wind speed/direction and fuel consumption, are expected to provide more accurate inputs to the model. One element, plume height, will be used in setting an important parameter of the model. The remaining two elements, on-site calibration data and concentration data on the ground and aloft will be used in evaluating the model outputs.

* The Rx-CADRE study at Eglin AFB is scheduled for February 4-13, 2011. There will be a total of 2 to 3 burns.

2 Objectives

This study is part of a larger project which aims to develop a simulation framework that can accurately predict the impacts of prescribed burns (PB) on regional air quality. One of the models in this framework is Daysmoke, a plume model developed by the Forest Service specifically for tracking the dispersion of PB plumes. The goal of this study is to collect data that have been identified during prior years of this project as most important elements for a more rigorous evaluation of the Daysmoke model.

Specific objectives of this study are to (1) provide Daysmoke with more accurate inputs, namely wind speed/direction and emissions; (2) set an important model parameter, namely the number of updraft cores; (3) calibrate the real-time instruments on site for more accurate smoke measurements; and (4) collect smoke concentration data, both on the ground and aloft, for more robust evaluation of Daysmoke outputs. The field study will be followed by a re-evaluation of the model with the collected data.

A doppler sodar and an anemometer mounted on a balloon-lofted and tether-maneuvered aerostat will periodically provide vertical profiles of wind speed and direction near the fire. These data will be used as direct inputs to Daysmoke; they will also be used to evaluate the vertical “soundings” provided by the Weather Research and Forecasting (WRF) model, which is the meteorological modeling component of the simulation framework being developed.

To provide more accurate emissions inputs to Daysmoke, fuel loading and fuel consumption data will be collected. Each fuelbed type in a burn unit will be sampled before and following the burn for fuels, which include trees, shrubs, grasses, small woody fuels, and litter. For a burn unit average, Fuel Characteristic Classification System (FCCS) fuelbeds will be built to represent the fuelbed types. This technique will also be compared to the previously used photo-series method. The consumption model Consume (Version 3.0) will be used to predict unit average consumption and emissions based on the area coverage of each fuelbed type.

A ceilometer will be used to measure the height of the smoke plume. These measurements will be used to determine the appropriate number of updraft cores, which is an important parameter of the Daysmoke model.

During the study, ground-based measurements will be made using stationary and mobile platforms. The objective of the mobile platforms is to capture downwind concentrations of $PM_{2.5}$ as well as its composition. The objective of the stationary site is to provide $PM_{2.5}$ measurements by non-portable instruments using the federal reference method. These measurements will be used for calibration of mobile instruments. In addition, CO , CO_2 measurements at the stationary site will provide essential combustion information.

Aerial measurements will be made using a tethered balloon lofting the same or similar mobile instruments used on the ground. The objective of the aerial measurements is to provide $PM_{2.5}$ and other burn-related data for use in Daysmoke evaluations.

3 Methods and analysis

This section describes the data to be collected, our sampling design, and instrumentation. Dr. Roby Greenwald of Emory University will be setting up a ground-based network with significant improvements over the prior year networks. Dr. Brian Gullett of the US Environmental Protection Agency (EPA) will conduct aerial sampling with a balloon-lofted and tether-maneuvered aerostat. Dr. Roger Ottmar of the US Forest Service (FS), who is the principal investigator of Rx-CADRE, will sample the fuelbeds while Dr. Scott Goodrick of USFS will characterize the fuels using the photo-series approach for comparison. Dr. Warren Heilman of USFS will measure vertical wind profiles using a Doppler sodar. Dr. Yongqiang Liu of the Forest Service will operate a ceilometer to measure plume height.

Post-sampling activities will include data analysis and interpretation, as well as model evaluation and preparation of the reports for the monitored burns. This section also describes how each data element will be used in model evaluation. Dr. Gary Achtemeier and Dr. Talat Odman of Georgia Tech will evaluate the model using the collected data. Applying the Daysmoke model to the monitored burns and comparing its PM_{2.5} predictions with measured PM_{2.5} will enable a final assessment of the model's predictive skills and a determination of its potential limitations.

3.1 Wind measurements

Our prior evaluations of the Daysmoke model identified a significant uncertainty in wind speeds and directions that our previous experimental design did not address. Therefore, we would like to measure the vertical profile of the winds. The measured wind speeds and directions will be directly input to Daysmoke, whenever possible, instead of the winds predicted by WRF. The measured winds will also be compared to WRF winds to determine the level of uncertainty introduced to Daysmoke by using predicted wind fields. Our analyses during the first two years of the project suggest that Daysmoke can be sensitive to wind direction shifts from 2-5 degrees – well within the expected range of WRF modeling errors. Since the smoke impact prediction system is planned to operate with predicted winds, a more accurate wind model may be necessary in the future.

3.1.1 Remotely sensed wind measurements

We plan to use the USFS Doppler sodar to obtain vertical wind profiles in the lowest 500 m of the atmosphere. The sodar will provide wind speed and direction from 100-500 m with 10 m height resolution. We plan to compare WRF winds from 100-500 m with the Doppler sodar winds, which will be assumed to be ground-truth. If there is a difference between the modeled and observed winds that is considered to compromise the comparisons between Daysmoke and ground-truth PM_{2.5} measurements, then we will substitute the Doppler sodar winds into the WRF soundings. We will compare Daysmoke/PM_{2.5} measurements for Daysmoke run with WRF only and WRF/Doppler

sodar winds. The purpose is to see whether small differences between WRF winds and Doppler sodar winds lead to improvements in Daysmoke/PM2.5 comparisons.

REMTECH Doppler sodar system consists of one sole antenna (phased array type of transducer elements), one computer, one transceiver, one power amplifier, cables and a small mount for the antenna. The system allows for full control of the antenna beams: four of the electronically steered beams are tilted (30° or 15°) from vertical and turned 90° from each other to provide the horizontal component of wind velocity. The last beam is pointed vertically and provides that component of the wind. The system software controls the sequence and rate of operation for each beam.

Linux OS based software provides a signature to the transmitted pulse. The basic coding consists of transmitting 9 (up to 15 optional) frequencies in the pulse. Upon reception, this coded pulse is easily detected from noise and fixed echoes within the backscattered signal. This is particularly useful for turbulence studies since it allows quicker detection for full analysis on the noise spectrum. The frequency transfer function (in phase and amplitude) between the “active antenna” and the “reference antenna” (made of 4 transducers at the 4 antenna corners) allows a very efficient noise subtraction (especially for a fixed noise source such as an air conditioner, an aspirated shield on a meteorological tower close to the sodar). The final acoustic frequency power spectrum can be cleaned by more than 15dB’s decrease of the jamming source in the considered frequency zone.

USFS Doppler sodar has 52 transducer elements. Its nominal central operating frequency is 3500 Hertz (9 frequencies are emitted on each tilted beam during one “beep”). The size of the antenna is 0.4×0.4 m. Its maximum range is 1,000 m with an average range in typical conditions of 200–600 m.

3.1.2 Aerial wind measurements

As a supplemental means of wind measurements, we plan to take advantage of the US EPA aerostat. The aerostat will be operated near the burn unit and it will have vertical as well as some horizontal mobility. Therefore, it can be used to measure vertical wind profiles at different downwind positions than the Doppler sodar. We plan to use the wind speed and direction measurements from the aerostat for model evaluation in the same way as those measured by the Doppler sodar.

A 3D sonic anemometer will be affixed to the Flyer instrument pack sufficiently beyond the boundary layer of the aerostat balloon. The anemometer will have a GPS-aided Attitude and Heading Reference System (AHRS) which is an inertial measurement unit that allows for 3D orientation data. These data will be used with the velocity measurements to calculate an accurate determination of ground-reference wind vectors by altitude. The anemometer will likely be a Model 81000 ultrasonic anemometer (Figure 1) from R. M. Young Co. (or similar) weighing 1.7 kg. It measures 3D wind velocity and speed of sound based on the transit time of ultrasonic acoustic signals. Output data include 3D orientation (360°), 3D position and velocity (aided and unaided by inertial sensors), 3D acceleration, 3D rate of turn, and 3D magnetic field. Data will be recorded

with a National Instruments circuit board lofted on the aerostat using a program in LabView.



Figure 1. 3D sonic anemometer.

3.2 Fuel load and consumption measurements

One of the goals of this study is to have access to fuel loading data that does not rely on photo series and fuel consumption data that does not completely rely on estimates from the model CONSUME. As part of Rx-CADRE, Dr. Roger Ottmar of USFS will conduct a field study at Eglin AFB in February 2011 to collect fuel loading data in advance of the burn and post-fire consumption field data. The overall objective of that study is to measure the fuelbed component characteristics and fuel consumption for each of the Rx-CADRE prescribed burns. The questions to be answered are: (1) How much fuel exists for the tree, shrub, grass, small woody, and litter categories for each unit? (2) How much of each fuelbed category is consumed during the fire? A detailed plan for Rx-CADRE fuel loading and fuel consumption measurements is in preparation and it will be appended to this study plan when it is ready.

The fuel loading and fuel consumption measurements are expected to provide better inputs for the emissions modeling components of our smoke impact prediction system. In particular, the sampled fuelbeds will be compared to fuelbeds estimated from photo-series. This comparison will give us an idea about the error introduced through the Fuel Characteristic Classification System (FCCS). Similarly, the consumption measurements will be compared to the consumptions estimated by the model Consume for each fuelbed type. These comparisons will allow us to determine the level of uncertainty in the emissions inputs to Daysmoke. The level of uncertainty in emissions factors (mass of gas or particle emissions per unit mass of fuel consumed) is expected to be available through SERDP project SI-1649.

We would also like to get a better picture of ignition progression. For aerial burns, and hand-lit burns, the sequence and GPS coordinates of ignition points will be tracked. Because Daysmoke has proven to be sensitive to the location and timing of smoke production in prior evaluations, this data will allow us to determine exactly where the

igniters were and when. The data will be processed through an experimental fire spread model, Rabbit Rules that can provide temporal and spatial detail in relative emissions production.

3.3 Plume height measurements

The number of updraft cores is an important parameter of Daysmoke that needs to be set by the user. The modeled plume height is very sensitive to the number of updraft cores. Using prior years' data, we have developed certain criteria for setting the number of updraft cores. However, these criteria are not fully tested and more plume height measurements are needed to verify their veracity. First, a number of updraft cores will be assigned to each burn based on the earlier developed criteria. Then, the plume height estimated by Daysmoke for that number of updraft cores will be compared to the measured plume height. If there is a difference significant enough to affect the comparison of modeled and measured PM_{2.5} concentrations, plume height measurements will be used in making a more adequate selection for the number of updraft cores. When an agreement is reached between the Daysmoke estimated and measured plume heights, the criteria for setting the number of updraft cores will be reviewed and revised as necessary. In prior years, USFS lidar support has proven to be very helpful for determining the actual plume height.

Smoke plume rise will be measured using a CL31 Ceilometer (Figure 2). This device employs laser LIDAR (Light Detection and Ranging) technology. It emits short, powerful laser pulses in a vertical or slant direction. The directly backscattered light caused by haze is measured as the laser pulses traverse the sky. This is an elastic backscatter system and the return signal is measured at the same wavelength as the transmitted beam. As many as three smoke layers can be detected with the height up to 7.5 km. The detection frequency is 2 second. This device was used to measure nearly 20 prescribed burns in the past two years. Figure 3 shows the measured smoke plume structure for a prescribed burn at Ft Benning on April 9, 2009.

During the measurements at Eglin AFB in 2011, the CL31 Ceilometer will be mounted in a mobile or on a leveled plate on the ground. The instrument will be set up before the start of the burn at a certain distance from a burn in the downwind. The distance ranges between 1 and 5 miles, depending on burn intensity and wind speed. The collected data are vertical distribution and temporal variations of backscatter light intensity. They provide smoke plume properties of plume rise and vertical profile of smoke intensity.



Figure 2. CL31 Ceilometer with smoke plume from a prescribed burn.

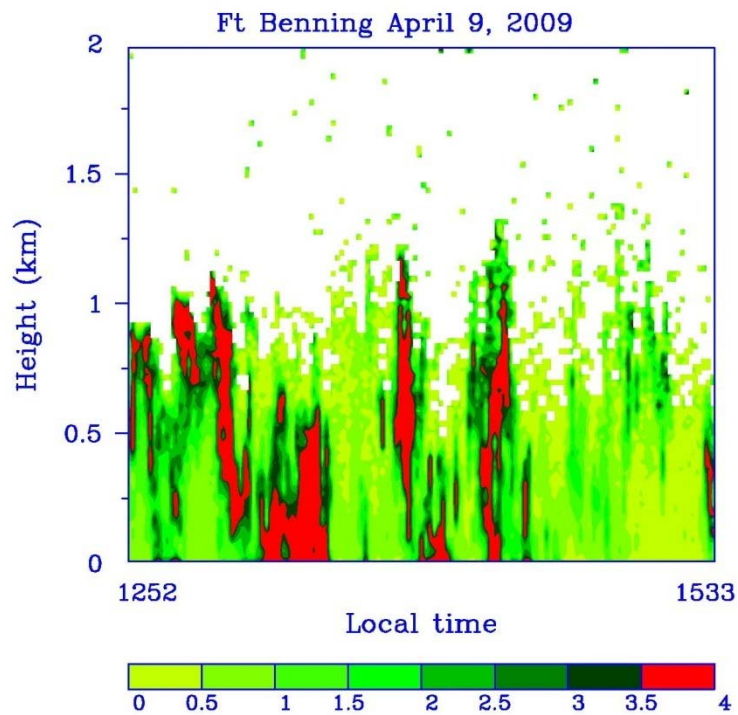


Figure 3. Time-height section of backscattered light of CL31 Ceilometer measurement for the prescribed burn at Ft Benning on April 9, 2009.

3.4 Smoke concentration measurements

The smoke concentration measurements, especially PM_{2.5} measurements are compared in evaluating the Daysmoke predictions. Due to the turbulent nature of the atmosphere, the measurements are time-averaged before comparison. The model predictions at the same location as the measurements are also time averaged and compared to time-averaged measurements. Typically a 15-minute or 30-minute time averaging is used. An averaging in space, within a certain radius of the measurements, is also being considered. In prior years, PM_{2.5} concentrations were only collected at the ground level. In 2011, we would like to measure PM_{2.5} concentrations aloft.

We will coordinate the ground-level sampling with the US EPA aerostat-based measurements aloft of PM_{2.5}, CO, and CO₂ concentrations. These data will enable the evaluation of the vertical smoke distribution predicted by Daysmoke. In the smoke impact prediction system that we are developing, Daysmoke provides the vertical distribution of smoke for input into the Community Multiscale Air Quality (CMAQ) model, which is the regional scale air quality modeling component. Simultaneous measurements of PM_{2.5}, CO₂, and CO will allow further characterization of the plume, including evaluation of emission factors using the carbon balance method.

Our experience in prior year field studies have shown that stationary but more precise PM mass measurements can be helpful for calibrating the less accurate instruments on mobile platforms. We will operate a Tamper Element Oscillating Microbalance (TEOM) at a stationary site in the short range (~ 1km) side-by-side with a sample of the real-time PM_{2.5} instruments which will be used on mobile platforms. These real-time particle counters will be operated on two trucks chasing the PB plume in the mid (1-5 km) to long ranges (5-10 km) for real-time PM_{2.5} mass sampling as well as on the balloon lofted and tether maneuvered aerostat.

The stationary site will also include measurements of the gas-phase combustion products CO and CO₂. These measurements will be used in detecting the transition of the burn from flaming phase to smoldering phase. These data will enable us to better estimate the emissions being input to Daysmoke and determine how each phase contributes to the smoke concentrations downwind.

3.4.1 Ground-Based Gas and PM Sampling

We will operate instrumentation to measure the concentration, size distribution and carbon speciation (elemental carbon and organic carbon as primary and secondary) of ambient particulate matter (PM) at both a stationary site and on two mobile platforms in the field. One mobile platform will be operated at a downwind distance of 1-5 km while the other will be 5-10 km downwind. The stationary site is necessary for non-portable instruments (specifically, the TEOM and CO and CO₂ instruments described below). These instruments are required for the proper calibration and interpretation of mobile instruments as well as for determining the amount of biomass being combusted. The

mobile platforms are required for determining spatial dispersion of the prescribed burn plumes both in the lateral and downwind directions. The instrumentation packages for the mobile platforms were developed by Dr. Roby Greenwald at Emory University, and a similar mobile platform is currently being used to measure in-vehicle pollutant exposures as part of the Atlanta Commuters Exposure (ACE) Study*. The measurements will include both real-time data from continuously-operating devices as well as time-integrated data from high flow-rate filters. In order to account for the influence of method artifacts, all filter-based measurements will include analysis of both laboratory and field blanks.

The stationary site for PM measurements will be located ~1 km downwind from the burns. The US Forest Service Doppler sodar and Lidar Ceilometer will be positioned at the same location to measure vertical wind profiles and plume heights, respectively. One of the objectives is to duplicate some of the instruments on the mobile platform at the stationary site so that they can be compared with higher precision non-portable instruments for calibration and interpretation. The stationary site will be powered using a Honda Model EU3000IS 3000 Watt gasoline generator. The generator will be placed 100 ft from the stationary site in the downwind direction. The mobile instrumentation packages will be mounted on two trucks that will continuously sample in the intermediate (1-5 km) and long (5-10 km) ranges downwind from the burns. During active sampling periods, the mobile platform vehicles will be parked on the upwind sides of the service road with the engine turned off.

3.4.1.1 Continuous measurements

PM_{2.5} mass. Continuous measurements of PM_{2.5} concentrations will be performed at the stationary site using the Tapered Element Oscillating Microbalance or TEOM (Thermo Scientific). This device calculates particle mass as a function the resonant frequency of an oscillating filter element and is a U.S. EPA recognized instrument for continuous measurement of PM_{2.5} mass. On the stationary platform and both mobile platforms, particle mass will be measured using an AeroTrak handheld particle counter (TSI Inc., Model 9306). The AeroTrak measures the light scattered by aerosols as they intercept a laser diode to count the number of particles in six size ranges in real-time. The largest size range will be configured to correspond to particles larger than 2.5 μm. The measured number concentration for each channel will be converted to a volume concentration by assuming particles are spherical with diameter equal to the log-midpoint of each channel. The volume concentration of particles smaller than 2.5 μm will be converted to a mass concentration using a “synthetic density” factor derived from calibration with the TEOM. The synthetic density will be estimated from simultaneous operation of the TEOM and the stationary platform AeroTrak and will be independently estimated during all phases of the burn (pre-burn, flaming phase, and smoldering phase). The measurement range of the AeroTrak is 0-70 particles/cm³ with a resolution of 1 particle/cm³. This measurement

* The ACE Study is a Center for Disease Control (CDC) funded program to assess the health effects on automobile commuters of exposure to motor-vehicle emissions on Atlanta’s highways.

range in terms of PM_{2.5} mass is variable depending on particle size and synthetic density, but is generally in the range 0-70 µg/m³.

Particle number concentration. The real-time number concentration of ambient aerosols will be characterized on the mobile platforms using condensation particle counters (CPC), the TSI P-Trak (TSI Inc., Model 8525). This model of CPC is capable of measuring particles in the size range of 20 to 1000 nm by condensing isopropyl alcohol vapor onto the particles until they have grown large enough to scatter a detectable amount of light from a laser diode. The measurement range of the P-Trak is 0-500,000 particles/cm³ with a resolution of 1 particle/cm³. Although this instrument does not provide information on particle size, the ambient aerosol number concentration is typically dominated by particles in the ultrafine size mode (< 0.1 µm).

Carbon monoxide. The concentration of CO will be measured continuously using the ThermoScientific Model 48i. This device measures the CO-specific absorption of infrared light at a wavelength of 4.6 µm. The measurement range of the 48i is 40 ppb to 10,000 ppm with a resolution of 1 ppb and response time of 60 seconds. This instrument will only be installed on the stationary platform.

Carbon dioxide. The concentration of CO₂ will be measured using the ThermoScientific Model 410i. This device uses the non-dispersive infrared (NDIR) method to measure the absorption of infrared light by CO₂ gas with excellent sensitivity. The measurement range of the 410i is 200 ppb to 10,000 ppm with a resolution of 10 ppb and response time of 90 seconds. The CO₂ concentration is very closely related to the amount of biomass that is combusted, and precise CO₂ measurements will be essential to calculating emission factors. This instrument will only be installed on the stationary platform.

3.4.1.2 Time-integrated measurements

Coarse and fine mode mass. The mass concentration of coarse mode (> 2.5 µm) and fine mode (< 2.5 µm) particles will be measured on both mobile platforms using a Harvard Compact Cascade Impactor operated at a flow rate of 30 L/min. For this study, this impactor will use a single impaction stage with an aerodynamic cutpoint of 2.5 µm; hence particles collected on the impaction plate will be greater than 2.5 µm in aerodynamic diameter while those collected on the after-filter will be smaller than 2.5 µm. The impaction filter is a Polyurethane Foam (PUF) substrate with dimensions of 1×7 cm while the after filter is a 47 mm Teflon filter. Flow rate spot checks will be performed at the beginning and end of each sampling period. Gravimetric measurement of particle mass will be conducted in a dedicated clean room facility at Georgia Tech. The clean room temperature is maintained at 25°C and the relative humidity is maintained at 20%. Both Teflon and PUF filters will be equilibrated to the clean room environmental conditions for 48 hours prior to weighing. Each filter will be weighed three times. The clean room microbalance has a precision of ±5 µg.

Analysis of elemental and organic carbon. Additional time-integrated characterization of PM_{2.5} elemental and organic carbon (EC-OC) content will be performed using two

parallel filter samples on both mobile platforms. Each sample line will be operated at a flow rate of 30 L/min and will be equipped with a 2.5 μm cutpoint impactor upstream of the filters to remove coarse-mode particles. One sample line will be equipped with a 47 mm Teflon filter followed by a 25 mm quartz fiber filter while the other sample line will only contain a quartz fiber filter. Flow rate spot checks will be performed at the beginning and end of each sampling period. EC-OC analysis will be performed using the Thermal-Optical Transmittance (TOT) method. The TOT method is a two-step thermal evolution process. In the first step, the filter is heated in an oxygen-free helium atmosphere to vaporize organic compounds; in the second step, the filter is heated in the presence of oxygen in order to oxidize elemental carbon. Throughout this process, the optical transmittance of the filter is monitored to provide a measure of the amount of organic carbon incidentally charred during the oxygen-free heating step. Each filter will be split using a semi-circular punch resulting in two halves each with an area of 1 cm^2 . Filter punches will be analyzed independently, and the mean of both analyses will be used for data analysis. The sampling artifact produced by the adsorption of volatile and semi-volatile organic compounds onto quartz fiber filters will be assessed by subtracting the OC content of the quartz filter which follows the Teflon filter from the stand-alone quartz filter.

Analysis of water-soluble organic carbon and ion speciation. The Teflon filter placed upstream of the quartz filter used for OC artifact analysis will be used to produce a duplicate gravimetric measurement of $\text{PM}_{2.5}$ mass (as described above) as well as an aqueous extract of water-soluble compounds. The extract will be produced by immersing the filter in 30 mL of ultrapure water and sonicating in an ultrasonic bath for 20 minutes at a temperature of 30°C. A 20 mL aliquot of this extract will be analyzed for water-soluble organic carbon (WSOC) content using a Sievers Model 900 Portable Total Organic Carbon (TOC) analyzer. The TOC analyzer that will be used for this study employs the UV/Chemical Oxidation method to oxidize all organic carbon in the aqueous extract to CO_2 , which is then detected using a conductivity cell. The ratio of WSOC to EC is useful for parameterizing secondary organic aerosol content. In addition, two separate 200 μL aliquots will be analyzed for ion content using a Dionex ICS-2000 ion chromatograph. One aliquot will be analyzed for anions including acetate, formate, chloride, nitrite, nitrate, sulfate and phosphate while the other will be analyzed for cations including sodium, ammonium, potassium, magnesium, and calcium.

Filter handling procedures. PUF filters will be immersed in ultrapure water and sonicated for 20 minutes. The water will be changed, and this process will be repeated. PUF filters will then be dried under a laminar flow hood. Teflon filters will have 50 mL of ultrapure water drawn through the filter membrane and will then be dried under a laminar flow hood. Quartz filters will be similarly treated, but will in addition be baked in a muffled furnace for 16 hours at a temperature of 550°C. A PLAS Labs Model 800 glove box will be installed at the stationary site for purposes of filter loading and unloading. Given the limited number of filter samples required for this study, it will be feasible to produce and analyze a field blank for each filter sample. Field blanks will be prepared in an identical fashion to filter samples, transported to the field, loaded into filter holders, and then immediately removed. In addition, for each filter substrate

preparation procedure, two laboratory blanks will be produced. Lab blanks will be prepared in an identical fashion, but will not be transported to the field.

3.4.2 Aerostat-Based Sampling

Aerial sampling will use a balloon-lofted instrument package called the “Flyer.” The Flyer is lofted with a helium-filled balloon and maneuvered by one or two tethers (Figure 4) connected to all-terrain-vehicles (ATVs). The Flyer collects batch gas and particle samples from ambient air or plumes. The Flyer (Figure 5) is typically comprised of multiple instruments powered by rechargeable 12-24 V Li-ion and AA batteries. The Flyer can make continuous measurements of CO₂, sampling of PM_{2.5} or PM₁₀, metals, volatile organic compounds, and semi-volatile organic compounds. Emission factors can be determined by use of C measurements (e.g., CO₂, CO, and PM) and the carbon balance method.

Measurements from the Flyer will be pre-planned to ensure that the appropriate target analytes are sampled and that the spatial and temporal parameters satisfy the data needs for Daysmoke evaluation. Field sampling will be coordinated with the installation, the burn boss, and the other sampling teams. In general, the Flyer will be as close to the burns as is safely possible in order to minimize the sampling times required to exceed the method detection limits. Likely sampling distances from the flame front are 200 m to 1,000 m at an altitude of less than 650 m.



Figure 4. Sampling design to be used by the US EPA aerostat.

The aerostat is a Kingfisher (K13N) 13×10.3 foot-diameter (3.96×3.14 m-diameter) helium balloon which lofts approximately 25 lb (11 kg). The balloon is tethered using Spectra line (1,000 or 2,000 ft length, 2.5 mm diameter) to a pair of ATVs equipped with electrically powered winches. The combination of one or two ATVs and tethers permit the positioning of the balloon, and therefore the Flyer, at a specific location and height downwind of burns.



Figure 5. The balloon and the instrument package in operation.

The Flyer (Figure 6) will be configured for this project with a 3D sonic anemometer (not shown in Figure 6), a PM_{2.5} sampler, a summa canister and/or electrochemical cell for CO, and a CO₂ CEM. Additional sampling instruments may be included to assist emission factor determination. CEM data and flow rate will be logged to an on-board HOBO data logger which also measures temperature plus relative humidity.

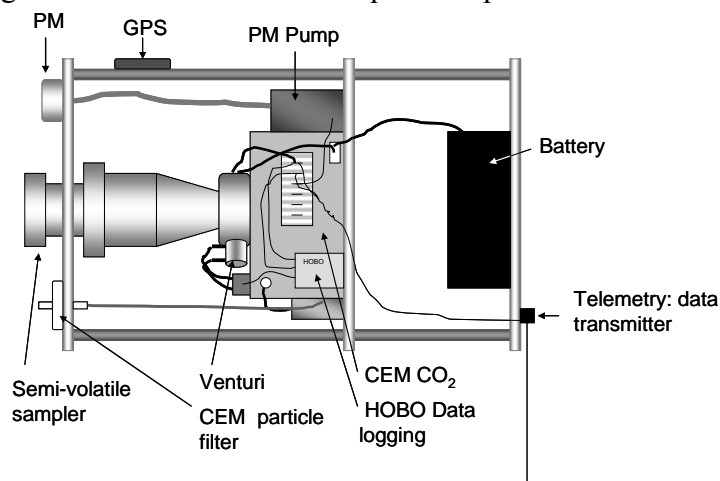


Figure 6. Aerial instrument package.

3.4.2.1 CO₂ Measurements

CO₂ is continuously measured in accordance with EPA Method 3A using non-dispersive infrared (NDIR) instrument (LI-820 model, LI-COR Biosciences, USA). This unit is configured with an optional 14 cm optical bench, giving it an analytical range of 0-20,000 ppm with an accuracy specification of less than 2.5% of reading. The LI-820 calibration range is set to 0-4,500 ppm. A particulate filter precedes the optical lens. The LI-820 is equipped with a programmable trigger circuit which activates collection of all samples at a user-set CO₂ concentration above background levels, indicating that the Flyer is within the emission plume. This trigger conserves batteries and avoids dilution of the sample with ambient air. The CO₂ level also can trigger a PM sampler comprised of a 47 mm tared Teflon filter (pore size of 2.0 μm) and a Leland Legacy sample pump (SKC Inc., USA) with a constant airflow of 13 L/min. An internal flow sensor on the Leland pump

measures flow directly and acts as a secondary standard to constantly maintain the set flow. PM is measured gravimetrically using pre-tared filters transported in sealed petri dishes.

3.4.2.2 CO Measurements

Summa canisters (6 L capacity) or an electrochemical cell will be used for collection of CO. Summa canisters are outfitted with an electronic valve that is opened at an operator-set threshold CO₂ concentration which provides sampling durations on the order of minutes. Analyses will be via GC, utilizing EPA method 25C, in which an aliquot of the collected Summa canister sample was injected into a sample loop equipped GC/FID. CO data will be background-corrected by subtracting the ambient air contribution to the sample. The electrochemical cell (Model RCO1000, Transducer Technology Division, Newark CA) is supplied with a standard range of 0-1,000 ppm, but will be calibrated at 0-100 ppm (± 2 ppm) for anticipated CO levels. From 0 ppm to 90% of full scale takes 20 seconds. For sampling periods in the order of minutes or longer, this lag should not compromise the data.

3.4.2.3 Telemetry and Positioning

The Flyer also has a Geko 301 (Garmin, USA) global position system (GPS) for location and height above sea level, saving data every 10 seconds (adjustable). A wireless telemetry and data recorder system (Seagull Sea Pro 900, Eagle Tree Systems, LLC) on the Flyer transmits signals to the ground crew. This 9 V system transmits (for example) CO₂ concentrations (as a voltage), flowrate (as a voltage), ambient temperature, and battery output to the aerostat crew to aid in positioning the aerostat within the plume, monitoring volumetric sampling rate to determine whether a filter change was necessary, and conveying residual battery capacity. These data, together with the telemetry's GPS data, can be saved every millisecond and used as a secondary data logger.

4 Quality Assurance

Sodar measurements will be compared with available tower measurements to assess the quality of near-surface sodar measured winds. Upper level sodar wind measurements will be compared with radiosonde measurements, if available, and/or measurements from a WLS70 Doppler Wind Lidar system.* Sample data obtained from the sodar are shown in Figure 7. These sodar measurements were taken in New Jersey earlier this year (2010) during the Joint Fire Science Program (JFSP) burn experiment. The lower level sodar measurements matched up really well with the 30 m tower wind measurements made at the site over the duration of the monitoring period.

* Dr. Craig Clements of San Jose State University is planning to bring a WLS70 Doppler Wind Lidar system to the Rx-CADRE burns.

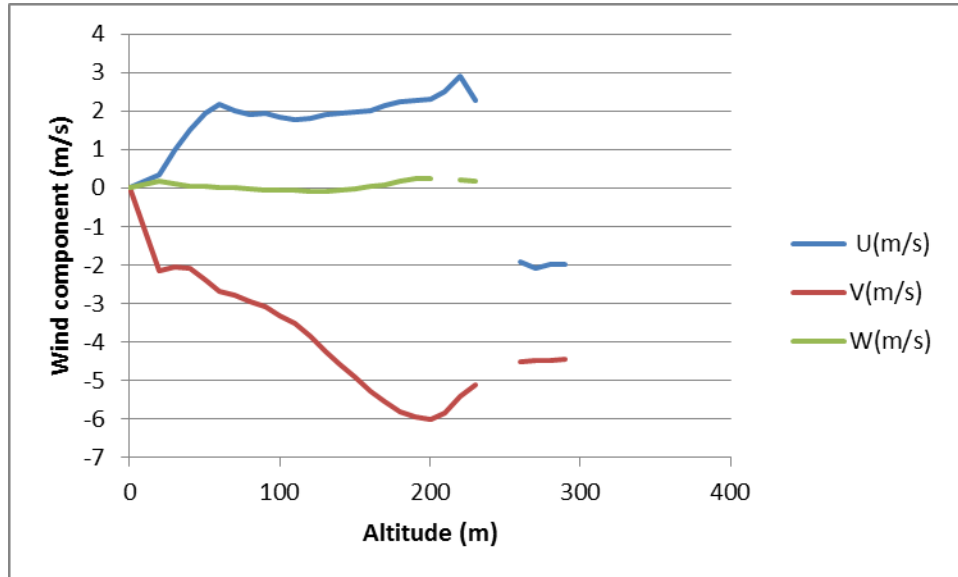


Figure 7. Sample wind profiles obtained with the Doppler sodar

The Ceilometer CL31 manufactured by Vaisala will be used to detect smoke plume rise and vertical profile. The quality assurance for the measurements is threefold. (1) Comparisons of atmospheric particles and clouds have been made by many other institutions. One comparison provided by Vaisala indicates a correlation coefficient of 0.83 between the particulate matter detection between CL31 Ceilometer and the ground measurement. (2) Comparisons with more sophisticated instruments like the Doppler sodar will be conducted during the experiment. (3) The following guidance and procedure will be used to assure normal operation of CL31 during the measurement: (i) At least two operators will be at the scene, (ii) arriving at least one day before the burn date to prepare for the measurements. (iii) CL31 will be placed at the best possible site for measurement, (iv) The instrument will be set up and shut down strictly following the steps showed in a note. (iv) The operation and data collection and storing of the instrument will be continuously monitored and changes will be made as needed. (vi) Finally, all data will be backed up before shutting down the instrument.

All ground-based instrumentation will undergo routine maintenance and calibration immediately prior to transport to the field. The Thermo 48i and 410i instruments for CO and CO₂ measurement will be calibrated at Georgia Tech following the manufacturer's recommended procedures. These instruments as well as the TEOM will be operated for a period of three days in co-location with identical instruments in the ambient air quality laboratory in the Environmental Science & Technology Building at Georgia Tech. Following transport to the field, instrumental flow rates will be verified using a BIOS Definer dry calibrator. These instruments will be zeroed in the field, and in addition, the TEOM will be field checked using calibration weights on the microbalance. All handheld instruments will be zeroed, have their flow rates verified, and operated simultaneously at

a co-location prior to burn ignition to verify agreement between instruments. The flow rates of all filter-based measurements will be verified at the beginning and end of each sampling period. A field blank will be produced for each filter sample, and in addition, multiple laboratory blanks will be produced for each filter preparation procedure.

All laboratory equipment involved in the analysis of filter samples will undergo recommended maintenance and calibration procedures. The environmental controls of the clean room facility at Georgia Tech will be verified during the 48-hour equilibration period and during gravimetric analysis of filter weights. Microbalance performance will be verified using standard weights. Each filter will be weighed three times with each measurement separated by at least twenty minutes. Performance of the TOT instrument for EC-OC analysis will be verified by applying known concentrations of sucrose to filter blanks. The TOC analyzer will be zeroed prior to use, and its performance will be verified by the injection of multiple calibration standards. Sample aqueous extracts for TOC analysis will be divided into two aliquots and analyzed separately. Similarly, ion chromatography analysis will be performed on two aliquots of each sample, and calibration curves will be generated using standard solutions that are analyzed on the same day as samples.

Prior to the onset of measurements, a Quality Assurance Project Plan (QAPP) will be written for the US EPA effort to ensure that planned measurements with the aerostat (both wind and smoke concentration) will meet the data quality objectives. This will ensure that the operation of the instruments, sampling procedures, analytical data, and calculations are consistent with level of quality necessary to meet the data quality objectives and intended use of the data.

Appendix E: Evaluation of Daysmoke with collected data

Re-Analysis of Smoke Data and Daysmoke Simulations for 9 April 2008 at Fort Benning, GA

Gary L. Achtemeier
USDA Forest Service
Athens, GA

Field projects collecting PM_{2.5} data were conducted at Fort Benning, GA, during 9, 14, and 15 April 2008. These data were presented by day and broken into categories referencing truck locations, risk of contamination, and analysis of 30-min averaged data. The following summarizes a re-analysis of Daysmoke predictions for smoke on 9 April 2008 based on lessons learned. The re-analysis corrects for georeferencing WRF wind data and calibration of the observed PM_{2.5} data.

Background for 9 April 2008.

Three trucks were positioned at distances roughly 1.5 mi, 3.0 mi, and 4.0 mi (2.4, 4.8, and 6.4 km) downwind from the 300 acre 9 April 2008 burn. The experiment was designed so that the trucks could be moved if and when wind shifted to blow smoke in different directions. The latitudes and longitudes of truck locations were measured by the UGA team using GPS units. Some of the GPS data was thought to be compromised however by mid-2009, the date were recovered. The UGA team also took field notes regarding map locations and times the trucks were moved during the burn. The truck coordinates provided by both methods were plotted on Google Earth. Those coordinates that best matched with road locations with particular emphasis on clearings next to roads were selected for the truck locations.

The positions of the three trucks are numbered and color-coded in Figure 1. Truck 1 (blue), initially 2.2 mi (3.5 km) from the burn centroid and co-located with the UMASS lidar (point 10) from 1112 – 1233 LST, was stationed closer to the burn (1.4 mi, 2.3 km) from 1240 – 1312 LST, then moved to point 3 2.5 mi (4.1 km) from the burn from 1325 – 1413 LST. Truck 2 (yellow), initially at point 4 - (3.9 mi, 6.2 km) from the burn centroid at 1153 LST, was moved to point 5 (4.2 mi, 6.7 km) at 1245 LST where it remained until 1424 LST. Truck 3 (red) was positioned at four locations during the burn: point 6 (5.0 mi, 7.9 km) at the southern edge of the Daysmoke-simulated plume (white line), point 7 (4.2 mi, 6.7 km), point 8 (4.8 mi, 7.7 km), and point 9 (4.7 mi, 7.6 km). Truck 3 was at the first location from 1200 – 1230 LST, left the second location at 1315 LST, and departed the third location at 1405 LST.

Two DustTrak PM_{2.5} samplers per truck were turned on at roughly the time of ignition (1130 LST) and were turned off shortly after firing was complete at 1430 LST. The dual sampler system was done so that measurements at each truck could be inter-compared to be certain the instruments were functioning properly. Five-minute averaged PM_{2.5} measurements for Truck 1 are shown on the upper panel of Figure 2. The smoke plume arrives at approximately 1155 LST, peaks at 50 $\mu\text{g m}^{-3}$ at 1210 LST, peaks near 70 $\mu\text{g m}^{-3}$ between 1240 -1310 LST, and again after 1330 LST. Smoke arrives at Truck 2 (middle panel) before 1230 LST with several peaks in concentrations near 70 $\mu\text{g m}^{-3}$. Similar traces are found for Truck 3 (lower panel).

Wind directions at 200 m agl (a simple representation for the transport wind carrying the plume just above ground) were calculated from WRF weather data soundings that served as hourly initialization for Daysmoke. Winds blew from the east-southeast during the period of the burn but were not steady in direction. During the period 1600-1800 GMT (1100-1300 LST) winds blew from 110-106 degrees. Then winds began shifting to blow from a more easterly direction (96 degrees) by 2000 GMT (1500 LST). Thus the WRF wind directions shifted by 14 degrees during the course of the burn. These directions shifts – if not accurate – can significantly impact Daysmoke-predicted PM2.5 concentrations over the truck locations.

Daysmoke PM2.5 Reanalysis for 9 April 2008

Another critical factor for executing Daysmoke regards the assignment of updraft core numbers appropriate for the 9 April 2008. Daysmoke provides no mechanism for determining updraft core number. Updraft core number is determined by a complex interaction among a number of factors. Some of these factors are:

- Size of burn area – a small burn area should be expected to produce only one updraft core; large burn areas can support many updraft cores.
- Shape of burn area – a burn area that is highly irregular in shape will require an irregular distribution of fire leading to many updraft cores. This problem can be amplified when wind direction maximizes irregularities.
- Heterogeneity of fuels – fuels that burn hot relative to surrounding fuels will develop stronger convective currents and will tend to form updraft cores.
- Fuel type, moisture, and loadings – all three factors relate to heat production. High heat production will develop convective columns and lead to fewer updraft cores; low heat production will lead to many updraft cores
- Distribution of fire on landscape - fire distributed along a long linear line will produce many updraft cores; fire spread evenly over length and depth (mass ignition, stripping) will organize convective columns into fewer updraft cores.
- Amount of fire on landscape – a small amount of fire will reduce emissions per second but decrease heat thus minimizing convective organization. Result: many updraft cores. A large amount of fire will produce the opposite. Result: fewer updraft cores
- Distribution of canopy gaps. Hot air trapped beneath a dense canopy will flow to the gaps thus creating convective columns that produce updraft cores there. Thin (or no) canopies will not be a factor in updraft core development.
- Transport wind speed – strong winds inhibit convective organization thus leading to many updraft cores. Weak winds allow convective organization resulting in few updraft cores.
- Mixing layer depth – a shallow mixing layer inhibits convective organization thus leading to many updraft cores. A deep mixing layer has less adverse impact on convective organization so fewer updraft cores should be expected.

Past experience with Daysmoke applied to a burn of size 300 acres leads to the assignment of 6-core updraft plumes. However, six cores may not be representative of the plume

structures for the 9 April 2008 burn. Therefore, Daysmoke was run for 4-core, 6-core, 8-core, and 10-core plumes and the results tallied below.

Figure 3 shows 30-min averaged PM_{2.5} generated by Daysmoke for 6-core updraft plumes (left panel) and 8-core updraft plumes (right panel) compared with 30-min averaged observed PM_{2.5} at the Truck 1 locations. The 30-min averages of the observed PM_{2.5} show a pyramid with a peak at 1300 LST. Neither the 6-core (left panel) nor the 8-core (right panel) Daysmoke solutions reproduced this pattern. The 6-core solution is mostly flat from 1200 – 1430 LST with small variations in PM_{2.5}. The 8-core solution peaks at 1200 LST and declines slowly thereafter. Correspondences between observed and simulated PM_{2.5} appear more likely due to chance than to model accuracy.

The 30-min averaged data for the Truck 2 location (Figure 4) show much closer correspondence with the observations. The observed peak in PM_{2.5} between 1300 – 1330 LST falls within the range of Daysmoke simulations for both 6-core (left panel) and 8-core (right panel) updraft plumes.

The increase PM_{2.5} after 1200 LST at Truck 3 (Figure 5) is simulated by Daysmoke albeit the magnitude of the increase is underestimated. Daysmoke systematically underestimated smoke at Truck 3 for both the 6-core (left panel) and the 8-core (right panel) updraft plumes.

Results showing average PM_{2.5} for the whole burn are more encouraging. Figure 6 shows the 3.5-hr average observed and ensemble averaged Daysmoke PM_{2.5} for the four updraft core selections. The comparisons between the observations and the 6-core solutions for Truck 1 (24 vs 28 $\mu\text{g}\text{m}^{-3}$), Truck 2 (27 vs 24 $\mu\text{g}\text{m}^{-3}$), and Truck 3 (27 vs 19 $\mu\text{g}\text{m}^{-3}$) can be judged as quite good given the sources of error in the calculations.

Discussion of Discrepancies for 9 April 2008

The major discrepancies between observed and Daysmoke-simulated PM_{2.5} concentrations – the flat pattern of simulated PM_{2.5} at Truck 1 and under-estimation of PM_{2.5} at Truck 3 need further discussion. It is proposed that the source of the discrepancies is related to three factors – the shape of the burn area, the hourly emissions production model, and the wind directions in the WRF model.

Figure 7 shows the block burned on 9 April 2008. As the winds were blowing from the east-southeast, ignition would have begun at the leftmost point and proceeded toward the right encompassing a wider area of the block. This could explain the gradual increase in observed PM_{2.5} between 1130 – 1300 LST as shown in Figure 3. However burn crews manned four-wheelers and it can be argued that the rate of ignition was a constant throughout the course of the burn. This argument is the basis for the hourly emissions production model shown in Figure 8.

Given a constant rate of ignition, the shape of the burn area still remains a factor regarding the flat pattern of simulated PM_{2.5} at Truck 1. In the list of factors that determine plume updraft core number are found shape of the burn area and distribution of fire on the landscape. Fire crews would have been able to lay more strips of fire over the narrow area of the block thus spreading fire more evenly over length and depth of the burn. This distribution favors the organization of the plume into fewer updraft cores – perhaps 2-3 updraft cores – thus providing more efficient vertical transport of smoke out of the lower boundary layer immediately downwind from the burn. As ignition worked

back toward the wider part of the block, the ignition pattern would have been spread more linearly thus favoring more updraft cores – perhaps 6-8 updraft cores. Thus more smoke would have been found at the ground at the location of Truck 1 as the burn proceeded. This explanation could account for the gradual increase in PM2.5 observed at Truck 1. Daysmoke is currently not set up to account for the time-rate of change of updraft core number.

As regards the underestimation of smoke at Truck 3, the shape of the burn area and WRF wind directions could have been important factors. Daysmoke releases particles within a square equal in area to the area of the block of land burned. Figure 7 shows that the burn area was elongated along the wind direction. The outcome is the Daysmoke plume would have been too broad and PM2.5 concentrations spread in reduced amounts. The observed plume would have been narrower with higher local concentrations of PM2.5.

Wind direction could also have been a factor in the underestimation of smoke at Truck 3. Daysmoke generates gradients of smoke going from the plume centerline to the plume edge. Small differences in wind direction between observed winds and WRF winds of up to 5 degrees – well within the margin of error for a numerical weather prediction model – could have placed truck locations nearer to the edge of the plume and resulted in significant reductions between Daysmoke-simulated and observed PM2.5 at the location of Truck 3.

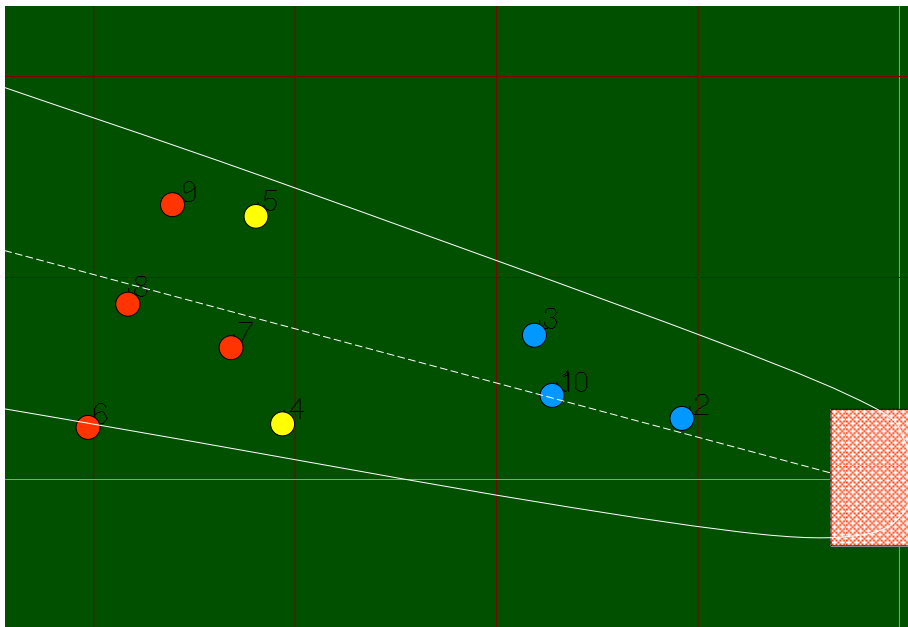


Figure 1. Locations of the three PM_{2.5} collection trucks (blue, yellow, and red circles) and the University of Massachusetts radar/lidar van (point 10) relative to the 9 April 2008 burn site (hatched area) at Fort Benning, GA. The white curve gives the boundaries of the Daysmoke-simulated smoke plume at 1300 LST. Each square is 1 mi (1.6 km).

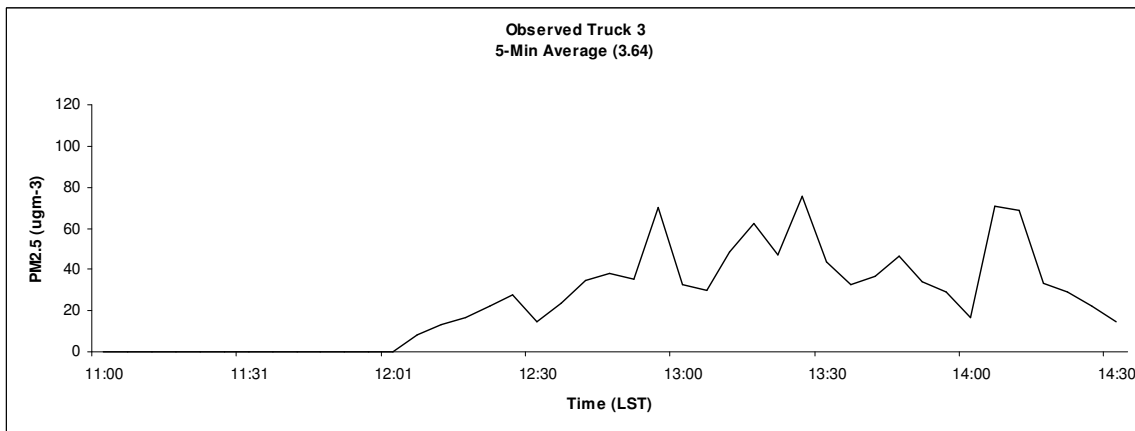
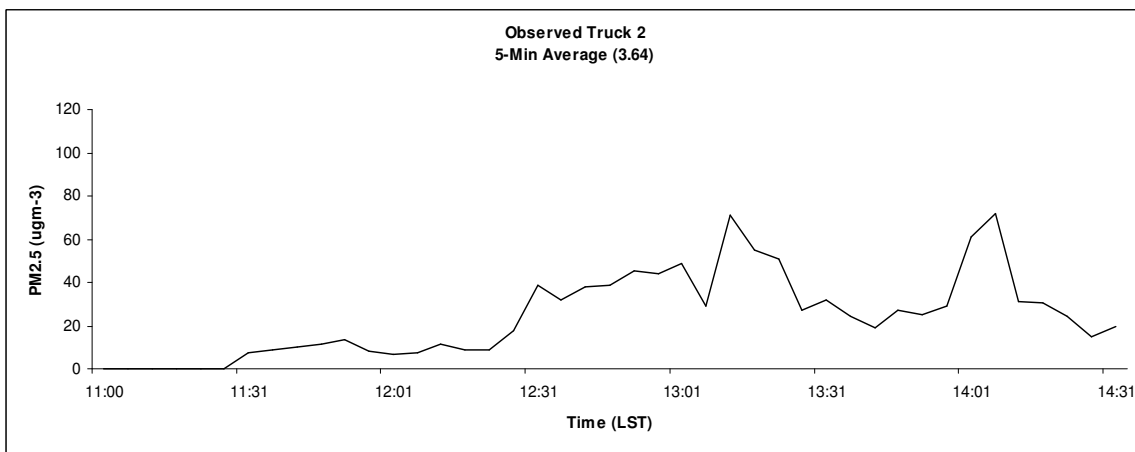
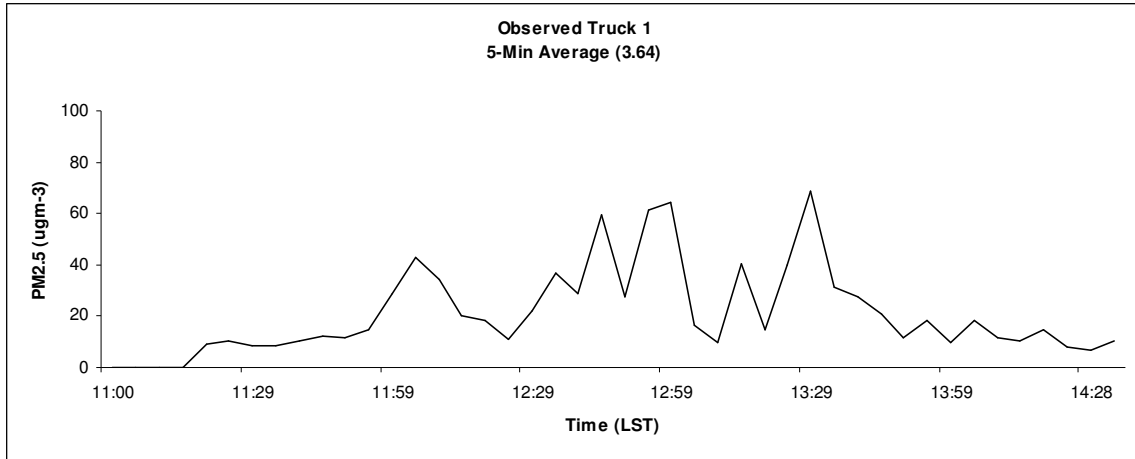


Figure 2. Time series of five-minute average PM_{2.5} concentrations as measured by DustTrak samplers rigged to the three trucks for 9 April 2008. Measurements have been calibrated for wood smoke through division by a factor of 3.64.

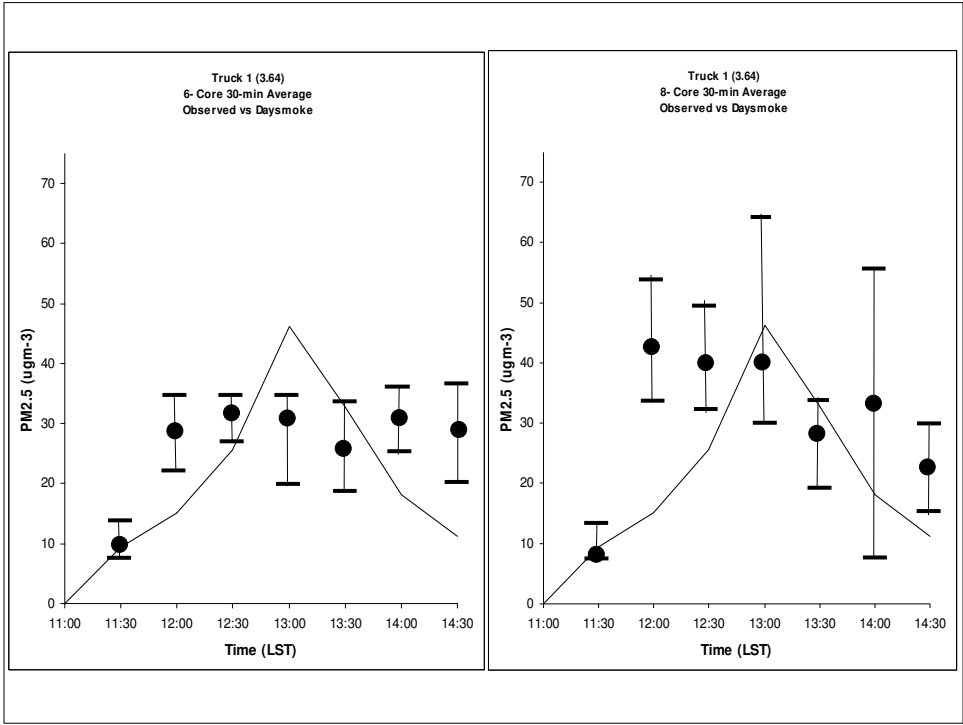


Figure 3. 30-min averaged PM2.5 generated by Daysmoke for 6-core updraft plumes (left panel) and 8-core updraft plumes (right panel) compared with 30-min averaged observed PM2.5 at the Truck 1 locations.

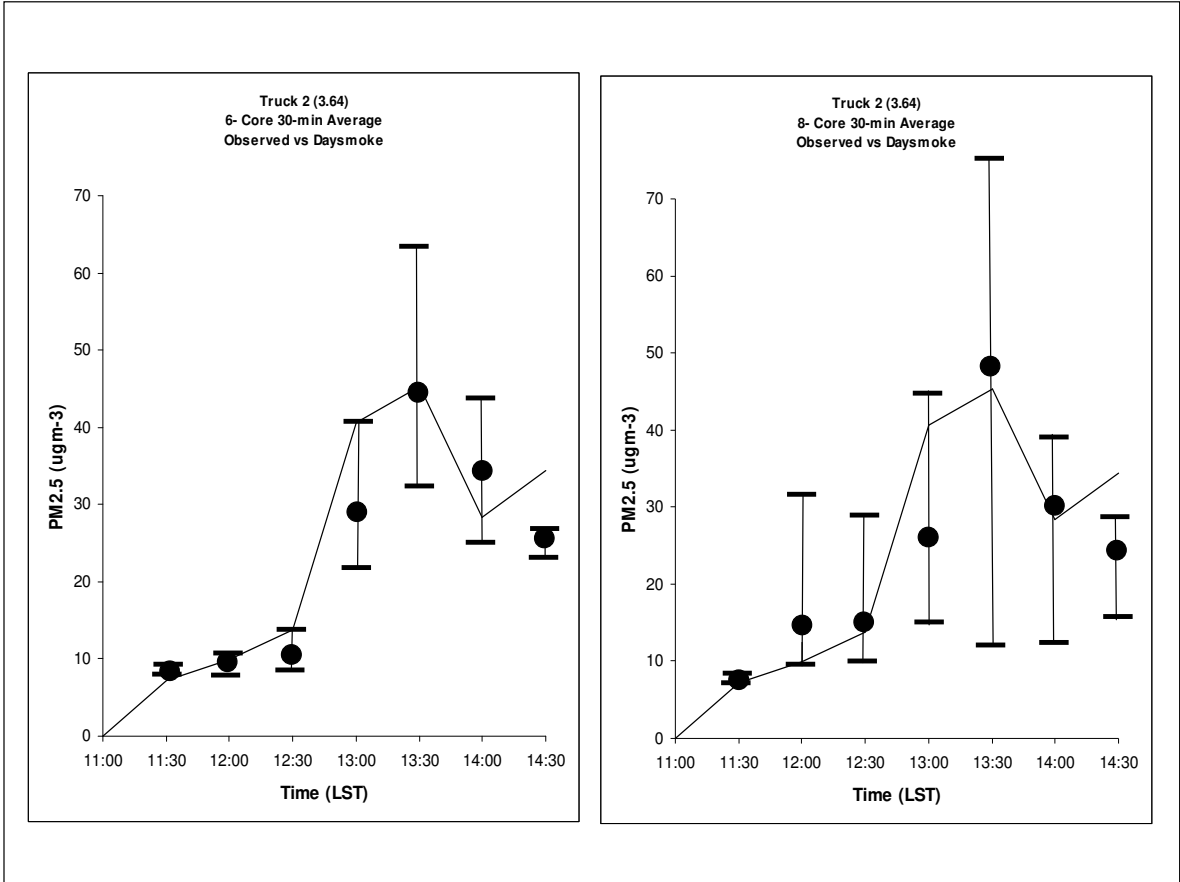


Figure 4. Same as for Truck 3 but for Truck 2.

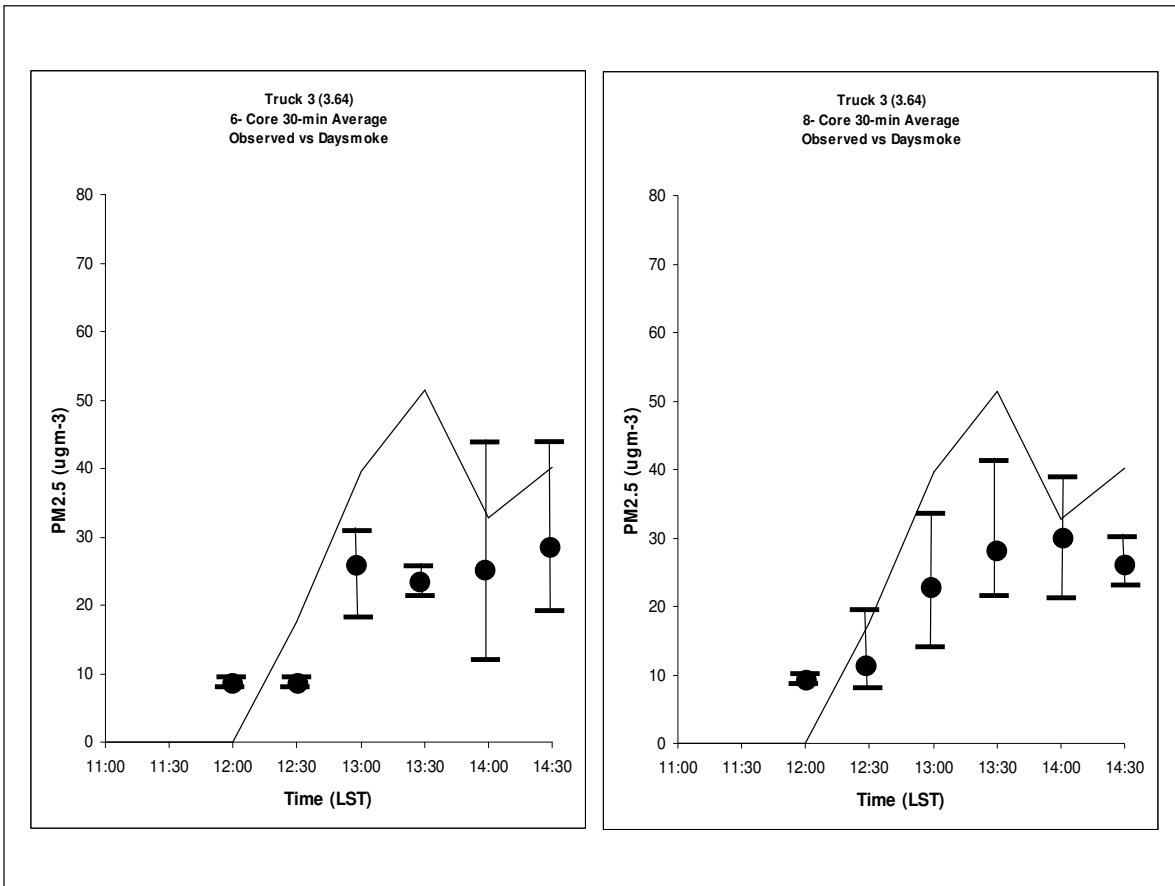


Figure 5. Same as for Figure 3 but for Truck 3.

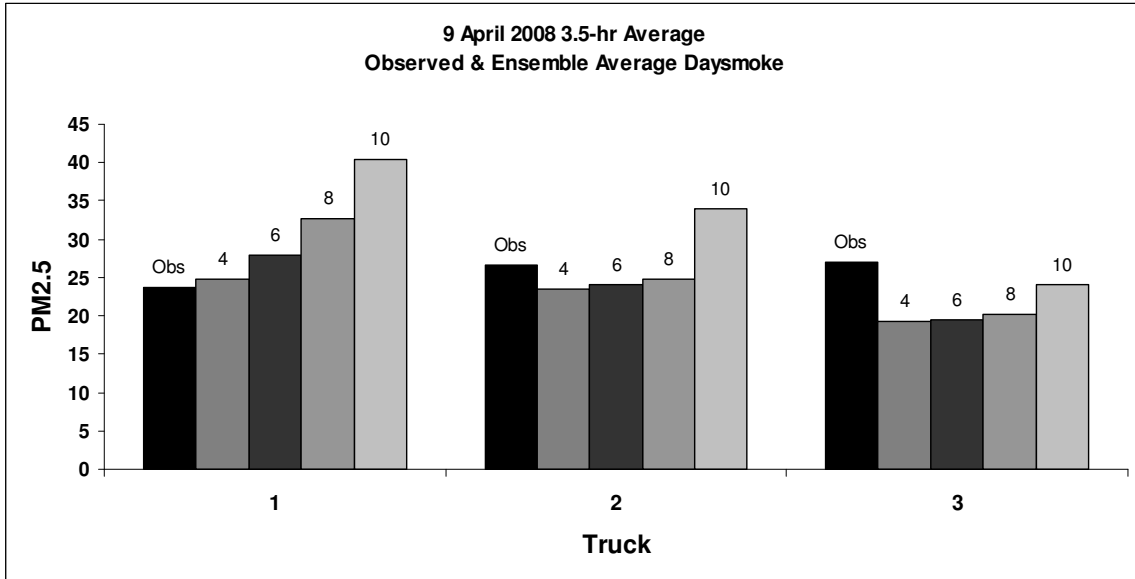


Figure 6. Smoke concentrations averaged for the duration of the observations (1200 – 1430 LST) at the three truck locations for the observed PM2.5 (black), the 4-core updraft (medium gray), 6-core updraft (dark gray), 8-core updraft (medium gray) and the 10-core updraft (light gray).



Figure 7. The 300 acre block burned on 9 April 2008.

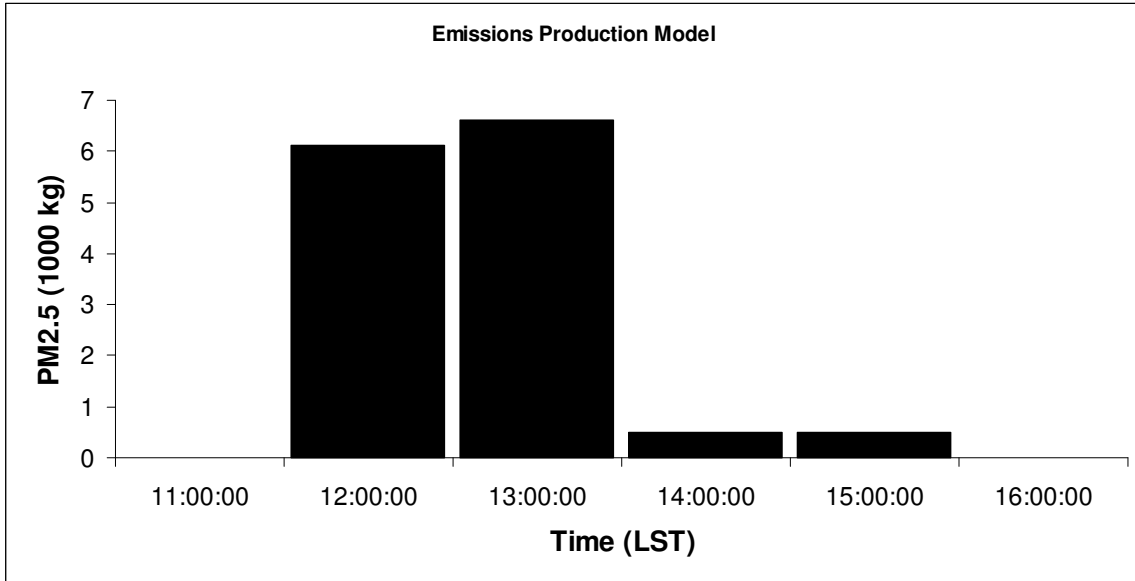


Figure 8. Distribution of hourly emissions for the 9 April 2008 burn.

Re-Analysis of 14 April 2008 at Fort Benning, GA

Gary L. Achtemeier
USDA Forest Service
Athens, GA
26 February 2010

Introduction.

Field projects collecting PM_{2.5} data were conducted at Fort Benning, GA, during 9, 14, and 15 April 2008. These data have been compared with Daysmoke simulations for the same locations as reported by 3 mobile trucks. Results are summarized in the report: **Analysis of Smoke Data and Daysmoke Simulations for April 2008 at Fort Benning, GA** by Gary L. Achtemeier (June 2009). The outcome of these analyses in combination with results from data/model cycles is a greater understanding of the models used and the sensitivity of these models to the data used to run them. For example:

1. The WRF meteorological model that supplies weather data for Daysmoke was found to generate unstable winds in the lower boundary layer for 15 April 2008.
2. The wind data for all WRF soundings supplied for Daysmoke were not geo-referenced.
3. The PM_{2.5} data measurements had not been calibrated for wood smoke.

Problems (2) and (3) above have been corrected.

Some additional findings are:

Observations:

1. Observations of PM_{2.5} were subject to contamination from dust kicked up by passing vehicles and when the parent truck was moved. Further analysis showed that possible contamination from dust was equal in magnitude to the smoke signal. However, the duration of the contamination was short (1-2 min) so that the contribution to increasing the total PM_{2.5} was small. The problem of dust contamination from passing vehicles was eliminated by having crews park their trucks on the upwind side of the road.
2. Canopy sheltering occurs when/if trucks are parked where dense forested areas are close to the road on both sides but particularly on the upwind side. Relatively clear air below canopy height can be trapped or move slowly past the truck while the bulk of the plume is transported at higher speeds just above. Mixing of smoke down to the road is limited by the narrow gap. The outcome is that the observations taken at such sites underestimate the PM_{2.5} that would have been present had the truck been parked at a cleared area. Crews were instructed to park at clearings but that was not always possible.

WRF weather data:

1. Numerical weather prediction models should be expected to produce errors in predicted wind direction of 3-10 degrees. This error is large enough to shift Daysmoke-generated plumes away from truck locations so that trucks are located at the edge of the Daysmoke plumes where in fact trucks were located near the

centers of actual plumes. The reverse situation could also exist. Observations to validate WRF predicted winds were not part of the original project design.

The following summarizes a re-analysis of Daysmoke predictions for smoke on 14 April 2008 based on lessons learned. The re-analysis takes two parts. The first analysis is based on the “standard method” for using Daysmoke as a smoke injector for atmospheric chemistry models. The second detailed analysis incorporates the methods fire bosses used in conducting the burn into the fire spread model, Rabbit Rules, and breaks the 14 April event into five separate burns.

Background for 14 April 2008.

Three trucks were positioned at distances roughly 1.7 mi, 3.0 mi, and 3.5 mi (2.7, 4.8, and 5.6 km) downwind from the 400 acre 14 April 2008 burn. The positions of the three trucks are numbered and color-coded in Figure 1 and superimposed on the Daysmoke map with the 400 acre burn site constructed as the square at the upper left corner of the figure. Truck 1 (blue), initially 0.7 mi (1.1 km) from the burn centroid was moved at 1137 LST to point 2 (1.7 mi, 2.7 km) where the instruments remained for the duration of the burn. Truck 2 (yellow), at point 3- (2.3 mi, 3.7 km) from the burn centroid from 1130 - 1245 LST, was moved to point 4 (2.9 mi, 4.6 km) where it remained until 1435 LST. Truck 3 (red) was positioned at five locations during the burn: point 5 (3.3 mi, 5.3 km), point 6 (3.6 mi, 5.7 km), point 7 (3.8 mi, 6.1 km), point 8 (2.7 mi, 4.3 km), and point 9 (3.2 mi, 5.1 km). Truck 3 was at the first location from 1114 – 1144 LST, left the second location at 1220 LST, departed the third location at 1310 LST, departed the fourth location at 1400 LST, and remained at the fifth location until 1430 LST. Point 10 locates the position of a radar/lidar system operated by the University of Massachusetts.

Two DustTrak samplers were rigged to each truck. The dual sampler system was done so that measurements at each truck could be inter-compared to be certain the instruments were functioning properly. Five-minute averaged PM_{2.5} measurements for Truck 1 are shown on the upper panel of Figure 2. Smoke concentrations slowly build during the course of the burn reaching a peak of 148 $\mu\text{g}\text{m}^{-3}$ near the end of the burn. Similar traces are found for Truck 2 (middle panel) and Truck 3 (lower panel) which show slow buildup in smoke concentration reaching a peak near the end of the burn. There were peak concentrations of 90 $\mu\text{g}\text{m}^{-3}$ and 78 $\mu\text{g}\text{m}^{-3}$ respectively.

Wind directions at 200 m agl (a simple representation for the transport wind carrying the plume just above ground) were calculated from WRF weather data soundings that served as hourly initialization for Daysmoke. Winds blew from the northwest during the period of the burn but were not steady in direction. During the period 1600-1800 GMT (1100-1300 LST) winds blew from 318-312 degrees. Then winds began shifting to blow from a more northerly direction (329 degrees) by 2000 GMT (1500 LST). Thus the WRF wind directions shifted by 17 degrees during the course of the burn. These direction shifts – if not accurate – can significantly change Daysmoke-predicted PM_{2.5} concentrations over the truck locations.

Analysis 1: Standard Method for 14 April 2008.

The simple, straightforward method for using Daysmoke is summarized in Figure 1. The burn area is represented as a box centered at GPS coordinates given for the burn site and equal in size to the number of acres burned. Since the pattern of ignition is not known, smoke is emitted equally from all points within the square. The amount of PM_{2.5} emitted per hour is shown in Figure 3. It is assumed that burn crews operating 4-wheelers equipped with drip torches spread a set amount of fire over the landscape per unit time via stripping ignition until all of the block of land to be burned has been ignited. The four hour duration of the ignition phase explains the “box car” shaped emissions profile shown in Figure 3. Given light fuel loadings, some smoldering was continued for only several hours.

The burn area assumed in Figure 1 and linked with the emissions profile shown in Figure 3 provided emissions source data for Daysmoke. Daysmoke was then initialized with WRF hourly weather soundings to model smoke plumes from the 14 April 2008 burn. Five-minute average time series of PM_{2.5} concentrations from 6-core updraft plumes simulated by Daysmoke for 14 April 2008 at the three truck locations are shown in Figure 4. Two simulations (solid and dashed lines) demonstrate that inclusion of stochastic terms for updraft core diameter and convective mixing terms in Daysmoke lead to concentration spikes that are not reproducible.

The results from Figure 4 show that the time series of simulated smoke does not match with the observations (Figure 2). Concentration data averaged over 30-min (Figure 5) confirms Figure 4 for Truck 1. Ignition was at 1100 LST. Daysmoke overestimates smoke concentrations from 1130-1300 LST and underestimates concentrations thereafter. The outcome is a flat, relatively uniform, distribution of smoke throughout the simulation. The results for Truck 2 (Figure 6) are similar to the results for Truck 1 with the exception that Daysmoke overestimated concentrations for the duration of the burn excepting 1430 LST. At Truck 3 (Figure 7), Daysmoke-simulated smoke concentrations peaked at 1200 LST instead of at 1430 LST as observed.

Given the assumptions made in the standard method for Daysmoke as shown in Figure 1 and Figure 3, namely that the burn area could be represented as a square and that fire was spread on the landscape at the same rate throughout the burn, the relatively uniform magnitude of smoke simulated for the duration of the burn should not have been unexpected. Therefore, the analysis for 14 April 2008 is revisited with respect to the shape of the burn area and how fire was placed on the landscape.

Analysis 2: Detailed Analysis for 14 April 2008.

Figure 8 is a map showing the elongated burn area and fire lines used during the 14 April burn. This burn area cannot be represented by a square as done for the standard analysis. Figure 8 also shows the burn area sectored into five distinct sub-areas. Burn crews began at the first sub-area at the bottom of the figure and progressed to the northernmost sub-area. Thus the method for spreading fire on the landscape violated the second assumption used for the standard analysis, namely, that smoke is emitted uniformly within the square burn area throughout the course of the burn.

Therefore, the 14 April burn was re-analyzed subject to the following conditions. The five sub-areas were designated as five separate burns. These areas were re-mapped into

the model domain of the experimental fire spread/relative emissions model, Rabbit Rules and color-coded (Figure 9). The centroid for each burn site was geopositioned via Google-Earth. Rabbit Rules was started at the ignition lines shown in Figure 8. Then the interiors of the areas were subjected to ignition by stripping. The outcome was a sort of “area characterization by fire” as summarized in Table 1.

Table 1. Statistics of the five burn “sub-areas” as calculated through Rabbit Rules or designated for Daysmoke.

| Red | Orange | Yellow | Burn sub-area | | Totals | Comments |
|--------|--------|--------|---------------|---------|---------|-----------------|
| | | | Lt Blue | Blue | | |
| 18,214 | 31,171 | 40,213 | 26,297 | 136,280 | 252,175 | Total Rabbits |
| 0.07 | 0.12 | 0.16 | 0.10 | 0.54 | 1.00 | Fractional area |
| 29 | 49 | 64 | 42 | 216 | 400 | Acres burned |
| 17 | 30 | 38 | 25 | 130 | 240 | Burn minutes |
| 1,017 | 1,740 | 2,245 | 1,468 | 7,608 | 14,078 | PM2.5 (kg) |
| 3 | 3 | 4 | 2 | 6 | | Core number |

The first line of Table 1 lists the number of rabbits – a rabbit is an autonomous agent representing an element of fire – involved for each burn area. From these were calculated the fractional area burned (line 2), the number of acres burned out of 400 acres (line 3), the number of minutes of active ignition (line 4), and the mass of PM2.5 released from each burn as a fraction of total active burn phase emissions (Figure 3) (line 5).

Another factor of the detailed analysis is the assignment of updraft core numbers appropriate for the five burns. The standard method for analysis uses six updraft cores for a 400 acre prescribed burn. However several of these burns are much smaller and the arbitrary assignment of six updraft cores for these burns may not be representative of the plume dynamics. Daysmoke provides no mechanism for determining updraft core number. Updraft core number is determined by a complex interaction among a number of factors. Some of these factors are:

- Size of burn area – a small burn area should be expected to produce only one updraft core; large burn areas can support many updraft cores.
- Shape of burn area – a burn area that is highly irregular in shape will require an irregular distribution of fire leading to many updraft cores. This problem can be amplified when wind direction maximizes irregularities.
- Heterogeneity of fuels – fuels that burn hot relative to surrounding fuels will develop stronger convective currents and will tend to form updraft cores.
- Fuel type, moisture, and loadings – all three factors relate to heat production. High heat production will develop convective columns and lead to fewer updraft cores; low heat production will lead to many updraft cores
- Distribution of fire on landscape - fire distributed along a long linear line will produce many updraft cores; fire spread evenly over length and depth (mass ignition, stripping) will organize convective columns into fewer updraft cores.
- Amount of fire on landscape – a small amount of fire will reduce emissions per second but decrease heat thus minimizing convective organization. Result: many

- updraft cores. A large amount of fire will produce the opposite. Result: fewer updraft cores
- Distribution of canopy gaps. Hot air trapped beneath a dense canopy will flow to the gaps thus creating convective columns that produce updraft cores there. Thin (or no) canopies will not be a factor in updraft core development.
 - Transport wind speed – strong winds inhibit convective organization thus leading to many updraft cores. Weak winds allow convective organization resulting in few updraft cores.
 - Mixing layer depth – a shallow mixing layer inhibits convective organization thus leading to many updraft cores. A deep mixing layer has less adverse impact on convective organization so fewer updraft cores should be expected.

Most of these factors contribute to the development of multiple-core updrafts for the five burns. At this time the choice for updraft core is completely subjective. The selections for this study rely most heavily on the size and shape of the burn area. The number of updraft cores assigned to the five burns are listed on line 6 of Table 1.

With the aid of Table 1, each burn has an assigned acreage, mass of PM_{2.5}, time of burn, and plume updraft core number. Daysmoke was run for each burn to produce smoke plumes that drifted downwind partly over the Truck locations. When a burn was completed, it was assumed that it took 5-min to move and set up equipment for the next burn and that, once ignition began, it took another 5-min to develop a plume.

The contribution from each burn was added to the total concentration at each truck location. Results for the locations of Truck 1 are shown in Figure 10. These detailed analysis Daysmoke simulations follow the measured PM_{2.5} more closely than do the simulations by the standard method (Figure 5). The trend in concentration for the Truck 2 locations simulated in the detailed analysis (Figure 11) also better matches with the observations in comparison with the standard method (Figure 6) albeit the detail analysis overestimates concentrations as do the standard method simulations. Similar results are found for Truck 3 (Figure 12). Gone is the spurious peak in concentrations at 1200 LST (Figure 7).

Figure 13 shows the cumulative total concentrations of PM_{2.5} at the three truck locations for the observations, standard method, and the detailed analysis. At Truck 1, the standard method slightly overestimates smoke concentrations by 4%. The detailed analysis underestimates smoke concentrations by 8%. Given uncertainties of estimation in the many quantities that enter into the Daysmoke simulations, these results are quite good.

Both analyses overestimate the total concentrations at Truck 2 and Truck 3. For the standard method, the overage is by a factor of 2.37 for Truck 2 and 2.45 for Truck 3. Results for the detailed analysis are better - factors of 2.12 for Truck 2 and 2.20 for Truck 3.

14 April 2008 Analysis – Conclusions

The re-analysis of the 14April 2008 prescribed burn at Fort Benning with the standard method and the detailed analysis revealed the following: For the standard method, the representation of the burn area as a square and the release of emissions at all points in the

square uniformly throughout the duration of the burn, is admittedly crude. However the standard method is simple and, in the absence of information regarding physical specifics of the burn site, and how a burn was conducted, it may be the only method available for running Daysmoke. The detailed analysis was shown to be superior to the standard method in the time series representation of smoke in comparison with observations. As regards simulations of smoke at the ground – for which we have measurements – both methods performed equally well. The standard method was best at Truck 1 while the detailed analysis was best at Truck 2 and Truck 3. Both approaches greatly overestimated smoke at Truck 2 and Truck 3.

Although the detailed analyses improve on the standard method in comparison with measured PM_{2.5} concentrations, it is the cumulative concentration totaled for the whole burn that is most important for smoke injection into atmospheric chemistry models. In other words, air chemistry models need (1) the correct amount of smoke placed at (2) the correct levels in the atmosphere at (3) the correct times. Simulating the correct amount of smoke is of first importance. In this regard, a claim that the detailed analysis gave a statistically significant improvement over the standard method would be difficult to prove. Operationally, the additional labor required to implement the detailed analysis seems difficult to justify.

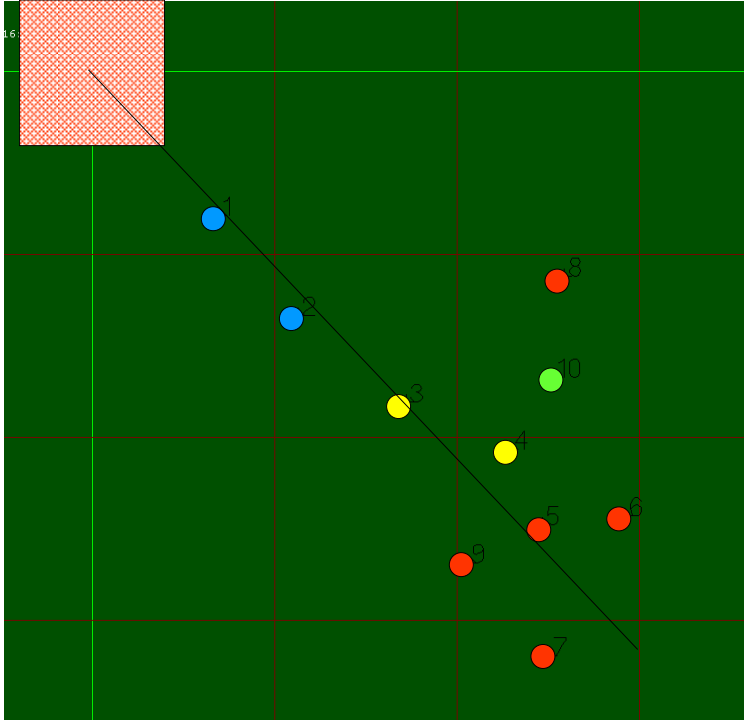


Figure 1. Locations of the three trucks (blue, yellow, red) relative to the 400 acre burn site (red shaded square) for the 14 April 2008 burn. (see text for explanation). The black line identifies the expected wind direction. Squares on the map denote 1-mile intervals.

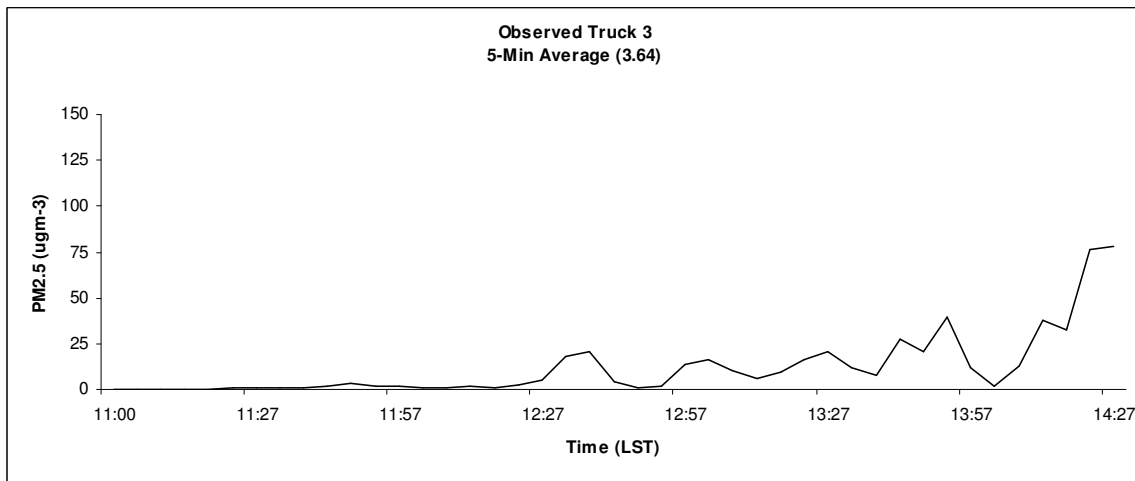
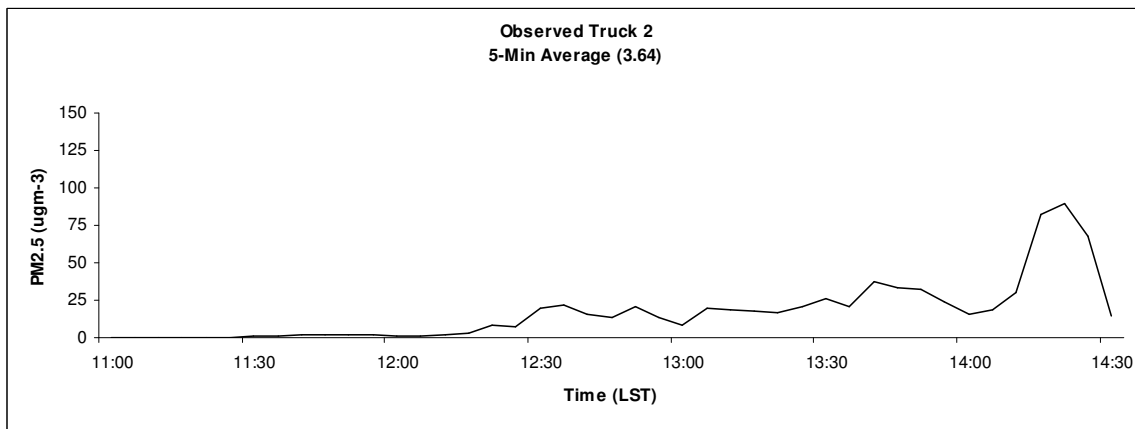
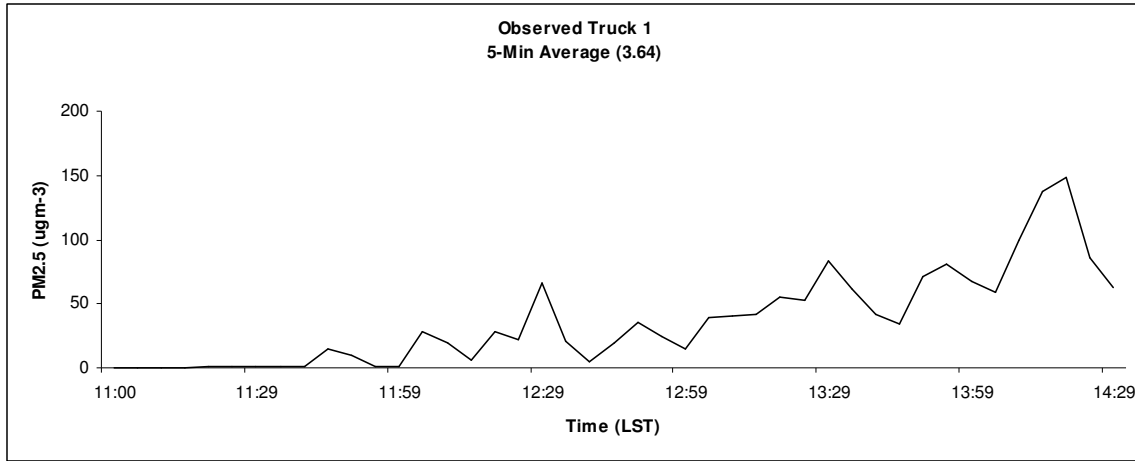


Figure 2. Time series of five-minute average PM_{2.5} concentrations as measured by DustTrak samplers rigged to the three trucks. Measurements have been calibrated for wood smoke through division by a factor of 3.64.

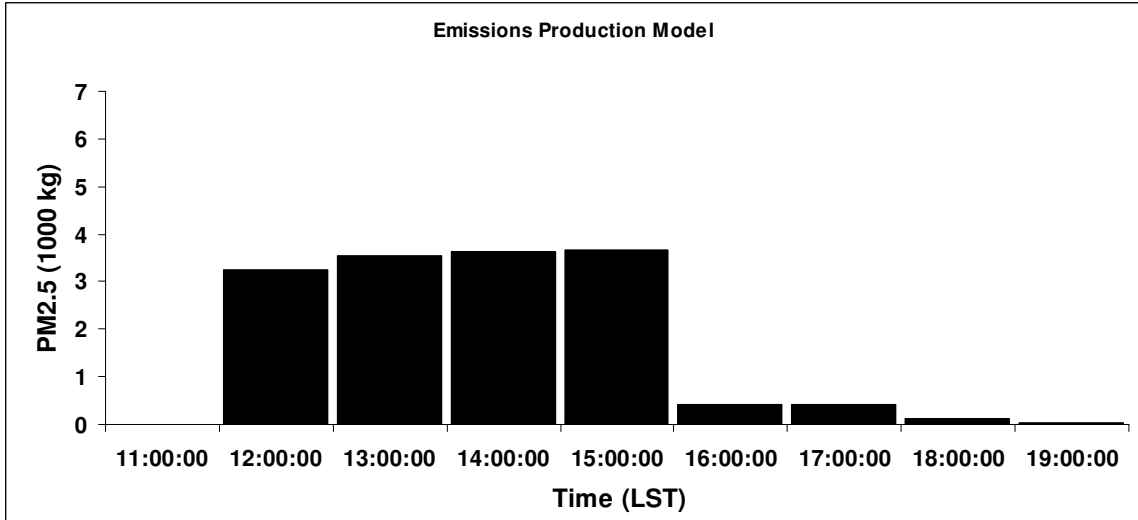


Figure 3. Hourly PM2.5 emissions used for 14 April 2008.

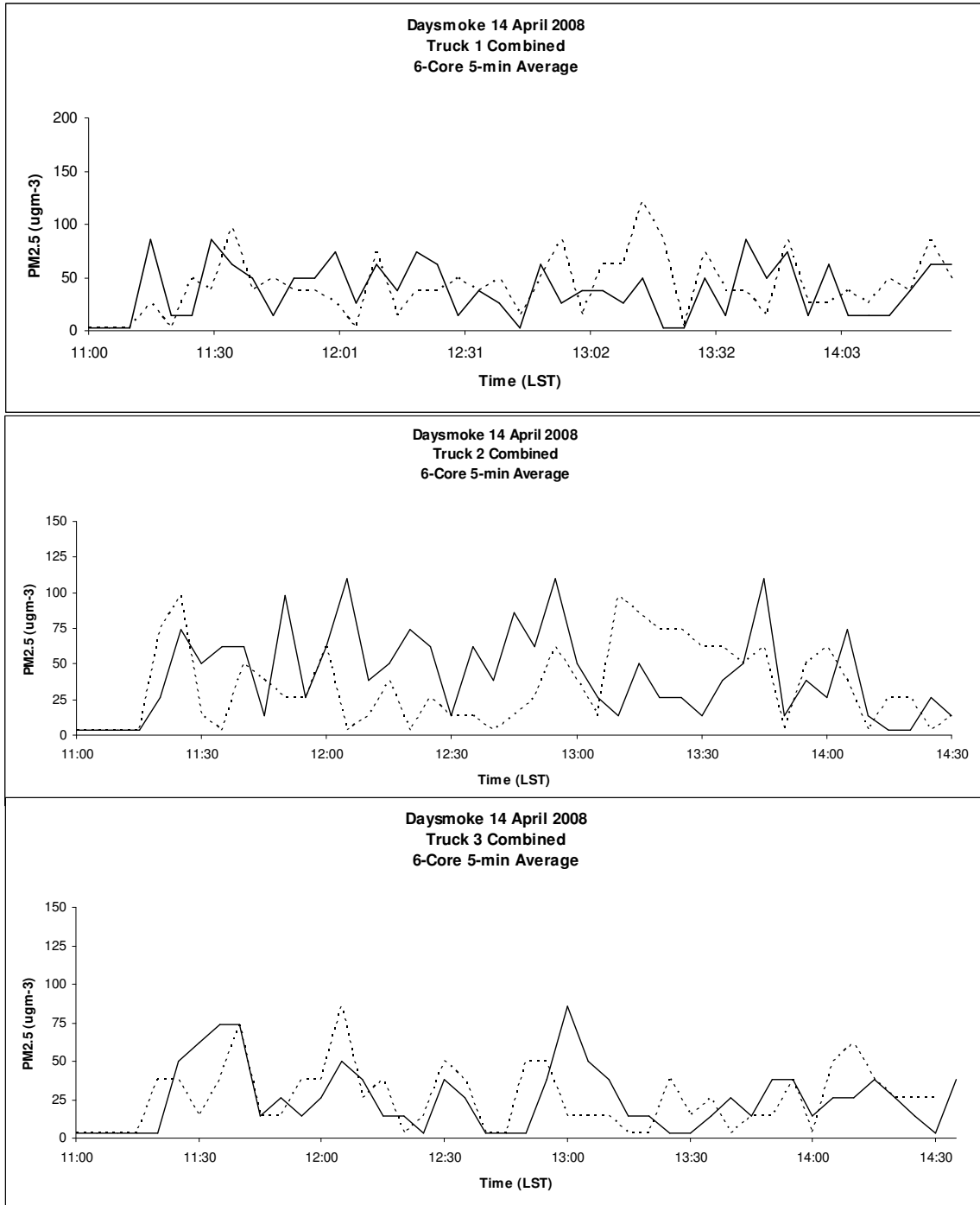


Figure 4. Time series of five-minute average PM_{2.5} concentrations for each truck location simulated by two runs with Daysmoke using the standard method (solid and dashed lines).

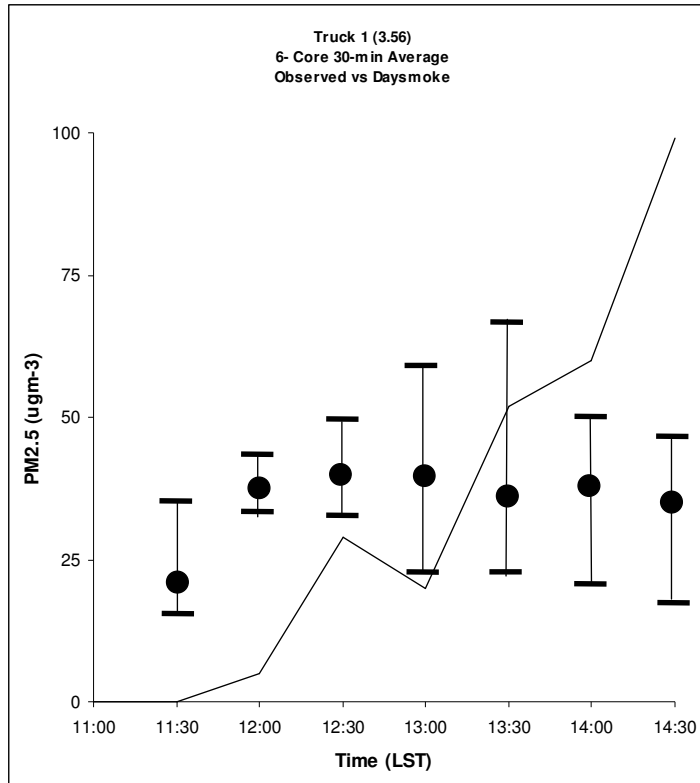


Figure 5. Time series of 30-min averaged PM2.5 from an ensemble of 5 Daysmoke simulations set for 6-core updraft smoke plumes for Truck 1. The averages are represented by the dots and the range of concentrations are given by the bars.

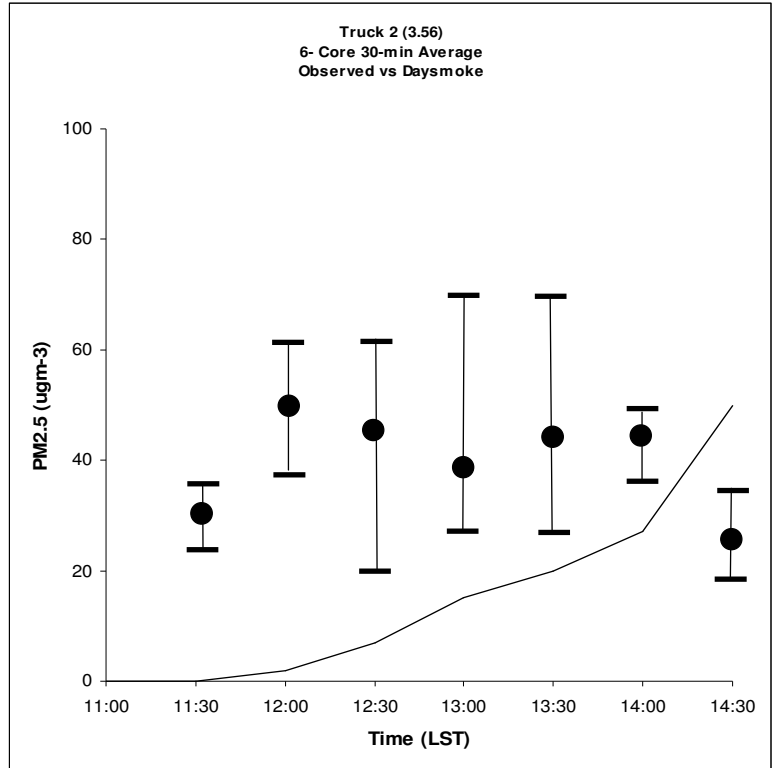


Figure 6. Same as for Figure 5 but for Truck 2.

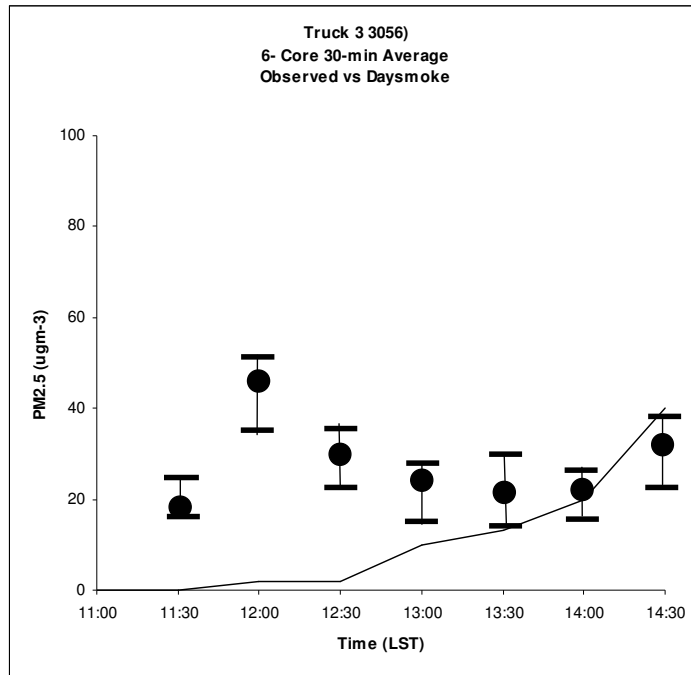


Figure 7. Same as for Figure 5 but for Truck 3.

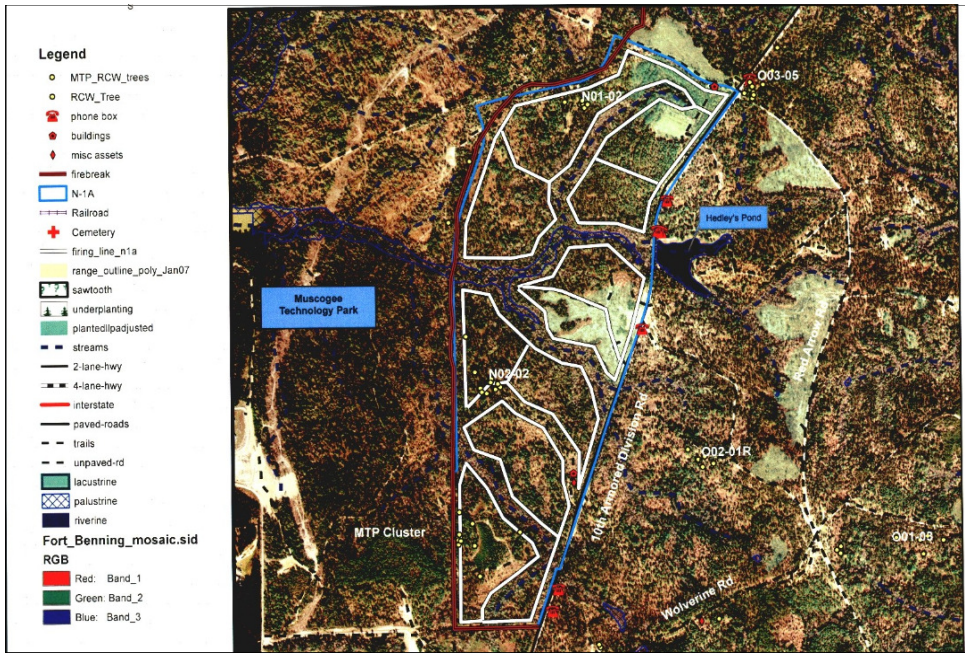


Figure 8. Map of the 14 April 2008 burn area showing fire lines (white).

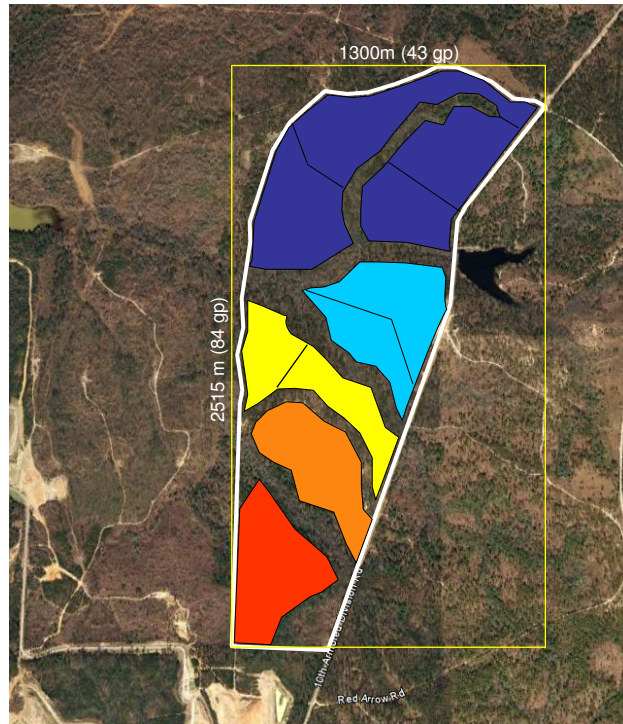


Figure 9. The 14 April 2008 burn area re-mapped and color coded for insertion into the fire spread model Rabbit Rules.

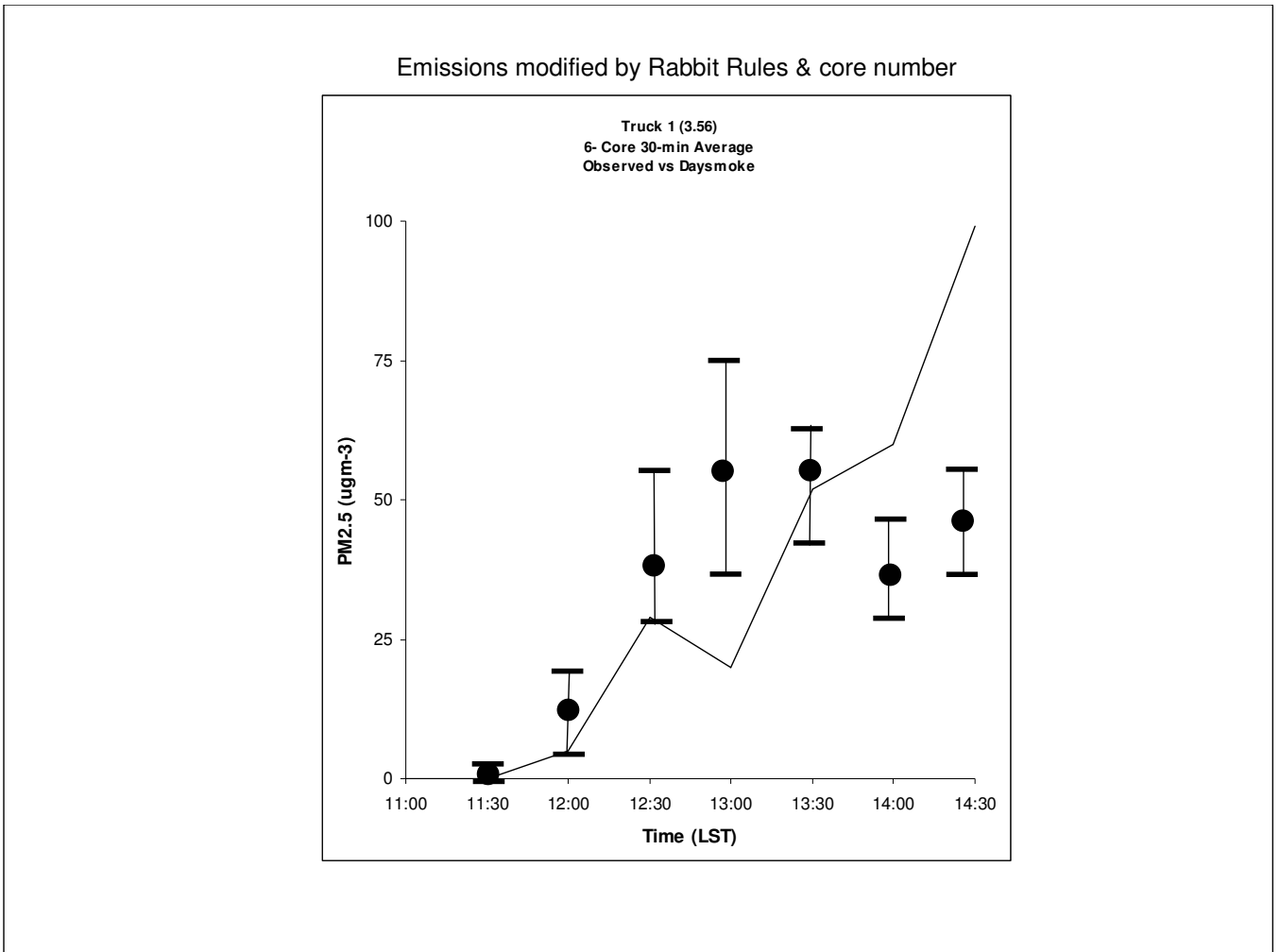


Figure 10. Time series of 30-min averaged PM_{2.5} from an ensemble of 5 Daysmoke simulations at the location of Truck 1. The concentrations are summed through the five burns (red – blue) shown in Figure 9 as part of the detailed analysis of the 14 April 2008 prescribed burn. The averages are represented by the dots and the range of concentrations are given by the bars.

Emissions modified by Rabbit Rules & core number

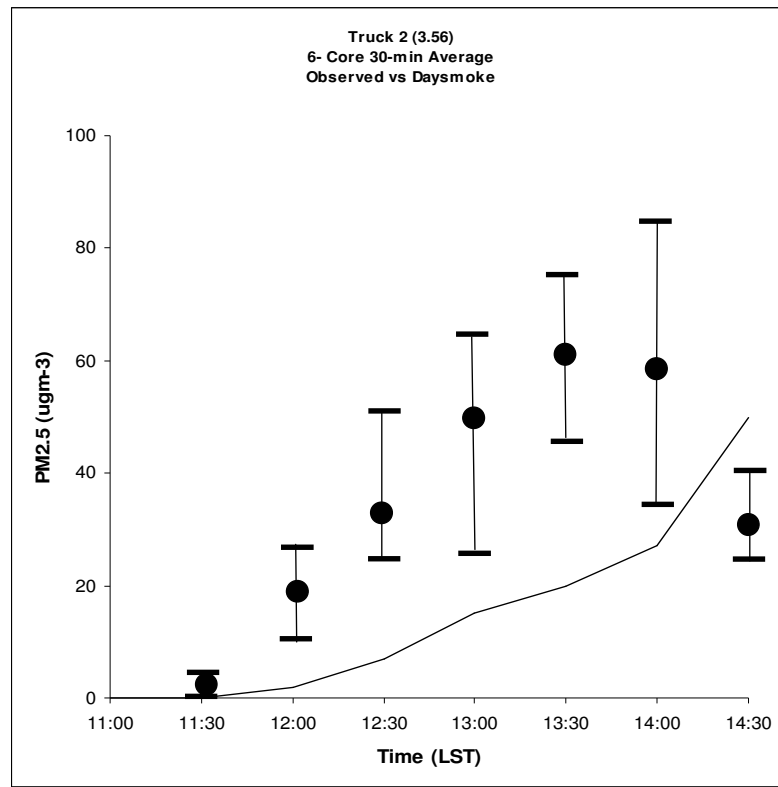


Figure 11. Same as for Figure 10 but for Truck 2.

Emissions modified by Rabbit Rules & core number

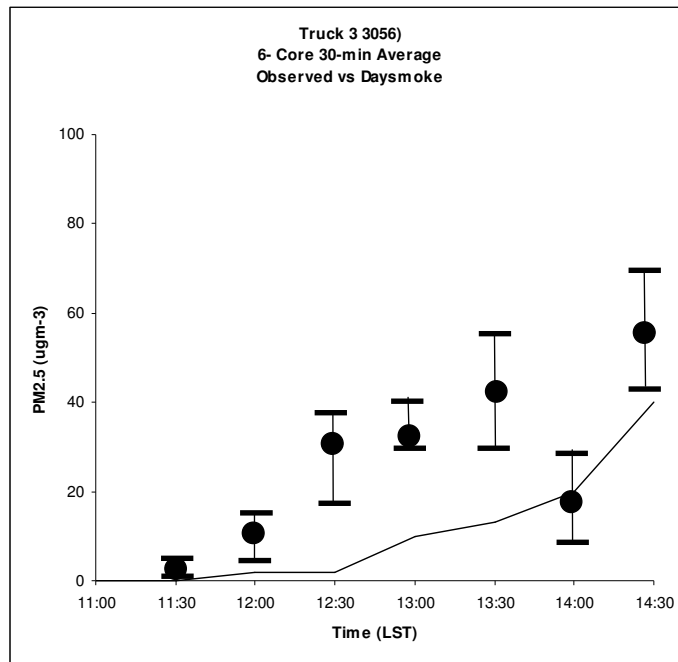


Figure 12. Same as for Figure 10 but for Truck 3.

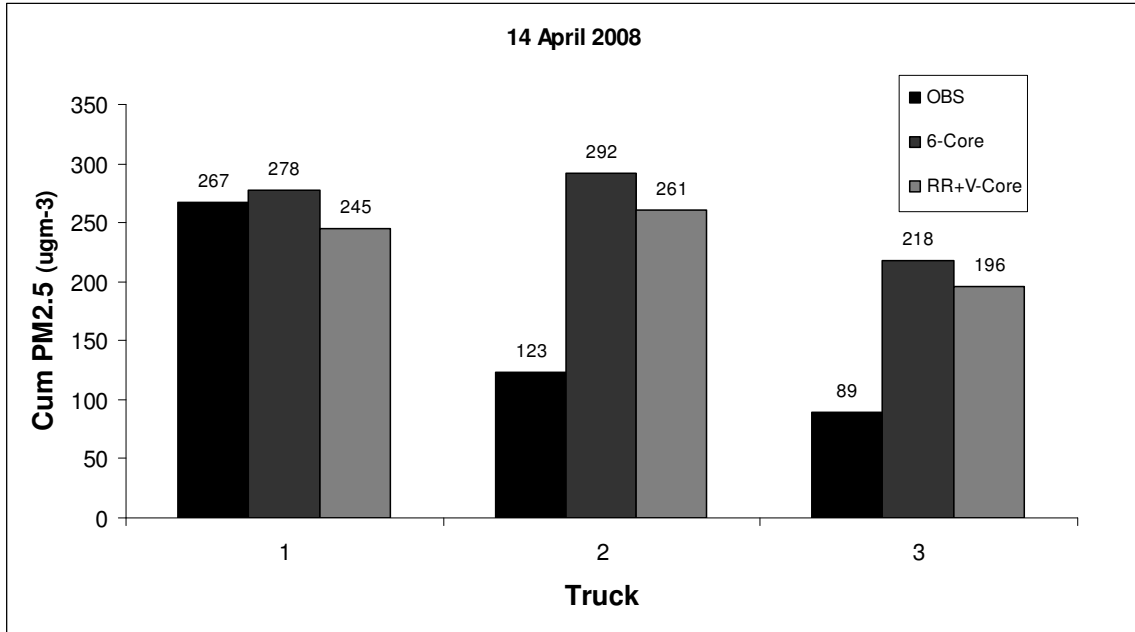


Figure 13. Cumulative smoke concentrations at the three truck locations for the observed PM2.5 (black), the 6-core updraft standard method (dark gray), and the detailed analysis (light gray).

Re-Analysis of 15 April 2008 at Fort Benning, GA

Gary L. Achtemeier
USDA Forest Service
Athens, GA
22 April 2010

Introduction.

On 15 April 2008 compartment BB3 consisting of 201 acres was burned. Ignition began at approximately 1130 LST and was completed at 1330 LST. Figure 1 shows a Google Image of the burn area.

Two trucks were positioned at distances roughly 1.3 mi and 2.5 mi (2.1 and 4.0 km) downwind from the 201 acre 15 April 2008 burn. The positions of the two trucks are numbered and color-coded in Figure 2. This case was limited by road inaccessibility. Truck 1 (blue), initially 1.3 mi (2.1 km) from the burn centroid was moved at 1144 LST to point 2 (2.6 mi, 4.2 km) very close to Truck 2 where it was found that road access needed to position under the plume was denied. Truck 1 then returned to point 1 where it remained for the duration of the burn. Truck 2 (yellow) remained at point 3- (2.1 mi, 4.0 km) from the burn centroid for the duration of the burn. Road access restrictions prohibited Truck 2 from positioning beneath the plume and therefore no smoke was observed at the Truck 2 site. The white circle locates positions of the UMASS lidar.

Winds at 200 m (approximation to the transport winds) developed by the WRF model were characterized by relatively constant speeds (4.4 m sec^{-1} at 1100 LST to 4.9 m sec^{-1} at 1400 LST). Wind directions shifted from 024 deg at 1100 LST to 353 deg at 1400 LST. The range of wind shift is shown by the beginning direction (solid line) and the ending direction (dashed line) in Figure 2.

Observations

The upper panel of Figure 3 shows the 30-sec PM_{2.5} record from 1100–1400 LST for Truck 1. The truck was moved from 1144 – 1149 LST during a time little smoke was being observed. Most of the smoke arrived after 1300 LST with numerous peaks in concentration exceeding $100 \mu\text{gm}^{-3}$. The lower panel shows the 30-sec PM_{2.5} record for Truck 2. No smoke was observed at Truck 2 until after 1345 LST. The peak of $19 \mu\text{gm}^{-3}$ at 1405 LST, if it was from smoke, indicated a brief residence time of smoke in very low concentrations.

Daysmoke Results for PM_{2.5}

For the Daysmoke simulations, the block BB3 burn was treated as a square of area equal to the area of block BB3. Ignition was at 1130 LST.

The Daysmoke results are based on a subjective determination of the updraft core number that would be typical for the 15 April burn. Daysmoke provides no mechanism

for determining updraft core number. Updraft core number is determined by a complex interaction among a number of factors. Some of these factors are:

- Size of burn area – a small burn area should be expected to produce only one updraft core; large burn areas can support many updraft cores.
- Shape of burn area – a burn area that is highly irregular in shape will require an irregular distribution of fire leading to many updraft cores. This problem can be amplified when wind direction maximizes irregularities.
- Heterogeneity of fuels – fuels that burn hot relative to surrounding fuels will develop stronger convective currents and will tend to form updraft cores.
- Fuel type, moisture, and loadings – all three factors relate to heat production. High heat production will develop convective columns and lead to fewer updraft cores; low heat production will lead to many updraft cores
- Distribution of fire on landscape - fire distributed along a long linear line will produce many updraft cores; fire spread evenly over length and depth (mass ignition, stripping) will organize convective columns into fewer updraft cores.
- Amount of fire on landscape – a small amount of fire will reduce emissions per second but decrease heat thus minimizing convective organization. Result: many updraft cores. A large amount of fire will produce the opposite. Result: fewer updraft cores
- Distribution of canopy gaps. Hot air trapped beneath a dense canopy will flow to the gaps thus creating convective columns that produce updraft cores there. Thin (or no) canopies will not be a factor in updraft core development.
- Transport wind speed – strong winds inhibit convective organization thus leading to many updraft cores. Weak winds allow convective organization resulting in few updraft cores.
- Mixing layer depth – a shallow mixing layer inhibits convective organization thus leading to many updraft cores. A deep mixing layer has less adverse impact on convective organization so fewer updraft cores should be expected.

For the 15 April 2008 burn, the relatively weak 200 m transport winds ($4.4\text{--}4.9\text{ m sec}^{-1}$) serves to decrease updraft core number. The deep mixing layer (2040-2444 m) also serves to decrease the number of updraft cores, however the organization of weak plume updrafts within this deep mixing layer is problematic. The shape of the burn area, with the long axis oriented normal to the wind direction, favors an increase in the number of updraft cores. An updraft core number of 4 cores is assigned for this burn.

Figure 4 compares the 3.5 hr average PM_{2.5} for the period of the burn with the results from a 5-ensemble Daysmoke average for 4-core updraft plumes for the locations of the trucks. Daysmoke predicted smoke at Truck 1 ($26\text{--}30\text{ }\mu\text{gm}^{-3}$). However, Daysmoke produced an average $18\text{ }\mu\text{gm}^{-3}$ at the Truck 2 location. No smoke was observed at Truck 2. Examination of the truck positions relative to wind direction in Figure 2 show that Truck 1 was located left of the plume axis (looking downwind) early then near the plume axis later as winds shifted from 024 deg to 353 deg near the end of the burn. The implication is that high concentrations of smoke should have arrived late in the burn period as the wind shifted to place Truck 1 along the plume axis. See also Figure 3 (upper panel). However, Figure 5 (left panel) shows that smoke in high concentration arrived too soon at 1230 LST suggesting that the wind shift occurred too soon. Even though Truck 1

was near the plume axis late in the burn, lower level winds with stronger westerly components blew the smoke more toward Truck 2 thus resulting in slightly diminished concentrations at Truck 1 after 1230 LST. Regarding Truck 2, Truck 2 was located outside of the plume early, then close enough to the plume axis later as the wind shifted for Daysmoke to place higher smoke concentrations there after 1330 LST.. This could not have occurred because no smoke was observed at Truck 2.

In summary, the 15 April 2008 burn has been plagued by faulty wind direction problems. The winds provided for Daysmoke turned from blowing from the northeast to blowing from west of north with stronger westerly components near the ground. It is clear from the observations that winds could not have blown from directions simulated by WRF and there have been no smoke observed at Truck 2 unless the burn was not done at block BB3.

Daysmoke Results for Plume Top Height

Figure 6 shows images for the lidar (upper panel) and 3 mm radar (lower panel) as measured by UMASS for the period 1200-1230 LST (time in the figure are in GMT – subtract 5 hr to convert to LST) for the 15 April 2008 burn. The lidar is highly attenuated above 1000 m. Both panels show the plume rising to between 1000-1500 m. The plume also appears as a disjointed series of towers rising from the ground.

The vertical cross section for the 4-core updraft plume at 1300 LST is shown in Figure 7. The white lines identify the mixing heights. For the first several miles (km) downwind from the burn, Daysmoke tended to run the plumes with plume tops just 400 m above the ground. Mixing to higher heights above 1000 m occurred beyond 2.5 miles (4.0 km). Convective mixing in Daysmoke has ordered the plume into a series of towers rising from the ground to between 1500-2000 m.

Therefore, both the observations and Daysmoke show a smoke plume broken into vertical towers rising from the ground. Daysmoke apparently overestimated the height of the plume by 500 m but this was downwind from the location of the lidar/radar. Furthermore, growth from 400 m to the maximum plume height occurred 4 miles (6.4 km) downwind from the burn. The observations show the plume had already grown to at least 1500 m by 1.3 miles (2.1 km).



Figure 1. Google Earth image of compartment BB3 outlined in yellow for the 15 April 2008 burn at Fort Benning, GA.

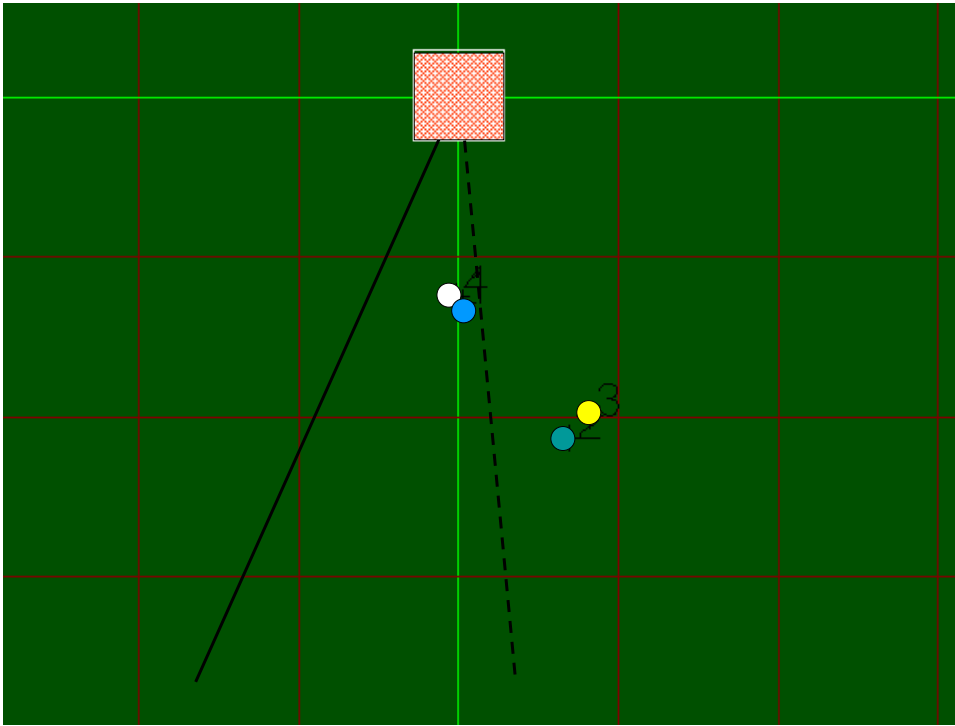


Figure 2. Locations of the three trucks relative to the Daysmoke depiction of the compartment BB3 burn with reference to the compartment center point. The diagonal solid and dashed black lines delineate prevailing wind directions.

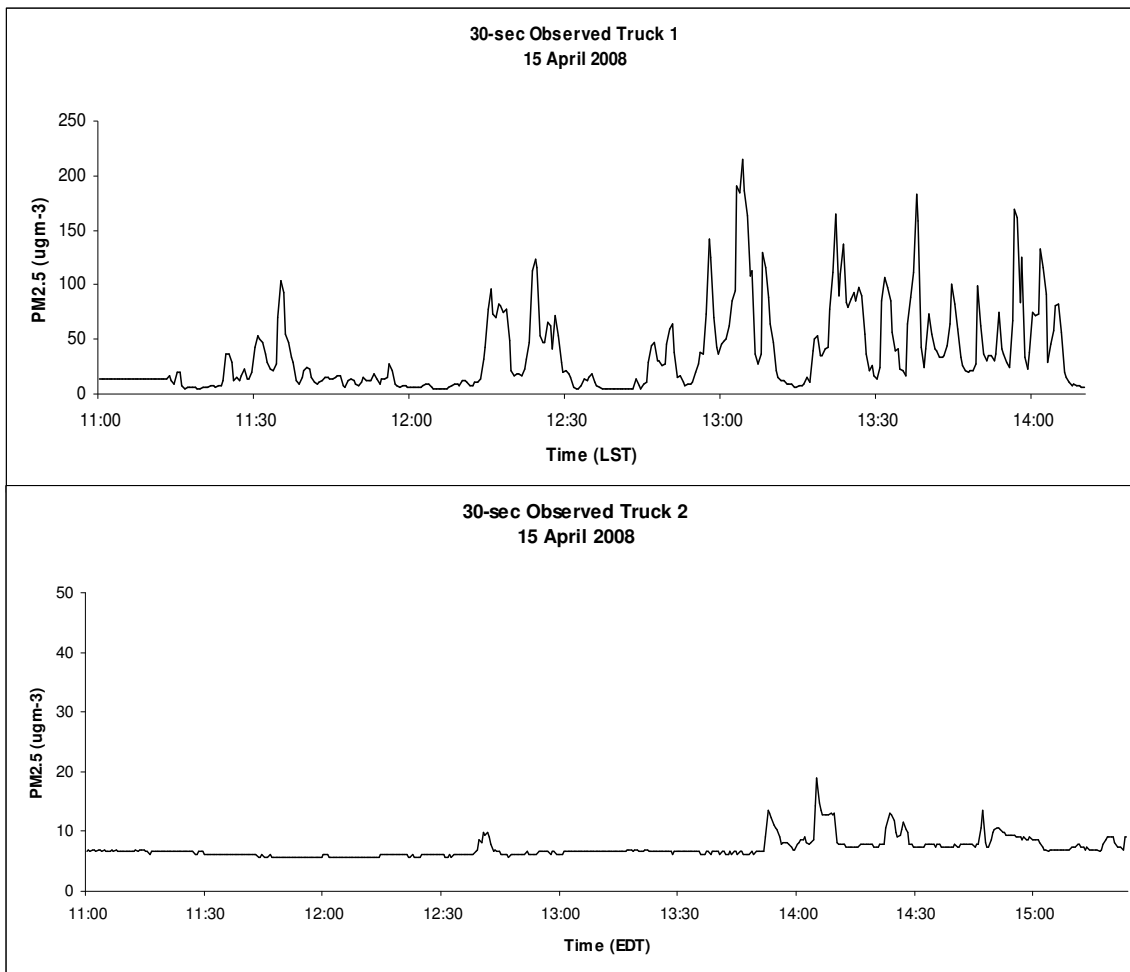


Figure 3. Traces of the 30-sec observed PM_{2.5} measured at the locations of Truck 1 (top panel) and Truck 2 (lower panel) for the 15 April 2008 burn.

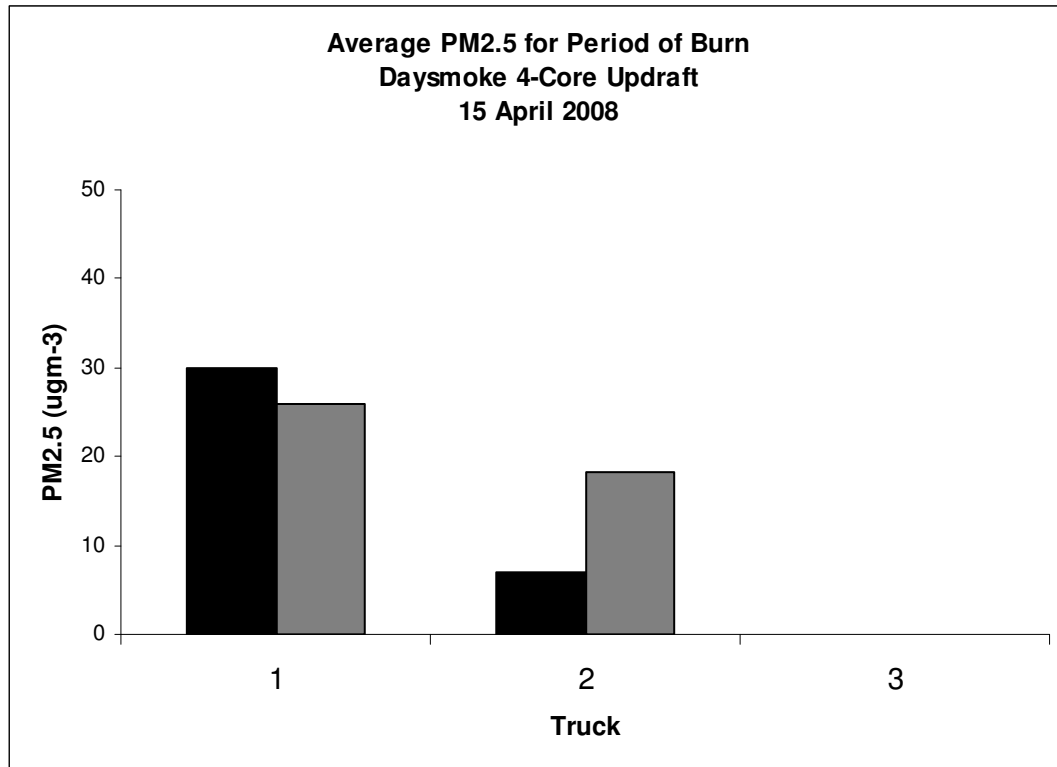


Figure 4. The average PM2.5 for the 2.5 hr period of the burn (black bars) compared with the 5-ensemble average 4-core updraft Daysmoke simulations (gray bars) for the 15 April 2008 burn.

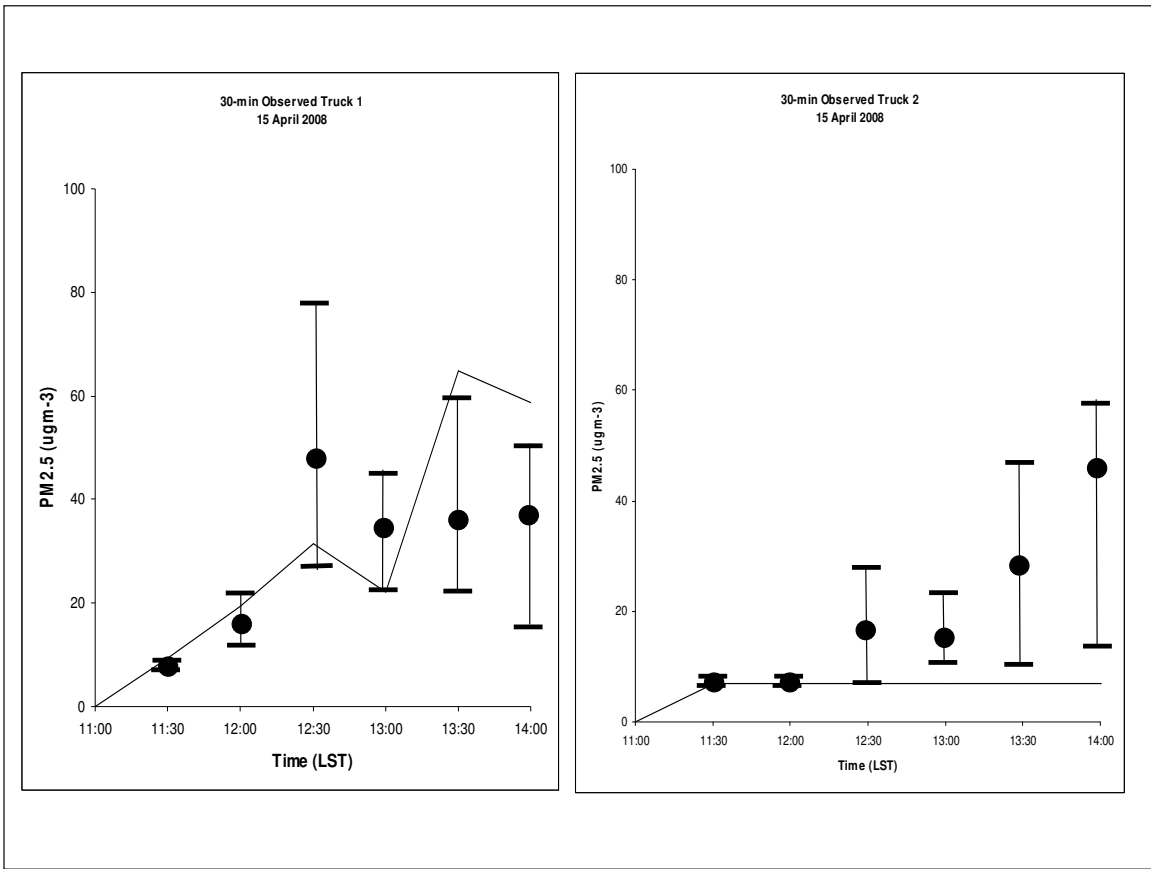


Figure 5. 30-min averaged PM2.5 generated by Daysmoke for 4-core updraft plumes at Truck 1(left panel) and 4-core updraft plumes at Truck 2 (right panel) compared with 30-min averaged observed PM2.5.

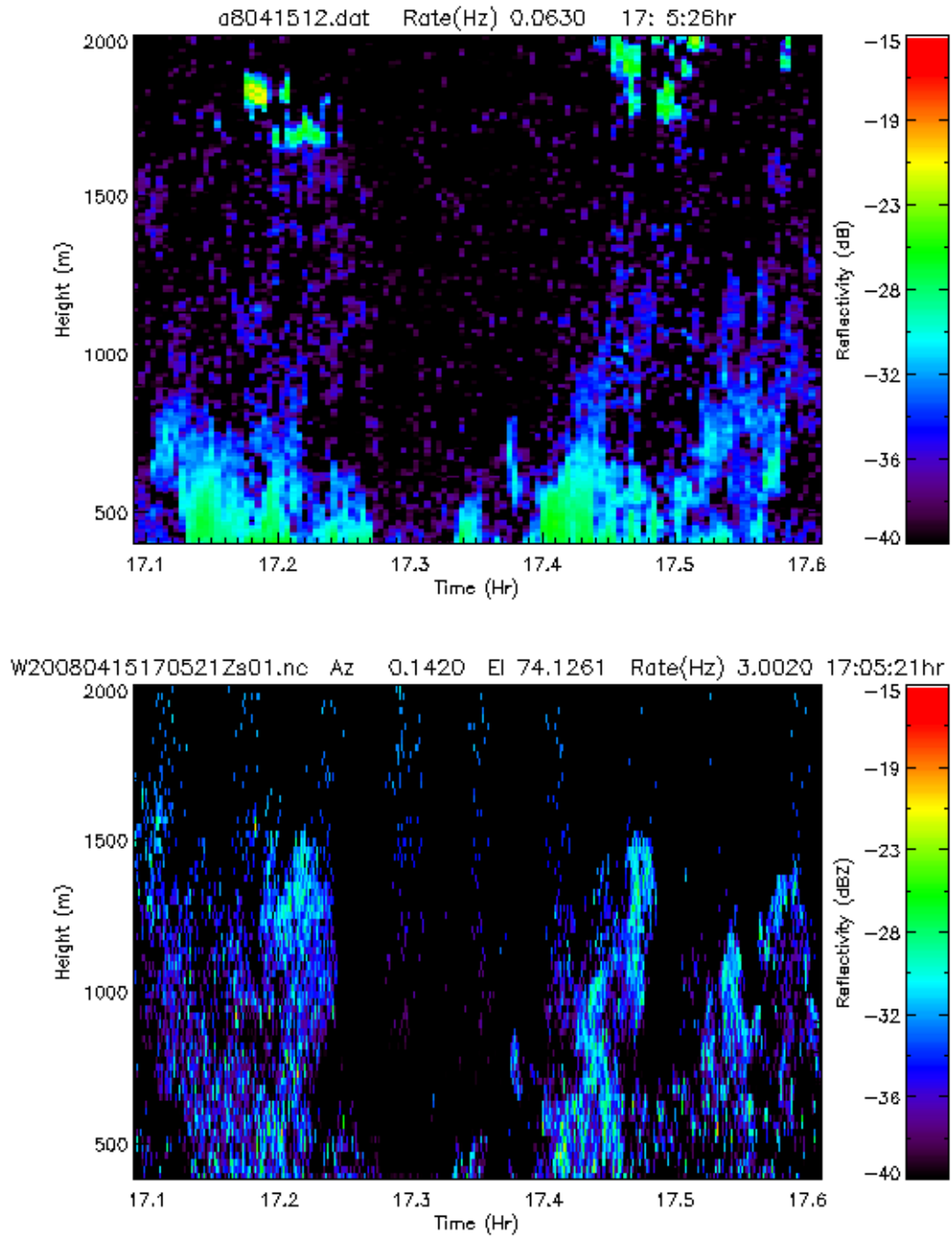


Figure 6. Vertical cross sections of the 15 April 2008 Ft Benning plume from 1200-1230 LST (1700-1730 GMT) for the UMASS lidar (upper panel) and UMASS 3 mm radar (lower panel).



Figure 7. Vertical cross section for a 4-core updraft plume modeled by Daysmoke for 1300 LST 15 April 2008. The white horizontal tic marks denote 100 m intervals. The vertical tic marks denote 1.0 mile (red) and 1.0 km (white) intervals.

Analysis of 13 January 2009 at Fort Benning, GA

Gary L. Achtemeier
USDA Forest Service
Athens, GA
5 March 2010

Introduction.

On 13 January 2009 compartment O7 consisting of 276 acres was burned. Ignition began at approximately 1230 LST and was completed at 1430 LST. Due to very limited access to the area, the UGA teams set up along a north-south road to the southeast of the burn site. This was the first case where trucks were located at distances in the range 5-10 miles downwind from the burn. Truck 1 (blue square in Figure 1) was the farthest away (13.92 km, 8.63 mi), then Truck 2 (yellow square) (11.77 km, 7.27 mi), and Truck 3 (red square) being the closest (11.35 km, 7.09 mi).

Winds were light and variable at the beginning of the burn period. Winds shifted to blow from the northwest by approximately 5 m sec^{-1} by the end of the period.

Observations

Because smoke concentrations were so low for the 13 January burn, discussion of the observations is in reference to graphs of the raw 30-sec data (calibrated for wood smoke). The top panel of Figure 2 shows the PM_{2.5} trace for Truck 1 located at the southernmost position (Figure 1). This trace is flat at the background concentration of 4 ug m^{-3} with the exception of prominent peaks at 1303 LST and at 1512 LST. Thus the trace for Truck 1 most likely shows that the smoke plume never impacted Truck 1 and that the peaks in PM_{2.5} concentration were caused by traffic contamination. Truck 1 crews reported a tractor trailer passed by at 1311 LST and multiple trucks and other vehicles passed by again from 1511-1514 LST.

The middle panel of Figure 2 shows the PM_{2.5} trace for Truck 2. Peak concentrations are only $10\text{-}15 \text{ }\mu\text{g m}^{-3}$ above the background of $5 \text{ }\mu\text{g m}^{-3}$. Sharp spikes in concentration between 1300 – 1330 LST are suggestive of non-smoke contamination. Truck 2 crews reported frequent traffic along the road throughout the sampling period. At Truck 3 (lower panel), the presence of elevated PM_{2.5} is more continuous (suggestive of smoke) than at other locations albeit concentrations are only about 10 ug m^{-3} above background. Spikes after 1500 LST are suggestive of non-smoke contamination.

With truck positions and smoke measurements taken together, the concentration traces imply that 45-min after ignition the northernmost trucks were impacted by the edge of the smoke plume. Light smoke was present at Truck 3 throughout most of the period from 1315 – 1500 LST. Scattered smoke was present at Truck 2 during the same period. Smoke was never at the location of Truck 1. If smoke from ignition traveled the 11 km to Truck 3, the calculated windspeed for travel would have been 4.2 m sec^{-1} .

Daysmoke Results

Daysmoke was initialized with fire activity data: block size = 276 acres, time of ignition = 1230 LST, time of ignition completion = 1430 LST. Emissions data were based on period of ignition (2-hr) for fuels typical of fuels measured elsewhere at Ft. Benning. Hourly WRF weather soundings provided weather data for Daysmoke.

What remains is the determination of the updraft core number that would be typical for the 13 January burn. Daysmoke provides no mechanism for determining updraft core number. Updraft core number is determined by a complex interaction among a number of factors. Some of these factors are:

- Size of burn area – a small burn area should be expected to produce only one updraft core; large burn areas can support many updraft cores.
- Shape of burn area – a burn area that is highly irregular in shape will require an irregular distribution of fire leading to many updraft cores. This problem can be amplified when wind direction maximizes irregularities.
- Heterogeneity of fuels – fuels that burn hot relative to surrounding fuels will develop stronger convective currents and will tend to form updraft cores.
- Fuel type, moisture, and loadings – all three factors relate to heat production. High heat production will develop convective columns and lead to fewer updraft cores; low heat production will lead to many updraft cores
- Distribution of fire on landscape - fire distributed along a long linear line will produce many updraft cores; fire spread evenly over length and depth (mass ignition, stripping) will organize convective columns into fewer updraft cores.
- Amount of fire on landscape – a small amount of fire will reduce emissions per second but decrease heat thus minimizing convective organization. Result: many updraft cores. A large amount of fire will produce the opposite. Result: fewer updraft cores
- Distribution of canopy gaps. Hot air trapped beneath a dense canopy will flow to the gaps thus creating convective columns that produce updraft cores there. Thin (or no) canopies will not be a factor in updraft core development.
- Transport wind speed – strong winds inhibit convective organization thus leading to many updraft cores. Weak winds allow convective organization resulting in few updraft cores.
- Mixing layer depth – a shallow mixing layer inhibits convective organization thus leading to many updraft cores. A deep mixing layer has less adverse impact on convective organization so fewer updraft cores should be expected.

For the 13 January 2009 burn, the size of the burn area – 276 acres – should be sufficient to support six updraft cores considered typical for a medium sized prescribed burn. The shape of the burn area was fairly regular and thus not a factor for increasing the number of updraft cores. Other factors, heterogeneity of fuels, fuel type, moisture and loadings, distribution and amount of fire on the landscape, and distribution of canopy gaps are considered typical for the area and neither increase or decrease the number of updraft cores.

The transport wind speed is a major factor in the selection of updraft core number. At time of ignition, wind speeds for the lowest 1200 ft (400 m) were nearly calm. Plume rise would have been nearly vertical – a condition that minimizes the impact of entrainment – thus feeding back to increase the efficiency of vertical transport. Thus the near-calm winds would have assisted the organization of the plume into one or two updraft cores.

Further inspection of the hourly WRF transport winds led to the following scenario for a wind speed / core number relationship: one updraft core for 1200-1300 LST, two updraft cores for 1300-1400 LST, four updraft cores from 1400-1500 LST, and six updraft cores after 1500 LST. The current version of Daysmoke does not allow for changing the updraft core number during the course of a burn. Thus Daysmoke was run for a range of from 1-6 updraft core numbers with no change in results at the truck locations. Thus the Daysmoke plumes shown in the figures to follow are from the 6-core updraft solution.

Figure 3 shows the pattern of ground-level smoke concentrations generated by Daysmoke at 1300 LST, 30 minutes after ignition. Given near-calm winds, smoke is concentrated at and nearby the burn site. Locations for the three trucks southeast of the burn site are shown in the figure. By 1330 LST (Figure 4) weak southwesterly winds have transported the smoke several miles east and northeast of the burn. From Figure 2 smoke was measured at Trucks 2 and 3 by 1345 LST. However, the Daysmoke-simulated concentration pattern at 1400 LST (Figure 5) continues to show the modeled plume was moving east-northeast and narrowing – an indication the transport winds speeds were increasing.

Ignition was completed by 1430 LST. The Daysmoke simulation (Figure 6) shows that winds had shifted to blow from the west-northwest and the edge of the plume approached Truck 3. At 1500 LST (Figure 7) the edge of the plume had reached Truck 3. The emissions model switched to the smoldering stage after 1430 LST. By 1530 LST (Figure 8), the last plume map as the observations ceased at 1530 LST, weaker concentrations associated with a narrower plume follow the main plume located mostly north of the trucks. Trucks 2 and 3 are contained within the edge of the plume. Smoke never moved over Truck 1.

Figure 9 shows the cumulative PM_{2.5} simulated at the three trucks. Smoke did not arrive at any of the trucks until 1500 LST, one hour and 15 min after smoke was observed (1345 LST, Figure 2). The implication is that model wind directions did not match with observed wind directions. RAWS wind data for station FBGG1 show that winds shifted from the southwest to the northwest by 1310 LST. Had the wind shift been representative of the transport wind directions, the northwest winds could have placed smoke in the vicinity of Truck 3 by 1400 LST. The WRF data used to initialize Daysmoke placed the wind shift between 1400 – 1430 LST – about an hour after the RAWS data show the wind shift occurred. Thus the cumulative PM_{2.5} concentrations reveal smoke not arriving at Truck 3 until an hour after it was observed.

Figure 10 shows average PM_{2.5} for the period of the burn. The results are excellent at Truck 1 smoke was not observed nor modeled there. Daysmoke-simulated average smoke concentrations at Trucks 2 and 3 are, as expected, lower than observed for reasons described above.

Figures

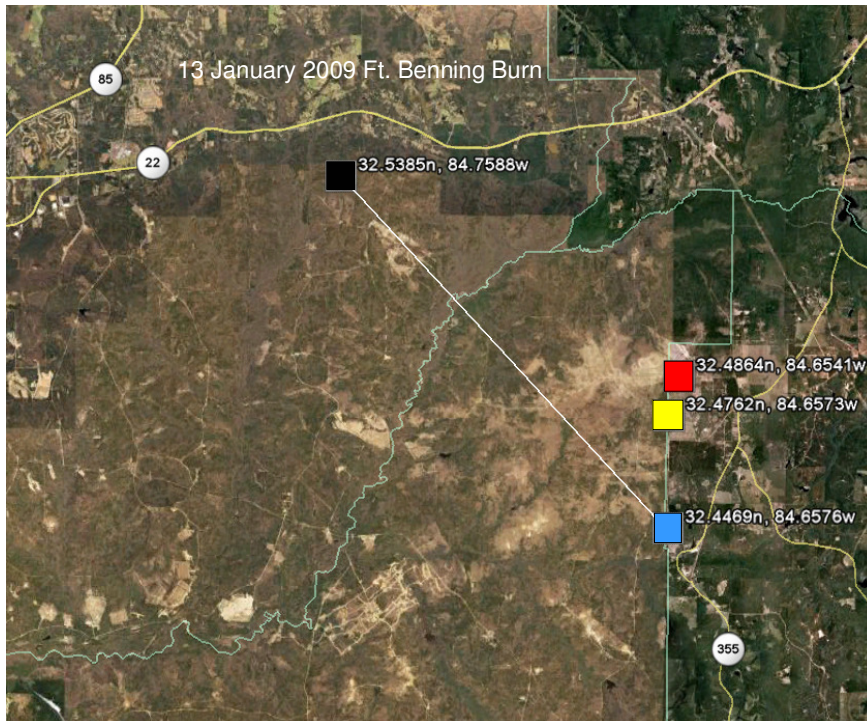


Figure 1. Google map showing the location of the burn (black square) and the locations of Truck 1 (blue square), Truck 2 (yellow square), and Truck 3 (red square).

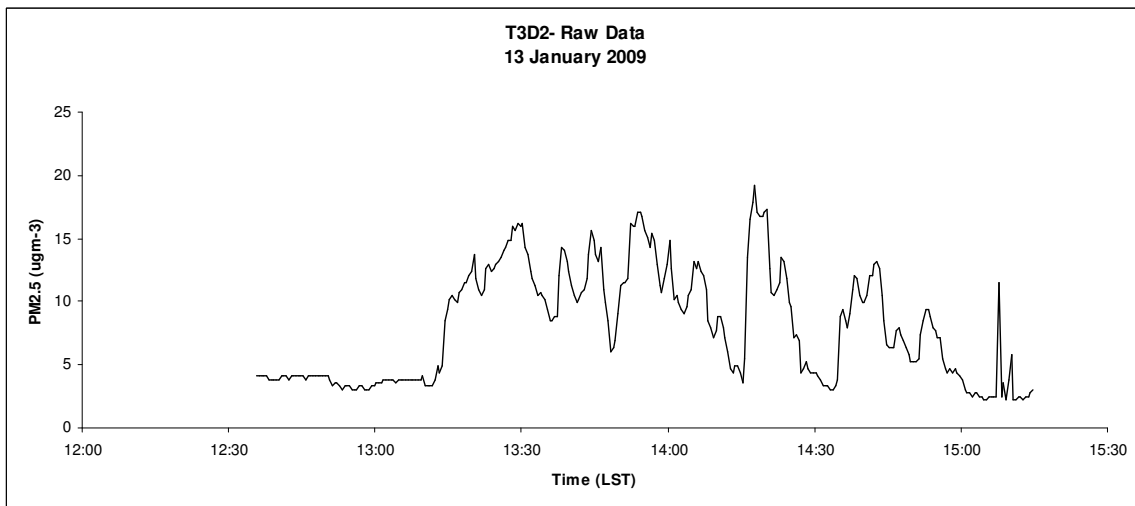
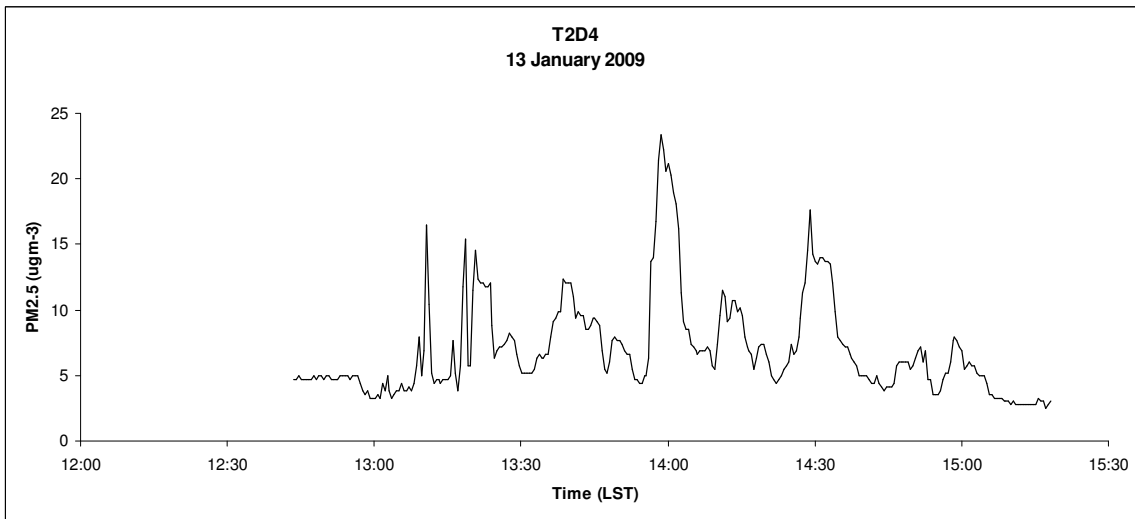
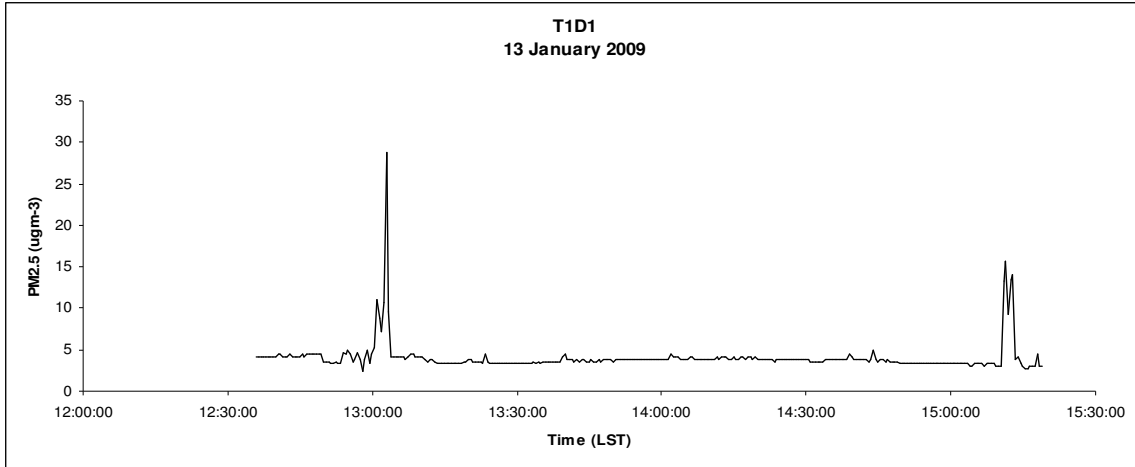


Figure 2. Graphs of 30-sec observed PM2.5 (calibrated for wood smoke) for Truck 1 (top panel), Truck 2 (middle panel), and Truck 3 (bottom panel).

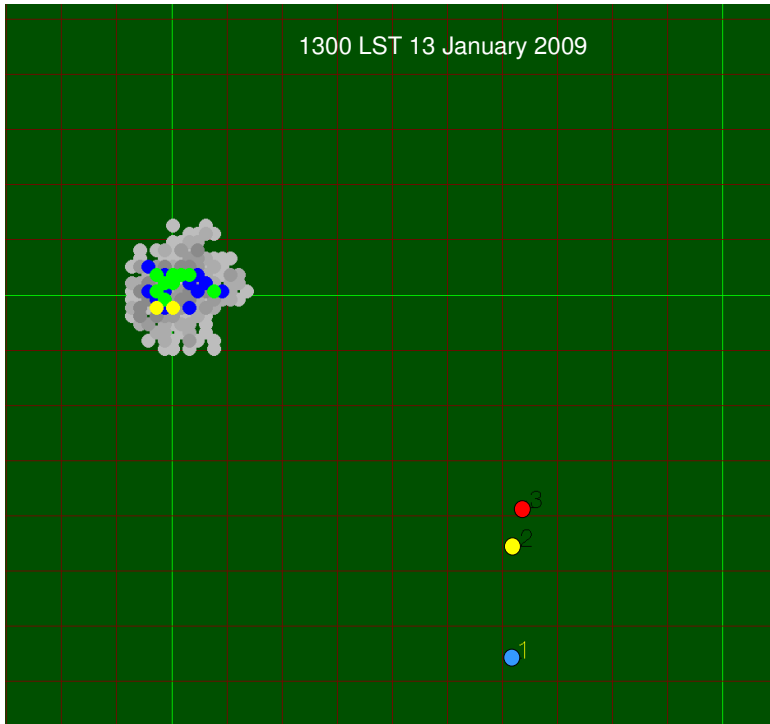


Figure 3. Ground-level PM_{2.5} concentrations simulated by Daysmoke for the 13 January 2009 burn at 1300 LST.

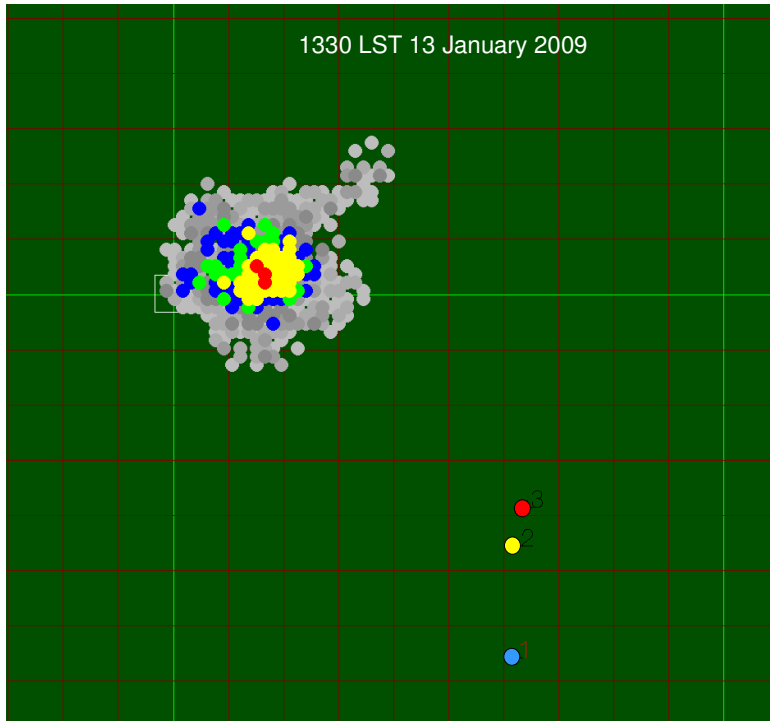


Figure 4. Same as for Figure 3 but for 1330 LST.

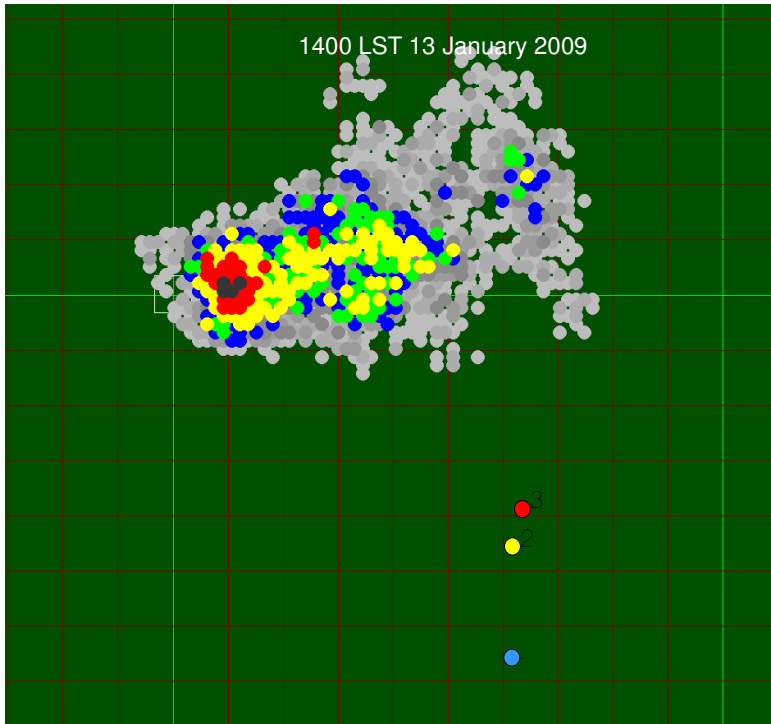


Figure 5. Same as for Figure 3 but for 1400 LST.

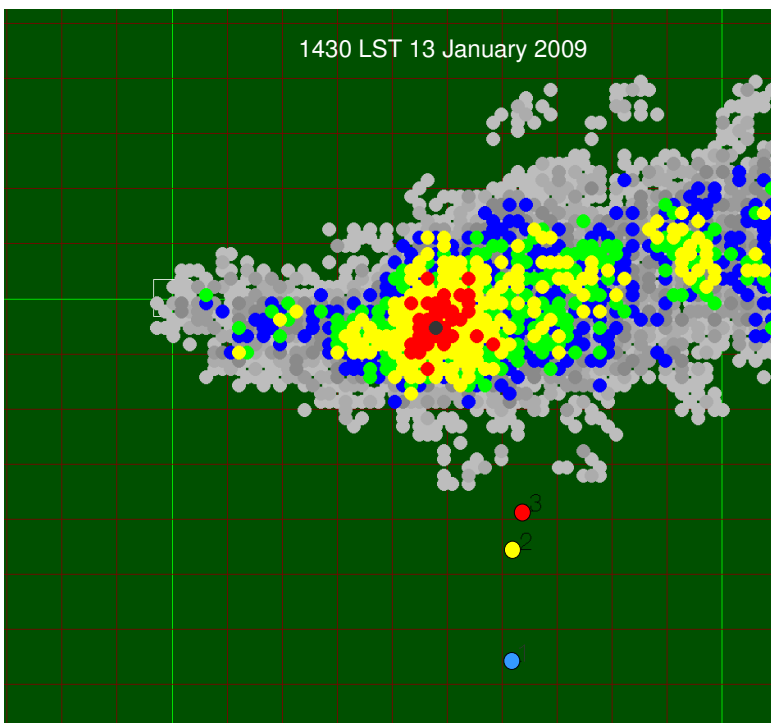


Figure 6. Same as for Figure 3 but for 1430 LST.

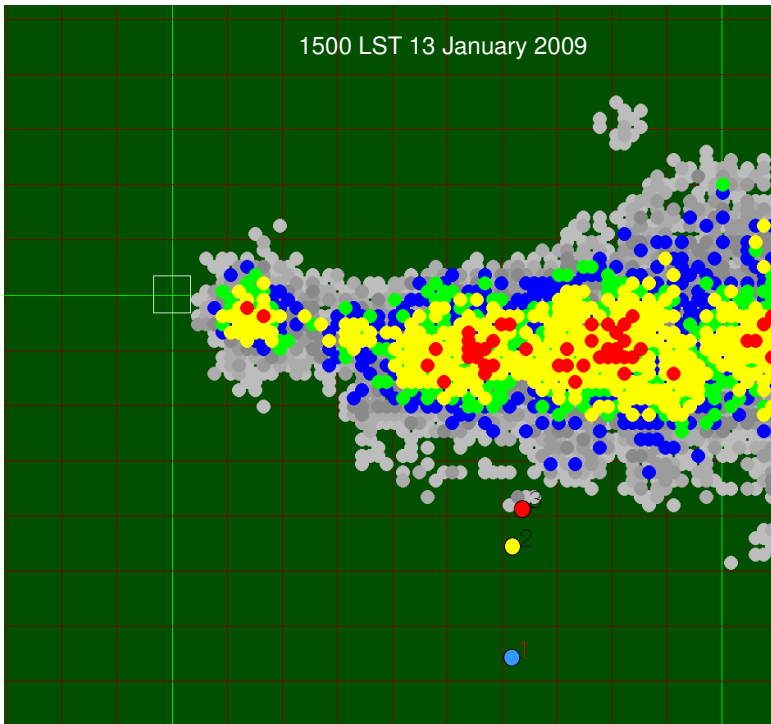


Figure 7. Same as for Figure 3 but for 1500 LST.

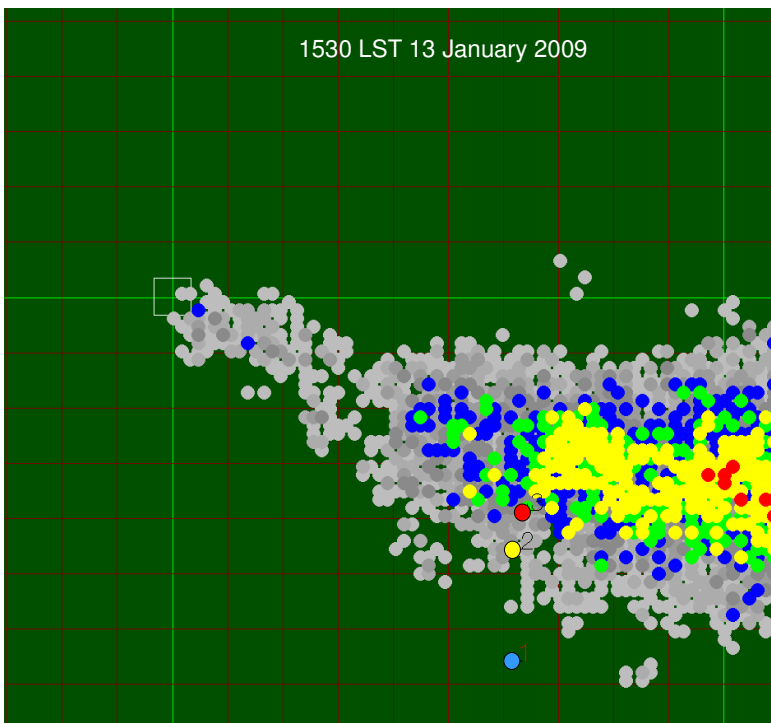


Figure 8. Same as for Figure 3 but for 1530 LST.

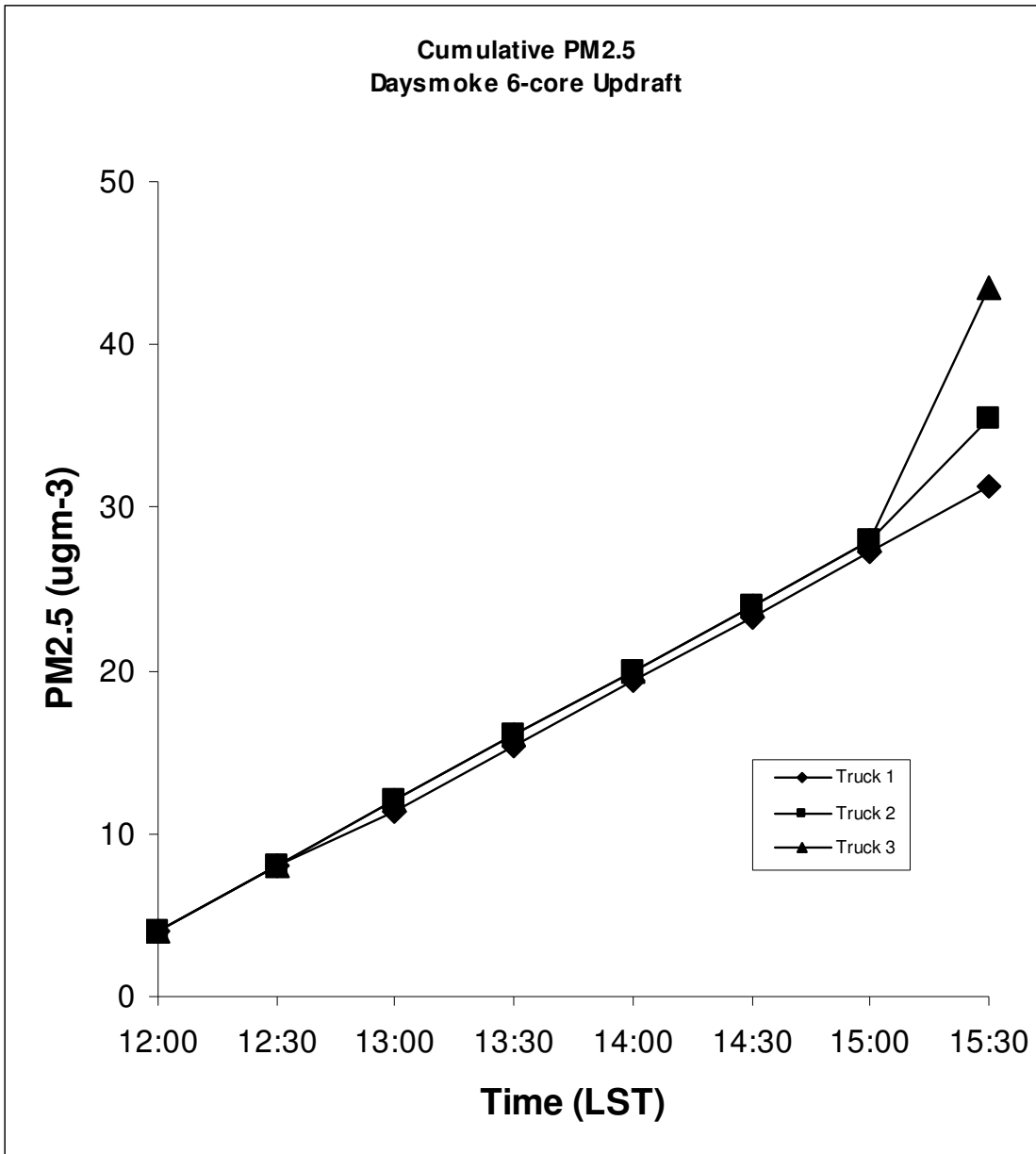


Figure 9. The cumulative PM2.5 simulated during the course of the burn for the three truck locations. Background PM2.5 from the observations of $4\text{-}5 \mu\text{g m}^{-3}$ have been added to the Daysmoke solutions.

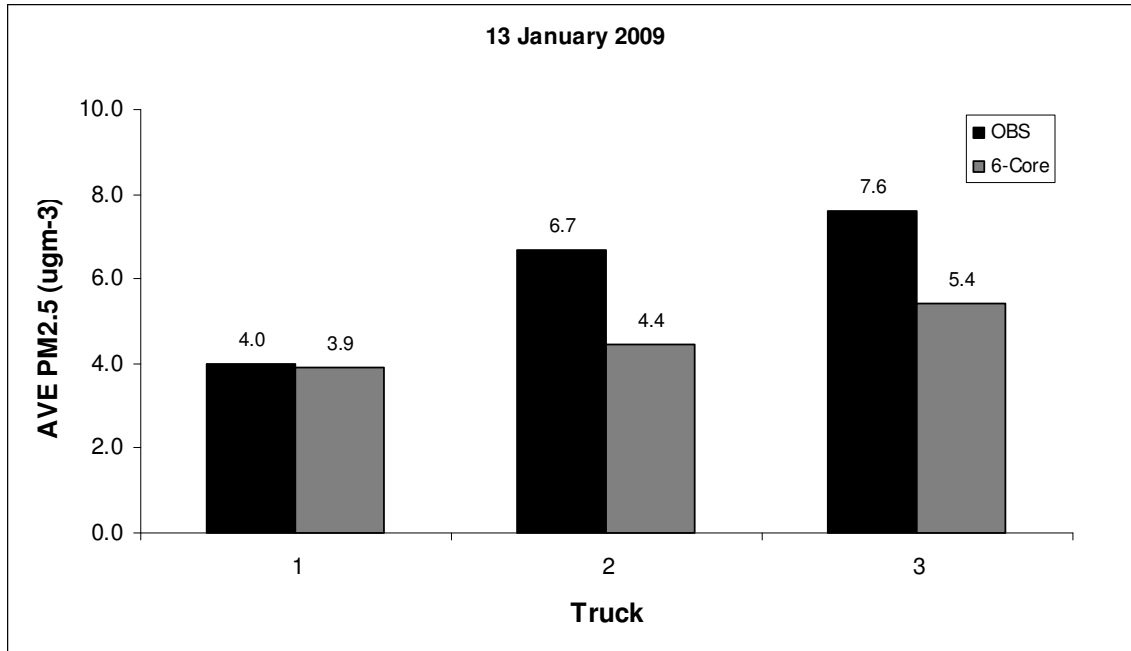


Figure 10. The average PM2.5 for the period of the burn.

Analysis of 14 January 2009 at Fort Benning, GA

Gary L. Achtemeier
USDA Forest Service
Athens, GA
5 March 2010

Introduction.

On 14 January 2009 compartments S1A, S2, and S3 consisting of 109, 163, and 150 acres (422 acres total) were burned. Ignition began at approximately 1215 LST and was completed at 1445 LST. The burns were conducted beginning at S1A (gray square in Figure 1). Then S3 (black square) was burned followed by S2 (light gray square).

All three trucks were deployed. However, faulty data downloads from Trucks 2 and 3 resulted in PM_{2.5} data collected only at Truck 1. Therefore, only information related to Truck 1 is presented. Figure 1 shows the positions of Truck 1 during the burn. From 1229-1326 LST, the truck was located at the dark blue square and from 1349-1530 LST, it was located at the light blue square. Location 1 is at the edge of a road immediately downwind from a large cleared area. Location 2 appears surrounded by canopy and thus could have been subject to canopy sheltering that could reduce measured PM_{2.5} relative to canopy level concentrations.

Winds blew steadily from 279 deg for most of the period. Wind speeds were also relatively steady at approximately 3.8 m sec⁻¹.

Observations

The graph of the raw 30-sec data (calibrated for wood smoke) is shown in the top panel of Figure 2. Most concentration peaks are below 100 μgm^{-3} . Exceptions are a peak to 200 μgm^{-3} at 1245 LST and an anomalous peak to 821 μgm^{-3} at 1341 LST. Data logs from Truck 1 reveal that data was collected at location 1 (dark blue square in Figure 1) from 1229-1326 LST and again from 1349-1530 LST (light blue square). The 23-min gap in data collection is shown in the top panel of Figure 2 as the thick horizontal line. This data gap includes the anomalous peak in PM_{2.5}. Therefore the raw data record was modified to eliminate PM_{2.5} data during the 23-min observation gap (bottom panel of Figure 2).

Daysmoke Results

For the Daysmoke simulations, the three blocks were treated as three separate burns. Block S1A was ignited at 1215 LST; block S3 ignited at 1245 LST and block S2 ignited at 1315 LST. Emissions data were based on period of ignition (2-hr) for fuels typical of fuels measured elsewhere at Ft. Benning. Hourly WRF weather soundings provided weather data for Daysmoke.

Daysmoke calculated 5-min PM_{2.5} concentrations at the truck locations for each burn. Then, to get the total impact of the burn, the concentrations for individual burns

were added. These results are contrasted with the 5-min averaged PM_{2.5} calculated from the observations in Figure 3. The top panel shows the 5-min averaged observed PM_{2.5} concentrations at Truck 1. A primary peak of 155 μgm^{-3} was found at 1245 LST. Secondary peaks of exceeding 50 μgm^{-3} were found around 1315 LST then again around 1430 LST and 1500 LST. The bottom panel shows a five ensemble average of 5-min averaged PM_{2.5} simulated by Daysmoke. Because the graph is constructed from an average of five simulations, the outcome is smoother than the graph for the observations. However, two peaks in PM_{2.5} are found – one of 118 μgm^{-3} at 1205 LST and the other at 1310 LST. PM_{2.5} generally exceeds 50 μgm^{-3} between 1420 LST and 1500 LST.

The Daysmoke results are based on a subjective determination of the updraft core number that would be typical for the 14 January burn. Daysmoke provides no mechanism for determining updraft core number. Updraft core number is determined by a complex interaction among a number of factors. Some of these factors are:

- Size of burn area – a small burn area should be expected to produce only one updraft core; large burn areas can support many updraft cores.
- Shape of burn area – a burn area that is highly irregular in shape will require an irregular distribution of fire leading to many updraft cores. This problem can be amplified when wind direction maximizes irregularities.
- Heterogeneity of fuels – fuels that burn hot relative to surrounding fuels will develop stronger convective currents and will tend to form updraft cores.
- Fuel type, moisture, and loadings – all three factors relate to heat production. High heat production will develop convective columns and lead to fewer updraft cores; low heat production will lead to many updraft cores
- Distribution of fire on landscape - fire distributed along a long linear line will produce many updraft cores; fire spread evenly over length and depth (mass ignition, stripping) will organize convective columns into fewer updraft cores.
- Amount of fire on landscape – a small amount of fire will reduce emissions per second but decrease heat thus minimizing convective organization. Result: many updraft cores. A large amount of fire will produce the opposite. Result: fewer updraft cores
- Distribution of canopy gaps. Hot air trapped beneath a dense canopy will flow to the gaps thus creating convective columns that produce updraft cores there. Thin (or no) canopies will not be a factor in updraft core development.
- Transport wind speed – strong winds inhibit convective organization thus leading to many updraft cores. Weak winds allow convective organization resulting in few updraft cores.
- Mixing layer depth – a shallow mixing layer inhibits convective organization thus leading to many updraft cores. A deep mixing layer has less adverse impact on convective organization so fewer updraft cores should be expected.

For the 14 January 2009 burn, relatively weak transport winds, amount of fire on the landscape (2-yr rough) and the size and shape of the burn area are main determiners for estimating the number of updraft cores. The updraft core numbers are assigned as follows: Block S1A (gray) – orientation of burn area is offset by transport wind direction plus weak transport wind speed – 3 updraft cores; Block S3 (black) – orientation of the area relative to the transport wind direction, weak transport wind speed, and shape of the

area – 3 updraft cores; Block S2 (light gray) – shape of the area offsets orientation of the area plus weak transport winds – 4 updraft cores. Note that the above selection is subjective.

Figure 4 shows the time series of 30-min averaged PM_{2.5} from the ensemble of 5 Daysmoke simulations set for the locations of Truck 1 as compared with 30-min averages for the observations (solid line). The averages are represented by the dots and the ranges of concentrations are given by the bars. The figure shows wide variation in the Daysmoke simulations and particularly for 1300 LST where the range was almost a factor of five. Regarding averages, Daysmoke performed very well from 1230 – 1400 LST but over-predicted concentrations thereafter.

Reasons for the over-predictions cannot be pinned down but several explanations exist. One explanation holds that Truck 1 had moved to location 2 (Figure 1) from 1349 LST. Google Earth showed dense woodlands surrounding location 2. Therefore canopy sheltering cannot be ruled out. Canopy sheltering occurs when relatively clean air below canopy level moves much more slowly than does smoke-laden air carried above the canopy. Weak down-mixing of smoke through the canopy dilutes the smoke thus yielding lower observed PM_{2.5} concentrations in comparison with smoke above the canopy. Thus the over-prediction after 1400 LST could have occurred because the observed smoke concentrations were too low and not representative of concentrations had location 2 been open as was location 1.

Figure 5 shows the cumulative PM_{2.5} for the observations (solid line) and for Daysmoke (dashed line). Daysmoke results closely parallel the observations through 1400 LST. Then the Daysmoke results diverge from the observations.

Another explanation holds that Daysmoke over-estimated smoke after 1400 LST. One reason for this is that the smoke plume for block S2 was accorded 4 updraft cores. Reducing the core number would have reduced the ground-level smoke concentrations and brought the cumulative concentrations more in line with the observations. Conceptually, it is possible to reduce the core numbers for all burns to reproduce the observed trace exactly. However the purpose of the 14 January 2009 analysis is to make the analysis an independent study. Therefore, given that the impact of canopy sheltering on the observations of smoke after 1400 LST is unknown, there is no reason to manipulate updraft core number.

Smoke concentrations averaged over the period of the burn were $38 \mu\text{gm}^{-3}$. Daysmoke-simulated concentrations averaged over the same period were $51 \mu\text{gm}^{-3}$. Daysmoke over-estimated the smoke by $13 \mu\text{gm}^{-3}$ or a factor of 1.35.

Daysmoke Results for Plume Top Height

The second factor in the validation of Daysmoke regards how well Daysmoke reproduces the altitude of the plume top. Figure 6 shows the time history of the 14 January plume as measured by lidar. After 1300 LST, plume top heights consistently ranged between 800-900 m. Dense smoke (red) was distributed throughout the plume. Figure 7 shows part of a 4-core updraft Daysmoke plume for 1400 LST. Dense smoke was confined to the upper part of the plume but was available to be down-mixed by convective mixing. The plume top height was consistently 800 m.

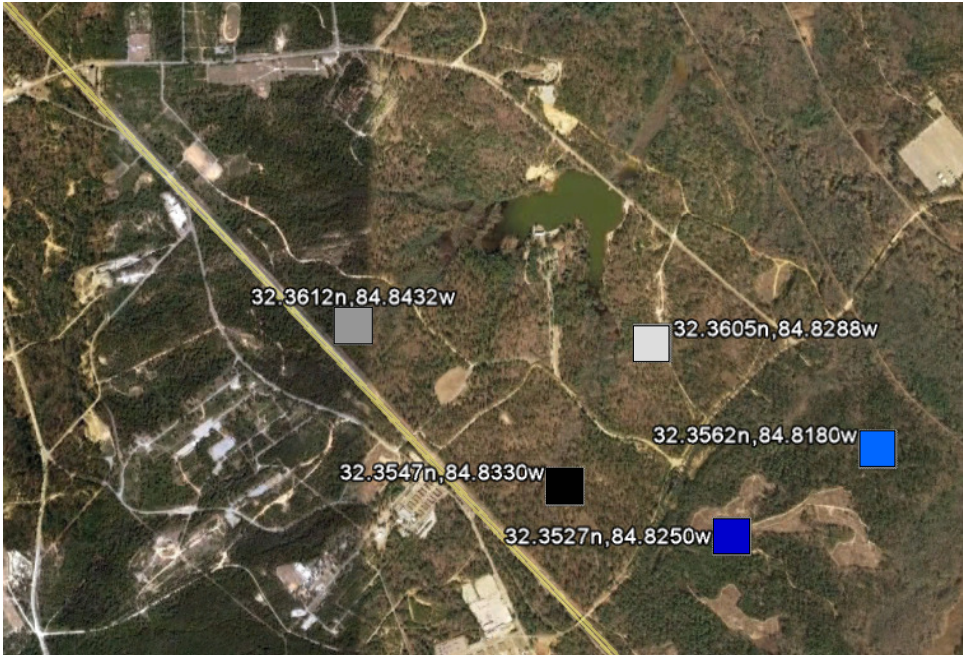


Figure 1. Google map showing the locations of the three burn sites (black, gray and light gray squares) and the locations of Truck 1 (blue and light blue squares) for the 14 January 2009 burns.

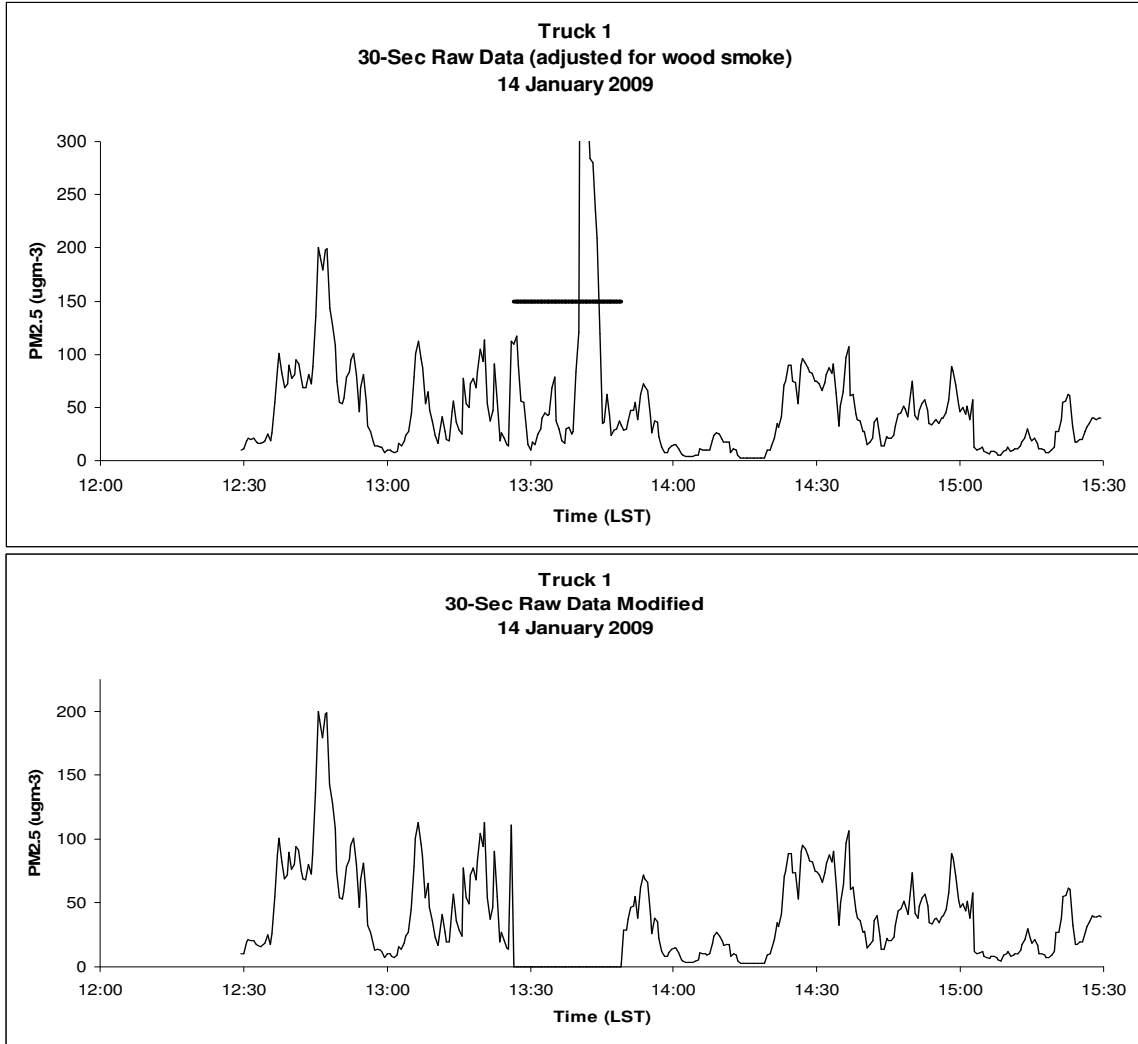


Figure 2. Graphs of 30-sec observed PM_{2.5} (calibrated for wood smoke) for Truck 1 (top panel) and with contamination removed (bottom panel).

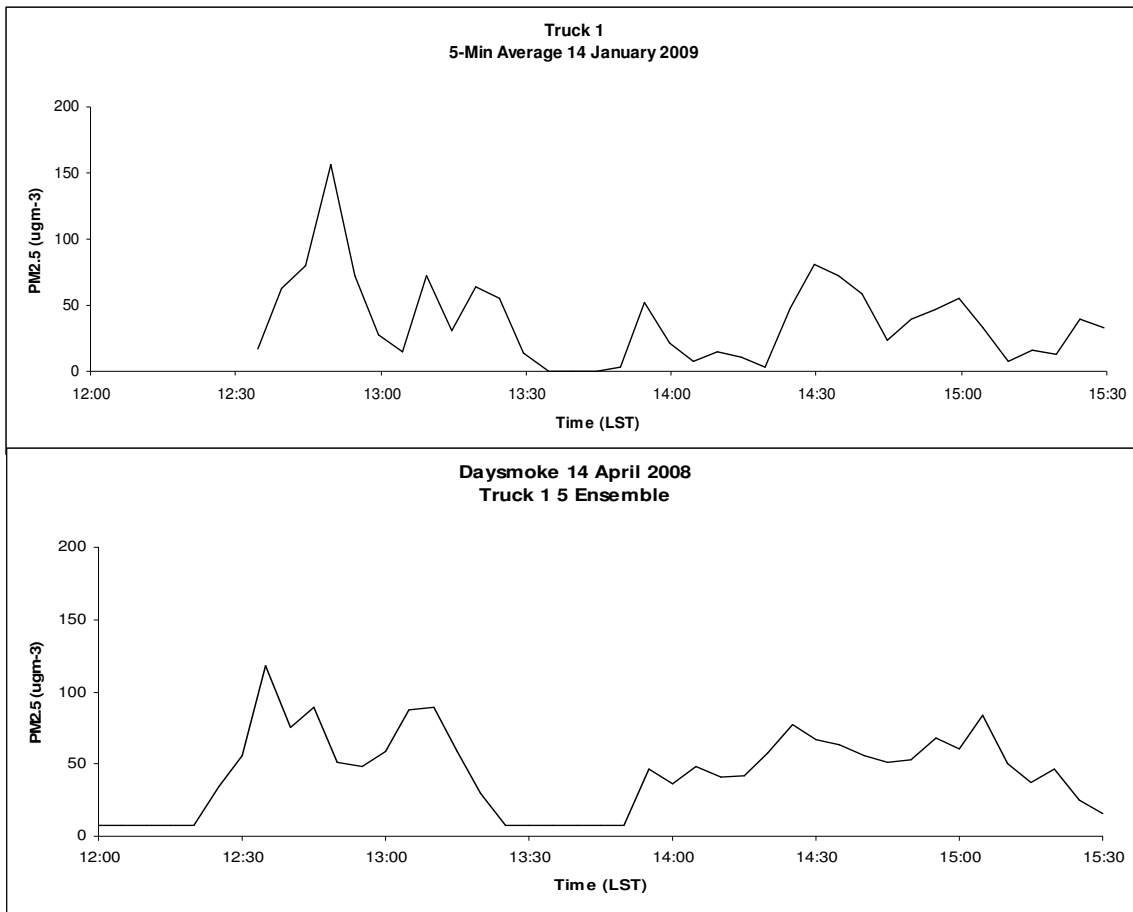


Figure 3. Graphs of 5-min averaged PM2.5 for the observations (top panel) and for a five ensemble averaged Daysmoke simulations (bottom panel).

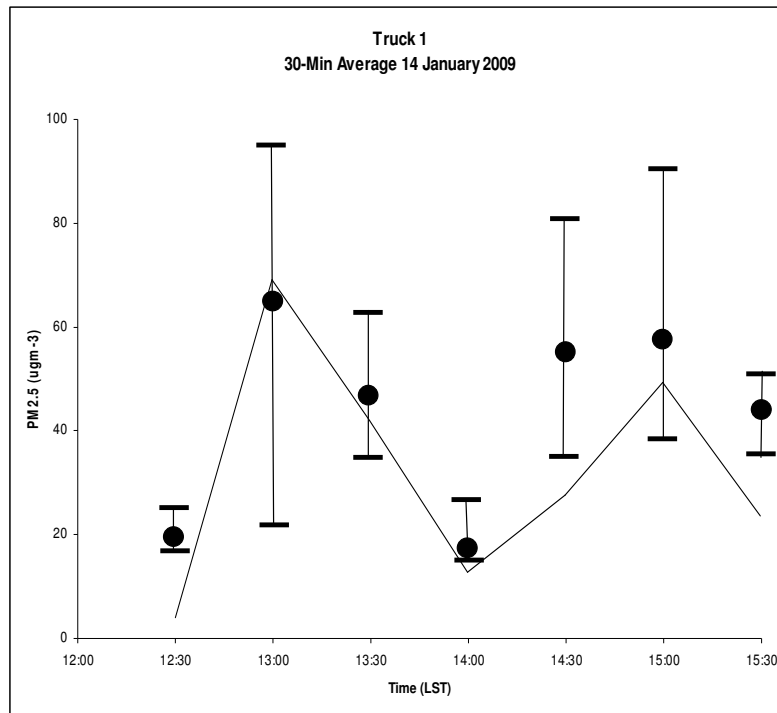


Figure 4. Time series of 30-min averaged PM_{2.5} from an ensemble of 5 Daysmoke simulations set for the locations of Truck 1. The averages are represented by the dots and the range of concentrations are given by the bars.

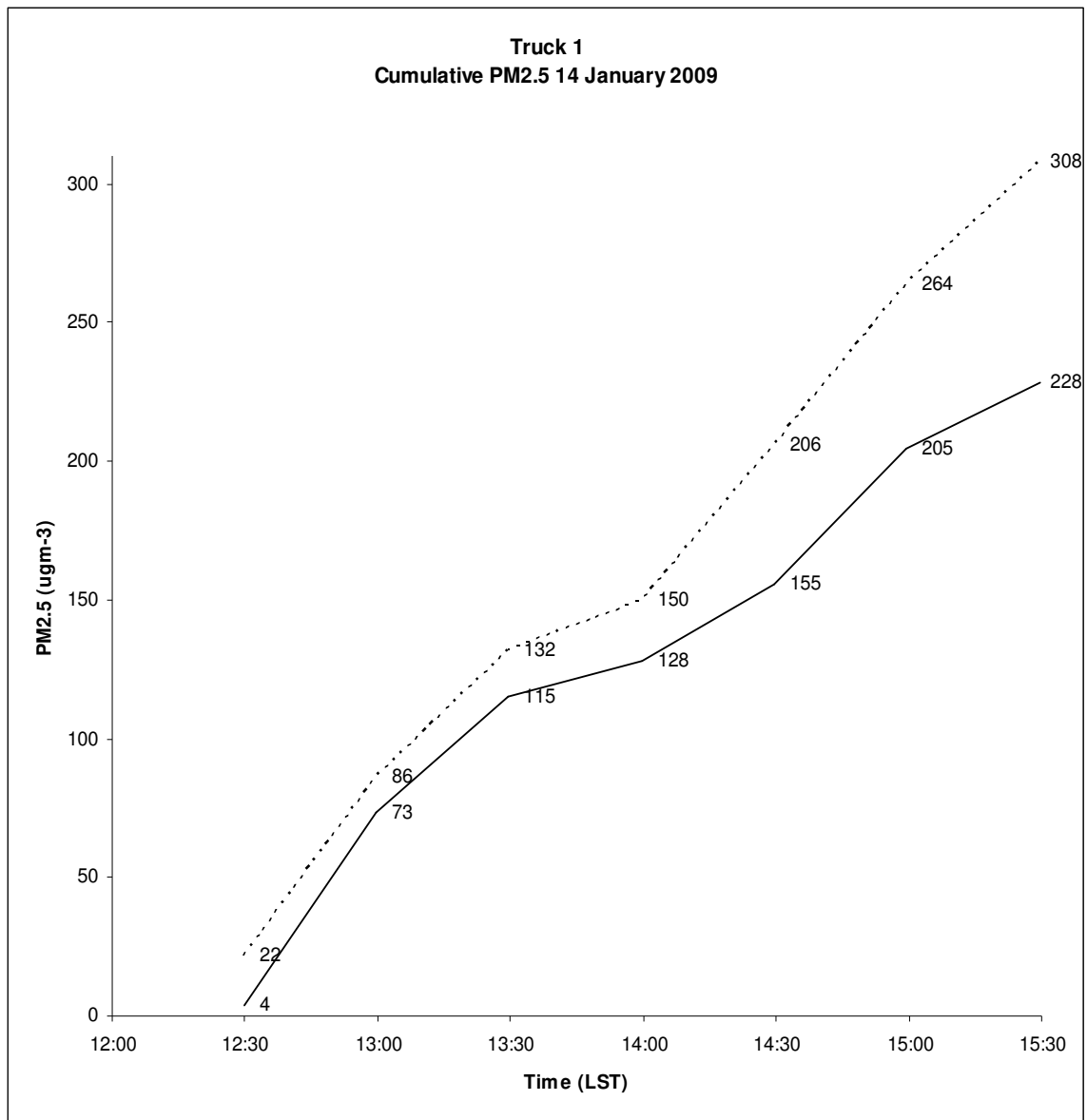


Figure 5. The cumulative PM2.5 simulated during the course of the burn for the observations (solid line) and for Daysmoke (dashed line). Background PM2.5 from the observations have been added to the Daysmoke solutions.

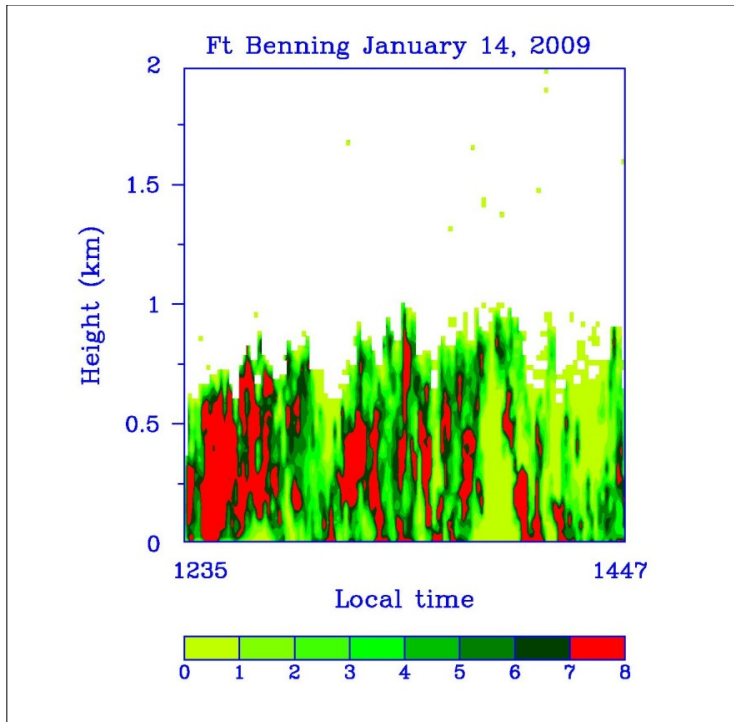


Figure 6. Time history of the 14 January 2009 plume as measured by lidar.

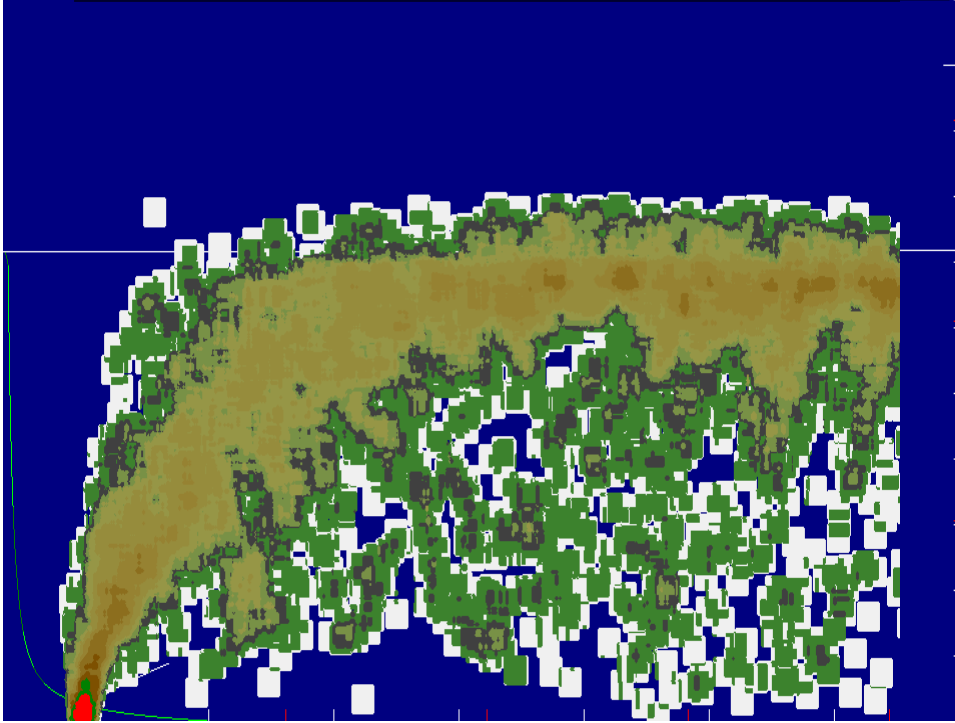


Figure 7. The 4-core updraft Daysmoke plume for 1400 LST 14 January 2009. White tic marks at the bottom of the figure denote 1 km intervals. White tic marks up the right side denote 100 m intervals. The solid white line shows the top of the mixing layer.

Analysis of 15 January 2009 at Fort Benning, GA

Gary L. Achtemeier
USDA Forest Service
Athens, GA
5 March 2010

Introduction.

On 15 January 2009 compartments A9A and A9B consisting of 302 and 281 acres (583 acres total) were burned. Ignition began at approximately 1215 LST and was completed at 1445 LST. The burns were conducted beginning at A9B (Figure 1). Then A9A was burned beginning at 1330 LST.

All three trucks were deployed. Figure 2 shows the positions of Truck 1 (blue) with respect to the A9B burn. From 1215-1320 LST, the truck was located at Point 1, from 1323-1353 LST at Point 2, and from 1407-1530 LST, it was located at Point 3. Truck 2 (yellow) was located at Point 4 from 1220-1315 LST, Point 4 from 1320-1415 LST, and at Point 5 from 1415-1530 LST. Truck 3 (red) was located at Point 7 from 1228-1530 LST.

Winds at 200 m (approximation to the transport winds) blew steadily from 316 deg (range 316-318 degrees) for most of the period. Wind speeds were also relatively steady at approximately 5.9 m sec^{-1} (range $5.6\text{-}6.0 \text{ m sec}^{-1}$).

Observations

The graph of the raw 30-sec data (calibrated for wood smoke) for Truck 1 is shown in the top panel of Figure 3. The record shows that smoke arrived at Truck 1 shortly after 1230 LST with concentrations exceeding $100 \mu\text{gm}^{-3}$ at 1245 LST and again at 1255 LST. Then, between 1255-1345 LST, there were observed large oscillations in the magnitude of smoke concentrations. Peak concentrations exceeding $400 \mu\text{gm}^{-3}$ (maximum concentration $584 \mu\text{gm}^{-3}$ at 1313 LST) were separated by minimum concentrations as low as $30 \mu\text{gm}^{-3}$ at 1309 LST and again at 1314 LST. Unfortunately, the first hour of data for Truck 2 (middle panel) was missing. A PM_{2.5} concentration of $113 \mu\text{gm}^{-3}$ at 1355 LST compares with concentrations exceeding $200 \mu\text{gm}^{-3}$ at Truck 1. The peak concentration at Truck 3 (lower panel) was only $71 \mu\text{gm}^{-3}$ at 1330 LST.

Daysmoke Results for PM_{2.5}

For the Daysmoke simulations, the compartments A9A and A9B were treated as two separate burns producing two separate plumes. Then the contributions to the total PM_{2.5} from each plume as a function of time were computed for each Truck location. Compartment A9B was ignited at 1215 LST and compartment A9A was ignited at 1330 LST. Emissions data were based on period of ignition (2-hr) for fuels typical of fuels measured elsewhere at Ft. Benning. Hourly WRF weather soundings for a grid point near A9 provided weather data for Daysmoke.

The Daysmoke results are based on a subjective determination of the updraft core number that would be typical for the 15 January burn. Daysmoke provides no mechanism for determining updraft core number. Updraft core number is determined by a complex interaction among a number of factors. Some of these factors are:

- Size of burn area – a small burn area should be expected to produce only one updraft core; large burn areas can support many updraft cores.
- Shape of burn area – a burn area that is highly irregular in shape will require an irregular distribution of fire leading to many updraft cores. This problem can be amplified when wind direction maximizes irregularities.
- Heterogeneity of fuels – fuels that burn hot relative to surrounding fuels will develop stronger convective currents and will tend to form updraft cores.
- Fuel type, moisture, and loadings – all three factors relate to heat production. High heat production will develop convective columns and lead to fewer updraft cores; low heat production will lead to many updraft cores
- Distribution of fire on landscape - fire distributed along a long linear line will produce many updraft cores; fire spread evenly over length and depth (mass ignition, stripping) will organize convective columns into fewer updraft cores.
- Amount of fire on landscape – a small amount of fire will reduce emissions per second but decrease heat thus minimizing convective organization. Result: many updraft cores. A large amount of fire will produce the opposite. Result: fewer updraft cores
- Distribution of canopy gaps. Hot air trapped beneath a dense canopy will flow to the gaps thus creating convective columns that produce updraft cores there. Thin (or no) canopies will not be a factor in updraft core development.
- Transport wind speed – strong winds inhibit convective organization thus leading to many updraft cores. Weak winds allow convective organization resulting in few updraft cores.
- Mixing layer depth – a shallow mixing layer inhibits convective organization thus leading to many updraft cores. A deep mixing layer has less adverse impact on convective organization so fewer updraft cores should be expected.

For the 15 January 2009 burn compartment 9B, relatively moderate transport winds (5.9 m sec^{-1}), amount of fire on the landscape (2-yr rough), size of the burn area and shallow mixing layer depth (400 m) are main determiners for estimating the number of updraft cores. An updraft core number of 10 cores was assigned for this burn. For compartment 9A, shape of the burn area also contributes to increased updraft core number. However, the orientation of compartment 9A, with the long axis oriented normal to the prevailing wind direction, is taken as evidence that most of the smoke did not impact the trucks. Therefore to compensate for Daysmoke placing all smoke within a square of area equal to the acreage burned, the burn for compartment 9A is assigned an updraft core number of three (3). Note that the above selection is subjective.

Figure 4 shows the time series of 30-min averaged PM_{2.5} from the ensemble of 5 Daysmoke simulations set for the locations of Truck 1 as compared with 30-min averages for the observations (solid line). The averages are represented by the black circles and the ranges of concentrations are given by the bars. The figure shows that Daysmoke simulated the overall trend of smoke at Truck 1 fairly well with the exception of 1330

LST where Daysmoke under-simulated the $171 \mu\text{gm}^{-3}$ peak by a factor of 2. Less noticeable but still significant was the Daysmoke over-simulation of smoke at 1500-1530 LST also by a factor of 2.

Figure 5 shows the time series of 30-min averages for the observations (solid line) after 1400 LST at Truck 2. This is overlaid with averaged PM_{2.5} from the ensemble of 5 Daysmoke simulations - represented by the black circles and the ranges of concentrations are given by the bars. Although the observations fall within the ranges of Daysmoke simulations for 1400-1430 LST, Daysmoke over-simulated smoke for the whole period of the observations. The over-simulation of smoke is worse still at Truck 3 (Figure 6) – the overage being greater than a factor of 4 from 1430-1530 LST.

Given the results of Figures 4-6, the over-estimation of PM_{2.5} for the whole burn is not unexpected (Figure 7). Daysmoke estimated PM_{2.5} at Truck 1 fairly well (observed = $59 \mu\text{gm}^{-3}$, modeled = $52 \mu\text{gm}^{-3}$) but for the wrong reasons. Daysmoke over-predicted smoke at Truck 2 (observed = $34 \mu\text{gm}^{-3}$, model = $74 \mu\text{gm}^{-3}$) by a factor of 2.2. Note that the calculations were done only for the period of the observations.) At Truck 3 (observed = $14 \mu\text{gm}^{-3}$, model = $50 \mu\text{gm}^{-3}$), the over-prediction was by a factor of 3.6.

In summary, it can be concluded that Daysmoke performed poorly in simulating the 15 January 2009 burn. There are several reasons for the low model performance. First, the steep gradient in PM_{2.5} ($59 \mu\text{gm}^{-3}$ to $14 \mu\text{gm}^{-3}$) over the 2.1 mile (3.4 km) distance between Truck 1 and Truck 3 for the whole burn is not found in other observed data to date. The inference is that fire behavior, hence smoke and heat production, was different in comparison with other burns. From a meteorological perspective, 15 January 2009 was cold, windy, and had low mixing heights. Under these conditions, Daysmoke lacked convective mixing strong enough to transport smoke aloft from near the ground. Thus smoke from the smoldering phase (after 1400 LST in Figure 8) stayed near the ground and gave relatively high PM_{2.5} concentrations at Truck 1 (Figure 4) after 1430 LST.

To further understand the impact of smoldering on the Daysmoke solutions for the 15 January 2009 burns, the model was rerun with the smoldering emissions set to zero for the A9B compartment. These results are plotted as the white circles in Figure 4. The 5-ensemble production yielded several runs with high PM_{2.5}. Thus the re-run ensemble averages are larger for 1230-1400 LST for Truck 1. The impact of the lack of smoldering on the simulated PM_{2.5} shows up from 1430-1530 LST when PM_{2.5} ranged between $19 \mu\text{gm}^{-3}$ and $12 \mu\text{gm}^{-3}$ – below the 30-min averaged observations.

The effects of removal of smoldering from the simulations also impact the simulated PM_{2.5} for Truck 2 (Figure 5) and Truck 3 (Figure 6). At both trucks, the PM_{2.5} at 1500-1530 LST has been roughly halved regardless that the re-run ensemble averages were much higher for the flaming phase emissions in comparison with the original simulations.

Second, though removal of smoldering in the Daysmoke simulations produces greater fidelity to the shape of the traces for the observations, both simulations (with and without smoldering) remain too low at Truck 1 (1330 LST), and far too high for Truck 2 and Truck 3. Daysmoke follows the assumption in the emissions production model that there is an active burn phase followed by a smoldering phase. From a physical perspective, the assumption implies that indrafts produced by the active burn phase sweep nearby smoldering emissions into the active burn plume. Thus all smoke during

the active burn phase is lofted some distance above ground by heat of combustion to be dispersed and mixed back to the ground by convective mixing. The distance downwind the plume mixes back to the ground is determined by the wind speed and the intensity of convective mixing. For strong winds and weak convective mixing observed during 15 January 2009, much of the plume was aloft when passing Truck 1 but had mixed to the ground before passing Truck 2 (see Figure 8). Thus the average modeled PM_{2.5} at Truck 2 was 74 μgm^{-3} compared with only 52 μgm^{-3} at Truck 1.

For the weak burns at Fort Benning, the assumption behind the emissions model may not hold. Not all smoke may be swept into the active burn phase plume. Thus the smoke available to drift along the ground would have greatest PM_{2.5} impact on trucks located closest to the burn as it slowly disperses. In this case, smoke concentrations at Truck 1 should be increased if smoldering existed during the active burn phase. Though the outcome could be over-predictions of smoke at all three trucks, the problem can be remedied by reducing the number of updraft cores.

Third, it is doubtful that the steep gradient in PM_{2.5} over the 2.1 mile (3.4 km) distance between Truck 1 and Truck 3 for the whole burn can be explained by any reasonable tinkering with Daysmoke. It would have to be argued that air passing over Truck 1 never passed over Truck 3, or that Truck 3 was subject to canopy sheltering, or that Truck 1 was located ideally downwind from dense smoldering fuels, or some other mechanism designed to explain away the data. Daysmoke, in its current configuration, is simply unable to satisfactorily model the distribution of smoke observed on 15 January 2009.

Finally, Figure 9 shows the distribution of 5 hr averaged PM_{2.5} for distances up to 30 miles (48 km) from the burn. The pencil-like concentration pattern is the outcome of steady winds for the duration of the burn period. Concentrations exceeding 50 μgm^{-3} are found as far as 15 miles (24 km) down wind.

Daysmoke Results for Plume Top Height

The second factor in the validation of Daysmoke regards how well Daysmoke reproduced the altitude of the plume top. Figure 9 shows the time history of the 15 January plume between 1250-1350 LST as measured by the USFS ceilometer from a location of 1 mile (1.6 km) from compartment A9B. From 1300-1320 LST, the plume top ranged between 400-600 m in altitude. Then the plume top climbed to between 700-800 m thereafter. Maximum backscatter was mostly below 250 m. Figure 10 shows the 10-core plume at 1330LST as simulated by Daysmoke. The plume top levels off around 500 m. However at the 1 mile (1.6 km) range the plume is still in ascent and its top is 400 m. Maximum smoke mass is found between 200-300 m. Thus, overall, the smoke plume of 15 January 2009 was not well-represented by Daysmoke. In addition, had Daysmoke placed the maximum smoke concentrations nearer to the ground – as measured by ceilometer, ground-level concentrations of PM_{2.5} would have been far higher than simulated by Daysmoke in this study – perhaps by a factor of 10.

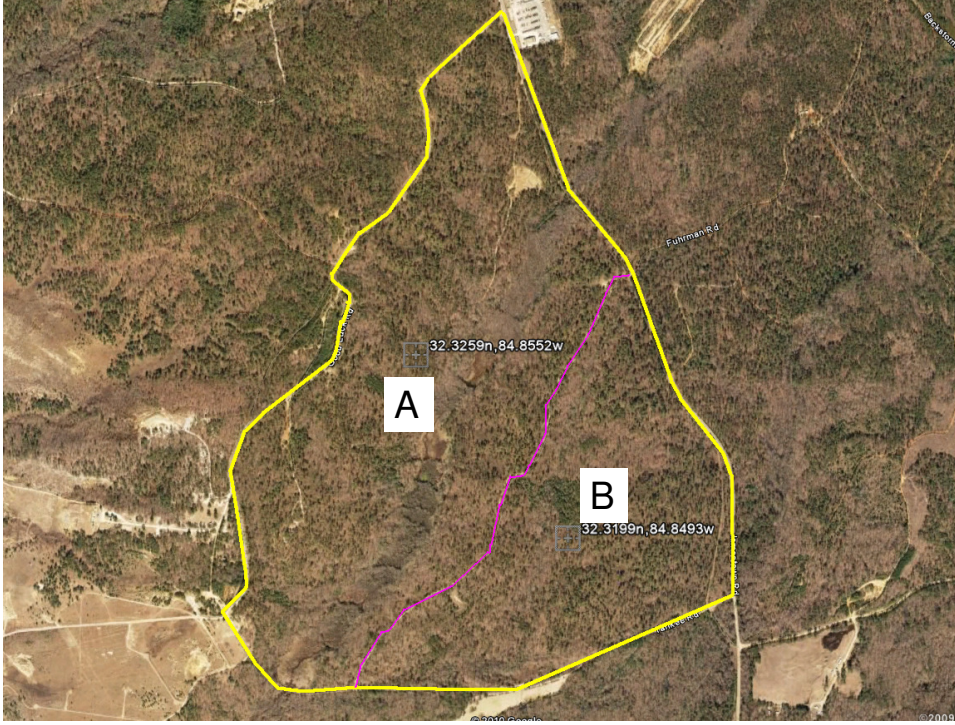


Figure 1. Google Earth image of Block A9 showing compartments A and B of the 15 January 2009 burn at Fort Benning, GA.

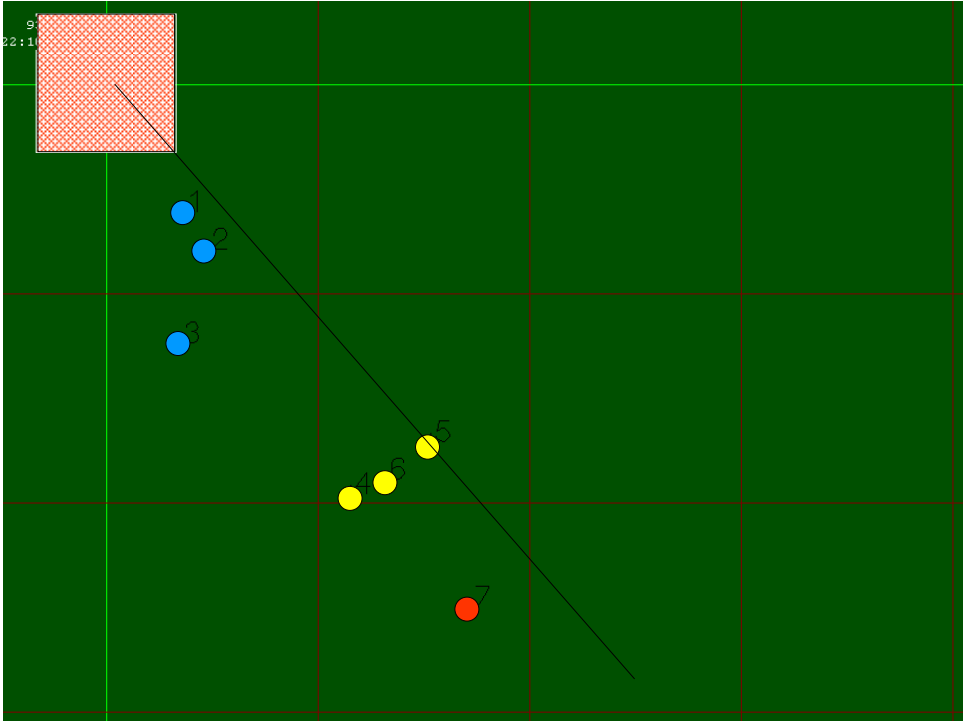


Figure 2. Locations of the three trucks relative to the Daysmoke depiction of the compartment A9B burn. The diagonal black line delineates prevailing wind direction.

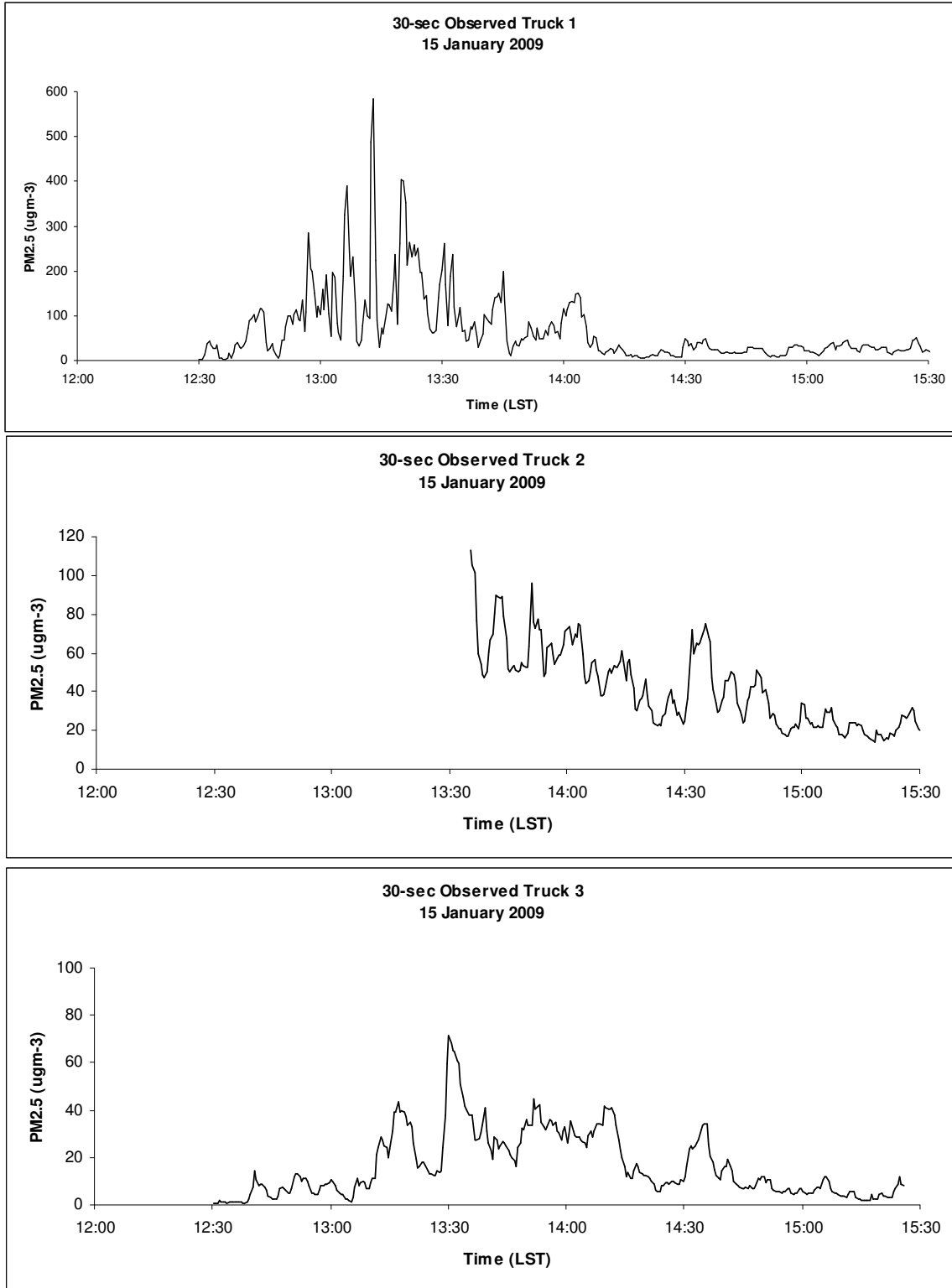


Figure 3. Traces of the 30-sec observed PM_{2.5} measured at the locations of Truck 1 (top panel), Truck 2 (middle panel), and Truck 3 (lower panel) for the 15 January 2009 burn.

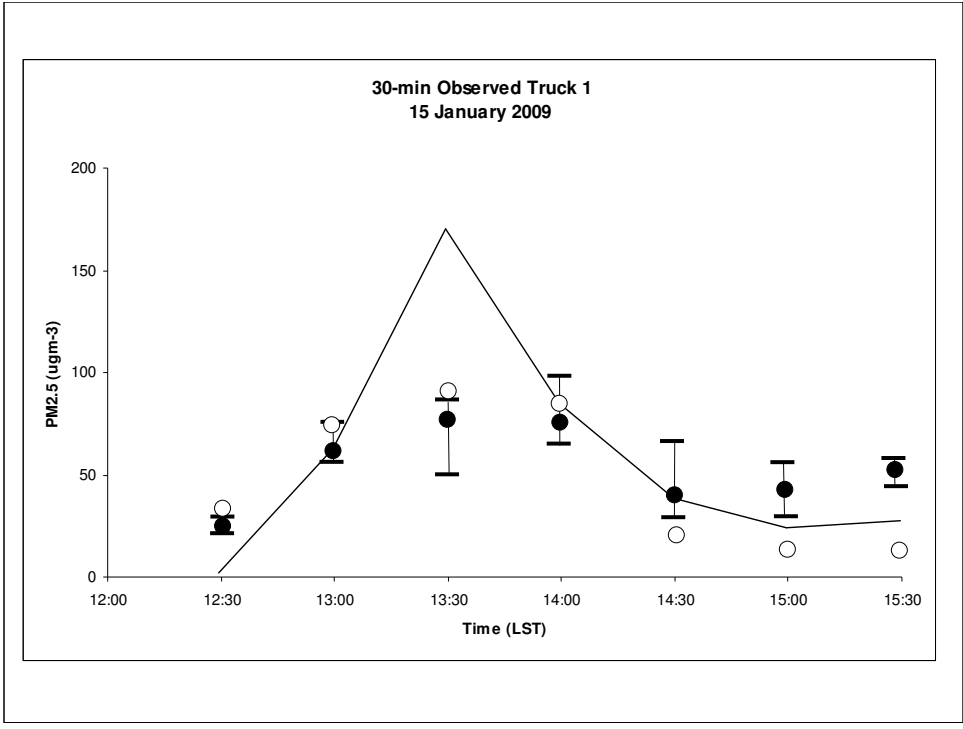


Figure 4. Time series of 30-min averaged PM2.5 from an ensemble of 5 Daysmoke simulations set for the locations of Truck 1. The averages are represented by the dots and the range of concentrations are given by the bars.

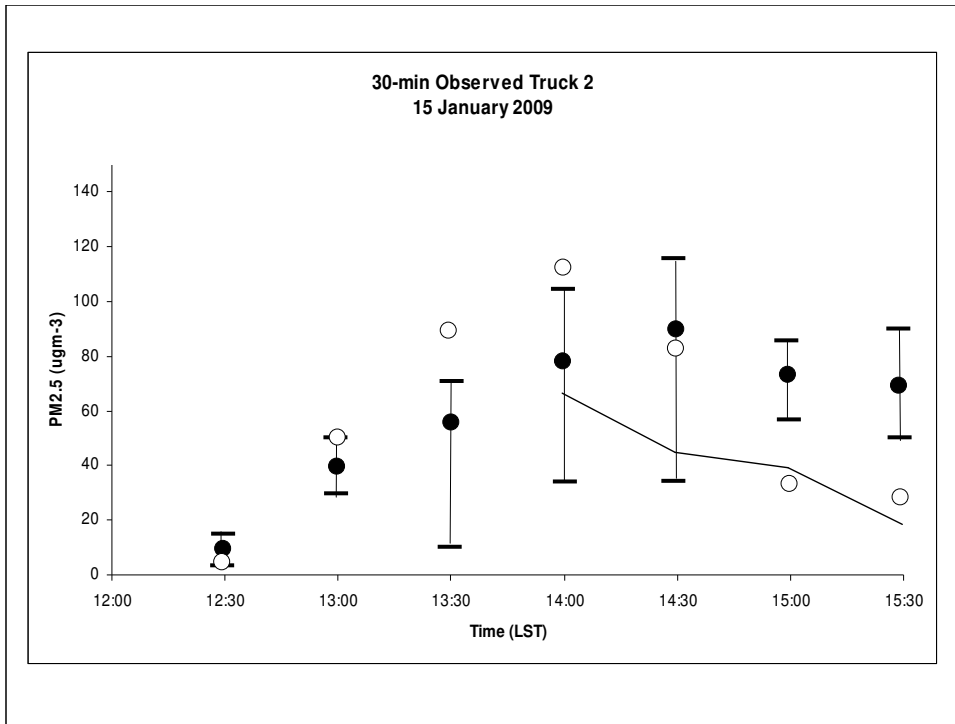


Figure 5. Time series of 30-min averaged PM2.5 from an ensemble of 5 Daysmoke simulations set for the locations of Truck 2. The averages are represented by the dots and the range of concentrations are given by the bars.

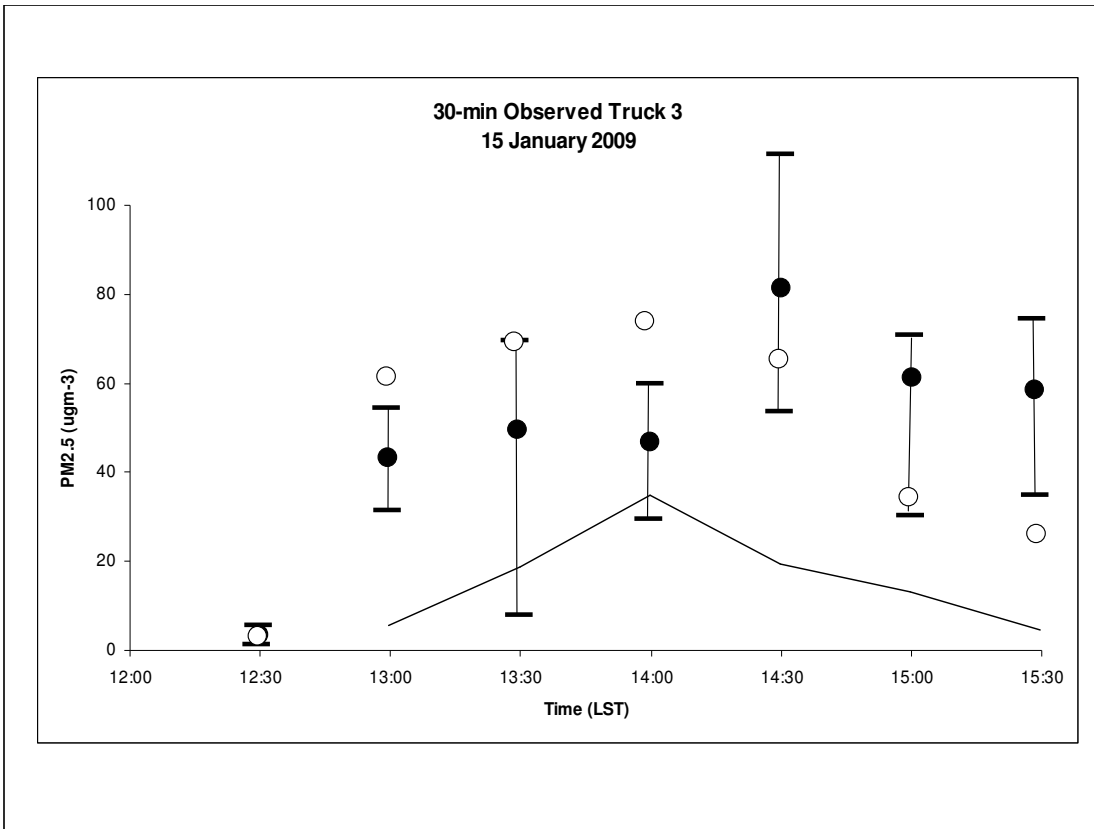


Figure 6. Time series of 30-min averaged PM2.5 from an ensemble of 5 Daysmoke simulations set for the locations of Truck 3. The averages are represented by the dots and the range of concentrations are given by the bars.

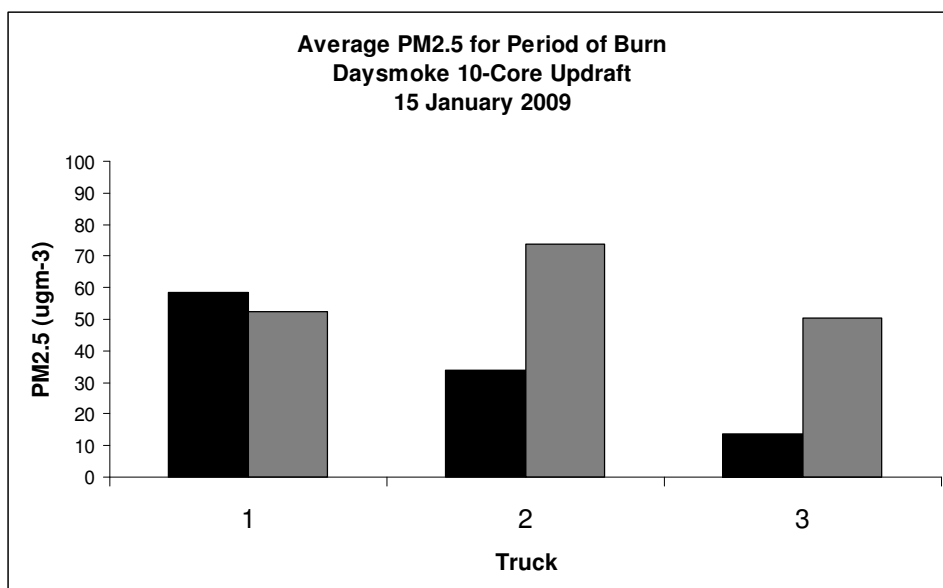


Figure 7. The average PM2.5 for the 3.5 hr period of the burn (black bars) compared with the 5-ensemble average 10-core updraft Daysmoke simulations (gray bars) for the 15 January 2009 burn.

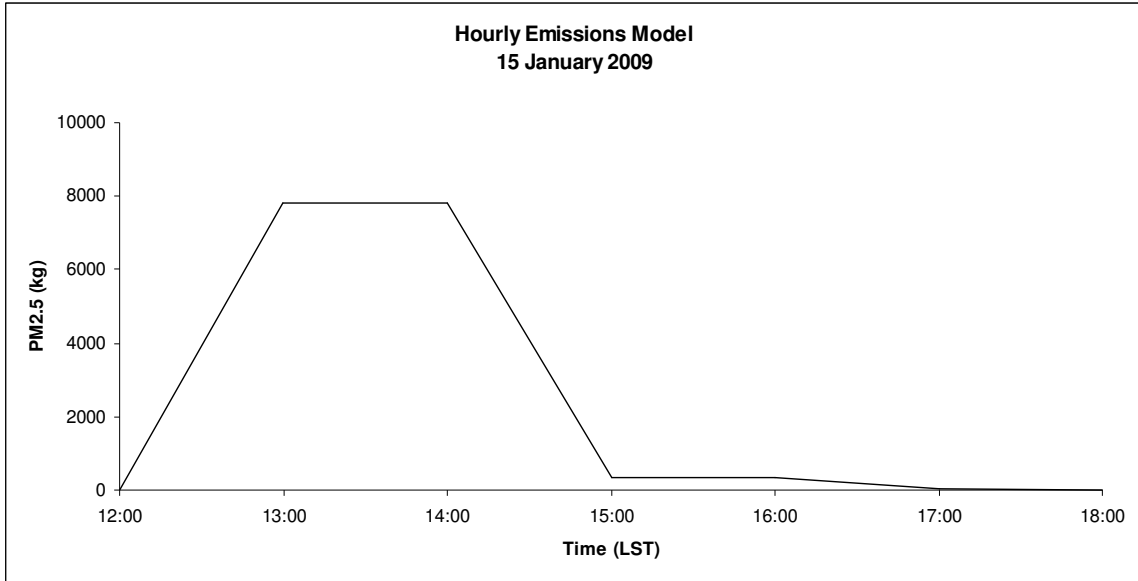


Figure 8. The hourly emissions model for the 15 January 2009 burn at compartment A9B.

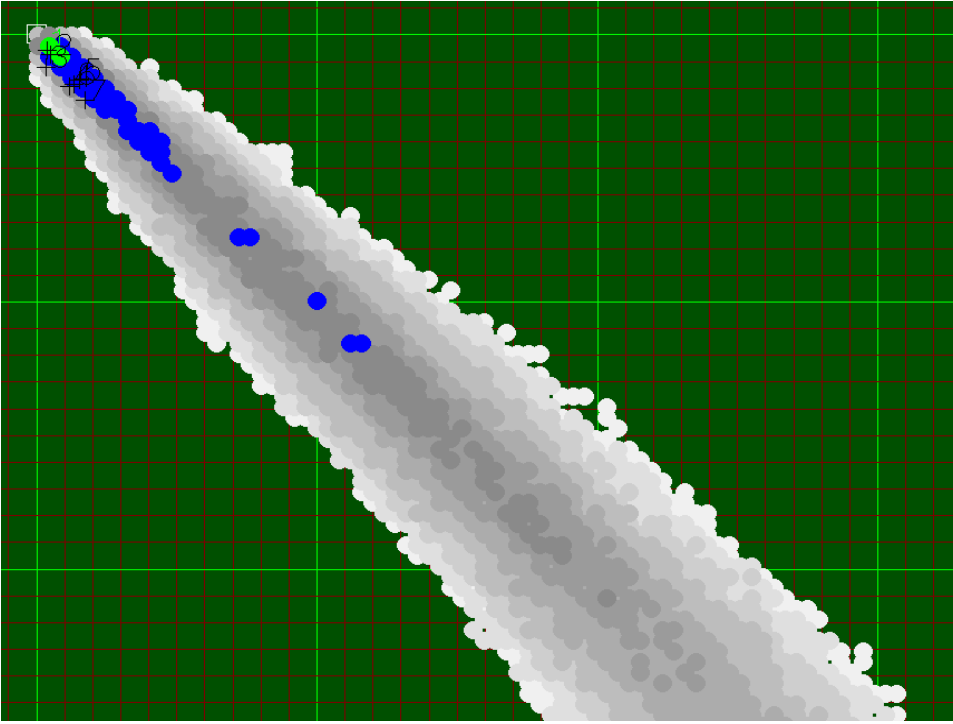


Figure 9. Five hour average PM_{2.5} concentrations from the 15 January 2009 burn. Brown squares represent 1 mile (1.6 km) squares and light green lines represent 10-mile (16 km) squares.

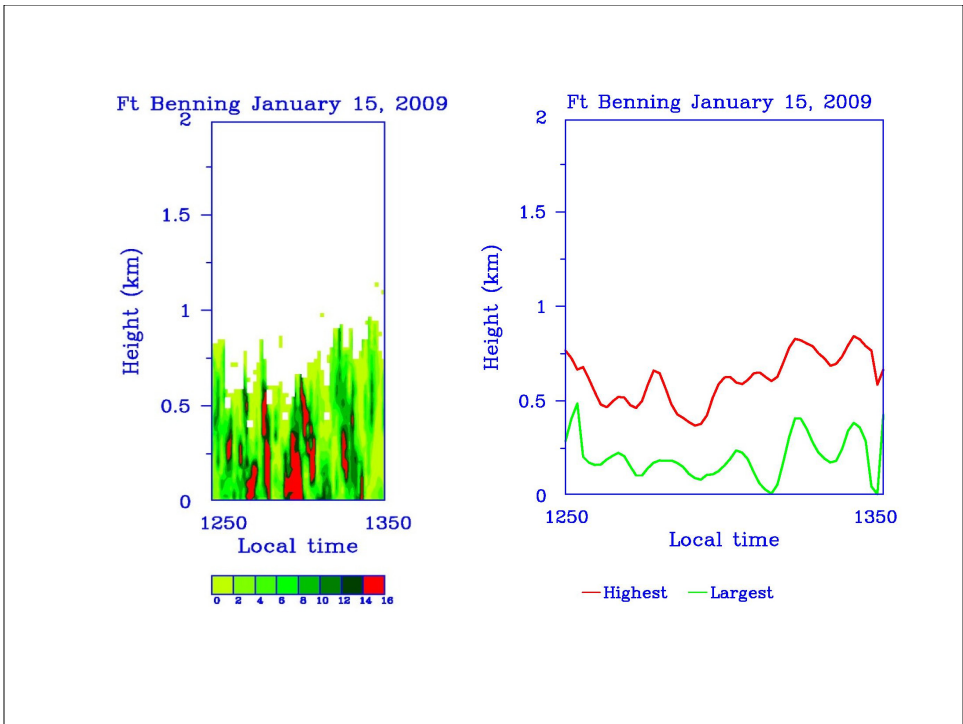


Figure 10. Ceilometer measurements of the smoke plume of 15 January 2009 from 1250-1350 LST. Left panel – time series of backscatter; right panel – time series of heights of plume top and maximum backscatter.

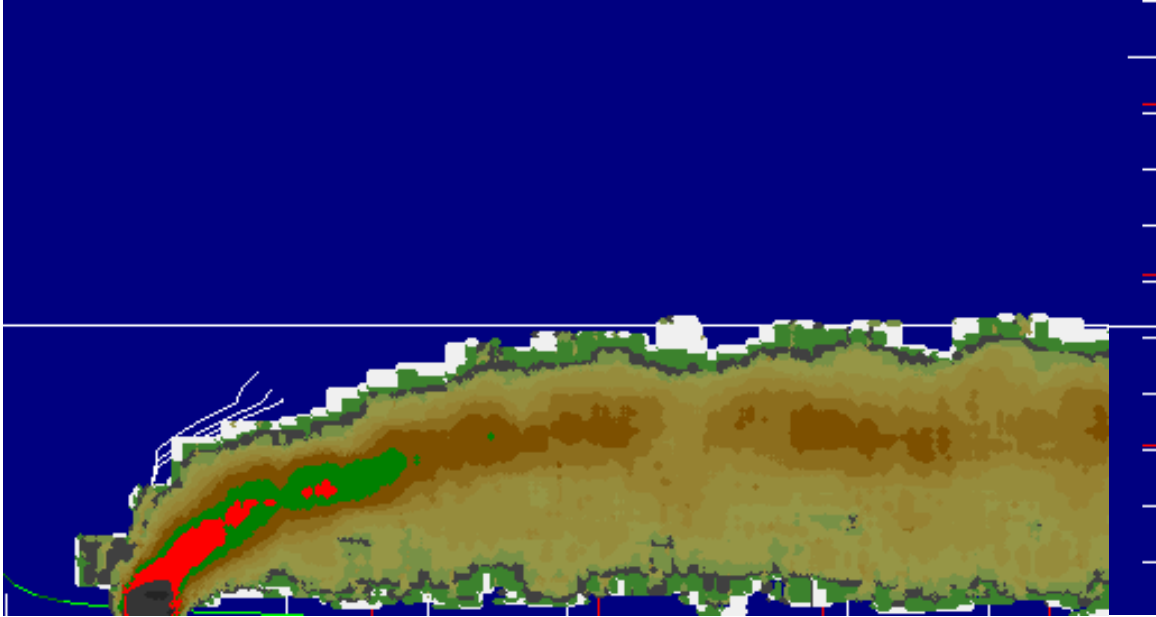


Figure 11. The plume simulated by Daysmoke at 1330 LST 15 January 2009.

Analysis of 20 January 2009 at Fort Benning, GA

Gary L. Achtemeier
USDA Forest Service
Athens, GA
5 March 2010

Introduction.

On 20 January 2009 compartment O11 consisting of 269 acres was burned. Ignition began at approximately 1220 LST and was completed at 1435 LST. Figure 1 shows a Google Image of the burn area. Save for the triangular extension at the lower right, the burn area can be well approximated by a square of equal area.

All three trucks were deployed. Figure 2 shows the positions of Truck 1 (blue) with respect to the O11 burn. From 1215-1430 LST, the truck was located at Point 1. Then Truck 1 was moved but got stuck in mud. Thus the record from 1430-1500 LST may have been contaminated and will be dropped from the analysis. Truck 2 (yellow) was located at Point 3 from 1220-1318 LST, Point 4 from 1324-1414 LST, and at Point 5 from 1415-1500 LST. Truck 3 (red) was located at Point 6 from 1225-1420 LST and at Point 7 from 1425-1500 LST.

Winds at 200 m (approximation to the transport winds) blew steadily from 320 deg (range 318-321 degrees) for most of the period. Wind speeds were also relatively steady at approximately 10.8 m sec^{-1} (range $10.0\text{-}11.6 \text{ m sec}^{-1}$). The diagonal black line in Figure 2 is oriented at 320 deg. It shows that positions 3, 6, and 7 may have been close to or beyond the edge of the plume.

Observations

The graph of the raw 30-sec data (calibrated for wood smoke) for Truck 1 is shown in the top panel of Figure 3. Though ignition was at 1220 LST, the record shows that smoke did not arrive at Truck 1 until shortly before 1400 LST with concentrations peaking at $60 \mu\text{gm}^{-3}$ at 1257 LST. Smoke arrived at Truck 2 (middle panel) at 1400 LST. No smoke was observed at Truck 3 (lower panel). The late arrival of smoke at Truck 1 and Truck 2 is suggestive that winds were initially blowing smoke away from the trucks until shortly before 1400 LST.

Daysmoke Results for PM_{2.5}

For the Daysmoke simulations, the block O11 burn was treated as a square of area equal to the area of block O11. Ignition was at 1220 LST.

The Daysmoke results are based on a subjective determination of the updraft core number that would be typical for the 20 January burn. Daysmoke provides no mechanism for determining updraft core number. Updraft core number is determined by a complex interaction among a number of factors. Some of these factors are:

- Size of burn area – a small burn area should be expected to produce only one updraft core; large burn areas can support many updraft cores.
- Shape of burn area – a burn area that is highly irregular in shape will require an irregular distribution of fire leading to many updraft cores. This problem can be amplified when wind direction maximizes irregularities.
- Heterogeneity of fuels – fuels that burn hot relative to surrounding fuels will develop stronger convective currents and will tend to form updraft cores.
- Fuel type, moisture, and loadings – all three factors relate to heat production. High heat production will develop convective columns and lead to fewer updraft cores; low heat production will lead to many updraft cores
- Distribution of fire on landscape - fire distributed along a long linear line will produce many updraft cores; fire spread evenly over length and depth (mass ignition, stripping) will organize convective columns into fewer updraft cores.
- Amount of fire on landscape – a small amount of fire will reduce emissions per second but decrease heat thus minimizing convective organization. Result: many updraft cores. A large amount of fire will produce the opposite. Result: fewer updraft cores
- Distribution of canopy gaps. Hot air trapped beneath a dense canopy will flow to the gaps thus creating convective columns that produce updraft cores there. Thin (or no) canopies will not be a factor in updraft core development.
- Transport wind speed – strong winds inhibit convective organization thus leading to many updraft cores. Weak winds allow convective organization resulting in few updraft cores.
- Mixing layer depth – a shallow mixing layer inhibits convective organization thus leading to many updraft cores. A deep mixing layer has less adverse impact on convective organization so fewer updraft cores should be expected.

For the 20 January 2009 burn, strong 200 m transport winds (10.8 m sec^{-1}) serve to increase updraft core number. Shape of the burn area and the deep mixing layer depth (1600-1800 m) serve to decrease the number of updraft cores. An updraft core number of 3 cores was assigned for this burn.

Figure 4 shows the time series of 30-min averaged PM_{2.5} from the ensemble of 5 Daysmoke simulations set for the locations of Truck 1 as compared with 30-min averages for the observations (solid line). The averages are represented by the black circles and the ranges of concentrations are given by the bars. The figure shows that Daysmoke simulated smoke at Truck 1 by 1300 LST with the maximum at 1330 LST.

Figure 5 also shows that smoke had arrived at Truck 2 by 1300 LST. The maximum concentrations occurred at 1430 LST in agreement with the observations. Figure 6 shows smoke scattered in a disorganized pattern at Truck 3. No smoke was observed there.

Given the results of Figures 4-6, the small average PM_{2.5} for the whole burn is not unexpected (Figure 7). Daysmoke over-estimated PM_{2.5} at all three trucks. However, the amounts were so small that little can be made of the discrepancies. The average PM_{2.5} values Truck 1 matched fairly well (observed = $4 \mu\text{gm}^{-3}$, modeled = $5 \mu\text{gm}^{-3}$). Daysmoke over-predicted smoke at Truck 2 (observed = $5 \mu\text{gm}^{-3}$, model = $9 \mu\text{gm}^{-3}$). At Truck 3, the over-prediction was by a factor of 2 (observed = $2 \mu\text{gm}^{-3}$, model = $4 \mu\text{gm}^{-3}$).

In summary, little can be concluded about the Daysmoke simulations. The late arrival of smoke at both Truck 1 and Truck 2 can be explained by winds having shifted to blow smoke away from the trucks prior to 1400 LST. The lack of smoke in the observations during the first 1.5 hr of the burn explains part of the discrepancies between the observations and Daysmoke.

Daysmoke Results for Plume Top Height

No ceilometer data was collected for the 20 January 2009 burn.

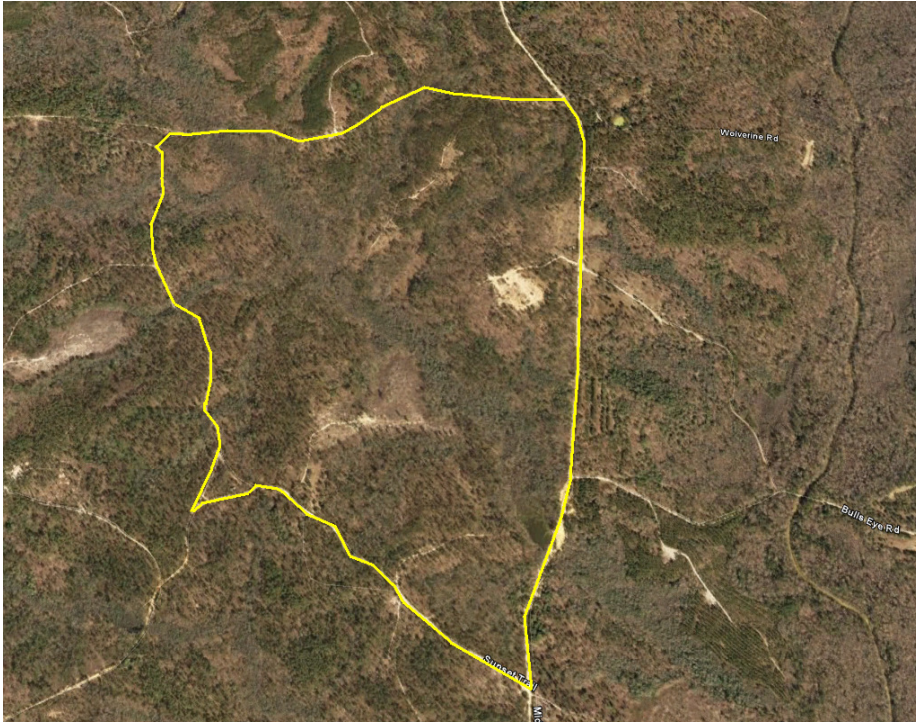


Figure 1. Google Earth image of Block O11 outlined in yellow 20 January 2009 burn at Fort Benning, GA.

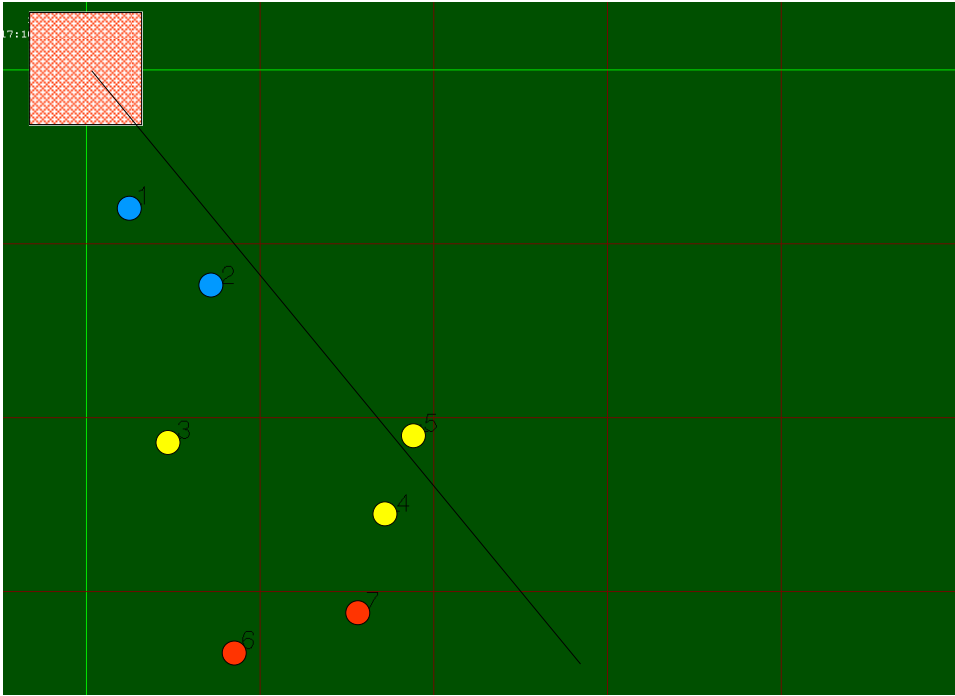


Figure 2. Locations of the three trucks relative to the Daysmoke depiction of the compartment O11 burn. The diagonal black line delineates prevailing wind direction.

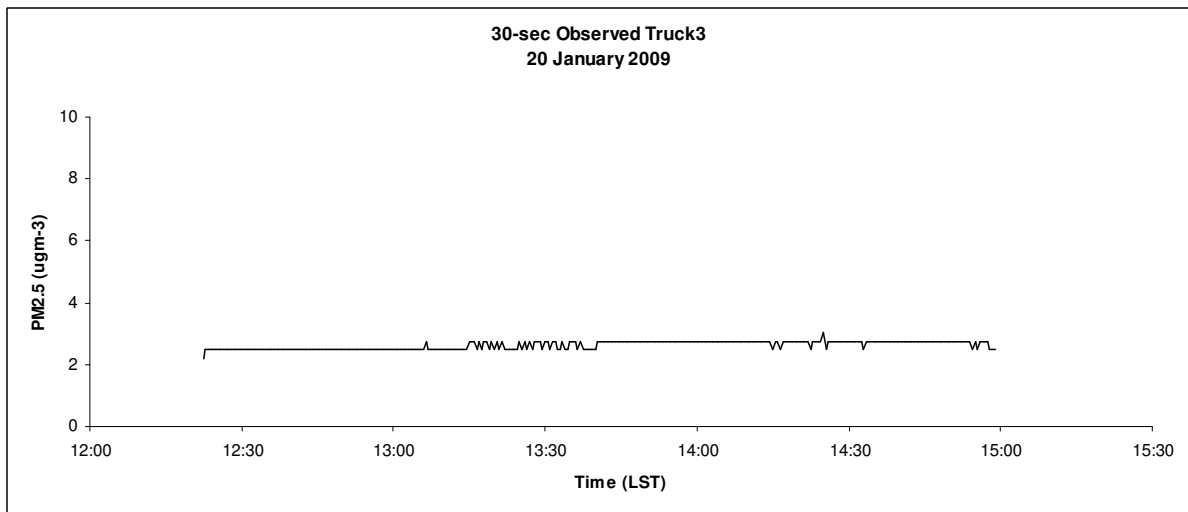
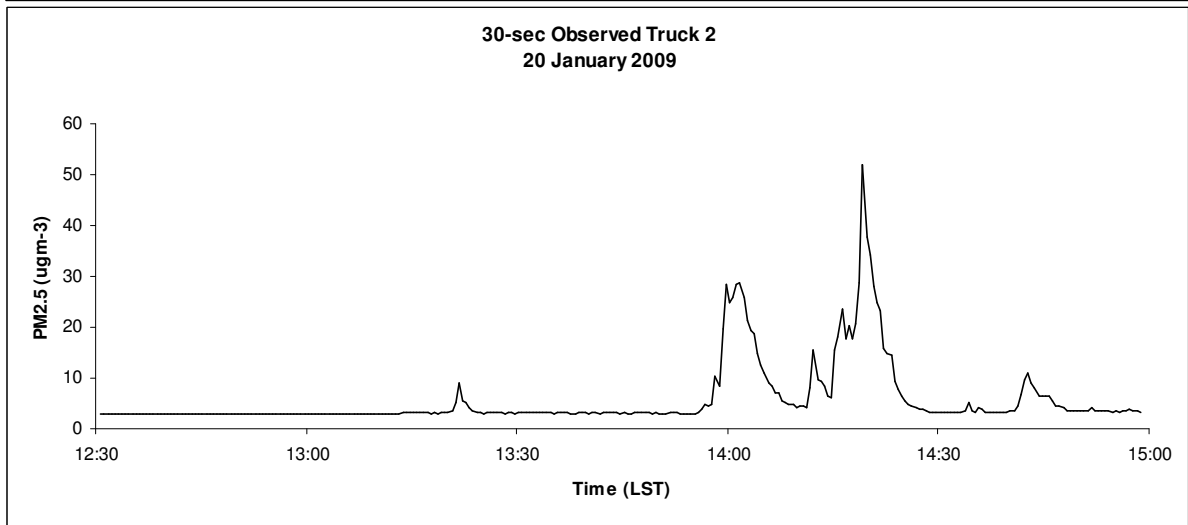
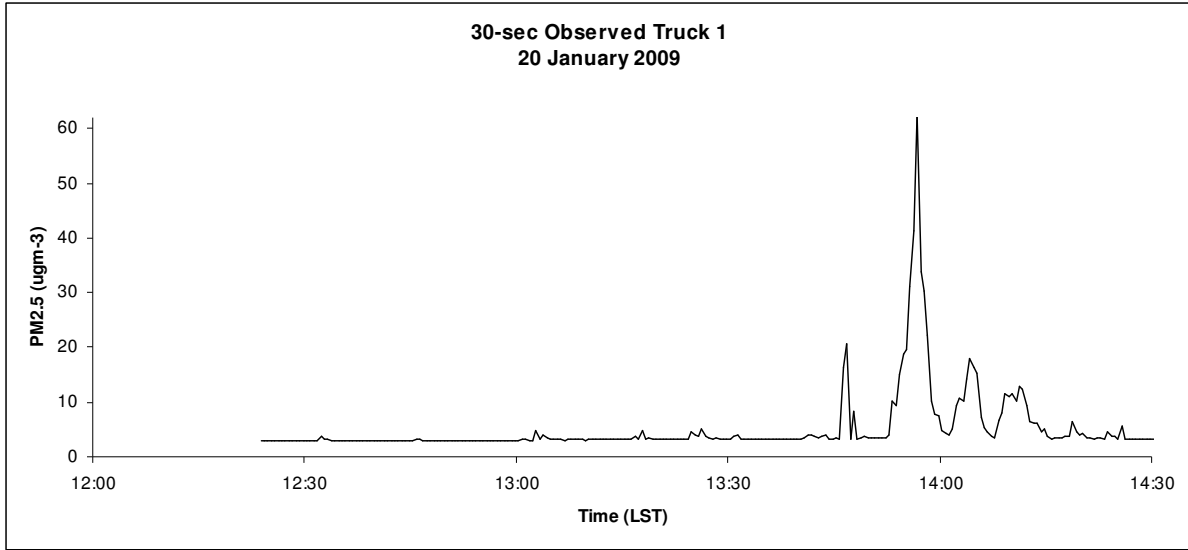


Figure 3. Traces of the 30-sec observed PM_{2.5} measured at the locations of Truck 1 (top panel), Truck 2 (middle panel), and Truck 3 (lower panel) for the 29 January 2009 burn.

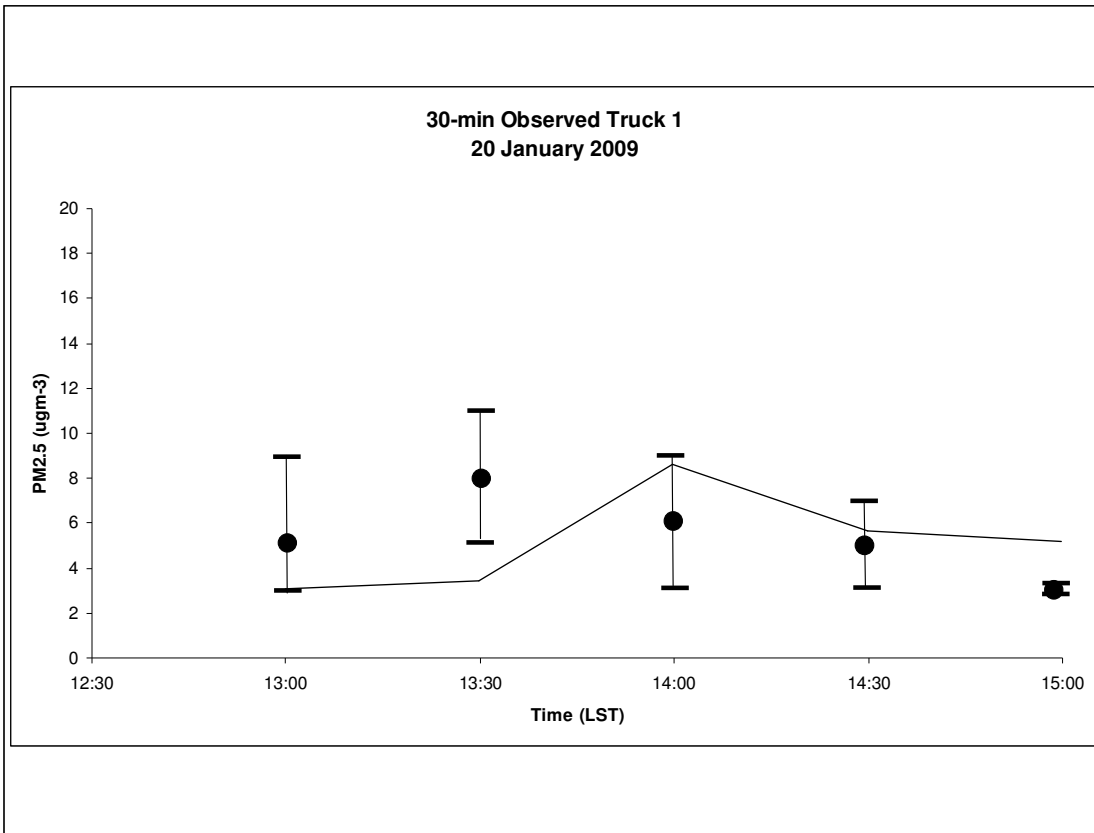


Figure 4. Time series of 30-min averaged PM2.5 from an ensemble of 5 Daysmoke simulations set for the locations of Truck 1. The averages are represented by the dots and the range of concentrations are given by the bars.

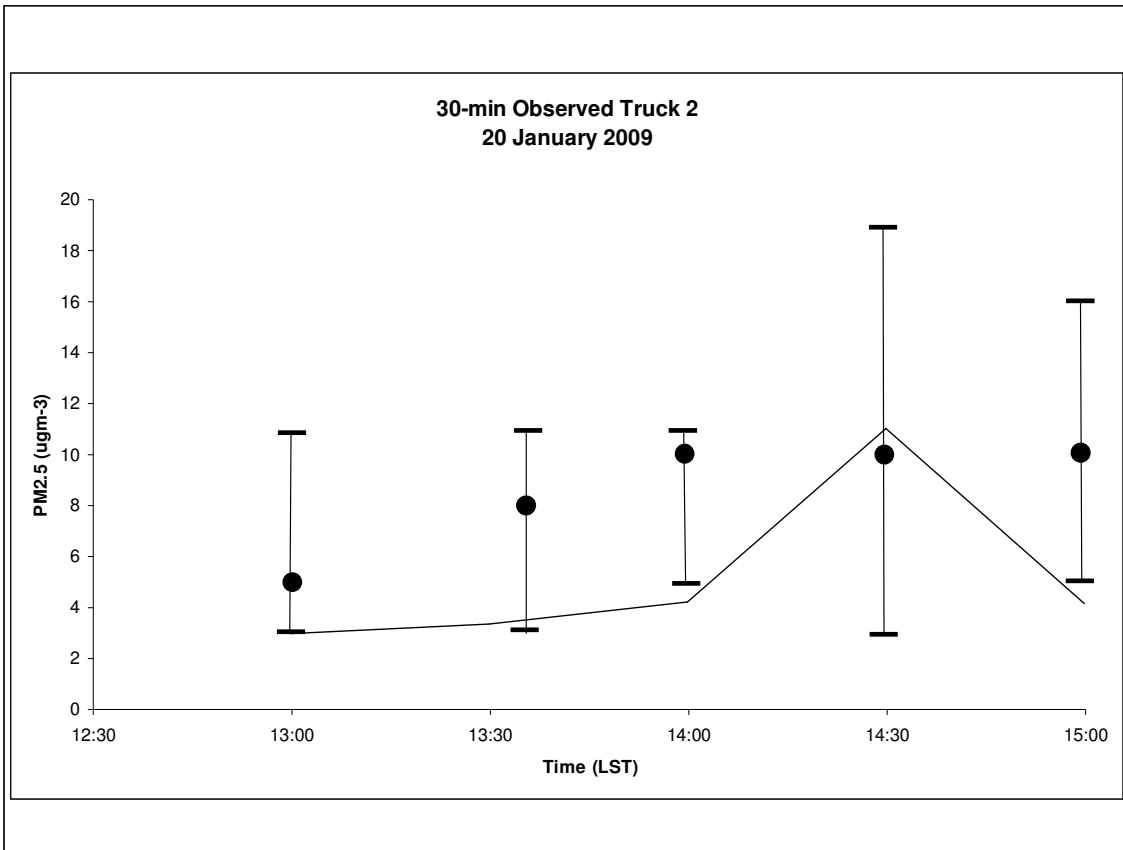


Figure 5. Time series of 30-min averaged PM2.5 from an ensemble of 5 Daysmoke simulations set for the locations of Truck 2. The averages are represented by the dots and the range of concentrations are given by the bars.

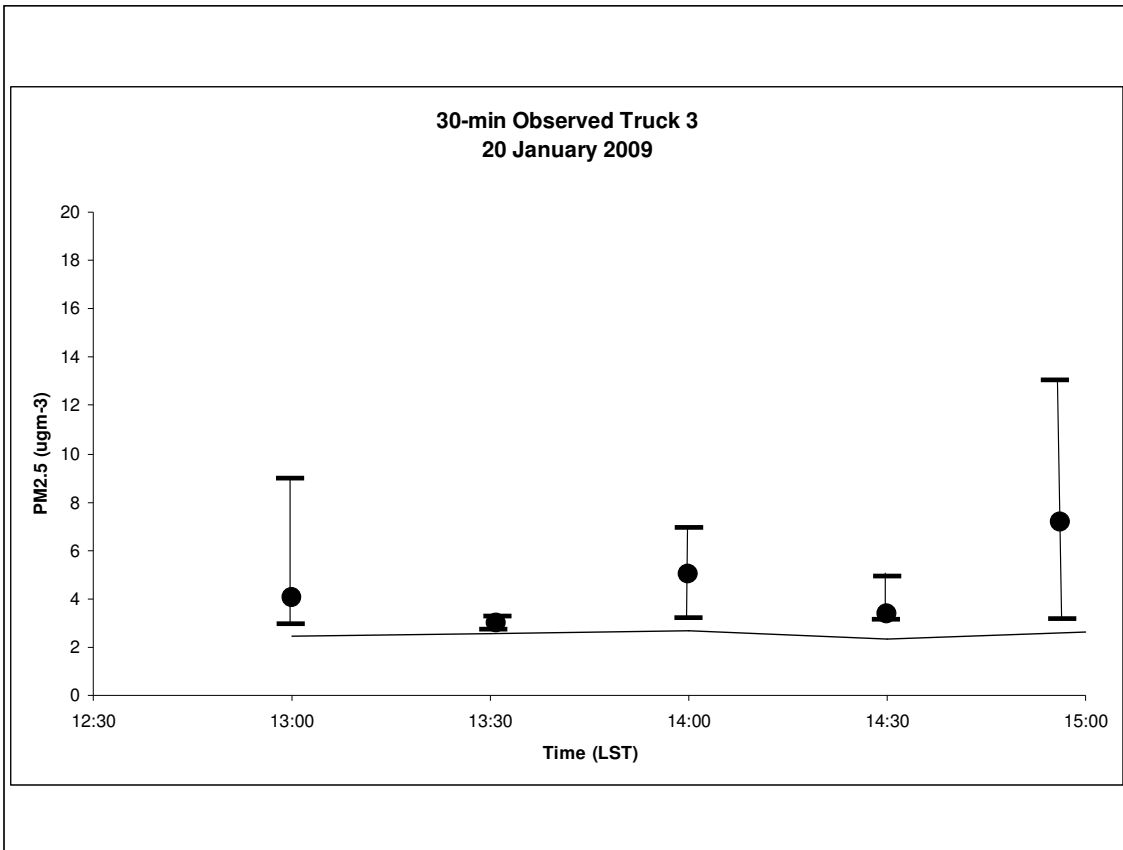


Figure 6. Time series of 30-min averaged PM2.5 from an ensemble of 5 Daysmoke simulations set for the locations of Truck 3. The averages are represented by the dots and the range of concentrations are given by the bars.

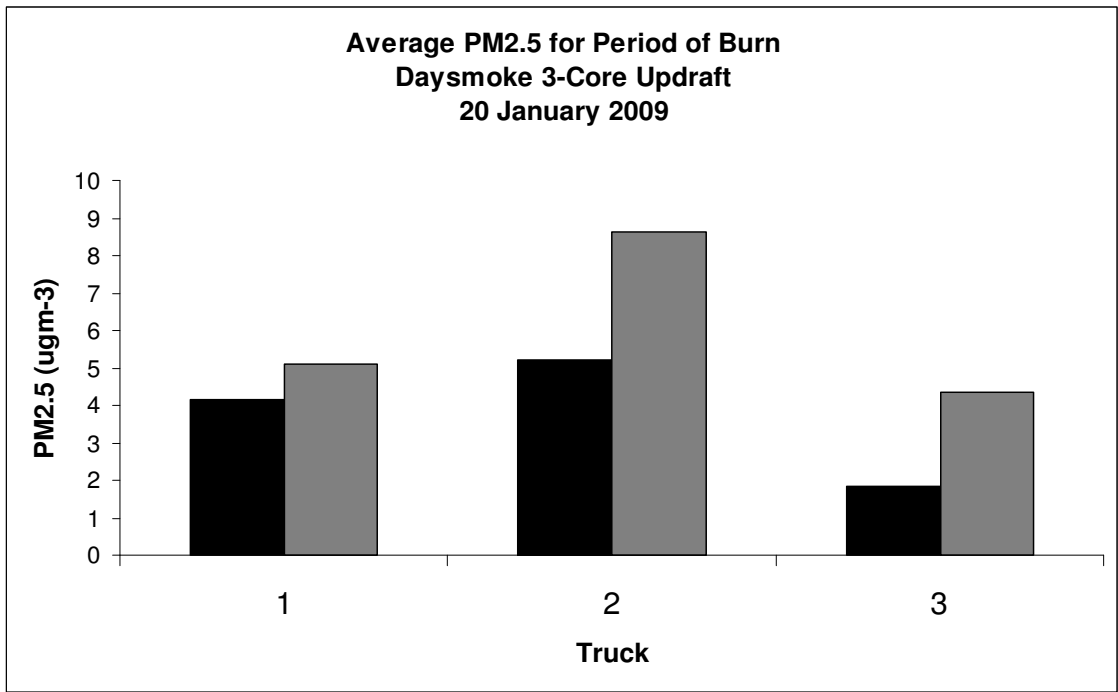


Figure 7. The average PM2.5 for the 3.5 hr period of the burn (black bars) compared with the 5-ensemble average 3-core updraft Daysmoke simulations (gray bars) for the 20 January 2009 burn.

Analysis of 21 January 2009 at Fort Benning, GA

Gary L. Achtemeier
USDA Forest Service
Athens, GA
5 March 2010

Introduction.

On 21 January 2009 compartment D15 consisting of 364 acres was burned. Ignition began at approximately 1230 LST and was completed at 1445 LST. Figure 1 shows a Google Image of the burn area.

All three trucks were deployed. Figure 2 shows the positions of Truck 1 (blue) with respect to the D15 burn. From 1243-1441 LST, the truck was located at Point 1 and from 1447-1532 LST was located at Point 2. Truck 2 (yellow) was located at Point 3 from 1237-1307 LST, Point 4 from 1308-1408 LST, and at Point 5 from 1415-1545 LST. Truck 3 (red) was located at Point 6 from 1235-1334 LST, at Point 7 from 1435-1434, and at Point 8 from 1435-1545 LST.

Winds at 200 m (approximation to the transport winds) developed by the WRF model were characterized by slowly increasing speeds and steadily shifting directions. At 1200 LST winds blew from 317 deg (diagonal black line) at 3.3 m sec⁻¹. Then WRF wind shifted so that winds blew at 1300 LST (304 deg at 3.6 m sec⁻¹), at 1400 LST (284 deg at 3.7 m sec⁻¹), at 1500 LST (276 deg at 3.9 m sec⁻¹) (dashed line), and at 1600 LST (267 deg at 4.3 m sec⁻¹). Figure 2 shows the trucks positioned to the left of the axis of the plume at 1200 LST and well to the right, if not outside, of the plume by 1500 LST.

Inspection of the truck positions in Figure 2 shows that the actions of field crews did not support the WRF wind history. Truck 1 was shifted in distance but not direction. Truck 2 was shifted southward meaning the observed winds were shifting to blow from a more northerly – not westerly – direction. Truck 3 remained essentially stationary. Additional uncertainty is added by an analysis of the hourly surface winds for FBGG1. At 1200 LST winds blew from the NNW, then blew from the WNW for 1300-1400 LST, then blew from the NNW at 1500 LST, and shifted to blow from the WSW at 1600 LST. This it is clear that the outcome of the Daysmoke analysis for 21 January 2009 is critically dependent on the accuracy of the wind directions supplied to the model by WRF.

Observations

The graph of the raw 30-sec data (calibrated for wood smoke) for Truck 1 is shown in the top panel of Figure 3. Smoke arrived in small concentrations (above background) at 1250 LST and in higher concentrations beginning at 1257 LST and remained through the sampling period. Numerous concentration peaks in excess of 100 µgm⁻³ were observed. Low concentrations of smoke arrived at Truck 2 (middle panel) at 1249 LST and in higher concentrations after 1300 LST with numerous peaks in excess of 100 µgm⁻³. Smoke concentrations tapered off after 1430 LST. Smoke in low

concentration arrived at Truck 3 at 1309 LST and in higher concentration after 1315 LST. Smoke was observed at Truck 3 throughout the sampling period.

Daysmoke Results for PM2.5

For the Daysmoke simulations, the block D15 burn was treated as a square of area equal to the area of block D15. Ignition was at 1230 LST.

The Daysmoke results are based on a subjective determination of the updraft core number that would be typical for the 21 January burn. Daysmoke provides no mechanism for determining updraft core number. Updraft core number is determined by a complex interaction among a number of factors. Some of these factors are:

- Size of burn area – a small burn area should be expected to produce only one updraft core; large burn areas can support many updraft cores.
- Shape of burn area – a burn area that is highly irregular in shape will require an irregular distribution of fire leading to many updraft cores. This problem can be amplified when wind direction maximizes irregularities.
- Heterogeneity of fuels – fuels that burn hot relative to surrounding fuels will develop stronger convective currents and will tend to form updraft cores.
- Fuel type, moisture, and loadings – all three factors relate to heat production. High heat production will develop convective columns and lead to fewer updraft cores; low heat production will lead to many updraft cores
- Distribution of fire on landscape - fire distributed along a long linear line will produce many updraft cores; fire spread evenly over length and depth (mass ignition, stripping) will organize convective columns into fewer updraft cores.
- Amount of fire on landscape – a small amount of fire will reduce emissions per second but decrease heat thus minimizing convective organization. Result: many updraft cores. A large amount of fire will produce the opposite. Result: fewer updraft cores
- Distribution of canopy gaps. Hot air trapped beneath a dense canopy will flow to the gaps thus creating convective columns that produce updraft cores there. Thin (or no) canopies will not be a factor in updraft core development.
- Transport wind speed – strong winds inhibit convective organization thus leading to many updraft cores. Weak winds allow convective organization resulting in few updraft cores.
- Mixing layer depth – a shallow mixing layer inhibits convective organization thus leading to many updraft cores. A deep mixing layer has less adverse impact on convective organization so fewer updraft cores should be expected.

For the 21 January 2009 burn, the shape and orientation of the burn area plus the relatively weak 200 m transport winds (3.6 m sec^{-1}) serve to decrease updraft core number. The relatively shallow mixing layer depth (900-1000 m) serve to increase the number of updraft cores. An updraft core number of 4 cores was assigned for this burn.

The left panel of Figure 4 shows the time series of 30-min averaged PM2.5 from the ensemble of five 4-core updraft plume Daysmoke simulations set for the locations of Truck 1 as compared with 30-min averages for the observations (solid line). The averages are represented by the black circles and the ranges of concentrations are given by the

bars. The 4-core updraft solutions fit the observations very well for 1300-1500 LST. The model results fall below the 30-min observed trace thereafter. The 6-core updraft solutions (right panel) are included to show that the drop-off in PM_{2.5} concentrations after 1400 LST was not the outcome of the selection of the 4-core updraft plume. The 6-core solution overestimates PM_{2.5} at 1330-1430 LST then falls below the observations after 1500 LST

The 4-core updraft solution for Truck 2 (Figure 5) follows the observations through 1400 LST then under-predicted PM_{2.5} thereafter. Figure 6 shows that the 4-core solution matched the observations from 1300-1330 LST. Then wind shifts placed Truck 3 on the plume edge and Daysmoke underpredicted smoke thereafter.

Figure 7 shows a 5-min average Daysmoke plume of PM_{2.5} at 1430 LST. Truck 1 is still within the plume, Truck 2 is on the edge of the plume and Truck 3 resides outside of the plume.

The 21 January 2009 burn was an example of PM_{2.5} concentrations increasing downwind from the burn (Figure 8). Concentrations increased from 33 $\mu\text{g m}^{-3}$ at Truck 1 to 42 $\mu\text{g m}^{-3}$ at Truck 3. Given the impacts of the wind shift in the WRF data, the 4-core updraft plume Daysmoke simulations systematically underestimated PM_{2.5} but were within acceptable limits. Results compare as follows: Truck 1 (29 $\mu\text{g m}^{-3}$ vs 33 $\mu\text{g m}^{-3}$), Truck 2 (33 $\mu\text{g m}^{-3}$ vs 42 $\mu\text{g m}^{-3}$) and Truck 3 (25 $\mu\text{g m}^{-3}$ vs 46 $\mu\text{g m}^{-3}$). Figure 9 is included to show the results for a 6-core updraft plume simulation. Results compare as follows: Truck 1 (39 $\mu\text{g m}^{-3}$ vs 33 $\mu\text{g m}^{-3}$), Truck 2 (42 $\mu\text{g m}^{-3}$ vs 42 $\mu\text{g m}^{-3}$) and Truck 3 (36 $\mu\text{g m}^{-3}$ vs 46 $\mu\text{g m}^{-3}$). Thus the 6-core solution improves over the 4-core solution but for the wrong reasons. The 6-core solution overestimate smoke at some times while underestimating smoke at other times (right panel of Figure 4).

In summary, the 21 January 2009 burn with relatively deep mixing layer and relatively light winds was an ideal case for Daysmoke as the model is best designed to simulate downwind down-mixing of smoke. Unfortunately, the WRF wind data on which the Daysmoke solutions are initialized shifted the winds from the northwest to the west too soon. The outcome for the 4-core solution was that Daysmoke underestimated smoke at all three trucks but the results were still quite good. Use of a 6-core updraft solution improved the average results but for the wrong reasons.

Daysmoke Results for Plume Top Height

No ceilometer data was collected for the 21 January 2009 burn.



Figure 1. Google Earth image of Block D15 outlined in yellow 21 January 2009 burn at Fort Benning, GA.

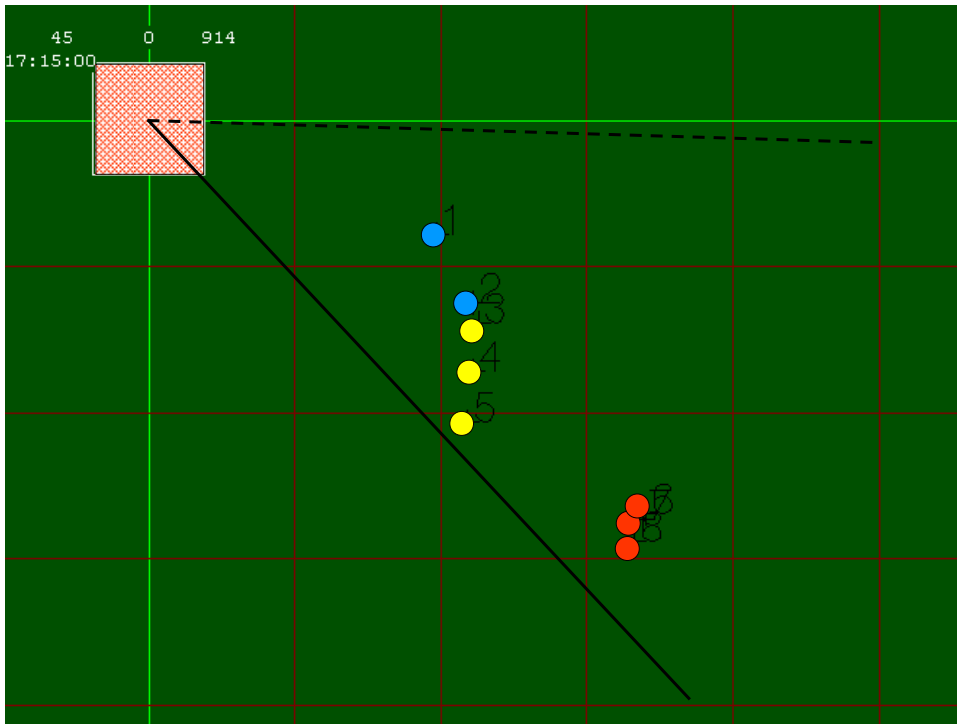


Figure 2. Locations of the three trucks relative to the Daysmoke depiction of the compartment D15 burn. The diagonal black line delineates prevailing wind direction.

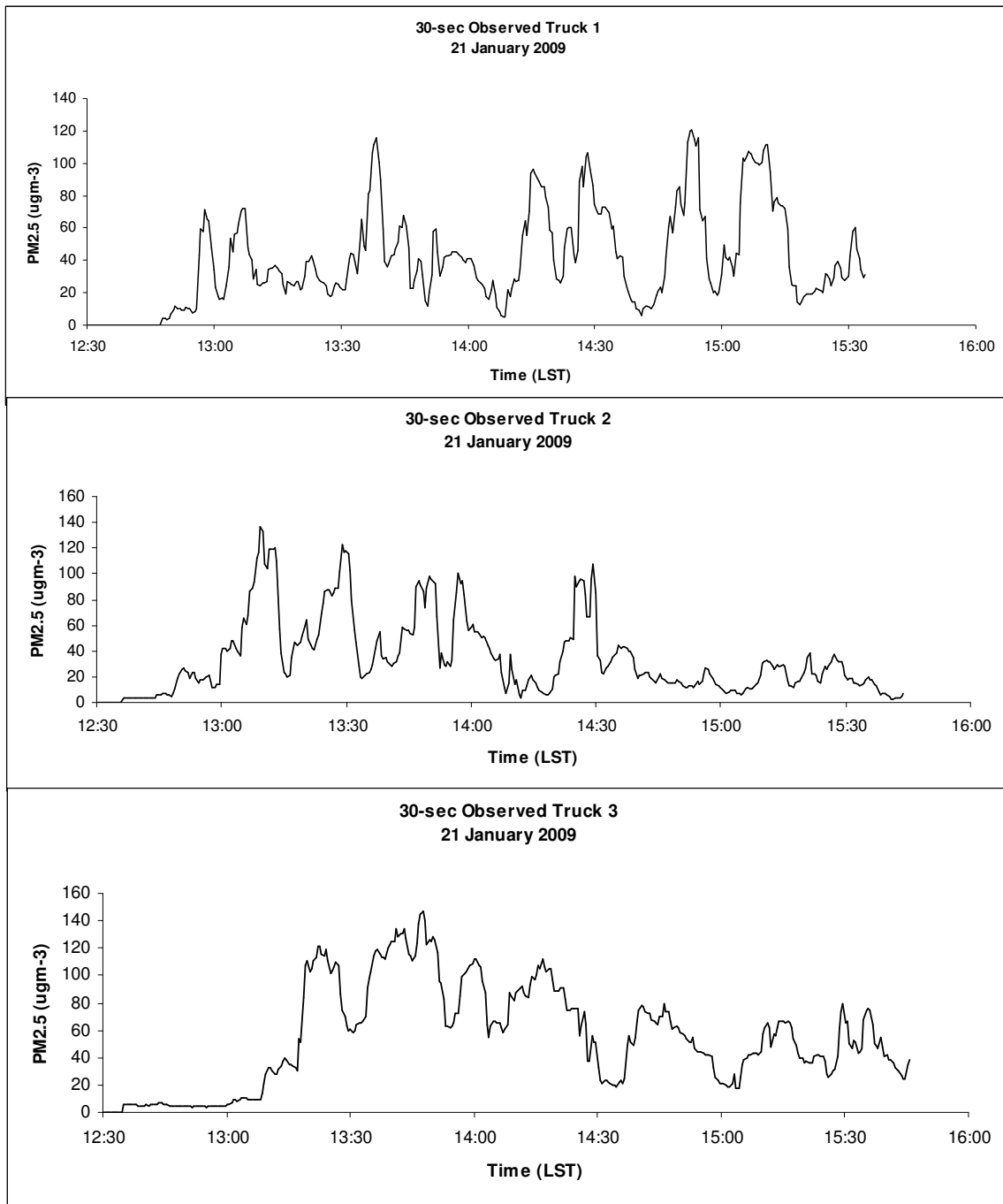


Figure 3. Traces of the 30-sec observed PM_{2.5} measured at the locations of Truck 1 (top panel), Truck 2 (middle panel), and Truck 3 (lower panel) for the 21 January 2009 burn.

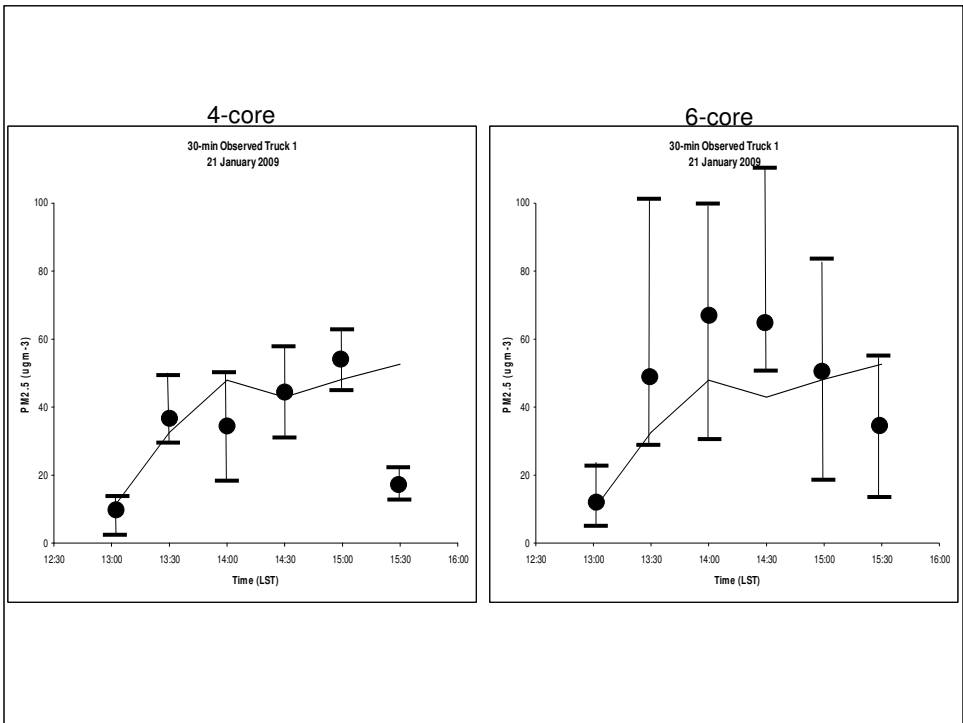


Figure 4. Time series of 30-min averaged PM_{2.5} from an ensemble of 5 Daysmoke simulations set for the locations of Truck 1 for 4-core (left panel) and 6-core updraft (right panel) updraft plumes. The averages are represented by the dots and the range of concentrations are given by the bars.

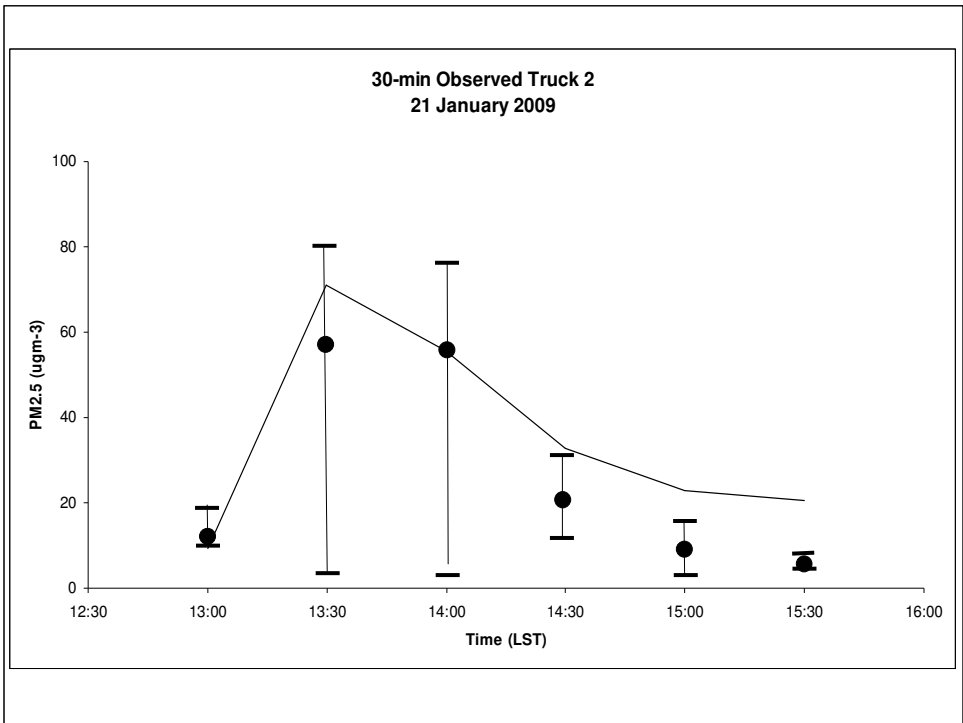


Figure 5. Time series of 30-min averaged PM_{2.5} from an ensemble of 5 Daysmoke simulations set for the locations of Truck 2. The averages are represented by the dots and the range of concentrations are given by the bars.

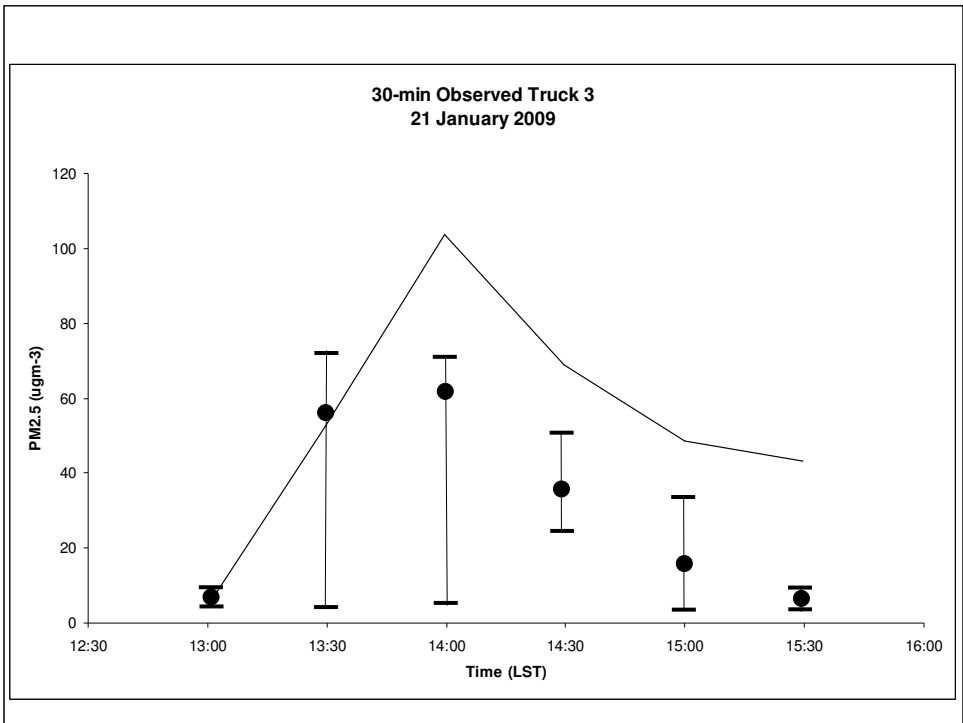


Figure 6. Time series of 30-min averaged PM2.5 from an ensemble of 5 Daysmoke simulations set for the locations of Truck 3. The averages are represented by the dots and the range of concentrations are given by the bars.

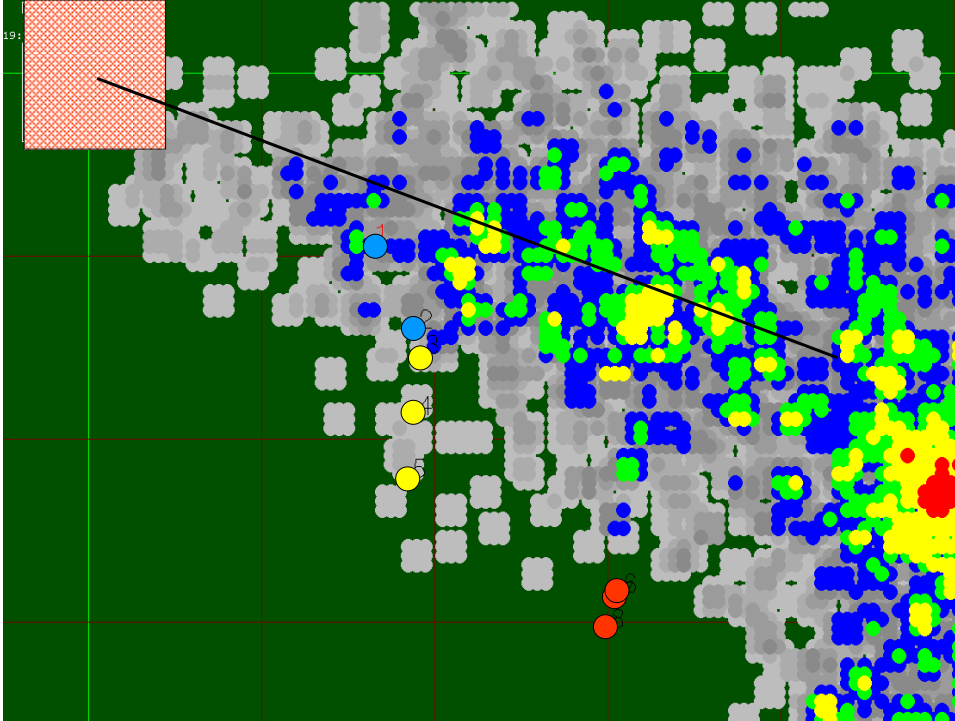


Figure 7. The 5-min Daysmoke 4-core plume for 1430 LST for the 21 January 2009 burn.

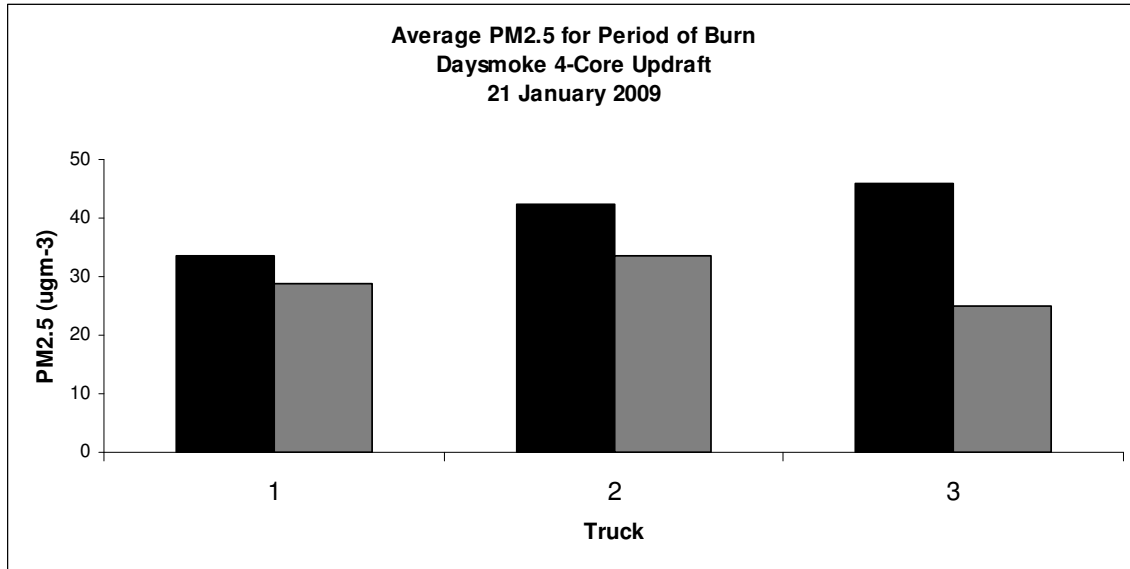


Figure 8. The average PM2.5 for the 3.5 hr period of the burn (black bars) compared with the 5-ensemble average 4-core updraft Daysmoke simulations (gray bars) for the 21 January 2009 burn.

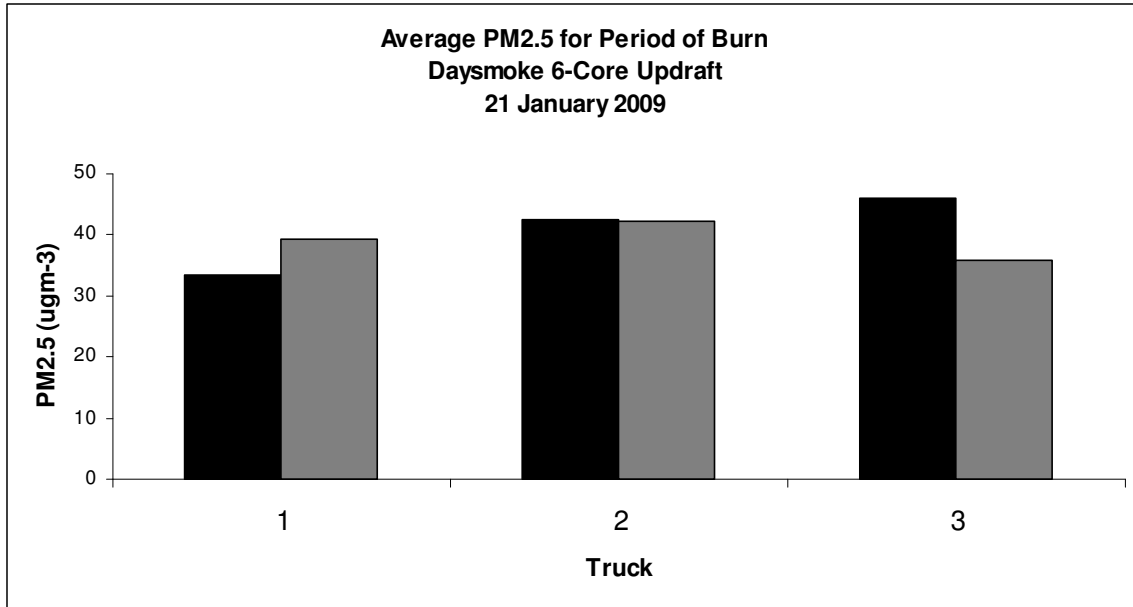


Figure 9. The average PM2.5 for the 3.5 hr period of the burn (black bars) compared with the 5-ensemble average 6-core updraft Daysmoke simulations (gray bars) for the 21 January 2009 burn.

Analysis of 23 January 2009 at Fort Benning, GA

Gary L. Achtemeier
USDA Forest Service
Athens, GA
5 March 2010

Introduction.

On 23 January 2009 Block I3 consisting of 455 acres was burned. Ignition began at approximately 1230 LST and was completed at 1430 LST. Figure 1 shows a Google Image of the burn area.

All three trucks were deployed. Figure 2 shows the positions of Truck 1 (blue) with respect to the I3 burn. From 1245-1440 LST, the truck was located at Point 1 and from 1446-1530 LST was located at Point 2. Truck 2 (yellow) was located at Point 3 from 1245-1315 LST, Point 4 from 1316-1345 LST, and at Point 5 from 1445-1530 LST. Truck 3 (red) was located at Point 6 from 1245-1344 LST, at Point 7 from 1445-1414, and at Point 8 from 1415-1530 LST.

Winds at 200 m (approximation to the transport winds) developed by the WRF model were characterized by slowly increasing speeds (6.6 m sec^{-1} at 1200 LST to 9.6 m sec^{-1} at 1500 LST). Wind directions remained steady at 233 deg until 1600 when the wind shifted to 227 deg. However, the wind shift occurred after the period of the burn.

Inspection of the truck positions in Figure 2 relative to the ambient wind direction (black line) shows that the trucks were positioned to the left of the axis of wind direction (looking downwind). Movement of the trucks, especially Truck 2 was apparently an adjustment for the wind direction. These actions of field crews support the notion that WRF winds were accurate for 23 January. Furthermore, the N-S elongation of the burn area would have placed the trucks in position to capture much of the smoke from the northern half of the burn area.

The long orientation of the burn site (Figure 1) and the location of the trucks to capture smoke from the northern half of the burn area led to a re-location of the burn center point from (32.3469n, 84.7302w) to (32.3529n, 84.7292w) or the red square in Figure 1. The revised locations of the trucks are shown in Figure 3.

Observations

The graph of the raw 30-sec data (calibrated for wood smoke) for Truck 1 is shown in the top panel of Figure 4. Smoke arrived at 1320 LST and in much higher concentrations beginning at 1340 LST. From 1340-1350 concentrations peaked above $600 \mu\text{gm}^{-3}$. Concentrations decreased after 1400 LST but peaks remained above $200 \mu\text{gm}^{-3}$. Smoke arrived at Truck 2 (middle panel) at 1315 LST followed by a peak concentration of $259 \mu\text{gm}^{-3}$. Concentrations peaked in excess of $100 \mu\text{gm}^{-3}$ for the remainder of the record. Smoke concentrations at Truck 3 increased gradually beginning at 1400 LST reaching concentrations of $72 \mu\text{gm}^{-3}$ at 1534 LST.

Daysmoke Results for PM2.5

For the Daysmoke simulations, the block I3 burn was treated as a square of area equal to the area of block I3. Ignition was at 1230 LST.

The Daysmoke results are based on a subjective determination of the updraft core number that would be typical for the 23 January burn. Daysmoke provides no mechanism for determining updraft core number. Updraft core number is determined by a complex interaction among a number of factors. Some of these factors are:

- Size of burn area – a small burn area should be expected to produce only one updraft core; large burn areas can support many updraft cores.
- Shape of burn area – a burn area that is highly irregular in shape will require an irregular distribution of fire leading to many updraft cores. This problem can be amplified when wind direction maximizes irregularities.
- Heterogeneity of fuels – fuels that burn hot relative to surrounding fuels will develop stronger convective currents and will tend to form updraft cores.
- Fuel type, moisture, and loadings – all three factors relate to heat production. High heat production will develop convective columns and lead to fewer updraft cores; low heat production will lead to many updraft cores
- Distribution of fire on landscape - fire distributed along a long linear line will produce many updraft cores; fire spread evenly over length and depth (mass ignition, stripping) will organize convective columns into fewer updraft cores.
- Amount of fire on landscape – a small amount of fire will reduce emissions per second but decrease heat thus minimizing convective organization. Result: many updraft cores. A large amount of fire will produce the opposite. Result: fewer updraft cores
- Distribution of canopy gaps. Hot air trapped beneath a dense canopy will flow to the gaps thus creating convective columns that produce updraft cores there. Thin (or no) canopies will not be a factor in updraft core development.
- Transport wind speed – strong winds inhibit convective organization thus leading to many updraft cores. Weak winds allow convective organization resulting in few updraft cores.
- Mixing layer depth – a shallow mixing layer inhibits convective organization thus leading to many updraft cores. A deep mixing layer has less adverse impact on convective organization so fewer updraft cores should be expected.

For the 23 January 2009 burn, the shape and orientation of the burn area plus the relatively strong 200 m transport winds ($6.6\text{-}9.6\text{ m sec}^{-1}$) serve to increase updraft core number. The relatively shallow initial mixing layer depth (512 m) also serves to increase the number of updraft cores. An updraft core number of 10 cores should be assigned for this burn. However, given the shape of the burn area, less smoke from the northern half of the burn area would impact the Trucks in comparison to smoke from the square burn area used in Daysmoke. Thus the number of updraft cores is reduced from 10 to 8.

Figure 5 compares the average PM2.5 for the period of the burn (1300-1530 LST) with the results from a 5-ensemble Daysmoke average for the three trucks. The event is characterized by the observations as a very steep gradient in smoke between Truck 1 and

Truck 3 – 106-14 μgm^{-3} – a decline of 92 μgm^{-3} over a distance of only 2.8 mi (4.5 km). It may be argued that Truck 3 was located to the left of the plume axis and was thus not in smoke much of the time. Furthermore, Figure 4 (panel 3) shows that smoke arrived at Truck 3 at a rather late 1400 LST and was still increasing when the observations were terminated at 1530 LST.

Truck 3 was located at the edge of the Daysmoke simulated plume but Daysmoke put an event averaged 22 μgm^{-3} at Truck 3 beginning at 1245 LST. Only by narrowing the plume unrealistically and increasing the updraft core number to 10 did Daysmoke begin to approximate observed smoke concentrations at Truck 2 (57 μgm^{-3} vs 74 μgm^{-3}) and at Truck 3 (25 μgm^{-3} vs 14 μgm^{-3}). Daysmoke never approximated the magnitudes of PM_{2.5} at Truck 1.

In summary, the 23 January 2009 burn could not be simulated with Daysmoke. Therefore there was no need to present detailed graphics at 5-min or 30-min intervals.

Daysmoke Results for Plume Top Height

No ceilometer data was collected for the 23 January 2009 burn. However, a vertical cross section of an 8-core updraft Daysmoke plume was obtained for 1800 LST. Figure 6 shows a concentrated plume core at 300 m above ground oriented roughly parallel to the ground for a distance of approximately 3 km. The plume climbs to the mixing height (720 m) between 5-6 km downwind.

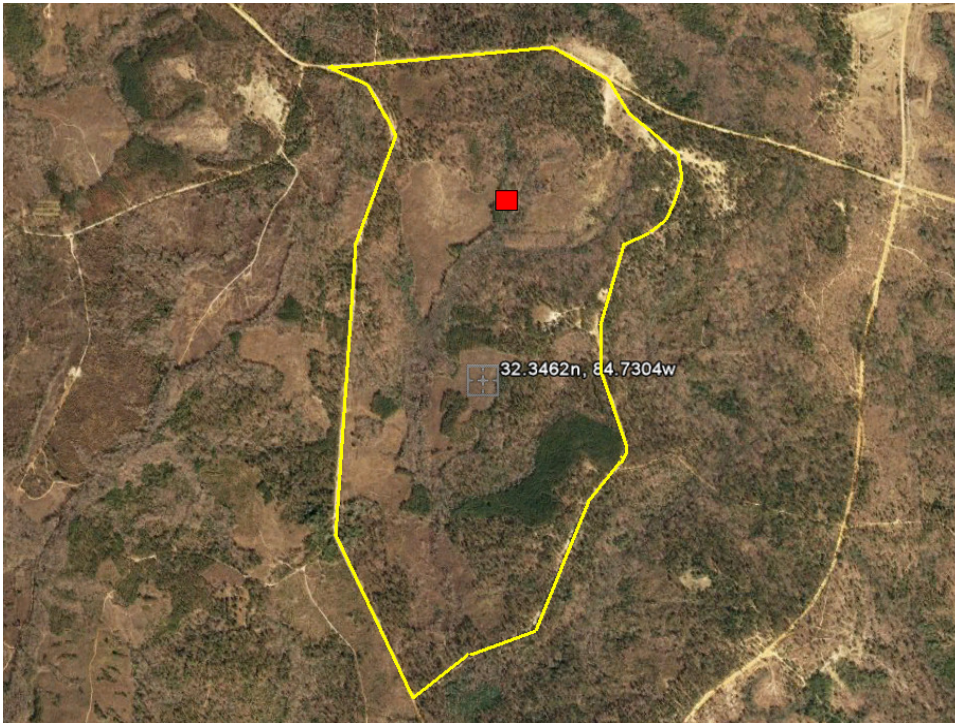


Figure 1. Google Earth image of Block I3 outlined in yellow 23 January 2009 burn at Fort Benning, GA.

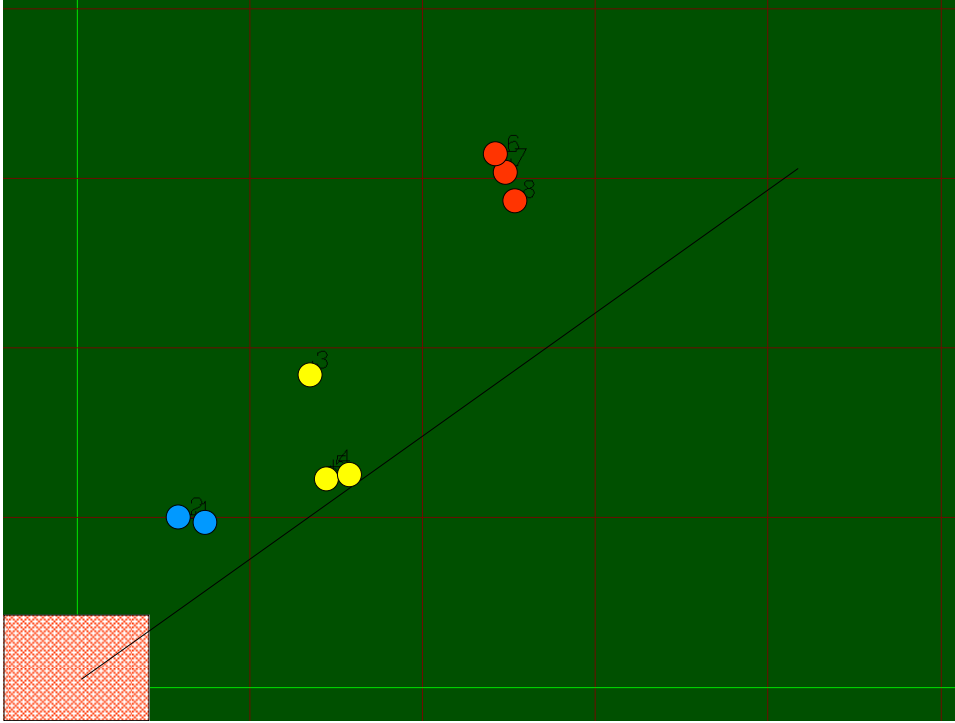


Figure 2. Locations of the three trucks relative to the Daysmoke depiction of the compartment I3 burn with reference to the compartment center point. The diagonal black line delineates prevailing wind direction.

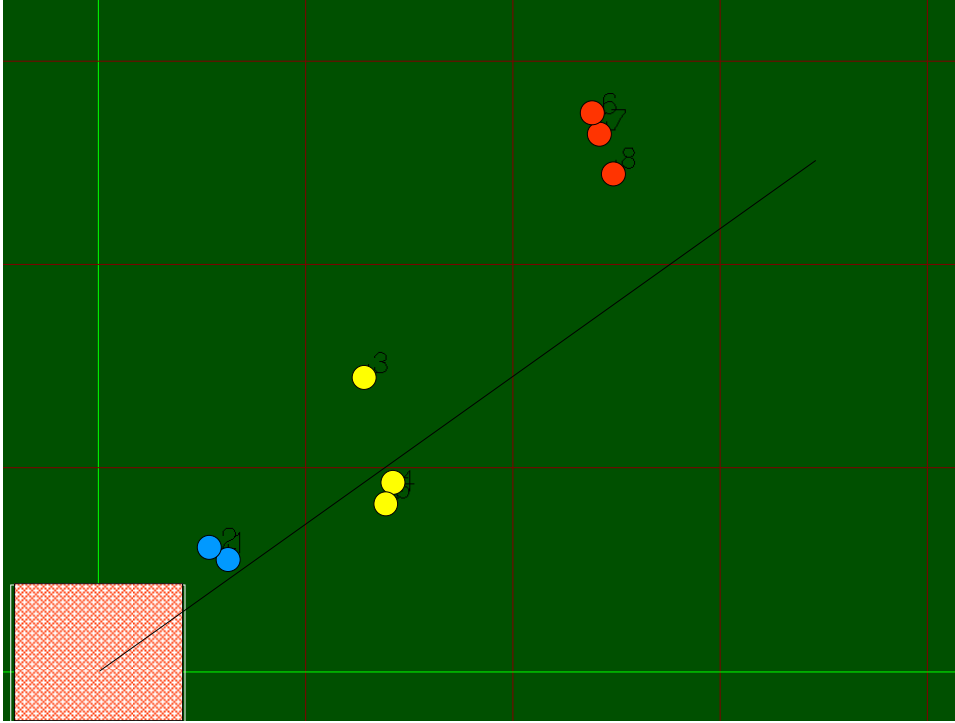


Figure 3. Locations of the three trucks relative to the Daysmoke depiction of the compartment I3 burn with reference to the red square in Figure 1. The diagonal black line delineates prevailing wind direction.

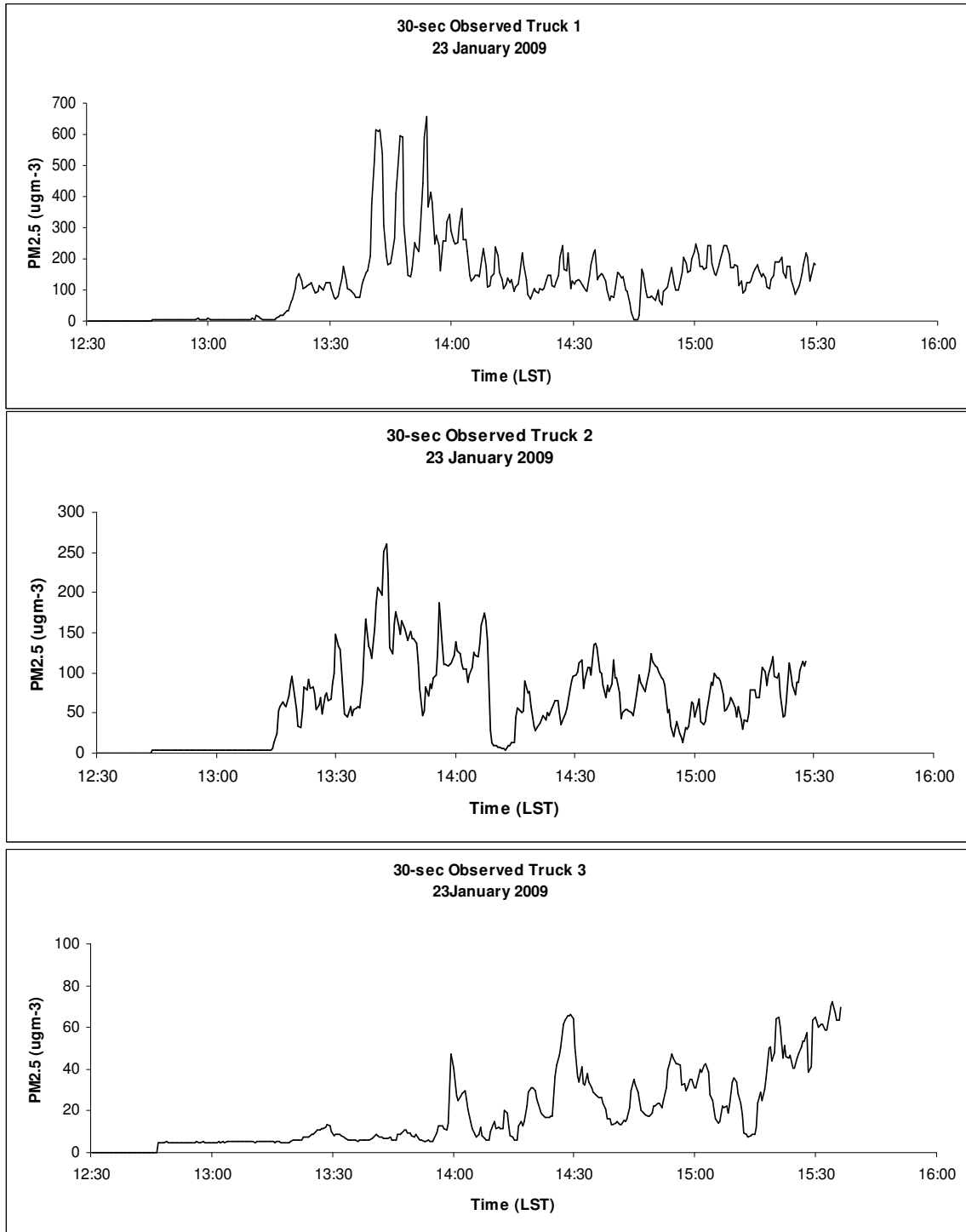


Figure 4. Traces of the 30-sec observed PM_{2.5} measured at the locations of Truck 1 (top panel), Truck 2 (middle panel), and Truck 3 (lower panel) for the 23 January 2009 burn.

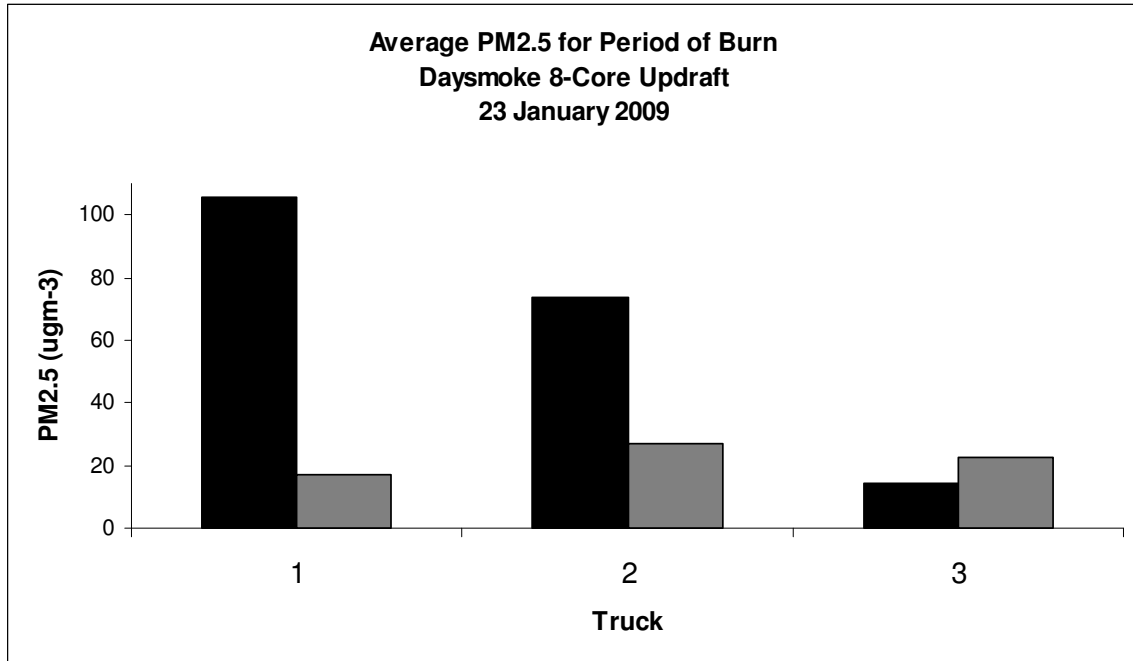


Figure 5. The average PM2.5 for the 2.5 hr period of the burn (black bars) compared with the 5-ensemble average 8-core updraft Daysmoke simulations (gray bars) for the 23 January 2009 burn.

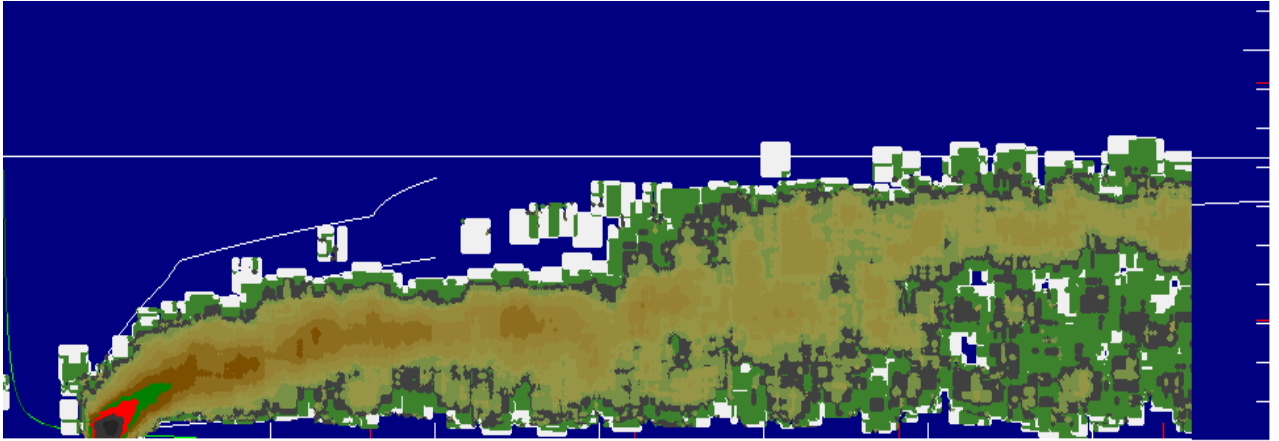


Figure 6. Vertical cross section of an 8-core plume modeled by Daysmoke for 1800 LST 23 January 2009. The white horizontal tic marks denote 100 m intervals. The vertical tic marks denote 1.0 mile (red) and 1.0 km (white) intervals.

Analysis of 08 April 2009 at Fort Benning, GA

Gary L. Achtemeier
USDA Forest Service
Athens, GA
5 March 2010

Introduction.

On 08 April 2009 two compartments of Block E3 consisting of 112 acres and 125 acres (337 acres total) were burned. Compartment A ignition began at approximately 1130 LST and was completed at 1230 LST. Compartment B ignition began at approximately 1300 LST and was completed by 1400 LST. Figure 1 shows a Google Image of the burn area.

All three trucks were deployed. Figure 2 shows the positions of Truck 1 (blue) with respect to the compartment A burn. From 1138-1232 LST, the truck was located at Point 1 and from 1240-1445 LST was located at Point 2. Truck 2 (yellow) was located at Point 3 from 1150-1220 LST, and at Point 4 from 1223-1430 LST. Truck 3 (red) was located at Point 5 from 1139-1225 LST and at Point 6 from 1232-1439 LST. The white circles locate positions of the USFS ceilometer. The positions of the trucks relative to the compartment B burn are shown in Figure 3. The distance from the burn site to Truck 3 was approximately 5.7 miles (9.1 km).

Winds at 200 m (approximation to the transport winds) developed by the WRF model were characterized by slowly increasing speeds (6.0 m sec^{-1} at 1100 LST to 9.5 m sec^{-1} at 1500 LST). Wind directions remained steady at 249 deg until 1500 LST when the wind shifted to 242 deg. However, the wind shift occurred after the period of the burn.

Inspection of the truck positions in Figure 2 and Figure 3 relative to the ambient wind direction (black line) shows that the trucks were positioned to the left of the axis of wind direction (looking downwind). Movement of the trucks, especially Truck 3 was apparently an adjustment for the wind direction. These actions of field crews support the notion that WRF winds were accurate for 08 April. Furthermore, the weather record for the surface weather station FBGG1 showed winds blowing from the WSW during most of the burn periods.

Observations

The graph of the raw 30-sec data (calibrated for wood smoke) for Truck 1 is shown in the top panel of Figure 4. Smoke arrived at 1230 LST in low concentrations until a spike to $50 \mu\text{gm}^{-3}$ at 1400 LST. Smoke arrived at Truck 2 (middle panel) at 1240 LST followed by a peak concentration $64 \mu\text{gm}^{-3}$ at 1245 LST and another peak to $61 \mu\text{gm}^{-3}$ at 1343 LST. Though these peaks were higher than maximum concentrations measured at Truck 1, the smoke residence time was less with an apparent smoke free period from 1246-1335 LST. Smoke concentrations at Truck 3 increased gradually beginning at 1205 LST then peaked at $27 \mu\text{gm}^{-3}$ at 1239 LST.

Daysmoke Results for PM2.5

For the Daysmoke simulations, the block E3 burn was treated as a square of area equal to the area of block E3. Ignition was at 1130 LST.

The Daysmoke results are based on a subjective determination of the updraft core number that would be typical for the 08 April burn. Daysmoke provides no mechanism for determining updraft core number. Updraft core number is determined by a complex interaction among a number of factors. Some of these factors are:

- Size of burn area – a small burn area should be expected to produce only one updraft core; large burn areas can support many updraft cores.
- Shape of burn area – a burn area that is highly irregular in shape will require an irregular distribution of fire leading to many updraft cores. This problem can be amplified when wind direction maximizes irregularities.
- Heterogeneity of fuels – fuels that burn hot relative to surrounding fuels will develop stronger convective currents and will tend to form updraft cores.
- Fuel type, moisture, and loadings – all three factors relate to heat production. High heat production will develop convective columns and lead to fewer updraft cores; low heat production will lead to many updraft cores
- Distribution of fire on landscape - fire distributed along a long linear line will produce many updraft cores; fire spread evenly over length and depth (mass ignition, stripping) will organize convective columns into fewer updraft cores.
- Amount of fire on landscape – a small amount of fire will reduce emissions per second but decrease heat thus minimizing convective organization. Result: many updraft cores. A large amount of fire will produce the opposite. Result: fewer updraft cores
- Distribution of canopy gaps. Hot air trapped beneath a dense canopy will flow to the gaps thus creating convective columns that produce updraft cores there. Thin (or no) canopies will not be a factor in updraft core development.
- Transport wind speed – strong winds inhibit convective organization thus leading to many updraft cores. Weak winds allow convective organization resulting in few updraft cores.
- Mixing layer depth – a shallow mixing layer inhibits convective organization thus leading to many updraft cores. A deep mixing layer has less adverse impact on convective organization so fewer updraft cores should be expected.

For the 08 April 2009 burn, the relatively strong 200 m transport winds ($6.0-9.5 \text{ m sec}^{-1}$) and light fuel loads (2T/acre) serve to increase updraft core number. The deep mixing layer (1600-1800 m) serves to decrease the number of updraft cores. Furthermore, the relatively small sizes of the burn areas (112 and 125 acres) serve to decrease the updraft core number. An updraft core number of 3 cores are assigned for this burn.

Figure 5 compares the average PM2.5 for the period of the burn (1130-1430 LST) with the results from a 5-ensemble Daysmoke average for 3-core updraft plumes for the locations of the trucks. The event is characterized by generally low concentrations of smoke punctuated by spikes of higher concentrations. Daysmoke overestimated smoke at Truck 1 by a factor of 2 ($18-8 \mu\text{gm}^{-3}$), matched Truck 2 ($10-9 \mu\text{gm}^{-3}$), and overestimated

smoke at Truck 3 (23-4 μgm^{-3}). Examination of Daysmoke plumes relative to truck positions in Figure 2 and Figure 3 show that Truck 1 was located within the plume but to the left of the plume axis. Truck 2 was located at the plume edge and Truck 3 was located along the plume axis once the truck was located at Point 6. Daysmoke simulated higher concentrations along the axis and it was the contribution to the total smoke at Point 6 from both compartment A and B burns that increased Daysmoke concentrations so far above the observations.

In summary, the 08 April 2009 burn produced relatively low smoke concentrations at all three trucks. Daysmoke over-predicted smoke at all three trucks with the greatest over-prediction at Truck 3. Given that smoke concentrations were quite low for both observations and Daysmoke, there is not much for which Daysmoke could be faulted. It can be argued that a small difference between observed and WRF modeled wind directions could account for most of the discrepancies. However, it can also be argued that a more judicious selection for the plume updraft core number would have produced better results.

Daysmoke was rerun for 1-core updraft plumes for the burns in both compartments. Figure 6 shows the results to be much improved. Daysmoke matched smoke at Truck 1 (10-8 μgm^{-3}), matched Truck 2 (7-9 μgm^{-3}), and overestimated smoke at Truck 3 (11-4 μgm^{-3}). These results show how sensitive is Daysmoke to the updraft core number.

Daysmoke Results for Plume Top Height

Vertical cross sections for the 3-core updraft (upper panel) and the 1-core updraft (lower panel) Daysmoke plumes obtained for 1800 LST are shown in Figure 7. The white line identifies the mixing height. Daysmoke tended to run the plumes just above the ground with mixing both to the ground and aloft as the plumes dispersed downwind. The 3-core plume typically remained below 500 m with the core of concentrations located at approximately 300 m. The 1-core solution (lower panel) dispersed slowly upward reaching 1300 m by 10 miles (16 km) downwind from the source. From Figure 2 and Figure 3, the location of the USFS ceilometer ranged from 2.0-2.5 miles (3.2-4.0 km) downwind from the burn. At those ranges, the Daysmoke plume tops ranged from 400 m (3-core) to 500-550 m (1-core). Examination of the Daysmoke plumes for 1900 LST showed little change in plume height for either of the 1-core or 3-core updraft plumes.

Figure 8 shows the traces for the highest plume height and largest return as measured by the USFS ceilometer. Time is local daylight time and one hour should be subtracted to bring the time to LST. The graph shows the plume first arriving at the location of the ceilometer shortly after 1230 LST (1330 EDT –eastern daylight time). Plume heights were found near 500 m. Plume heights climbed to 900 m by 1300 LST, then to 1250-1300 m thereafter. Daysmoke plumes did not attain to these heights until 6 miles (10 km) downwind. The slow growth in the Daysmoke plumes is attributed to the relatively strong transport winds simulated by the WRF model.

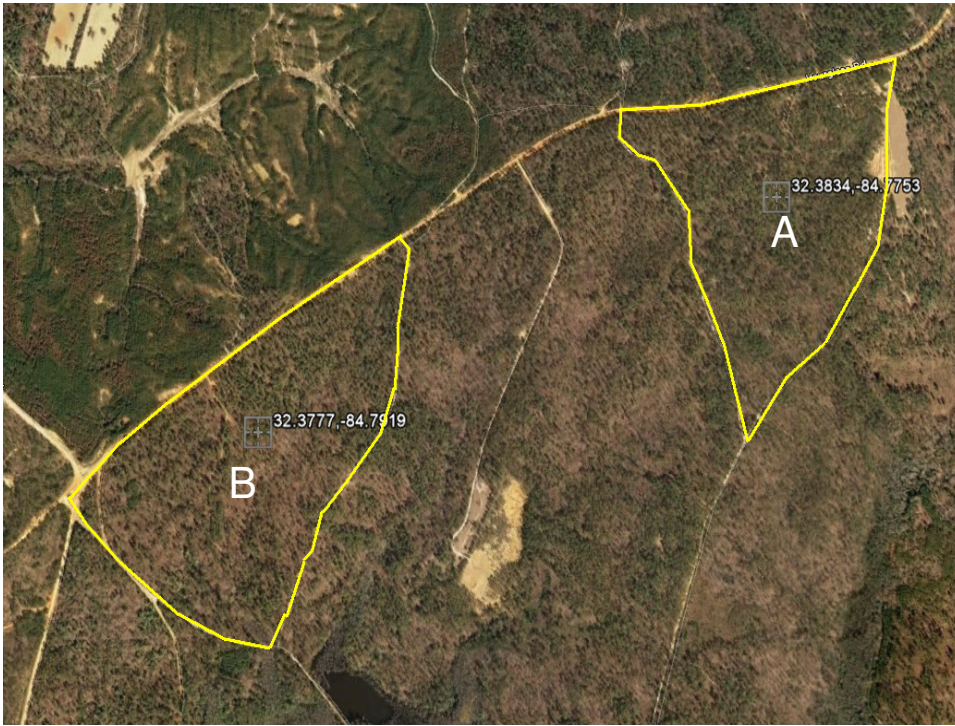


Figure 1. Google Earth image of Block E3 showing the two burned compartments outlined in yellow for the 08 April 2009 burn at Fort Benning, GA.

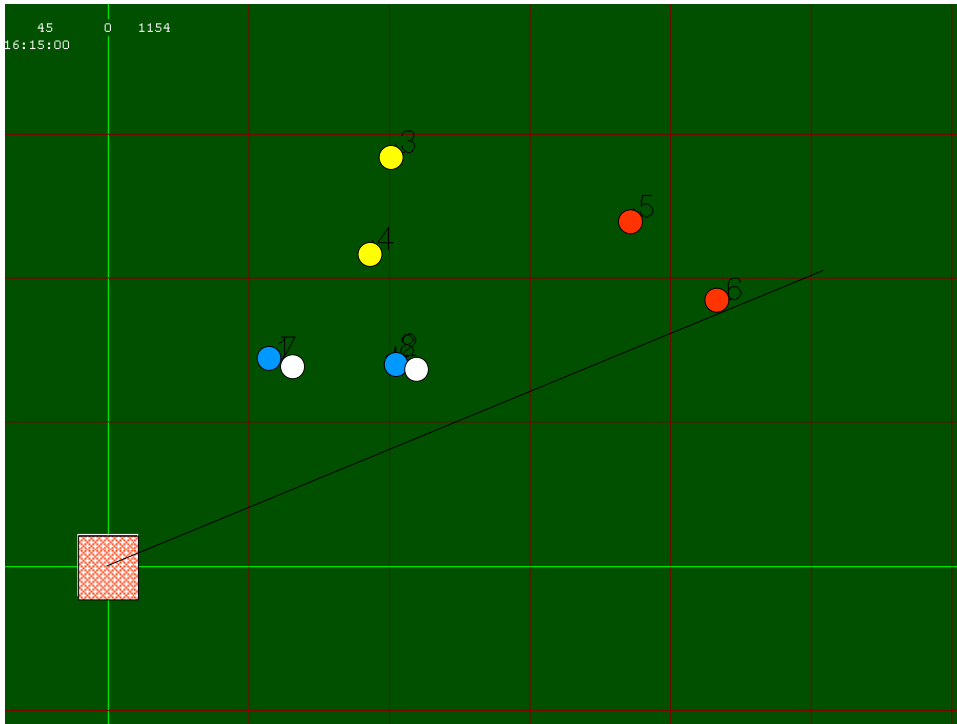


Figure 2. Locations of the three trucks relative to the Daysmoke depiction of the compartment E3-A burn with reference to the compartment center point. The diagonal black line delineates prevailing wind direction.

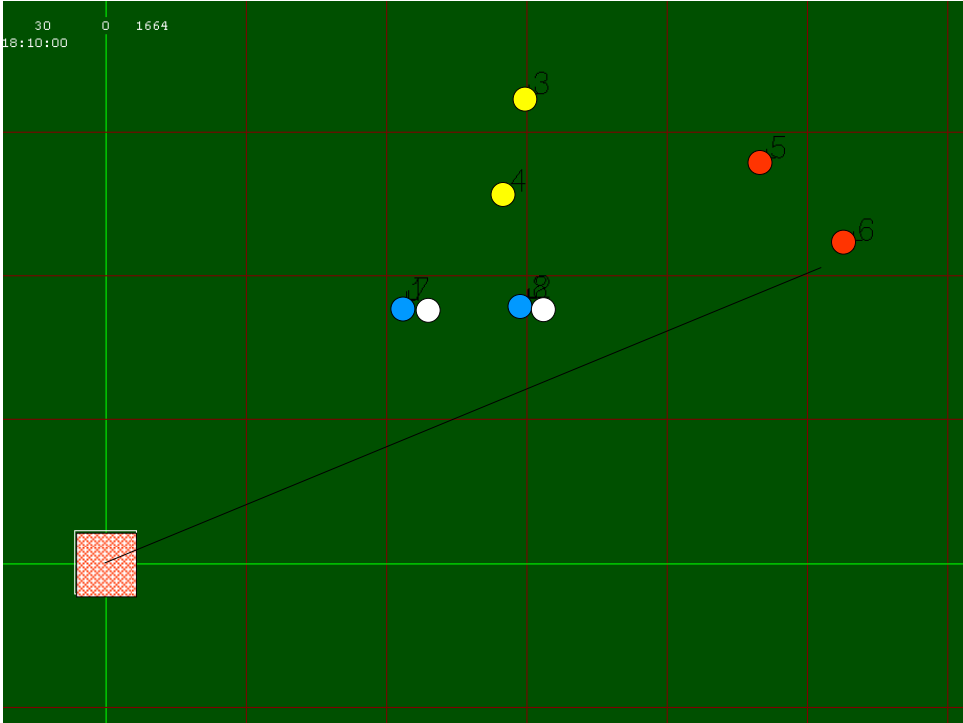


Figure 3. Locations of the three trucks relative to the Daysmoke depiction of the compartment E3-B burn with reference to the red square in Figure 1. The diagonal black line delineates prevailing wind direction.

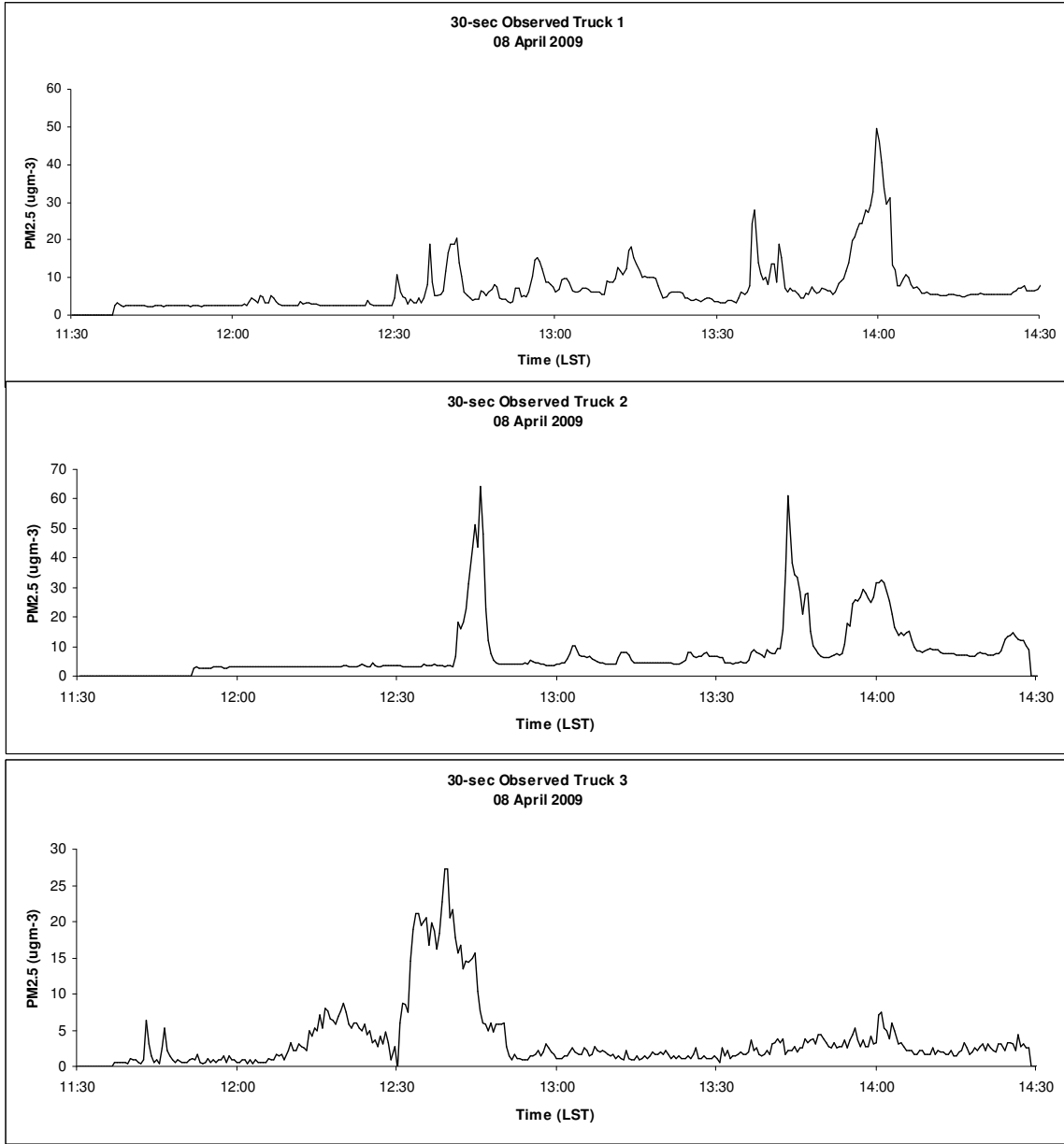


Figure 4. Traces of the 30-sec observed PM_{2.5} measured at the locations of Truck 1 (top panel), Truck 2 (middle panel), and Truck 3 (lower panel) for the 08 April 2009 burn.

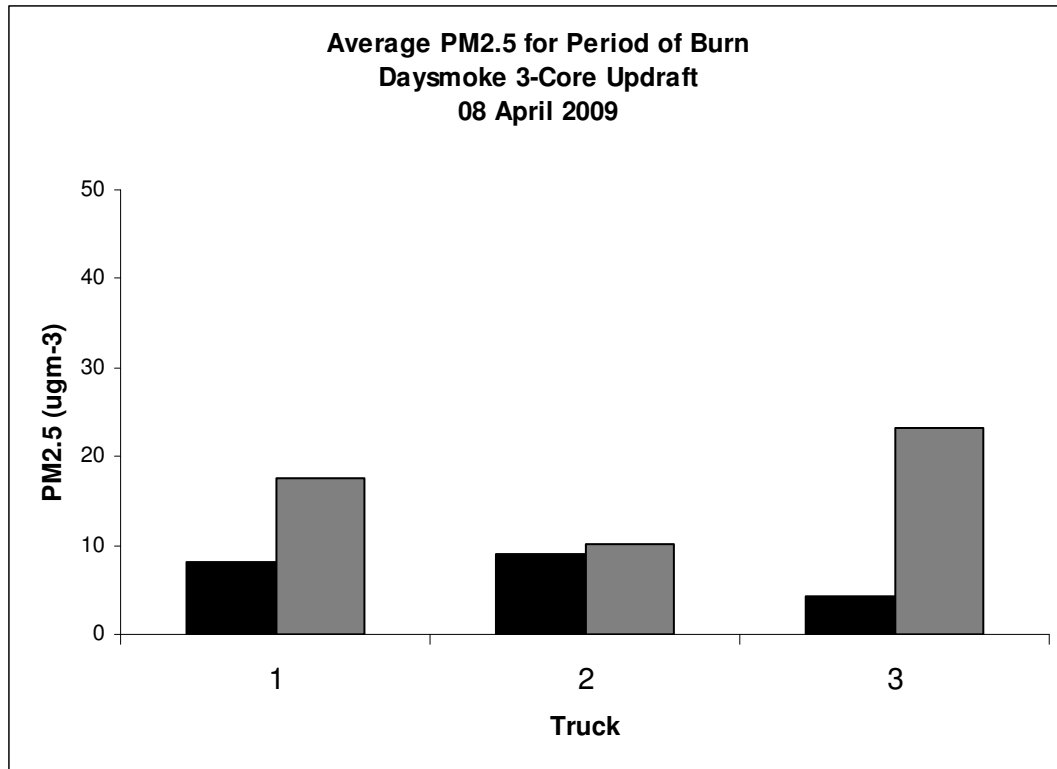


Figure 5. The average PM2.5 for the 2.5 hr period of the burn (black bars) compared with the 5-ensemble average 3-core updraft Daysmoke simulations (gray bars) for the 08 April 2009 burn.

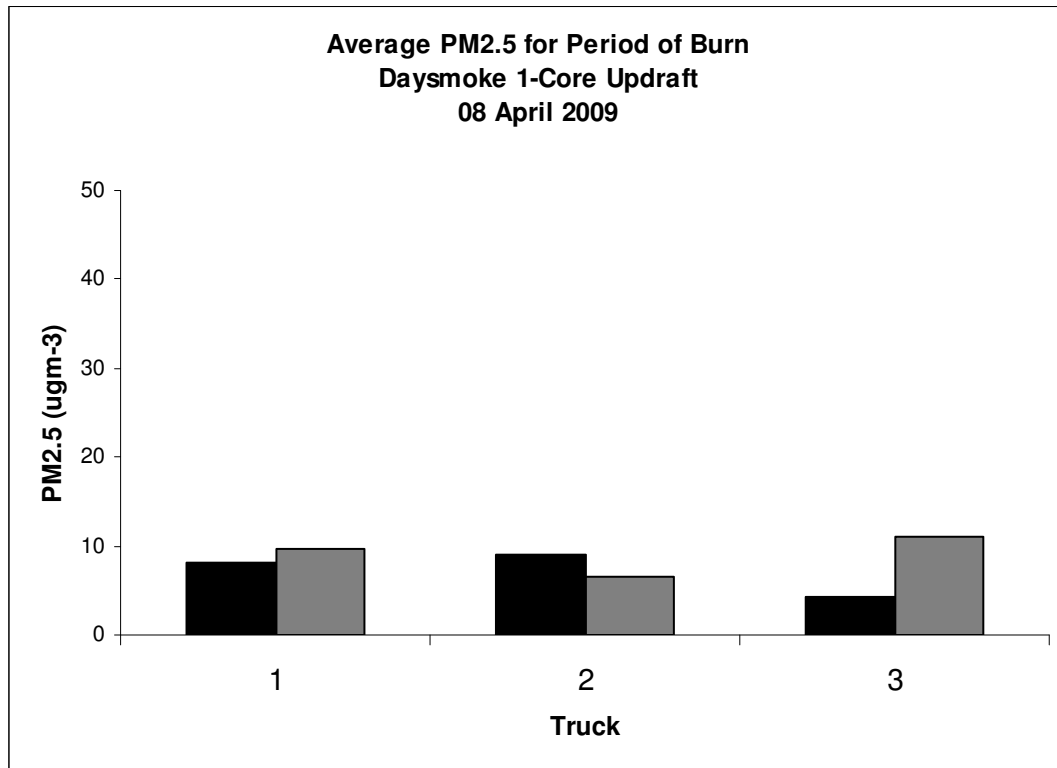


Figure 6. The average PM2.5 for the 2.5 hr period of the burn (black bars) compared with the 5-ensemble average 1-core updraft Daysmoke simulations (gray bars) for the 08 April 2009 burn.

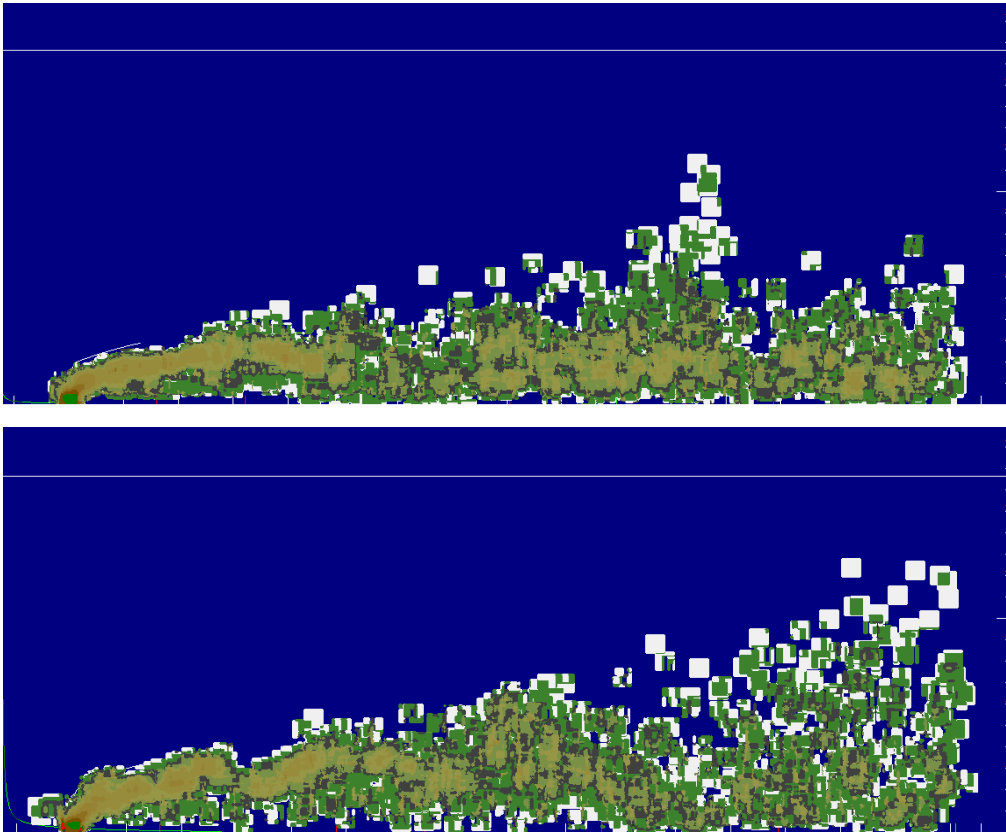


Figure 7. Vertical cross section for a 3-core (upper panel) and a 1-core plume modeled by Daysmoke for 1800 LST 08 April 2009. The white horizontal tic marks denote 100 m intervals. The vertical tic marks denote 1.0 mile (red) and 1.0 km (white) intervals.

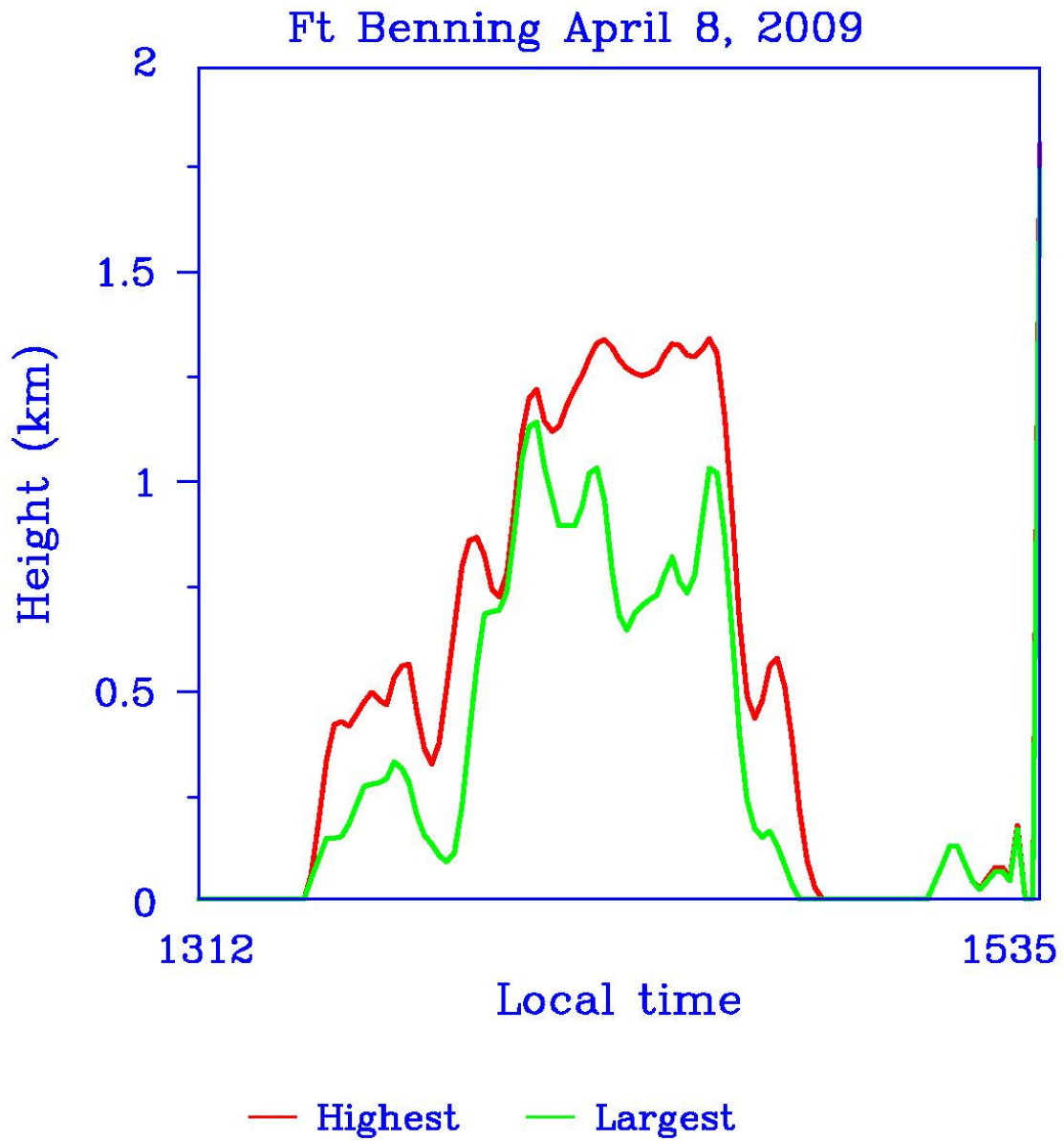


Figure 8. Traces for the highest plume height (red) and largest return (green) as measured by the USFS ceilometer. Time is local daylight time and one hour should be subtracted to bring the time to LST.

Analysis of 09 April 2009 at Fort Benning, GA

Gary L. Achtemeier
USDA Forest Service
Athens, GA
5 March 2010

Introduction.

On 09 April 2009 compartment J6 consisting of 383 acres was burned. Ignition began at approximately 1130 LST and was completed at 1320 LST. Figure 1 shows a Google Image of the burn area.

All three trucks were deployed. Figure 2 shows the positions of Truck 1 (blue) with respect to the burn. From 1100-1430 LST (the duration of the burn), the truck was located at Point 1. Truck 2 (yellow) was located at Point 2 from 1128-1247 LST, and at Point 3 from 1250-1430 LST. Truck 3 (red) was located at Point 4 from 1100-1430 LST. The white circle locates positions of the USFS ceilometer.

Winds at 200 m (approximation to the transport winds) developed by the WRF model were characterized by relatively constant speeds (6.3 m sec^{-1} at 1300 LST to 7.4 m sec^{-1} at 1500 LST). Wind directions shifted from 245 deg at 1200 LST to 222 deg at 1500 LST. The range of wind shift is shown by the beginning direction (solid line) and the ending direction (dashed line) in Figure 2.

Observations

The graph of the raw 30-sec data (calibrated for wood smoke) for Truck 1 is shown in the top panel of Figure 3. Smoke arrived at higher concentrations at 1200 LST followed by several spikes in excess of $100 \mu\text{gm}^{-3}$ from 1230 LST. Smoke arrived at Truck 2 (middle panel) shortly after 1200 LST followed by numerous peaks above $50 \mu\text{gm}^{-3}$. Smoke also arrived at Truck 3 at 1200 LST followed by peaks in excess of $40 \mu\text{gm}^{-3}$.

Daysmoke Results for PM_{2.5}

For the Daysmoke simulations, the block E3 burn was treated as a square of area equal to the area of block E3. Ignition was at 1130 LST.

The Daysmoke results are based on a subjective determination of the updraft core number that would be typical for the 09 April burn. Daysmoke provides no mechanism for determining updraft core number. Updraft core number is determined by a complex interaction among a number of factors. Some of these factors are:

- Size of burn area – a small burn area should be expected to produce only one updraft core; large burn areas can support many updraft cores.
- Shape of burn area – a burn area that is highly irregular in shape will require an irregular distribution of fire leading to many updraft cores. This problem can be amplified when wind direction maximizes irregularities.

- Heterogeneity of fuels – fuels that burn hot relative to surrounding fuels will develop stronger convective currents and will tend to form updraft cores.
- Fuel type, moisture, and loadings – all three factors relate to heat production. High heat production will develop convective columns and lead to fewer updraft cores; low heat production will lead to many updraft cores
- Distribution of fire on landscape - fire distributed along a long linear line will produce many updraft cores; fire spread evenly over length and depth (mass ignition, stripping) will organize convective columns into fewer updraft cores.
- Amount of fire on landscape – a small amount of fire will reduce emissions per second but decrease heat thus minimizing convective organization. Result: many updraft cores. A large amount of fire will produce the opposite. Result: fewer updraft cores
- Distribution of canopy gaps. Hot air trapped beneath a dense canopy will flow to the gaps thus creating convective columns that produce updraft cores there. Thin (or no) canopies will not be a factor in updraft core development.
- Transport wind speed – strong winds inhibit convective organization thus leading to many updraft cores. Weak winds allow convective organization resulting in few updraft cores.
- Mixing layer depth – a shallow mixing layer inhibits convective organization thus leading to many updraft cores. A deep mixing layer has less adverse impact on convective organization so fewer updraft cores should be expected.

For the 09 April 2009 burn, the relatively strong 200 m transport winds ($6.0\text{-}9.5\text{ m sec}^{-1}$) and light fuel loads (2T/acre) serve to increase updraft core number. The large size of the burn area (383 acres) would also contribute to increasing the updraft core number. The deep mixing layer (1200-1800 m) serves to decrease the number of updraft cores. An updraft core number of 4 cores are assigned for this burn.

Figure 4 compares the average PM_{2.5} for the period of the burn with the results from a 5-ensemble Daysmoke average for 4-core updraft plumes for the locations of the trucks. Daysmoke under-estimated smoke at Truck 1 by a factor of 0.6 ($15\text{-}26\text{ }\mu\text{gm}^{-3}$), matched Truck 2 ($20\text{-}20\text{ }\mu\text{gm}^{-3}$), and underestimated smoke at Truck 3 ($9\text{-}17\text{ }\mu\text{gm}^{-3}$). Examination of Daysmoke plumes relative to truck positions in Figure 2 show that Truck 1 was located within the plume near the plume axis. Truck 2 was located at the plume edge early and along the plume axis after the wind shifted. Truck 3 was located along the plume edge.

In summary, the 09 April 2009 burn was handled well by Daysmoke initialized with 4-core updraft plumes. Daysmoke under-predicted smoke at Truck1 and Truck 3 and matched the observations for Truck 2.

Daysmoke Results for Plume Top Height

Vertical cross sections for the 4-core updraft at 1230 LST (upper panel) and at 1400 LST (lower panel) are shown in Figure 5. The white lines identify the mixing heights. For the first several miles (km) downwind from the burn, Daysmoke tended to run the plumes with plume tops just 400 m above the ground. Mixing to higher heights above 1 km occurred beyond 2.5 miles (4.0 km).

Figure 6 shows the traces for the highest plume height and largest return as measured by the USFS ceilometer. Time is local daylight time and one hour should be subtracted to bring the time to LST. The graph shows the plume at the location of the ceilometer by 1152 LST. Plume tops range between 800-1000 m – about twice the heights shown by Daysmoke. Then shortly after 1215 LST (1315 EDT –eastern daylight time) plume heights fell to near 500 m. After that, large oscillations in plume top height were observed.



Figure 1. Google Earth image of compartment J6 outlined in yellow for the 09 April 2009 burn at Fort Benning, GA.

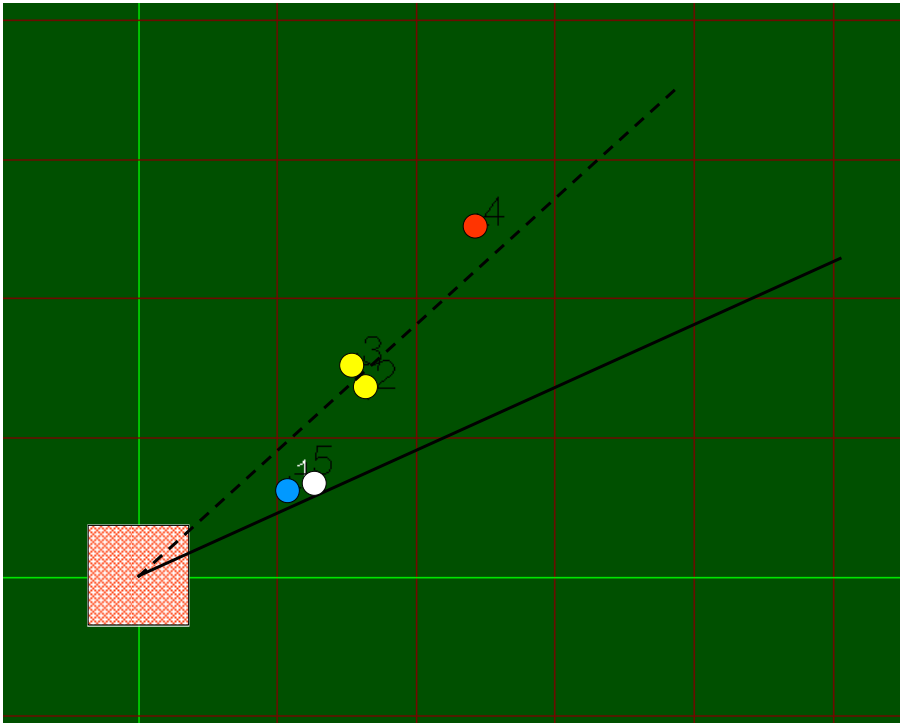


Figure 2. Locations of the three trucks relative to the Daysmoke depiction of the compartment J6 burn with reference to the compartment center point. The diagonal solid and dashed black lines delineate prevailing wind directions.

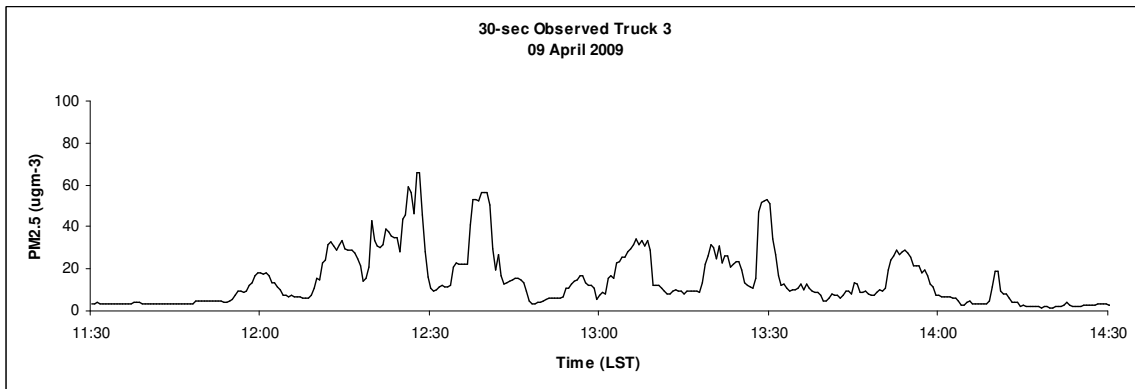
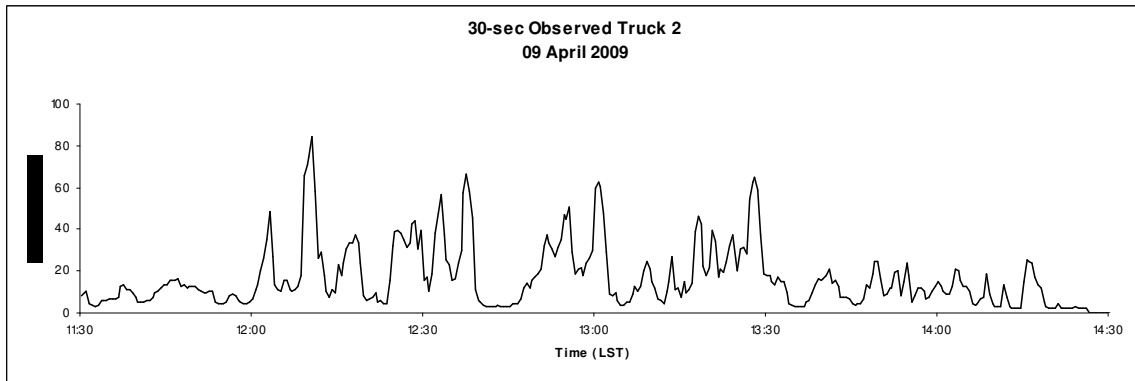
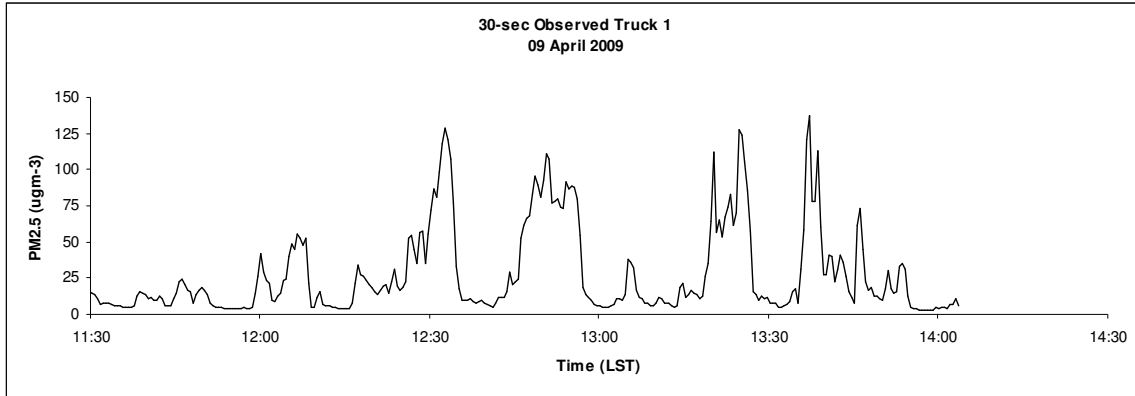


Figure 3. Traces of the 30-sec observed PM_{2.5} measured at the locations of Truck 1 (top panel), Truck 2 (middle panel), and Truck 3 (lower panel) for the 09 April 2009 burn.

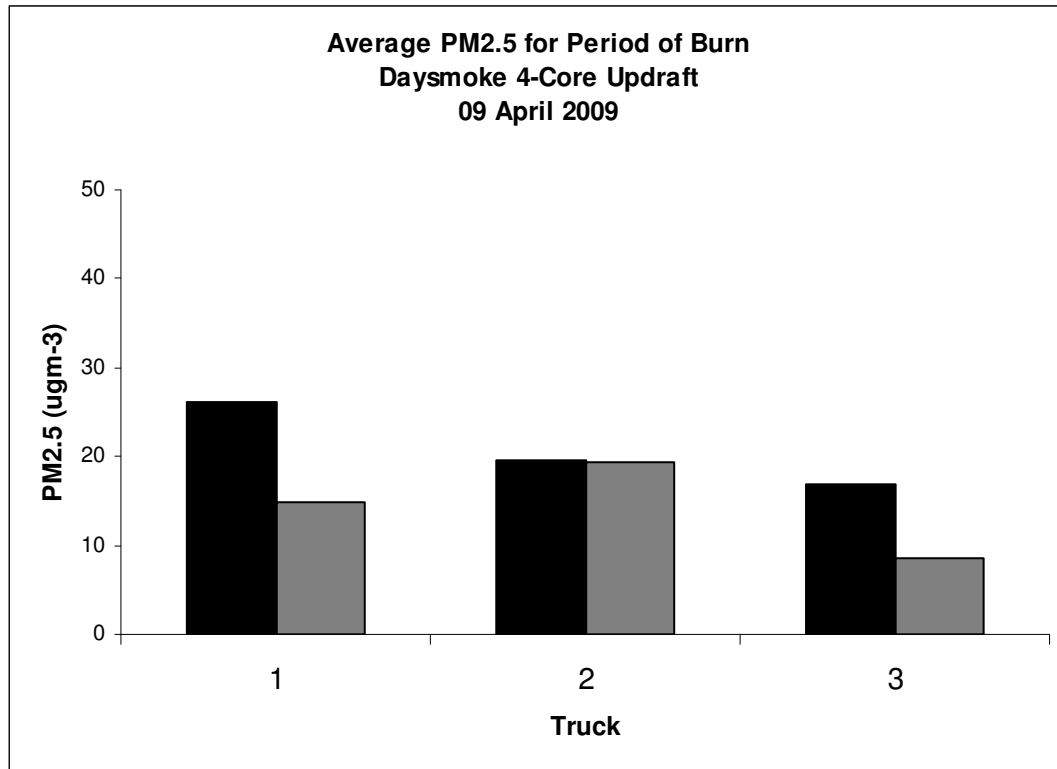


Figure 4. The average PM2.5 for the 2.5 hr period of the burn (black bars) compared with the 5-ensemble average 4-core updraft Daysmoke simulations (gray bars) for the 09 April 2009 burn.

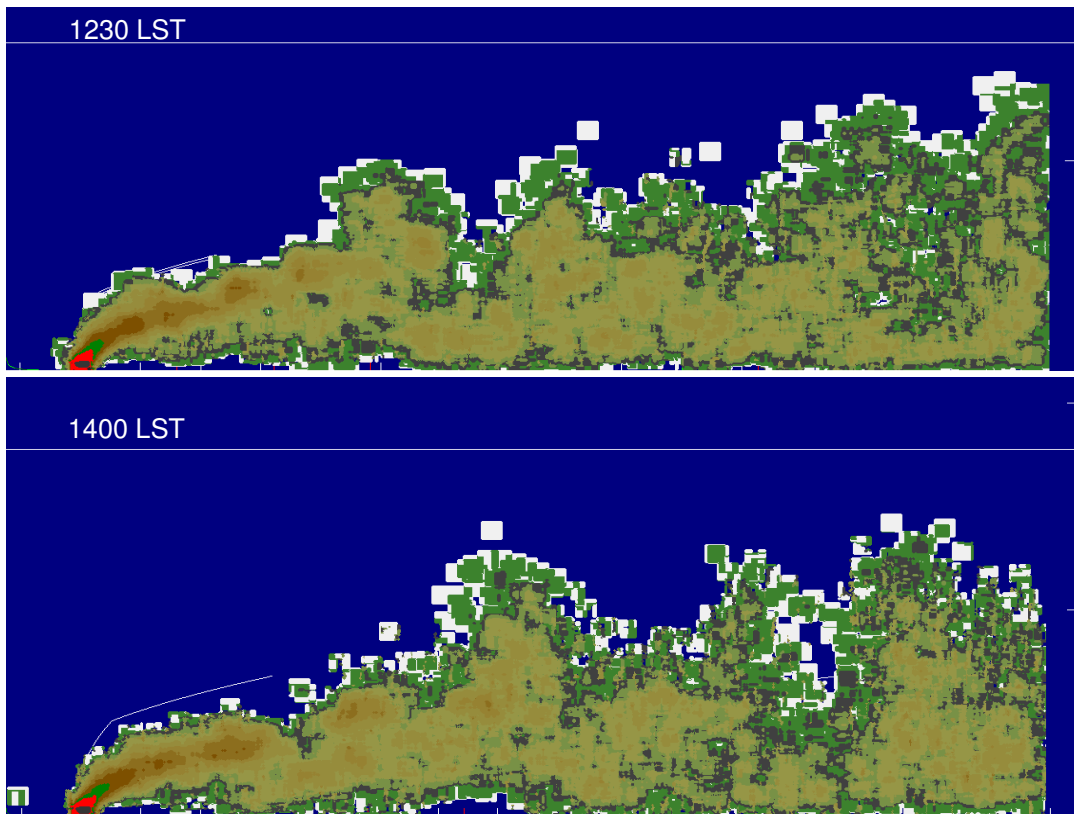


Figure 5. Vertical cross section for 4-core updraft plumes modeled by Daysmoke for 1300 LST (upper panel) and 1500 LST (lower panel) 09 April 2009. The white horizontal tic marks denote 100 m intervals. The vertical tic marks denote 1.0 mile (red) and 1.0 km (white) intervals.

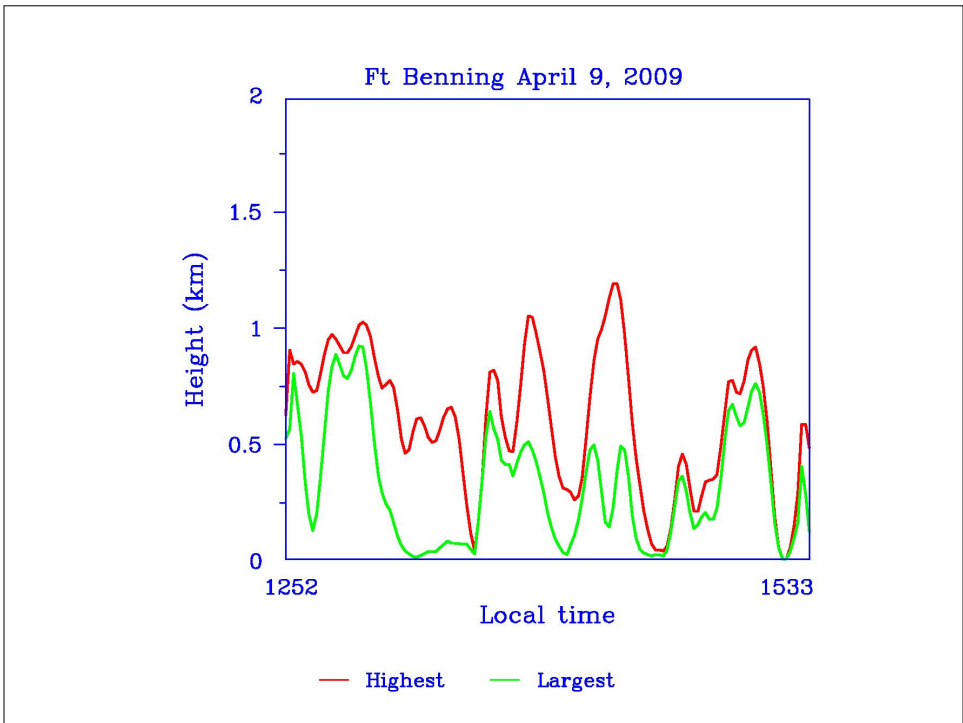


Figure 6. Traces for the highest plume height (red) and largest return (green) as measured by the USFS ceilometer. Time is local daylight time and one hour should be subtracted to bring the time to LST.